



The author(s) shown below used Federal funding provided by the U.S. Department of Justice to prepare the following resource:

Document Title: Fast On-Site Screening of Seized Drugs by Electrochemical and Spectroscopic Tools: Identification of Fentanyl and Novel Psychoactive Substances

Author(s): Luis E. Arroyo

Document Number: 308452

Date Received: January 2024

Award Number: 2019-DU-BX-0030

This resource has not been published by the U.S. Department of Justice. This resource is being made publicly available through the Office of Justice Programs' National Criminal Justice Reference Service.

Opinions or points of view expressed are those of the author(s) and do not necessarily reflect the official position or policies of the U.S. Department of Justice.

FINAL RESEARCH REPORT

Agency: National Institute of Justice

Award number: 2019-DU-BX-0030

Project Title: **Fast on-site screening of Seized Drugs by Electrochemical and Spectroscopic Tools: Identification of Fentanyl and Novel Psychoactive Substances**

PI: Luis E. Arroyo
Associate Professor
Luis.arroyo@mail.wvu.edu
304.293.6976

Submitting official: Luis E. Arroyo
Associate Professor, Department of Forensic and Investigative Science

Submission date: 12/30/22

DUNS: 191510239

EIN: 550665758

Recipient Organization: West Virginia University Research Corporation
886 Chestnut Ridge Road P.O. Box 6845, Morgantown, WV 26506-6845

Award Period: 01/01/2020 to 12/31/2022

Reporting Period End Date: 12/31/2022

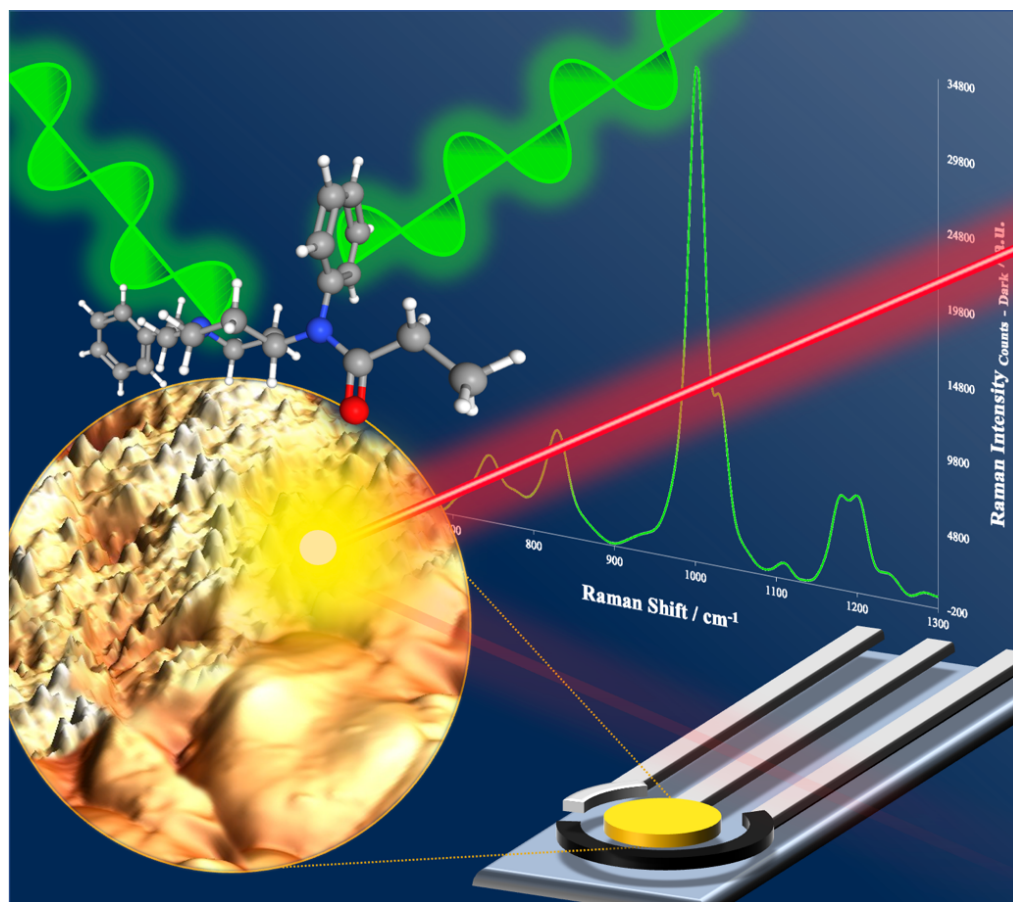
Award Amount: \$267,438.00

Signature of Submitting Official:



Authorized Organizational Representative:

Katie Schneller
Director, Office of Sponsored Programs



Fast on-site screening of Seized Drugs by Electrochemical and Spectroscopic Tools: Identification of Fentanyl and Novel Psychoactive Substances

NIJ Award 2019-DU-BX-0030

Final Research Report Master Document

WVU Forensic and Investigative Science Department
PI: Dr. Luis E. Arroyo

December 2022

Table of Contents

I PROJECT SUMMARY	5
1.1. Abstract	5
1.2. Problem Statement	7
1.3. Major Goals and Objectives of the Project.	9
1.4. Research Design, Methods, Data Analysis	10
1.4.1.1. Methods of Analysis	10
1.4.1.2. Data Analysis	11
1.5. Expected applicability of the research	11
2.1. Activities/accomplishments.	12
2.2. Results and Findings	13
2.2.1.1. Results and Findings for Task 1a: Master List of Target materials	13
2.2.1.2. Standard Preparation and Purity Verification.	13
2.2.1.3. Method Validation	15
2.2.1.4. Library Creation	15
2.2.1.5. Retention Indices Study	16
2.2.1.6. Method Validation Results	16
2.2.1.7. Library Creation Observations	17
2.2.1.8. Retention Indices Study	19
2.2.1.9. Chromatograms and mass spectra from GC/MS	21
2.3. Confirmatory LC-MS/MS Analysis of Target Analytes	23
2.3.1.1. Purpose of LC-MS/MS Method	23
2.3.1.2. Materials and Methods	23
2.3.1.3. Chromatographic Separation	26
2.3.1.4. Limits of detection	28
2.3.1.5. Bias and precision	29
2.3.1.6. Interference	30
2.3.1.7. Calibration Curves	30
2.4. Results and Findings for Tasks 1b-d. Generation of Voltammetric Profiles for target drugs and materials.	32
2.4.1.1. Instrumentation	32
2.4.1.2. Electrochemical characterization	32

2.4.1.3.	Electrochemical Behavior of Target Analytes	33
2.5.	<i>Results and Findings for Task 2a: Raman Spectra using Tactic ID Instrument.</i>	
	<i>Integration of Raman Data with Mass Spectrometry using DART-MS.</i>	41
2.5.1.1.	Establishing Bias, Precision, & Reproducibility for the Portable Raman	41
2.5.1.2.	Assessment of Mixtures	41
2.5.1.3.	Authentic Samples	43
2.5.1.4.	TacticID Results	43
2.5.1.5.	Performance Measures.	45
2.5.1.6.	Orthogonal Detection.....	46
2.5.1.7.	Authentic Sample Results.....	47
2.6.	<i>Results and findings for tasks 2a and 3b: Raman and Multivariate Analysis.</i>	48
2.6.1.1.	Machine Learning for Drug Identification in Portable Instruments.....	48
2.6.1.2.	Spectra Acquisition	49
2.6.1.3.	Spectral Comparison	49
2.6.1.4.	Pure Spectra Algorithms.....	49
2.7.	<i>Results and Findings for tasks 2b-c and 3a: SPELEC Raman and Performance measures.</i>	
	55	
2.7.1.1.	Surface-Enhance Raman Spectroscopy (SERS).....	55
2.7.1.2.	EC-SERS Experiment	56
2.7.1.3.	Determination of the electro-activity	57
2.7.1.4.	6.2. EC-SERS Electrode and Surface Characterization.	59
2.7.1.5.	Targeting the identification of Fentanyl and fentanyl analogs: MPD.....	68
2.7.1.6.	Differentiation of Analogs and Limits of Detection	70
2.7.1.7.	Quantitative Capabilities.....	76
2.7.1.8.	Interference Studies.....	77
2.7.1.9.	Assessment of Simulated Samples.....	82
2.7.1.10.	Performance on Authentic Samples	87
2.7.1.11.	Comparison to Chemical Color Tests	87
2.7.1.12.	Targeted Fentanyl EC-SERS Performance	90
2.8.	<i>PARTICIPANTS AND OTHER COLLABORATING ORGANIZATIONS.....</i>	94
2.9.	<i>CHANGES IN APPROACH.....</i>	98
2.10.	<i>LIMITATIONS.....</i>	98

I PROJECT SUMMARY

1.1. Abstract

Routine seized drug field testing uses color tests for the presumptive identification of illegal substances. Instrumental analyses are then conducted at the laboratory to confirm the drug's identity. As an attempt to speed up the process and compensate for the rapid increase in caseloads, several U.S. jurisdictions have accepted field test results at preliminary hearings. Nonetheless, the emergence of novel psychoactive substances (NPS) has brought additional challenges to color assays. Spot tests are not sensitive or selective enough to new drug formulations, increasing the number of false positive and false negative results and not meeting legal standards for preliminary hearings. The consequences are overwhelming to the judiciary system as the number of cases that require laboratory testing increase backlogs and raise the costs of analysis and incarceration. Moreover, novel fentanyl and fentalogs represent a safety concern to law enforcement personnel and first responders. Therefore, there is a critical need to develop alternative rapid, cheap, and reliable screening methods for in-situ drug identification.

The long-term objective of this project is to introduce smart and cost-effective portable instrumentation to integrate crime scenes with forensic laboratories in real time. The primary aim of this study is to develop and validate ultrafast screening methods that increase the reliability and productivity of drug identification. Powerful electrochemical (EC) techniques are presented as surrogate technologies to detect emerging drugs, like fentanyl and NPS, in drug trafficking and seized drug cases. Raman spectroscopy is proposed as an orthogonal approach to EC via spectroelectrochemistry experiment (EC-SERS) to enhance the scientific value of the evidence. Also, this study aims to evaluate chemometric tools for data mining of EC and Raman information for improved drug identification.

In this project, the utilization of simple, cheap, and disposable screen-printed carbon electrodes (SPCE) attached to portable electrochemical units, and Raman spectroscopy represents a feasible solution to streamline high-volume casework settings. Validation of the Spectro-electrochemical approach is proposed on a portable commercial instrument using case-like samples (mixtures of drugs and adulterants) and actual adjudicated casework specimens targeting the main drug. The significance of the proposed approach stems from its broad application in the criminal justice system and its ability to restructure the efficiency and efficacy of data collection against crime. We have achieved that through the following main contributions:

- 1) **Implementation of confirmatory mass spectrometry methods for drug identification in seized drugs scenarios.** This includes GC/MS single quadrupole full scan chromatographic separation of target drug and diluents (TIC generation) for purity evaluation and spectral drug database development. Also, an LC/MS-MS MRM Method for quantitative analysis of target drugs. A table containing the main transitions is included in this report.
- 2) **Validation of a Portable Raman Spectroscopy Instrument (Tactic ID, 785 nm)** towards the detection of native drugs and mixtures. Analytical performance and error rates are reported. Development of a Raman Spectral library.
- 3) **GC/MS mass spectral Monographs** containing information for target drugs and diluents (30 compounds). This monograph includes general information about the compound,

including IUPAC name, CAS#, Chemical Formula, molecular weight, GC/MS TIC spectra, as well as retention indices.

- 4) **Development of novel, fast methods for drug detection.** This includes information on the **qualitative electrochemical profiles** of main target drugs and materials summarized in a table format using a simple screen-printed carbon electrode (SPCE). Also, the **Rapid-On site Analysis of Fentanyl using EC-SERS targeted method** via silver screen printed electrodes, and a **general screening method of drugs using untargeted EC-SERS** approach via silver screen-printed electrodes are included. The use of gold screen printed electrodes is also included to demonstrate the efficiency of Spectro electrochemistry for the analysis of isomeric synthetic cathinones.
- 5) **EC-SERS Monographs** containing information for target drug and diluents (37 compounds). This monograph contains basic electrochemical profiles using screen-printed carbon electrodes (SPCE), Raman spectroscopy data of native materials, and SPELEC Raman using silver screen-printed electrodes via the Non-targeted EC-SERS Method.
- 6) **Development of novel machine learning algorithms to identify and classify drugs.** The use of neural networks and other approaches is presented to classify single compounds, binary, secondary, ternary, and quaternary mixtures by the compound name and compound's class using seized drugs and common diluents analyzed using a 785 nm portable Raman system. This innovative approach opens new research avenues for our field.

1.2. Problem Statement

The rapid detection and identification of drugs in the field and at the laboratory, especially opioids and novel psychoactive substances (NPS), is a challenging task due to their continuous street profile changes and their prevalence within the United States' illegal drug market. For instance, just in 2016, the Drug Enforcement Administration (DEA) reported sixty percent of the seized fentanyl and fentanyl-related compounds for the first time.¹ Data from U.S. Customs and Border Protection indicates an increase in seizures of fentanyl from 2800 pounds in 2019, reaching 10,200 pounds during FY2021.² Moreover, addressing the opioid epidemic becomes urgent as the death toll from overdose keeps escalating.

Forensic drug scientists employ hyphenated methods like gas chromatography-mass spectrometry (GC-MS) or liquid chromatography-mass spectrometry (LC-MS) due to their inherent confirmatory power. While these techniques provide excellent sensitivity and specificity, they may require complex sample preparation schemes, a higher level of expertise from the operator, and time to produce a result. The median turnaround time for a typical drug case is 36-40 days from evidence submission to report.³ The time it takes to process information prevents prompt administration of justice and increases costs in legal proceedings. Inevitably, innocent individuals may be unjustifiably waiting in jails, or offenders may escape the law enforcement radar.

Therefore, there is a critical need to implement more reliable on-site screening tools for the identification of the growing diversity of modern drugs of abuse. In the absence of immediate solutions, the implications to crime laboratories will become overwhelming, increasing backlogs and operational expenses. Moreover, extended incarceration drastically affects the overall cost-per-case and could bring distressing experiences to the involved suspects and families.

The use of portable Raman instrumentation has been investigated as a way to provide rapid and accurate results to crime scene investigators, first responders, and law enforcement officers. The use of Raman spectroscopy has gained momentum due to its portability, non-destructive nature, simplicity, and robustness in the detection of pure and adulterated samples. Some crime laboratories have conducted formal assessments to incorporate the use of these systems in their local law enforcement.^{4,5} Results have demonstrated that hand-held Raman devices are useful for narcotics field testing, are easy to implement, and are safer and cheaper than color tests.

Also, the Scientific Working Group for the Analysis of Seized Drugs (SWGDRUG) classifies Raman as a “Category A” technique due to its confirmatory potential. Despite this classification, some testing materials can show a lack of specificity and sensitivity, especially when dealing with mixtures of substances or when fluorescence is present. Fluorescence becomes particularly challenging for samples such as marijuana, ecstasy, and black-tar heroin. Surface Enhanced Raman Spectroscopy (SERS) and built-in background correction algorithms have shown promising results in overcoming fluorescence interferences and enhancing sensitivity. However, SERS is mainly available for bench-top instruments, and challenges remain for in-situ measurements.

The long-term goal of this research work was to develop and validate a more efficient, versatile, and reliable methodology for the analysis of controlled substances to modernize the analytical scheme by which evidence is processed in real-time. Improvements to the seized drug workflow will help combat the current opioid epidemic and will speed up law enforcement investigations.

We propose to combine electrochemical tools with Raman spectroscopy as a superior and practical approach for field testing. Spectro-electrochemistry will play a unique role in offering the best of two worlds: 1) a distinctive electrochemical signature of the target species, and 2) the ability to use electrochemistry to generate in-situ nanostructures to use surface-enhanced Raman Spectroscopy

(SERS) technology in portable devices with a particular emphasis on fentanyl. This orthogonal approach to interrogate unknown seized materials will offer a new avenue for analyte detection both in field and lab settings. Further, statistical models are proposed to improve the identification of the target drugs.

Electrochemistry (EC) is a mature analytical tool that is widely used for in-situ measurements in the pharmaceutical, environmental, energy, and medicine fields. However, its potential remains underexploited in drug analysis for forensic applications. The sensing concept in EC relies on the selective chemical oxidation or reduction of the active species (drug) present in a solution. This redox mechanism provides a profile (signal) of the testing material with information that complements Raman spectroscopy results. The use of a simple, cheap, and disposable electrode measuring platform in EC opens a new paradigm toward the detection and identification of seized drug entities.

Since this is early-stage research, we have developed strategic partnerships with a local forensic laboratory, other members of academia, and the private sector to provide a robust framework to assess the novel technology. The basic knowledge developed in this study has the potential to benefit the criminal justice system by increasing personnel safety, providing more cost-effective methods, enhancing the accuracy of results, and expediting the judiciary process. A summary of publications related to this research project is included in this technical report.⁶⁻¹⁰

1.3. Major Goals and Objectives of the Project.

This project aims to develop a comprehensive strategy to enhance the validity of the screening analysis and interpretation of seized drugs. We propose the development of versatile, fast, and reliable methodologies for the in-situ detection of common drugs of abuse, cutting agents, and novel psychoactive substances (NPS), including fentanyl and analogs. The specific objectives of this study are:

Objective 1. Develop and validate portable electrochemical (EC) methods using disposable, cheap, and selective electrodes for the detection of drugs of abuse.

Objective 2. Evaluate the utility of portable Raman spectroscopy for drug identification and the use of electrode-based nanostructures to apply Surface Enhanced Raman Spectroscopy (SERS) in handheld units.

Objective 3. Assess and validate the use of combined data from EC and Raman methods and chemometric tools for the on-site identification of drugs.

The central hypothesis of this study is that electrochemical techniques (EC) in tandem with Raman spectroscopy will provide screening methods that are faster, more selective, and more informative than the current presumptive laboratory-based and field identification tests. Our team will develop non-intrusive sampling techniques and more informative data to complement current practice and which are compatible with existing SWGDRUG and UNODC guidelines.

These goals will be accomplished through the following specific tasks and these activities are shown in figure 1:

Task 1a—Drug Master List Development.

Task 1b—Testing and selection of working electrode on screen-printed electrodes.

Task 1c—Generation of drug voltammetric profiles.

Task 1d—Evaluation of Nanomaterials deposition and its effect on analyte sensing.

Tasks 1e—Construction of a Drug Voltammetric Library.

Task 2a—Raman spectra acquisition of known drug materials, cutting agents and diluents.

Task 2b—Using SPELEC Raman Setup with silver electrodes for in-situ SERS spectra.

Task 2c—Development and optimization of nanostructures on screen-printed disposable electrodes (SPE) for SERS experiments.

Task 3a- Assessment of performance measures

Task 3b-Multivariate analysis and machine learning algorithms for the identification and classification of drug target compounds.

1.4. Research Design, Methods, Data Analysis

1.4.1.1. *Methods of Analysis.*

This project is designed to accomplish three main objectives, as described in section 1.3. A list of 30 different substances of forensic interest was selected to serve as model materials and demonstrate the analytical capability in presumptive drug identification of a novel Raman and Spectro-electrochemical approach. The selection of candidate drugs is based on their relevance according to recent drug trends reports. High-purity drug standards dissolved in a selected buffer medium were analyzed via SPCE electrodes using voltammetric techniques aiming at the later creation of an electrochemical drug library. The electrochemical behavior of each drug will be assessed individually using bare screen-printed carbon electrodes. Parallel cross-validation of the primary target drugs will be conducted using GC-MS and LC-MS/MS to generate mass spectral data (full scan and MRM transitions) of standards test samples to establish the ground truth.

Raman and Surface Enhanced Raman Spectra (SERS) were collected as a stand-alone technique and in synchronous mode with the electrochemical unit (SPELEC). Method development, screening, and full optimization stages will be conducted with standard drug materials (tasks 1b-1d and 2c) and standard drugs and common adulterants (tasks 1e, 2a, and 2b).

We also assessed the ability of the proposed orthogonal approach to detect and characterize unknowns via a single-blind validation study. Case-like samples (mixtures of native drugs with diluents at different ratios) and seized casework samples were used in this validation stage (task 3a). The performance of different commercial portable EC systems (Autolab 128 N/Metrohm), and Raman (Tactic ID and SPELEC/DropSens), is presented in this report.

In summary, this project involved the use of multiple analytical techniques and methods for different tasks. Two confirmatory analytical tools for drug analysis, GC/MS and LC/MS-MS were implemented and validated to support the emerging technology proposed in this project: Spectro electrochemistry (EC-SERS). The implementation and validation of this confirmatory instrumentation will be discussed in the results section. Raman Spectroscopy data were collected using a portable unit (Tactic ID) using a 785 nm laser, and its analytical performance for drug identification was evaluated. The general workflow developed in this project is summarized in **figure 1**, and more details of the methodology and experimental designs can be found in the published manuscripts.⁶⁻¹⁰

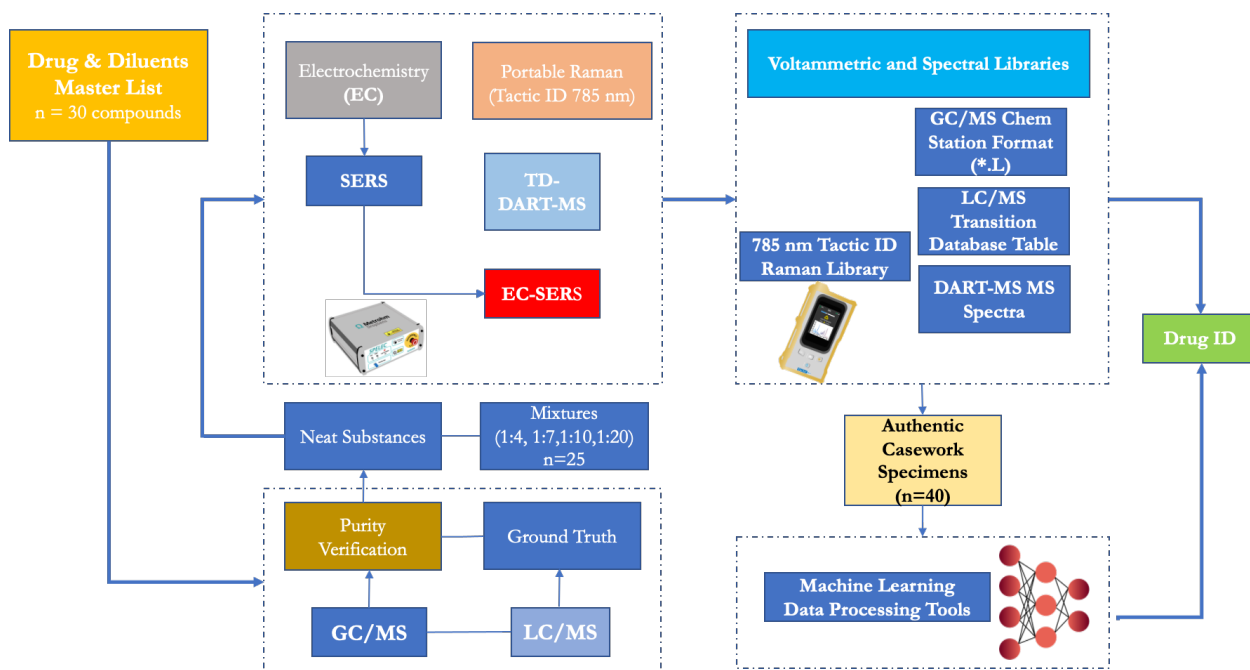


Figure 1: Analytical workflow for the analysis and testing of neat substances and mixtures using the proposed technologies and major outcomes of this research project.

1.4.1.2. Data Analysis

Data analysis in this project required using each analytical instrument's software for signal processing, such as background subtraction, smoothing, signal integration, and, when applicable, quantitative analysis. All statistical analyses were conducted using R Studio (open source, 1.2.1335). Depending on the data type and variables, various data normalization and scaling methods were applied (e.g., Min-Max normalization, Max, Z-score).

Exploratory and descriptive statistical analysis, machine learning algorithms, and classifier methods were used in this study to evaluate their ability to predict class membership on drug classification (Logistic Regression (LR), Naïve Bayes (NB), and Neural Networks (NN)). Misclassification outputs were used to assess the method's performance (sensitivity, selectivity, error rates, and accuracy).

1.5. Expected applicability of the research

This project addressed the challenges of seized drug screening identification as field tests and laboratory determinations. The results of this project can also be applied to, toxicology, law enforcement, and clinical medicine. A comprehensive strategy to enhance the reliability of analysis and the on-site interpretation of seized drug identification was developed. These proposed methodologies and techniques will influence current practices for the analysis of controlled substances within the forensic science community, both at the scene and within the laboratory. Furthermore, the implementation of these fast-testing methods will serve to reduce backlogs and improve the efficacy and efficiency with which controlled substance cases are processed.

The use of this methodology for testing is expected to aid in combating the current opioid epidemic affecting the country and will enhance the investigations of law enforcement due to the speed of analysis/identification and the improved detection capabilities for substances that may be present in low concentrations within a mixture. In addition, this study will serve to enhance presumptive identification as well as interpretation through statistical models. This will benefit the criminal justice system through reduced false positive and false negative results. This improvement in reliability offers superior results that will be defensible in preliminary hearings and trials.

In summary, the basic knowledge developed in this study has the potential to provide an overall benefit to the criminal justice system by increasing personnel safety, providing more cost-effective methods, enhancing the accuracy of results, and expediting the judiciary process. The community's interest in this research is reflected by the broad participation in scientific venues and awareness in social media and webinars. We are currently working towards the transfer of these technologies in case management, something we will be exploring in more detail in the second phase of this research if awarded.

II. OUTCOMES.

2.1. Activities/accomplishments.

Each of the proposed objectives and tasks was satisfactorily completed in this project. The four main tasks contained 50 specific research activities, including the following categories:

1. Selection of target drug materials
2. Sample preparation and purity verification using GC/MS. Implementation of LC/MS targeted method for suite of drugs.
3. Methods' development, optimization, and validation for electrochemistry, portable Raman System (Tactic ID) and SPELEC EC-SERS.
4. Data analysis.
5. Statistical analysis and data interpretation.
6. Reporting results in the scientific literature.
7. Disseminating findings at scientific meetings.
8. Creation of the GC/MS spectral database and Raman; EC-SERS database.

In addition, the project management included other activities: group meetings to discuss research results, planning meetings to monitor accountability for the main tasks and assignments, advisory meetings with practitioners, data analysis review sessions with students, preparation of progress reports, and submission of manuscripts.

The substantial dissemination of this study's research findings in peer-reviewed journals and scientific forums indicates the interest raised within the forensic community. We have **published the main results of this research in five scientific publications in peer-reviewed journals**, and three more are in progress. The research has been **published in high-impact factor journals** and read by a broad audience, including *Frontiers in Analytical Science*, *Sensors*, *Chemical Physics Letters*, *Forensic Chemistry*, and *Journal of Electroanalytical Chemistry*.

Also, two of our students completed and published their **master's thesis and two doctoral dissertations** from this effort (graduations occurred in Spring 2022 and December 2022).

Our research has been **disseminated at twenty-one scientific meetings**, some of which were invited contributions. Among the invited presentations is a webinar sponsored by the National Institute of Justice to present our spectroelectrochemical research results, which attracted multiple registrants. We have also received NIJ invitations to present the progress in this research at events dedicated to disseminating their funded research, like the Annual American Academy of Forensic Sciences and PITTCON 2021 and the upcoming PITTCON 2023 meetings. These events are broadcast and provide valuable opportunities to publicize WVU/FIS and NIJ-funded research.

Our research has also been featured on several local news, social media, and webinars, such as the Online Forensic Symposium organized by the Center for Forensic Science Research and Education (CFSRE), the Lightning Talk organized by the American Society of Crime Lab Directors (ASCLD), which crime laboratory managers and practitioners widely attend.

Specific results and details of the main milestones are discussed in the following sections.

2.2. Results and Findings

2.2.1.1. *Results and Findings for Task 1a: Master List of Target materials*

Table 1 below shows the suite of drug and diluent materials utilized in this work.

Table 1 shows the list of drugs and cutting agent/diluents describe in this monograph.

Target Drug	Diluent
Heroin	Phenacetin
Fentanyl	Paracetamol
Cocaine	Levamisole
Methamphetamine	Lidocaine
Alprazolam	Procaine
Naltrexone	Benzocaine
Codeine	Diltiazem
Morphine	Hydroxyzine
Sufentanil	Sorbitol
4-MMC	Maltose
4-MEC	Starch
PB-22	Caffeine
THC	Phenolphthalein
Mitragynine	Myo-inositol
Buprenorphine	Boric acid

2.2.1.2. *Standard Preparation and Purity Verification.*

Several available standards and reference materials were obtained from vendors like Cayman Chemical, Sigma, Across Organics, and Baker, and their purity was verified by GC/MS using the conditions shown in **table 2** and summary results presented in **table 3**.

Table 2. GC/MS conditions for purity evaluation.

Analytical Column	Agilent J&W DB-5MS UI, 30 m x 0.25 x 0.25µm (5 %phenyl-methylpolysiloxane)
GC	Agilent 7890 B GC
Carrier Gas	Helium, constant flow mode, 1.5 mL/min
Sample Introduction	Split/Splitless Inlet, 1 µL, 20:1 split ratio, 20 mL/min split flow, 22 mL/min total flow
Oven	60 °C (0 min); 20 °C/min to 188 °C for 0.15 min 5°C/min to 192°C for 0.15 min, 15°C/min to 280°C for 13 min Total Run time= 26.367
MSD	Agilent 5977 A MSD Mass Hunter GC/MS Rev B.07.00 SP.1549
Solvent Delay	2 min
MS Temperature	250 °C (source), 200 °C (quad)
Mass Range	50-500 m/z
Threshold	150
Scan Speed	1562 (N=2)
MS	EI, Full scan and SIM

Table 3. Standard preparation and purity verification

Compound	Vendor	Item #/ Lot #	Molecular weight (g/mol)	Amount weighed (mg)	Final Concentration (ppm)	Verified Purity (%)
4-Methylethcathinone	Cayman	10801/	227.7	10	8400.1	100.0
HCl	Chemical	0540916-13				
4-Methylmethcathinone	Cayman	9001069/	213.7	10	8293.9	100.0
HCl	Chemical	0474607-21				
Alprazolam	Cayman	14255/	308.8	10	10000.0	100.0
	Chemical	0525541-15				
Buprenorphine HCl	Cayman	14025/	504.1	10	9275.9	100.0
	Chemical	0574056-1				
Cocaine HCl	Cayman	22165/	339.8	10	8928.8	100.0
	Chemical	0522963-27				
Codeine	Cayman	15459/	299.4	10	10000.0	100.0
	Chemical	0524562-17				
Fentanyl HCl	Cayman	14719/	372.9	10	9022.3	99.7
	Chemical	0530926-29				
Heroin HCl	Cayman	9003076/	405.9	10	9100.8	99.9
	Chemical	0559234-9				
Methamphetamine HCl	Cayman	14216/	185.7	10	8036.1	100.0
	Chemical	0565231-8				
Mitragynine	Cayman	11151/	398.5	10	10000.0	100.0
	Chemical	0572828-14				
Morphine	Cayman	15464/	285.34	10	10000.0	100.0
	Chemical	0568085-6				
Naltrexone HCl	Cayman	15520/	377.9	11.7	10569.9	100.0
	Chemical	0539050-8				
PB-22	Cayman	ISO00122/	358.43	10	10000.0	99.5
	Chemical	0449164-38				
Sufentanil	Cayman	15917/	386.6	10	10000.0	99.6
	Chemical	0535925-12				
Delta-9 THC	Cayman	12068/	314.5		10000.0	99.8
	Chemical	0573609-14				
*Phenacetin	Tokyo	P1669/	179.22	10.4	10400.0	100.0
	Chemical	GFZED- OQ				
*Acetaminophen	Sigma	104K0154	151.16	9.9	9900.0	100.0
*Levamisole HCl	Acros	A0405532	240.75	11.8	10013.0	99.8
	Organics					
*Lidocaine HCl Monohydrate	Sigma	SLBR9987V	288.81	12	9736.8	100.0
*Procaïne HCl	Acros	A0407287	272.77	11.6	10049.5	99.7
	Organics					
*Benzocaine	Sigma	044K0697	165.19	10.2	10200.0	100.0
*Diltiazem HCl	Acros	A0403611	451	10.1	9282.6	100.0
	Organics					
*Hydroxyzine 2HCl	Spectrum Chemicals	HY125/ 11H0152	447.83	11.4	9543.5	99.7
*Caffeine	JT Baker	B34653	194.19	10	10000.0	100.0
*SKF 525A HCl	Cayman	15040/	390.5	10.9	9882.3	95.0
	Chemical	0457995-26				

*dilutents; +internal standard

Table 3 shows the amount of each drug dissolved in 1 mL methanol and the final concentration after the salt correction factor was applied. Equation 1 shows how this is performed for a target stock concentration.

$$\text{Drug amount required} = \frac{\text{target concentration}}{\left(\frac{\text{molecular wt of freebase(g/mol)}}{\text{molecular wt of salt(g/mol)}}\right)} \quad \text{Eq. (1)}$$

Where $(\text{molecular wt of free base})/(\text{molecular wt of salt})$ is the conversion factor. Each compound was analyzed via GC/MS with concentrations ranging from 382 to 503 ppm and used for purity verification. Purity was calculated using the quotient of the target drug peak area and the sum of all peak areas. Although the internal standard SKF 525A was the least pure, 95.0%, all other compounds were >99% pure.

2.2.1.3. Method Validation

Linearity, carryover, limits of detection, and selectivity were assessed. The analytical measurement range was 25.2– 200 ppm for cocaine, diltiazem, lidocaine, phenacetin, and procaine, 25.2- 250 ppm for 4-Methylethcathinone, 4-Methylmethcathinone, acetaminophen, alprazolam, caffeine, codeine, fentanyl, heroin, levamisole, methamphetamine, morphine, sufentanil, and THC, 50- 250 ppm for buprenorphine, and naltrexone, 100- 300 ppm for benzocaine, hydroxyzine, mitragynine, and PB-22. The low, medium, and high-quality controls were 50, 150, and 200 ppm for cocaine, diltiazem, lidocaine, phenacetin, procaine, 4-methylethcathinone, 4-methylmethcathinone, and methamphetamine; 50, 200, and 250 for acetaminophen, alprazolam, caffeine, codeine, fentanyl, heroin, levamisole, morphine, sufentanil, THC, buprenorphine, and naltrexone; 100, 250, and 300 for benzocaine, hydroxyzine, mitragynine, and PB-22 respectively. All calibrators were prepared in methanol daily and SKF 525A was used as the internal standard with a final concentration of 50 ppm. Carryover was assessed by analyzing a blank immediately after the highest calibrator. Calibration curves were prepared daily over five days, and residual plots and coefficients of variation were used to assess linearity. Acetaminophen calibrators were prepared separately as they coeluted with phenacetin. The limit of detection was evaluated through serial dilution. The retention times and mass spectra of the diluents and target drugs were compared for interferences.

2.2.1.4. Library Creation

An in-house library was created using the retention times and mass spectra from the selectivity data acquired. **Figure 2** shows the required information for the creation of a mass spectral library through Chemstation. In this example, the input information included the name of the compound, molecular formula, drug vendor, lot and item number, chemical abstract service number (CAS), and retention time. The observed match score at the limit of detection and at 50 ppm was compared to the match scores from a SWGDRUG library, version 3.5.

Figure 2. Screenshot of library creation in Chemstation.

2.2.1.5. Retention Indices Study

The retention index (RI) of selected compounds were evaluated by analyzing 100 ppm saturated alkanes before and after the compounds in triplicate over five days. The variability in retention time and RI were assessed. RI was calculated using Equation 2. The compounds' retention time are represented by $t_{r(x)}$, the retention time of the adjacent n-alkane with shorter retention time $t_{r(n)}$, the retention time of the adjacent n-alkane with longer retention time $t_{r(n+1)}$, and n is the number of carbon atoms in the n-alkane with longer retention time.

$$RI = 100n + 100 \left(\frac{t_{r(x)} - t_{r(n)}}{t_{r(n+1)} - t_{r(n)}} \right) \quad \text{Eq (2)}$$

2.2.1.6. Method Validation Results

Table 4. Regression equations from the linearity experiment.

Compound	R ²	Regression Equation
Phenacetin	0.9785	y = 0.3740x + 0.0153
Lidocaine	0.9318	y = 0.7136x + 0.3826
Procaine	0.9578	y = 0.6136x + 0.0743
Cocaine	0.9684	y = 0.2731x + 0.0535

Diltiazem	0.9816	$y = 0.9435x - 0.3535$
Methamphetamine	0.9883	$y = 0.9826x - 0.0319$
Mephedrone	0.9890	$y = 1.0595x - 0.1890$
4-Methylethcathinone	0.9888	$y = 0.9051x - 0.0159$
Caffeine	0.9871	$y = 0.3734x + 0.0565$
Levamisole	0.9907	$y = 0.2704x - 0.0688$
Codeine	0.9891	$y = 0.2173x - 0.0779$
Morphine	0.9845	$y = 0.1588x - 0.0908$
Δ^9 -Tetrahydrocannabinol	0.9902	$y = 0.2415x - 0.0634$
Heroin	0.9887	$y = 0.1551x - 0.0607$
Fentanyl	0.9892	$y = 0.4398x - 0.2159$
Sufentanil	0.9903	$y = 0.6022x - 0.2796$
Alprazolam	0.9873	$y = 0.1628x - 0.0765$
Acetaminophen	0.9904	$y = 0.6727x - 0.2554$
Naltrexone	0.9694	$y = 0.0585x - 0.0542$
Buprenorphine	0.9805	$y = 0.1530x - 0.1409$
Benzocaine	0.9513	$y = 0.3137x + 0.6282$
Hydroxyzine	0.9654	$y = 0.2496x - 0.4556$
Mitragynine	0.9758	$y = 0.1562x - 0.2816$
PB-22	0.9885	$y = 0.4111x - 0.6132$

2.2.1.7. *Library Creation Observations*

Compounds may fragment via complex pathways in a mass spectrometer resulting in multiple ions. Comparing each ion with that of a reference standard can be time-consuming and can be a subjective process. Although subjectivity is not eliminated, mass spectral libraries provide a comparison result using algorithms based on statistics. The operator is then responsible for concurring the results based on the ions present and their relative abundances. Several factors may influence a match score, including unknown differences in thresholds and type of statistical method used in various proprietary algorithms, the quality of the mass spectrum in a library, and the quality of the unknown mass spectrum.

At higher concentrations, higher match scores were observed. One reason for this observation is the loss of ions at lower concentrations. No score was observed for SKF 525A (proadifen) in the SWGDRUG library, as well as for buprenorphine at the limit of detection. At the LOD, higher match scores were observed from the in-house library, as shown in Table 2, because the library contained spectra at low and high concentrations. Match scores were >80% for the in-house library and >75% for the SWGDRUG library at 50 ppm, with the in-house library producing higher overall scores. Figure 3 shows the layout of Mass Hunter used for searching against the in-house library. Overall, this study highlights the importance of also creating an in-house library, when possible, for comparing unknown compounds.

Table 5. Match scores from the newly created in-house library compared to SWGDRUG library scores at the compounds LOD and 50 ppm. The signal to noise ratio (SNR) at the LOD is also reported for each compound.

Compound	LOD (ppm)	SNR _{LOD}	Match Score from In-House Library at LOD (%)	Match Score from SWGDRUG Library at LOD (%)	Match Score from In-House Library at 50 ppm (%)	Match Score from SWGDRUG Library at 50 ppm (%)
4MEC (4-Methylcathinone)	1.563	33.4	92.0	75.5	98.7	85.1
4MMC (mephedrone, 4-methylmethcathinone)	1.563	32.6	91.7	81.8	98.4	91.8
Alprazolam	3.125	8.7	63.2	51.2	91.0	90.0
Buprenorphine	12.500	24.6	71.8	NF	88.0	75.6
Cocaine	1.563	34.8	90.0	83.0	98.7	96.0
Codeine	3.125	15.0	73.7	69.3	99.1	96.2
Fentanyl	3.125	16.6	69.0	57.8	96.8	88.7
Heroin	3.125	12.2	62.3	53.3	98.9	95.2
Methamphetamine	1.563	41.4	92.6	81.9	98.6	92.3
Mitragynine	6.250	32.5	70.8	50.6	88.8	85.3
Morphine	3.125	9.6	66.7	53.5	98.4	93.9
Naltrexone	25.000	47.7	55.2	54.4	82.7	78.5
PB-22	6.250	32.1	68.3	50.5	86.0	80.5
Sufentanil	6.250	181.3	84.8	74.6	97.5	89.6
THC	1.563	30.7	78.6	60.0	99.1	97.1
Phenacetin	1.563	22.7	90.1	86.7	98.4	97.3
Paracetamol/ acetaminophen	12.500	19.0	94.7	90.6	99.5	91.5
Levamisole	1.563	18.0	84.6	73.9	98.9	96.2
Lidocaine	1.563	34.8	83.2	78.1	91.9	93.6
Procaine	1.563	27.2	94.6	85.4	93.3	93.9
Benzocaine	1.563	70.5	94.8	95.1	99.1	98.4
Diltiazem	6.250	104.6	70.4	64.5	88.8	85.1
Hydroxyzine	6.250	66.2	64.0	77.9	91.6	89.8
Caffeine	1.563	54.8	94.4	90.3	99.3	96.2
Proadifen	1.563	32.1	87.6	NF	95.3	NF

NF- compound not found in library

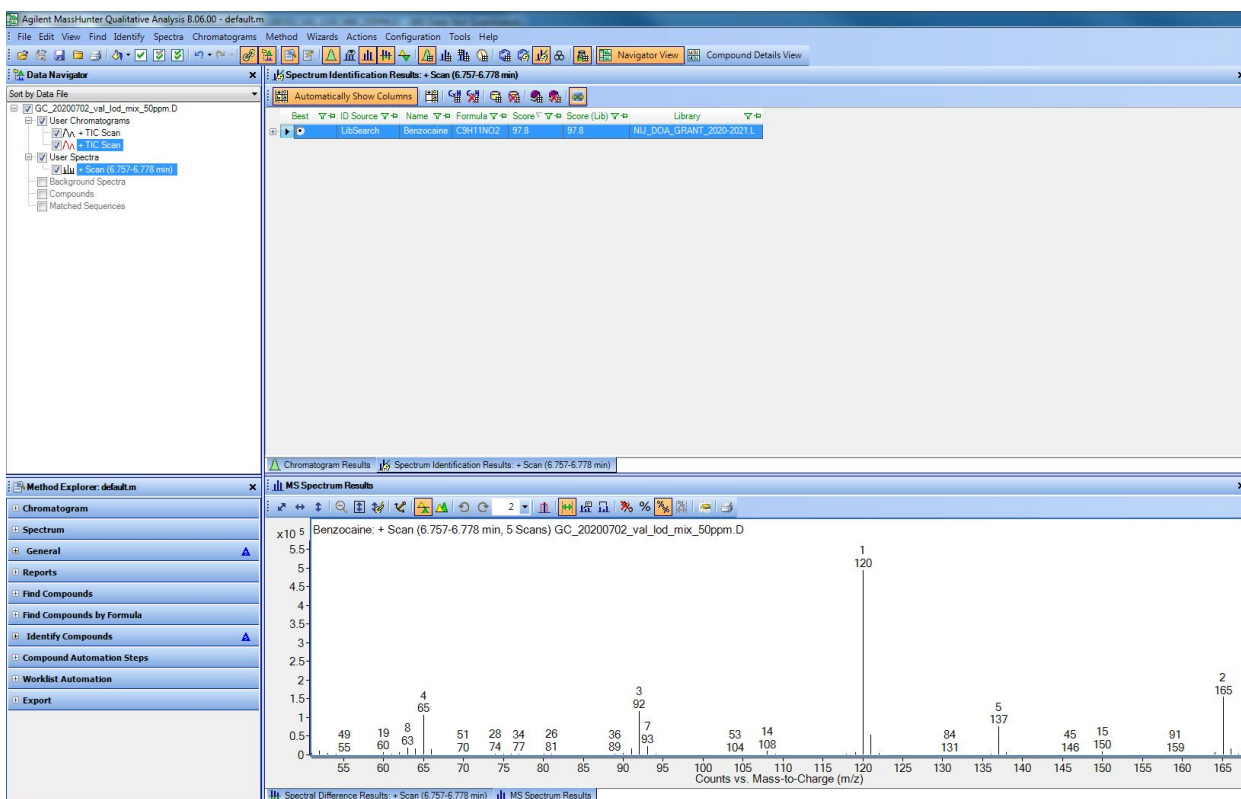


Figure 3. This figure shows an example of the match score—97.8, of benzocaine when searched in the in-house library.

2.2.1.8. Retention Indices Study

Retention time is one factor used to determine the probable identity of a compound when utilizing a chromatographic technique. However, the retention time of a compound is dependent on the method parameters, including the type of column and the temperature program. The retention time of a compound can vary between runs unexpectedly or if there has been a change in the instrument, such as a decrease in column length after maintenance. Such variation may make transferring methods between instruments a challenge and result in data analysis being time-consuming. Retention time locking and the use of retention indices (RI) have been used to circumvent this issue. Retention time locking (RTL) allows for retention times to be reproduced between gas chromatograph systems when the same nominal column is used. RTL methods must be maintained by relocking whenever the column has been cut or replaced, a method is transferred to another instrument, or there has been a change in the system that can influence the retention time of compounds. In a similar way, RI allows for the standardization of retention times to an n-alkanes ladder analyzed in each run.

The National Institute of Standards and Technology currently has a library of over 99,000 compounds with RI data with different column stationary phases (<https://chemdata.nist.gov/dokuwiki/doku.php?id=chemdata:ridatabase>). The creation of databases and a standardized method to compare unknown compounds make each a valuable tool. The retention indices (RI) of the compounds used in this study can be found in **Table 6**. No RI data was calculated for diltiazem, alprazolam, Mitragynine, PB22, and buprenorphine as these compounds eluted later than the longest n-alkane—one disadvantage of the RI method. As anticipated, the early eluting compounds had a lower RI than the later eluting ones. Methamphetamine eluted the earliest

with a RI value of 1356, whereas hydroxyzine had the highest RI value, 3035. **Figure 4** shows the chromatogram and the order of elution of the compounds. For compounds with RI values reported in the literature where a DB-5 column was used, the values were comparable to the findings reported in **Table 6**, although the column conditions may not have been identical. The primary source for the RI values was the NIST Chemistry Webbook (www.webbook.nist.gov). Although the NIST Chemistry Webbook contains RI data on most of the compounds in **Table 6**, only RI data from a similar column was selected for comparison. When the precision of the RI values was assessed by ANOVA, only methamphetamine showed high within day (27.2% CV) and between-run (70.7% CV) variability. The variability for other compounds was less than 0%. One possible reason for the high variability observed from methamphetamine (HCl salt form) is due to the split peaks, which may have influenced how the peak was auto-integrated.

Table 6. Average retention times and retention indices.

Compound	Retention Time (mins)		Retention Index	Retention Index from Literature
	Avg \pm SD	CV(%)	Avg \pm SD	
Methamphetamine	4.577 \pm 0.014	0.30	1356.0 \pm 1.99	1188 (30 m x 0.25 mm x 0.25 μ m) [3]
4-Methylmethcathinone	6.048 \pm 0.004	0.07	1572.4 \pm 0.61	NA
4-Methylethcathinone	6.374 \pm 0.002	0.02	1622.3 \pm 0.17	1535.1 (30 m x 0.25 mm x 0.25 μ m) [4]
Benzocaine	6.761 \pm 0.002	0.02	1681.7 \pm 0.16	NA
Acetaminophen	7.528 \pm 0.003	0.04	1786.5 \pm 0.19	1694.0 (12 m x 0.2 mm x 0.33 μ m) [5]
Phenacetin	7.642 \pm 0.002	0.03	1801.6 \pm 0.19	NA
Caffeine	8.790 \pm 0.002	0.02	1949.5 \pm 0.17	1842 (30 m x 0.25 mm x 0.25 μ m) [6]
Lidocaine	9.126 \pm 0.002	0.02	1993.7 \pm 0.17	1924 (25 m x 0.22 mm x 0.33 μ m) [7]
Levamisole	9.965 \pm 0.002	0.02	2110.1 \pm 0.21	NA
Procaine	10.307 \pm 0.002	0.02	2160.0 \pm 0.19	NA
Cocaine	11.483 \pm 0.002	0.01	2341.7 \pm 0.16	NA
SKF 525A	12.124 \pm 0.001	0.01	2448.6 \pm 0.16	NA
Codeine	12.670 \pm 0.002	0.01	2544.3 \pm 0.18	NA
Morphine	12.970 \pm 0.002	0.01	2598.4 \pm 0.16	NA
Δ^9 -THC	13.119 \pm 0.002	0.01	2626.1 \pm 0.15	NA
Heroin	14.016 \pm 0.002	0.01	2786.0 \pm 0.21	NA
Fentanyl	14.642 \pm 0.002	0.01	2880.5 \pm 0.20	NA
Sufentanil	15.197 \pm 0.002	0.02	2952.6 \pm 0.26	NA
Naltrexone	15.797 \pm 0.005	0.03	3022.4 \pm 0.27	NA

Hydroxyzine	15.919 ± 0.003	0.02	3035.0 ± 0.19	2838 (15 m x 0.25 mm x 0.2 µm) [8]
Diltiazem	16.657 ± 0.003	0.02	--	NA
Alprazolam	16.730 ± 0.004	0.02	--	2936 (15 m x 0.25 mm x 0.25 µm) [9]
Mitragynine	22.445 ± 0.010	0.05	--	NA
PB22	22.949 ± 0.259	1.13	--	NA
Buprenorphine	24.398 ± 0.011	0.04	--	NA

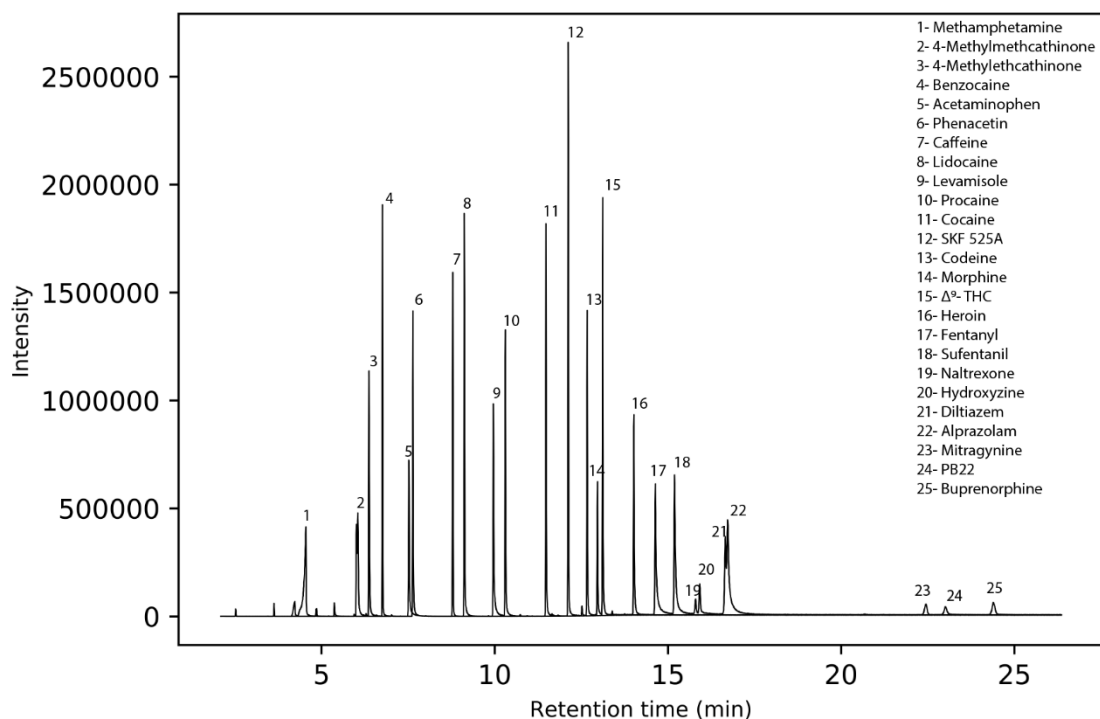


Figure 4. Full scan TIC Chromatogram of analyzed target compounds.

2.2.1.9. Chromatograms and mass spectra from GC/MS

All target drugs and cutting agents suitable for analysis on GC-MS were analyzed. The following **figures 5 and 6** show the TIC chromatograms and mass spectra for some of the target compounds (caffeine and cocaine). The rest of the spectra is compounded into the GC/MS in-house database created as a *.L library using the Agilent Chem Station Software. Additionally, a compilation of all GC/MS spectral information is provided as a separate monograph for easy access for practitioners (See Appendix A).

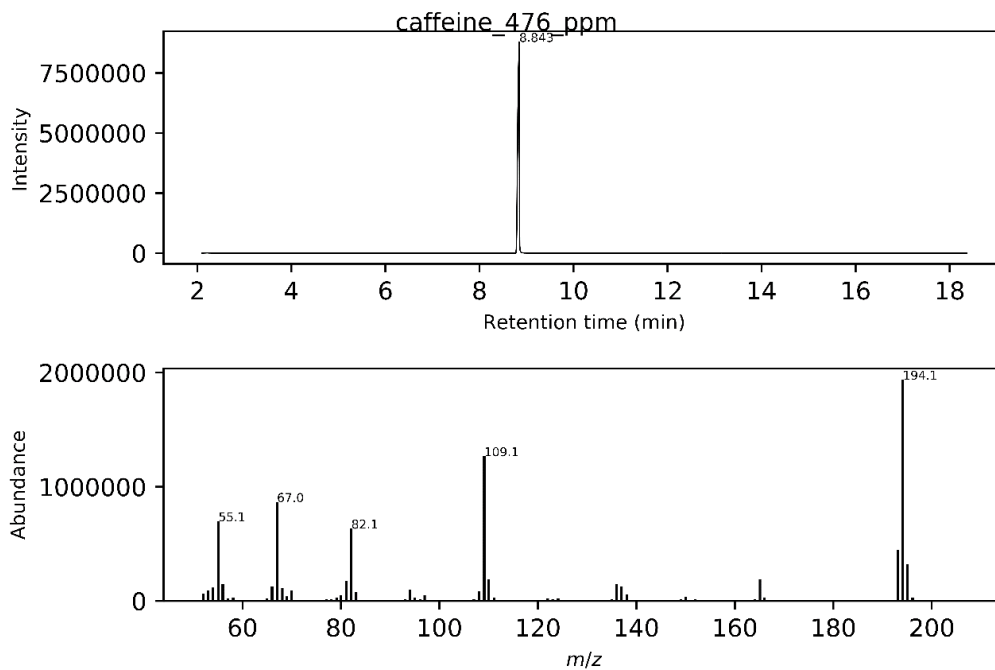


Figure 5: Caffeine GC/MS chromatogram and EI-mass spectra showing main fragmentation of the molecule.

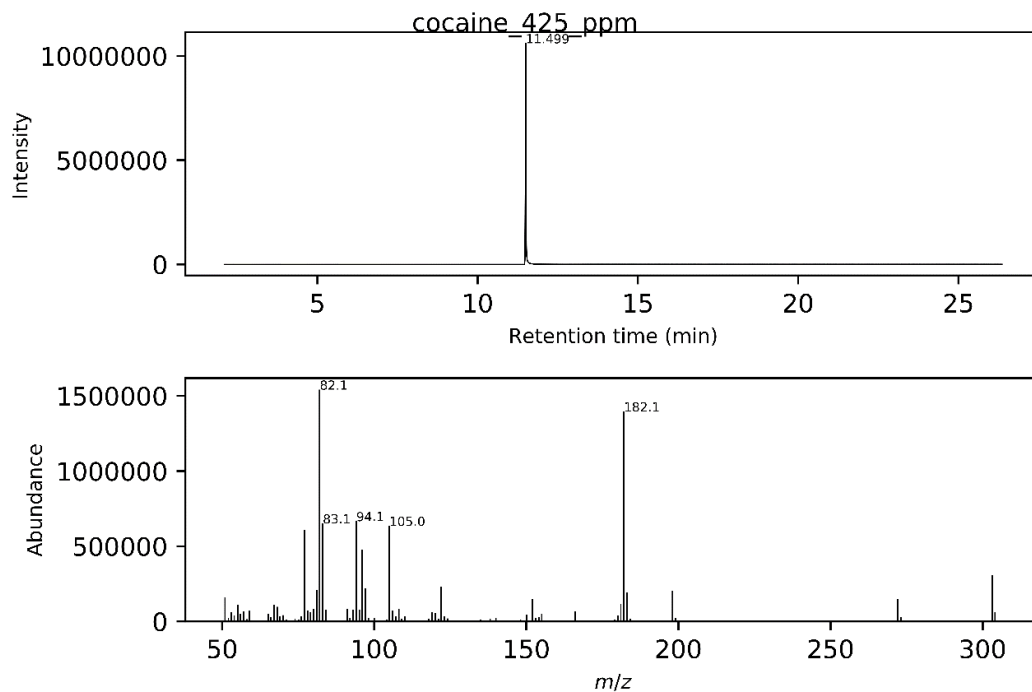


Figure 6: Cocaine GC/MS TIC chromatogram and EI-mass spectra showing main fragmentation of the molecule.

2.3. Confirmatory LC-MS/MS Analysis of Target Analytes

2.3.1.1. Purpose of LC-MS/MS Method

To serve as ground truth to the screening techniques under investigation (electrochemistry, Raman spectroscopy, and Spectro electrochemistry), a confirmatory method employing liquid chromatography-tandem mass spectrometry (LC-MS/MS) is needed. Forensic applications require confirmation of the results of other tests and techniques. This LC-MS/MS method will serve as the confirmatory method, providing the ground-truth results by which to compare the screening data. To ensure fit-for-purpose, the method will be optimized and validated according to SWGDRUG guidelines for the panel of target drug analytes and diluents.

2.3.1.2. Materials and Methods

Reagents

Methanol (Optima[®]), formic acid (Optima[®]), and ammonium formate were purchased from Fisher Scientific (Fair Lawn, NJ). 4-methylethcathinone (4-MEC), 4-methylmethcathinone (4-MMC, mephedrone), alprazolam, buprenorphine HCl, cocaine HCl, codeine, fentanyl, heroin, methamphetamine HCl, mitragynine, morphine, naltrexone HCl, PB-22, sufentanil, THC were purchased from Cayman Chemical (Ann Arbor, MI). Phenacetin was obtained from TCI Chemicals (Portland, OR). Acetaminophen, lidocaine HCl monohydrate and benzocaine were purchased from Sigma-Aldrich (St. Louis, MO). Levamisole HCl, procaine HCl, and diltiazem HCl were purchased from Acros Organics (Geel, Belgium). Hydroxyzine HCl was obtained from Spectrum Chemical MFG (New Brunswick, NJ), and caffeine was obtained from Baker (Radnor, PA). Table 1 provides the analyte panel of interest for this work. A Millipore Direct-Q[®] UV water purification system (Billerica, MA) was used to obtain purified, 18.2 MΩ water.

Instrumentation

Chromatographic separation and mass spectral analysis was achieved using an Agilent 1290 Infinity II Liquid Chromatograph system coupled to an Agilent 6470 Triple Quadrupole Mass Spectrometer (Santa Clara, CA). Optimization of transitions was performed using Agilent Optimizer software. Analysis of samples was completed using Mass Hunter Qualitative and Quantitative software version B.08.00.

Methods

Optimization of transitions was completed on the instrument using ~1 µg/mL solutions of each target analyte individually and injected using a zero-dead volume valve directly into the mass spectrometer. Transitions were selected based on relative abundance, fragment m/z , and collision energy. Chromatographic separation was achieved using an Agilent RR-HD Zorbax Eclipse Plus C18 column (3.0 x 100 mm, 1.8 microns). The column temperature was maintained at room temperature. Gradient elution using an organic phase of methanol with 0.1% formic acid (mobile phase B) and an aqueous phase of 0.1% formic acid and 5 mM ammonium formate in water (mobile phase A) was performed. Several different gradients were tested. Table 8 provides the initial gradient elution and instrument parameters used. **Table 9** provides the chosen transitions for the method along with the retention

times obtained from the optimal chromatographic separation, as well as the chosen internal standard for each analyte.

Table 8: Gradient elution and instrument parameters

Column Type	Agilent RR-HD Zorbax Eclipse Plus C18 column (3.0 x 100 mm, 1.8 micron)		
Column Temperature	25°C		
Injection volume	1.00 µL		
Flow rate	0.300 mL/min		
Gradient elution	Time (min)	Mobile Phase	
		A (%)	B (%)
	0.00	95.00	5.00
	1.00	80.00	20.00
	8.00	10.00	90.00
	9.00	0.00	100.00
12.00	0.00	100.00	
Mass spectrometry			
Ionization Mode	ESI + Agilent Jet Stream, Positive Mode		
Gas temperature	325°C		
Gas flow	9 (L/min)		
Nebulizer	30 psi		
Sheath gas temperature	350°C		
Sheath gas flow	10 (L/min)		
Capillary voltage	3500 V		
Collision gas	Nitrogen		

Table 9: Optimized transitions for the panel of target analytes via LC-MS/MS

Analyte	Retention Time (min)	Transition (m/z)	Fragmentor (V)	CE (V)	Internal Standard
Hydroxyzine	8.545	374 → 201	140	20	Methamphetamine-D5
		374 → 165		76	
Acetaminophen	4.371	151 → 93	86	24	Methamphetamine-D5
		151 → 65		36	
Caffeine	5.529	194 → 42	124	48	Diazepam-D5
		194 → 53		84	
Benzocaine	7.543	165 → 65	86	44	Methamphetamine-D5
		165 → 77		32	
THC	11.593	314 → 123	124	36	THC-D3

		314 → 41		80	
Naltrexone	4.489	341 → 324	124	24	Morphine-D3
		341 → 55		44	
Morphine	3.276	285 → 152	140	72	Morphine-D3
		285 → 51		84	
Heroin	5.926	369 → 165	156	64	6-MAM-D3
		369 → 58		32	
Codeine	4.234	299 → 152	140	84	Codeine-D3
		299 → 115		88	
Buprenorphine	7.730	467 → 55	180	56	Buprenorphine-D4
		467 → 414		40	
Alprazolam	8.882	308 → 281	164	28	Diazepam-D5
		308 → 205		48	
Diltiazem	7.915	414 → 178	124	28	Codeine-D3
		414 → 109		80	
Procaine	3.996	236 → 120	86	28	Cocaine-D3
		236 → 65		68	
Lidocaine	5.731	234 → 86	86	20	Methamphetamine-D5
		234 → 58		44	
Levamisole	4.625	204 → 91	124	44	Methamphetamine-D5
		204 → 51		100	
Sufentanil	7.917	386 → 111	124	44	Carfentanil Oxalate-D5
		386 → 77		76	
PB-22	10.649	358 → 214	86	20	THC-D3
		358 → 144		44	
Mitragynine	7.344	398 → 174	162	36	6-MAM-D3
		398 → 130		100	
Methamphetamine	5.331	149 → 91	86	24	Methamphetamine-D5
		149 → 65		48	
Fentanyl	7.220	336 → 105	124	48	Fentanyl-D5

			336 → 188		24	
Cocaine	6.208	303 → 77	124		80	Cocaine-D3
		303 → 51			132	
Mephedrone-4-methylmethcathinone	5.753	177 → 144	86		36	Methamphetamine-D5
		177 → 91			40	
4-methylethcathinone	6.047	191 → 144	86		36	Methamphetamine-D5
		191 → 91			44	
Phenacetin	7.468	179 → 110	124		24	Methamphetamine-D5
		179 → 65			44	

*Transitions in bold are quantitative transitions, and the transitions that are not in bold are qualitative transitions.

2.3.1.3. Chromatographic Separation

Initially, an 18-minute method was created to elute all analytes of interest from the sample injected onto the column. This method started at a ratio of water to methanol 95:5 and changed to 5:95 over the course of 18 minutes. Optimization of this method was performed using a mix of the 24 analytes at $\sim 1 \mu\text{g}/\text{mL}$ concentration from individual stock solutions. After experimentation, it was determined to add a two-minute hold at the end of 18 minutes from 19 to 21 minutes at 100% methanol to elute THC and PB-22 (cannabinoids). **Figure 7** shows the chromatogram and labeled analytes from 1-24 and identified in **Table 10**, including each analyte's retention time, mass, and monoisotopic mass. This method had good separation; however, it took a long time to complete the separation of target analytes, so the time needed to be decreased, and a new method was tested. A $10 \mu\text{g}/\text{mL}$ solution of all 24 analytes was created, and a mix of $250 \text{ ng}/\text{mL}$ working solution of all 24 analytes from the $10 \mu\text{g}/\text{mL}$ solution was created and used to test the new method on the LC-MS/MS shown in **figure 8**.

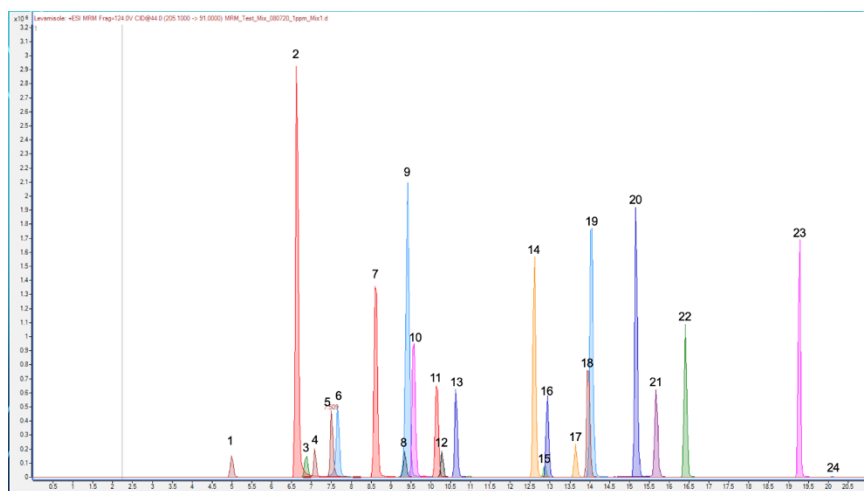


Figure 7. Initial Chromatographic separation of analytes at $\sim 1 \mu\text{g}/\text{mL}$ via LC-MS/MS

Table 10: Target Analytes obtained from chromatogram in figure 7 at $\sim 1 \mu\text{g}/\text{mL}$ with respective retention times and mass

	Compound	Retention Time (min)	Molecular Mass (g/mol)	Monoisotopic Mass (g/mol)
1	Morphine	4.990	285.34	285.14
2	Procaine	6.619	236.31	236.15
3	Acetaminophen	6.881	151.16	151.06
4	Codeine	7.074	299.4	299.15
5	Levamisole	7.499	204.29	204.07
6	Naltrexone	7.650	341.4	341.16
7	Methamphetamine	8.594	149.23	149.12
8	Caffeine	9.336	194.19	194.08
9	Lidocaine	9.416	234.34	234.17
10	Mephedrone-4-methylmethcathinone	9.548	177.24	177.12
11	4-Methylethcathinone	10.131	191.27	191.13
12	Heroin	10.273	369.4	369.16
13	Cocaine	10.619	303.4	303.15
14	Fentanyl	12.617	336.44	336.22
15	Benzocaine	12.888	165.19	165.08
16	Mitragynine	12.939	398.5	398.22
17	Buprenorphine	13.645	467.6	467.30
18	Sufentanil	13.942	386.6	386.20
19	Diltiazem	14.022	414.5	414.16
20	Hydroxyzine	15.154	374.9	374.18
21	Alprazolam	15.667	308.8	308.08
22	SKF525A	16.411	353.51	353.24
23	PB-22	19.288	358.43	358.17
24	THC	20.088	314.5	314.22

The ratio of the gradient elution for water to methanol was calculated for each analyte tested, and a shorter method was created based on the calculated ratios that the analytes preferred. The new method (method 1), shown in **Figure 8**, achieved the goal of being a shorter method without sacrificing chromatography for the separation of analytes. The separation gradient used to chromatographically separate analytes of interest is in **table 11** for this improved method.

Table 11: Elution gradient for improved method

Time	A	B	Flow	Pressure
1	80	20	0.300 mL/min	1000.00 bar
8	10	90		
9	0	100		
11	0	100		

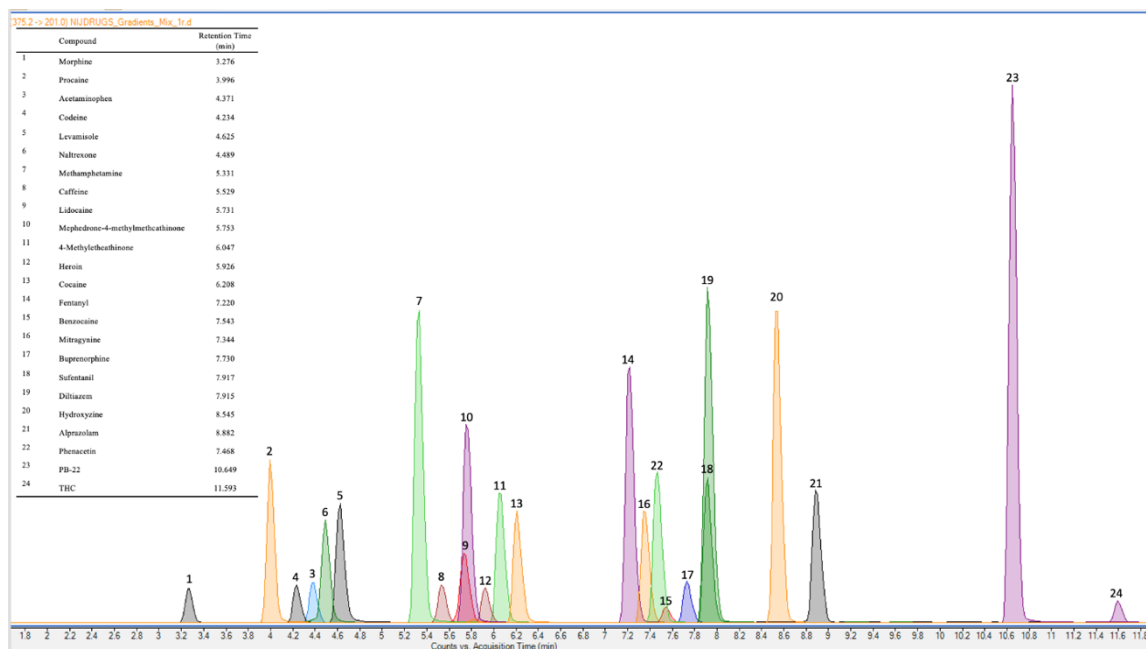


Figure 8. Chromatographic separation of analytes at 250 ng/mL for improved LC method

The optimal method for gradient elution offered better chromatographic separation for each of the analytes of interest. After adjusting the new method, chromatographic separation was achieved through the use of gradient elution, starting at a ratio of water to methanol of 95:5 and moving to a ratio of 80:20 at one minute. Then incrementally increasing the amount of methanol within the elution gradient to a ratio of 10:90 water to methanol at 8 minutes. Finally, increasing to 100% methanol solution from 9 to 12 minutes to elute the more nonpolar analytes of interest, namely THC and PB-22.

2.3.1.4. Limits of detection

The limit of detection for each of the analytes of interest was experimentally determined through a serial dilution at concentrations of 0.01 ng/mL, 0.1 ng/mL, 0.5 ng/mL, and 1 ng/mL. The limit of detection was determined by the analyte signal that is greater than the average signal of the blank matrix plus 3.3 times the standard deviation of the blank matrix signal. The limit of detection was run at six replicates, and the determined limit of detection for each analyte is listed in **table 12**, shown below.

Table 12. Limit of detection for each drug and diluent of interest in LC-MS/MS analysis.

Compound	Limit of Detection (ng/mL)
Morphine	0.1
Procaine	0.1
Codeine	0.1
Acetaminophen	0.5
Naltrexone	0.01
Levamisole	0.1

Methamphetamine	0.5
Caffeine	50
Lidocaine	0.1
Mephedrone (4-methylmethcathinone)	0.01
Heroin	0.1
4-Methylethcathinone	0.01
Cocaine	0.5
Fentanyl	0.5
Mitragynine	0.01
Phenacetin	0.5
Benzocaine	0.5
Buprenorphine	0.1
Diltiazem	0.1
Sufentanil	0.1
Hydroxyzine	0.01
Alprazolam	0.1
PB-22	0.1
THC	1

2.3.1.5. *Bias and precision*

The bias and precision were determined through the analysis of low, medium, and high concentrations of each of the drugs and diluents tested on the LC-MS/MS method. The low concentration was at 1.5 ng/mL for morphine, procaine, codeine, naltrexone, levamisole, methamphetamine, lidocaine, mephedrone-4-methyl methcathinone, heroin, 4-methylethcathinone, cocaine, fentanyl, mitragynine, phenacetin, benzocaine, buprenorphine, diltiazem, sufentanil, hydroxyzine, alprazolam, and PB-22. The low concentration was at 100 ng/mL for acetaminophen, caffeine, and THC. The medium concentration was at 400 ng/mL for morphine, procaine, codeine, naltrexone, levamisole, methamphetamine, lidocaine, mephedrone-4-methyl methcathinone, heroin, 4-methylethcathinone, cocaine, fentanyl, mitragynine, phenacetin, benzocaine, buprenorphine, diltiazem, sufentanil, hydroxyzine, alprazolam, PB-22, acetaminophen, caffeine, and THC. The high concentration was at 800 ng/mL for morphine, procaine, codeine, naltrexone, levamisole, methamphetamine, lidocaine, mephedrone-4-methyl methcathinone, heroin, 4-methylethcathinone, cocaine, fentanyl, mitragynine, phenacetin, benzocaine, buprenorphine, diltiazem, sufentanil, hydroxyzine, alprazolam, PB-22, acetaminophen, caffeine, and THC. The analytes of interest were run on the LC-MS/MS at the low, medium, and high concentrations in batches of 3 samples per concentration per run over the course of 5 runs. For each run, a calibration curve was run to determine the most accurate concentration for each of the analytes at low, medium, and high concentrations for each individual bias and precision run. The bias is calculated from the expected value at either low, medium, or high concentrations subtracted from the grand mean of all the runs (n=15) and divided by the expected value at either a low, medium, or high concentration and multiplied by 100 to get a percentage. A bias of less than 20% passes analytical standards and displays the accuracy of the method for each drug and diluent. The precision of the method is calculated from the grand mean of the sample, divided by the standard deviation of the analyte signal given by each sample during each run (n=15) and then multiplied by 100, thus giving an estimate of how close the measured values are to each other. The table of the bias and precision for each drug and diluent is shown in **table 13**.

Table 13. Bias and between run precision for each drug and diluent.

Compound	Bias (%)			Between Run (%CV)		
	Low	Med	High	Low	Med	High
Morphine	5.8	0.6	-1.0	7.8	4.8	4.7
Procaine	7.2	1.6	1.0	7.1	3.8	2.7
Codeine	5.7	-0.02	2.8	8.6	3.6	3.2
Acetaminophen	15.1	10.1	-3.4	8.4	4.6	4.2
Naltrexone	5.4	-0.5	-0.7	7.0	5.5	4.6
Levamisole	8.3	0.7	2.4	7.9	4.0	3.9
Methamphetamine	4.8	0.1	2.0	7.2	3.5	3.8
Caffeine	3.9	2.2	1.0	4.9	3.4	3.0
Lidocaine	6.6	0.5	1.2	6.5	3.7	3.5
Mephedrone/4methylmethcathinone	5.6	4.2	-0.5	7.4	3.3	3.8
Heroin	11.1	1.8	-1.3	7.0	4.8	4.0
4Methylethcathinone	5.6	-1.1	1.6	5.9	3.4	4.0
Cocaine	6.0	1.2	1.3	6.1	3.7	2.8
Fentanyl	6.4	-0.07	0.4	5.2	3.4	4.5
Mitragynine	2.0	1.2	-1.5	7.5	4.7	4.5
Phenacetin	8.9	1.1	1.3	5.8	3.6	3.9
Benzocaine	6.9	4.6	-0.5	13.6	4.3	3.7
Buprenorphine	5.1	-0.05	-0.9	6.3	3.3	3.9
Diltiazem	4.0	-0.2	2.7	6.1	3.5	3.6
Sufentanil	6.0	5.3	-1.0	8.8	5.4	4.2
Hydroxyzine	6.9	-0.6	2.3	5.6	3.6	4.2
Alprazolam	7.8	5.4	0.2	6.7	3.3	3.6
PB-22	14.7	0.8	-2.3	6.8	5.0	5.8
THC	2.2	0.2	0.7	4.8	4.6	4.2

2.3.1.6. Interference

An interference mix was created at a high concentration to determine the method's selectivity of analyzing analytes of interest and contained analytes that would be potentially run on the LC-MS/MS instrumentation to determine if any compounds were detected at interfering retention times. There were no interfering analytes found in the mix run on the same method and parameters as the standard mix run.

2.3.1.7. Calibration Curves

A calibration curve, or linear range, was created to determine the instrument's response to a compound at specific concentrations in known increasing incremental amounts. This will be utilized later to verify concentrations of analytes in a mixture, establish a ground-truth concentration and evaluate performance measures. The calibration curve was created from a stock mixed solution at 10 µg/mL of all 24 analytes. From this stock solution, the calibration curve was created at concentrations of 0.5, 1, 10, 50, 100, 250, 500, 750, and 1000 ng/mL. This is a wide linear range to consider the fact that most samples will be assessed in powdered forms first during the screening methods, meaning that

dilution of samples will most likely be needed before LC-MS/MS analysis. Then, the calibration curve was run on the LC-MS/MS with quality control samples at a low concentration of 10 ng/mL and a high concentration of 500 ng/mL. All concentrations of the calibration curve, quality controls, and negative had internal standards added to the samples as a quality measure and to allow for quantitation. The internal standard was a mix containing the analytes amphetamine's-D5, methamphetamine's-D5, buprenorphine's-D4, carfentanil oxalate's-D5, fentanyl's-D5, 6-MAM's-D3, THC's-D3, cocaine's-D3, codeine's-D3, diazepam's-D5, and morphine's-D3 in methanol. The 9-point calibration curve for morphine, procaine, codeine, naltrexone, lidocaine, mephedrone, heroin, 4-methyl methcathinone, cocaine, fentanyl, mitragynine, phenacetin, benzocaine, buprenorphine, diltiazem, sufentanil, hydroxyzine, and alprazolam are at concentrations 0.5, 1, 10, 50, 100, 250, 500, 750, and 1000 ng/mL and demonstrated good linearity for these analytes generally above 0.995, assessed as the R^2 value utilizing a linear regression model with a weighting of $1/x$. The calibration curve for acetaminophen is at concentrations 100, 250, 500, 750, and 1000 ng/mL because lower calibrators failed to be detected accurately. The calibration curve for levamisole, methamphetamine, PB-22, and THC are at concentrations 1, 10, 50, 100, 250, 500, 750, and 1000 ng/mL. The calibration curve for caffeine is at concentrations 50, 100, 250, 500, 750, and 1000 ng/mL, and this is due to the calibrators need to be at higher levels than the blank to indicate a true positive signal for the analyte of interest and at 50 ng/mL the analyte is giving off a higher signal than the blank sample.

In summary, optimization was achieved for all 24 analytes of interest at $\mu\text{g/mL}$ concentrations for each analyte for selection of optimal quantitative and qualitative ion selection. A long 18-minute gradient elution method was employed from a ratio of water to methanol 95:5 at one minute to 5:95 at the end of 18 minutes to determine ideal elution ratios for each analyte of interest. From the calculation of ratio conditions preferable to each analyte, an additional new method was created and tested to decrease the run time on the instrument. Method 1 was chosen as the optimal method for use since it had a shorter run time as well as it did not sacrifice the chromatographic separation of the analytes. Calibration curves were created at specific concentrations relative to each analyte of interest spanning at least five calibration points for each of the 24 analytes of interest. Bias and precision were completed for all 24 drugs and diluents over the course of 5 runs encompassing 15 samples and five calibration curves within the analytical measurement range for each analyte. The bias and precision passed according to SWGDRUG method validation guidelines. The limit of detection was experimentally performed at concentrations of 0.01 ppb, 0.1 ppb, 0.5 ppb, and 1 ppb, and then statistically analyzed to determine an accurate limit of detection for each of the drugs and diluents analyzed. The interference mix was run to determine the selectivity of the method for the drugs and diluents under investigation, and found no potential interferences. The LC/MS analytical method is fit for use based on the performance to detect and quantify analytical results from the blind samples quantitatively measured against a standard curve.

2.4. Results and Findings for Tasks 1b-d. Generation of Voltammetric Profiles for target drugs and materials.

2.4.1.1. Instrumentation.

Electrochemical techniques were carried out using a variety of electrochemical instruments at our disposal, including a benchtop potentiostat, portable potentiostat, and a combination potentiostat. The benchtop model was a Metrohm AutoLab PGSTAT128N potentiostat running the NOVA software (version 2.1.4) from Metrohm USA, Inc. (Tampa, FL). The portable potentiostat model was a PalmSens 4 running the PSTrace Software (Randhoeve, Netherlands). Finally, the combination potentiostat and the SPELEC Raman system running DropView SPELEC software (version 3.2.2 18LZ04) from Metrohm DropSens (Tampa, FL).

Many electrode types were used throughout this work; however, electrochemical characterization studies were performed predominantly with screen-printed carbon electrodes (SPCEs) obtained from Metrohm DropSens USA (Tampa, FL). These electrodes were purchased in the DRP-110 configuration, having a working and counter electrode made of carbon and a pseudo reference electrode made of silver. The geometric area of the working electrode was 0.126 cm². Additionally, a Mettler Toledo FiveEasy pH meter was used in the preparation of any buffer solutions and electrolytes (Columbus, OH).

2.4.1.2. Electrochemical characterization.

The general workflow for the analysis of drugs using electrochemical and later spectroscopic tools is presented in **figure 9**.

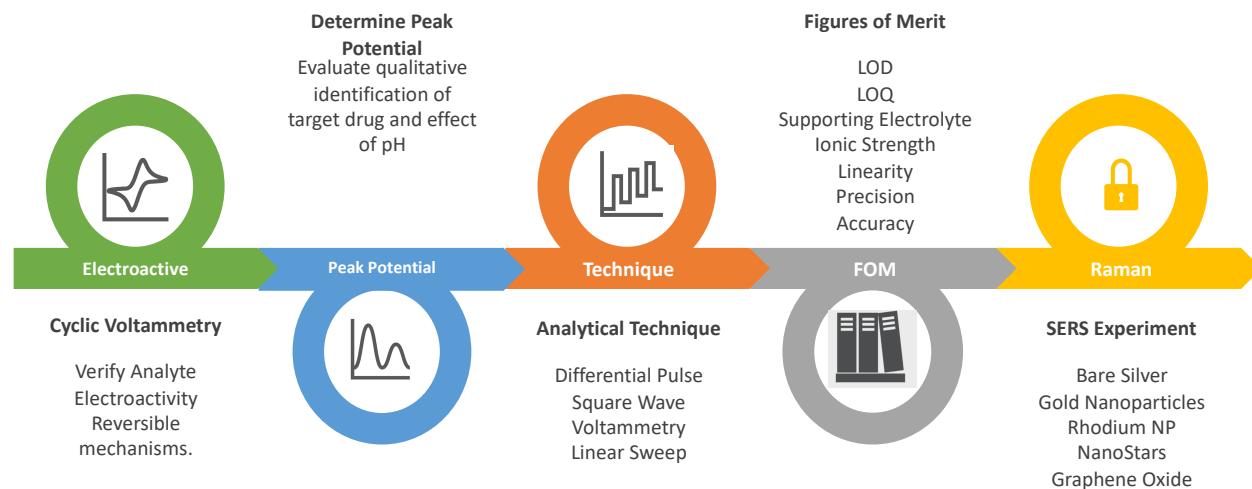


Figure 9: Analytical workflow for drug detection using electrochemical sensors and Raman

Cyclic voltammetry (CV) is initially used to obtain information about the electroactivity of the substance tested. This information could also serve to observe the behavior and later determine the peak potential of the target drug. To this end, different pH conditions and electrolytes are commonly employed to evaluate their effects in the sensing of the species of interest and potential interferences. Due to the versatility of electrochemistry (EC), several analytical techniques could be employed,

including differential pulse, square wave, and linear sweep voltammetry. Once the analytical technique is chosen, different figures of merit are evaluated, including limits of detection, limits of quantitation, linearity, precision, and accuracy. The final stage in the analytical workflow is the development of the Raman experiment. This experiment is conducted stand-alone using the SPELEC Raman Unit or in tandem with the potentiostat unit.

For the electrochemical characterization of samples, cyclic voltammetry was carried out using two different methods:

$$-0.8 \text{ V} \rightarrow 1.3 \text{ V} \rightarrow -0.8 \text{ V}$$

$$0 \text{ V} \rightarrow 1.3 \text{ V} \rightarrow -0.5 \text{ V} \rightarrow 0 \text{ V}$$

While the characterization samples were prepared to known concentrations, this was not the case for the simulated samples. In order to develop a method that could be used quickly, at the crime scene, and easily, a different sampling approach was taken. Therefore, the simulated mixtures were assessed by transferring approximately 1 mg of powder to a microfuge tube containing 0.1 M KCl as a supporting electrolyte. This electrolyte was used for all characterization experiments and testing of the simulated samples.

2.4.1.3. Electrochemical Behavior of Target Analytes

As not all compounds are electroactive, characterization of their electrochemical activity is a necessity. While the electrochemical aspect was not the focus of this work, as that was for Spectro electrochemical analysis, understanding the redox behavior of the analytes of interest was required to understand potentials that could be utilized later with method development. It was also discovered that electrochemistry could serve as an important first step in an orthogonal analytical scheme to identify the analytes present preliminarily. A summary of the characterization experiments can be seen in **Figure 10**, showing a graphical representation of where the potential overlap of analytes may occur, and **Table 14** shows the potentials of interest. This process was carried out and completed for all 30 target analytes in the panel.

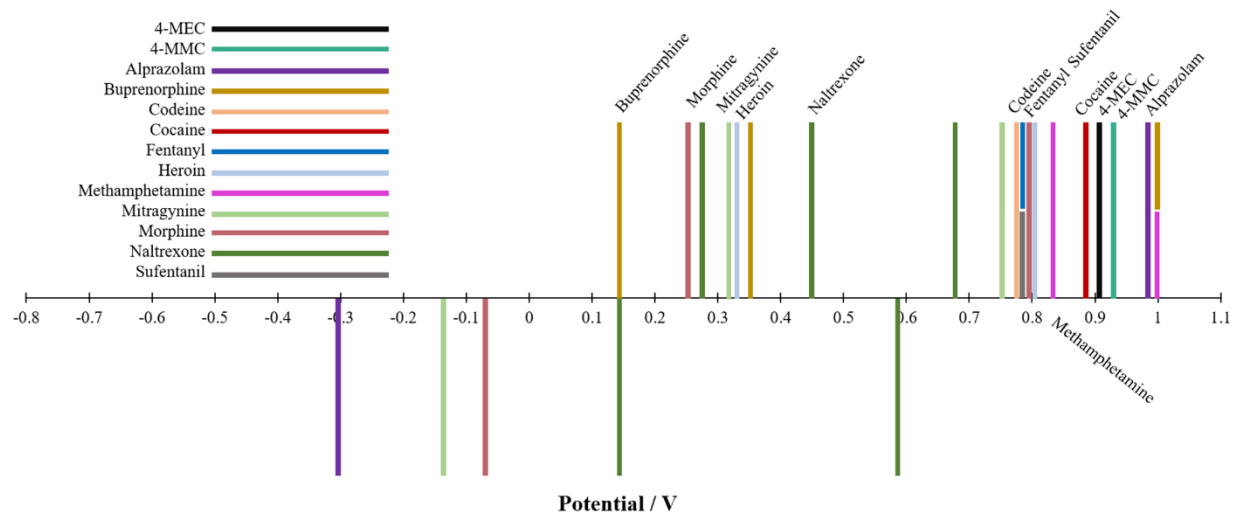


Figure 10. Visual representation of the location of oxidation (top) peaks and reduction (bottom) peaks for the drug analytes to demonstrate the distribution of potentials and the overlap of redox potentials for certain analytes.

Table 14. Oxidation potentials for the analytes of interest.

Drug	Oxidation (V)	Diluent	Oxidation (V)
4-MMC	0.91	Acetaminophen	0.22, 0.50
4-MEC	0.90	Benzocaine	0.62
Alprazolam	0.98	Boric acid	–
Buprenorphine	0.13, 0.34, 0.99	Caffeine	–
Codeine	0.73	Corn starch	–
Cocaine	0.85	Diltiazem	–
Fentanyl	0.74	Hydroxyzine	0.69, 0.98
Heroin	0.30, 0.76	Levamisole	1.03
Methamphetamine	0.84, 1.0	Lidocaine	0.71
Mitragynine	0.30, 0.71	Maltose	–
Morphine	0.25, 0.78	Myo-Inositol	–
Naltrexone	0.27, 0.45, 0.67	Phenacetin	0.60, 0.72
PB-22	–	Phenolphthalein	0.45
Sufentanil	0.74	Procaine	0.66
THC	–	Sorbitol	–

Figure 11 demonstrates several example voltammograms for selected analytes of interest to show the CV characterization and the oxidation and reduction potentials of interest for these analytes. Some of these analytes demonstrate complex electrochemical behavior compared to others (**Figure 12**). Several analytes did not demonstrate any electroactivity under the conditions tested, including THC, PB-22, diltiazem, maltose, Myo-inositol, caffeine, sorbitol, corn starch, and boric acid. It is important to remember that although these analytes did not demonstrate electroactivity on the carbon electrode, that does not mean that other methods, electrodes, or electrolytes cannot be used for their analysis. Our approach was to simplify the electrode platform to serve as a simple measuring device for a good number of target analytes while reducing the overall cost.

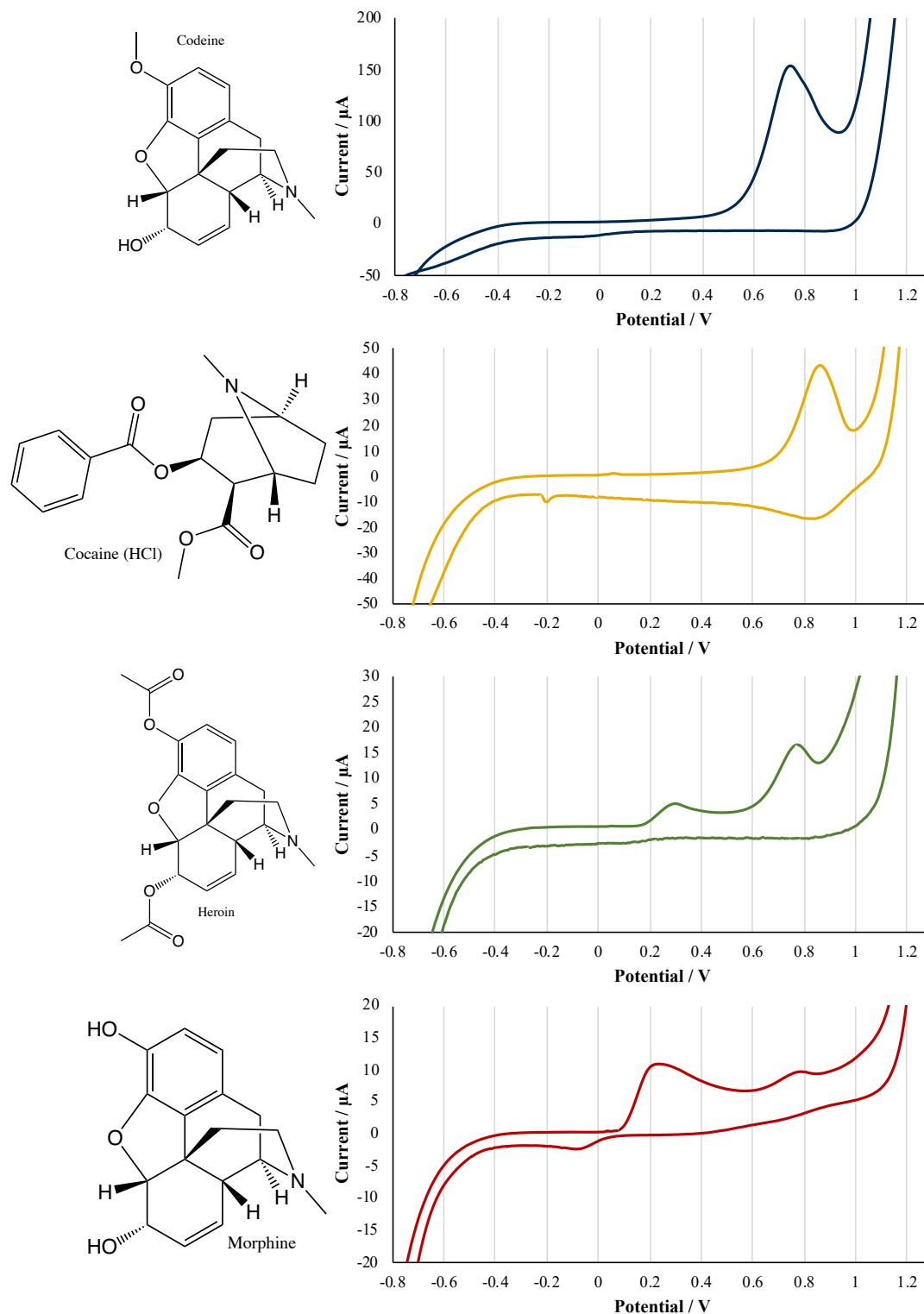


Figure 11. Cyclic voltammograms and the molecular structure for four examples of from the panel of analytes. Cyclic voltammograms were collected for codeine (blue, 2500 ppm), cocaine HCl (yellow, ~1000 ppm), heroin (green, ~300 ppm), and morphine (red, 238 ppm) analyzed with 0.1 M KCl supporting electrolyte.

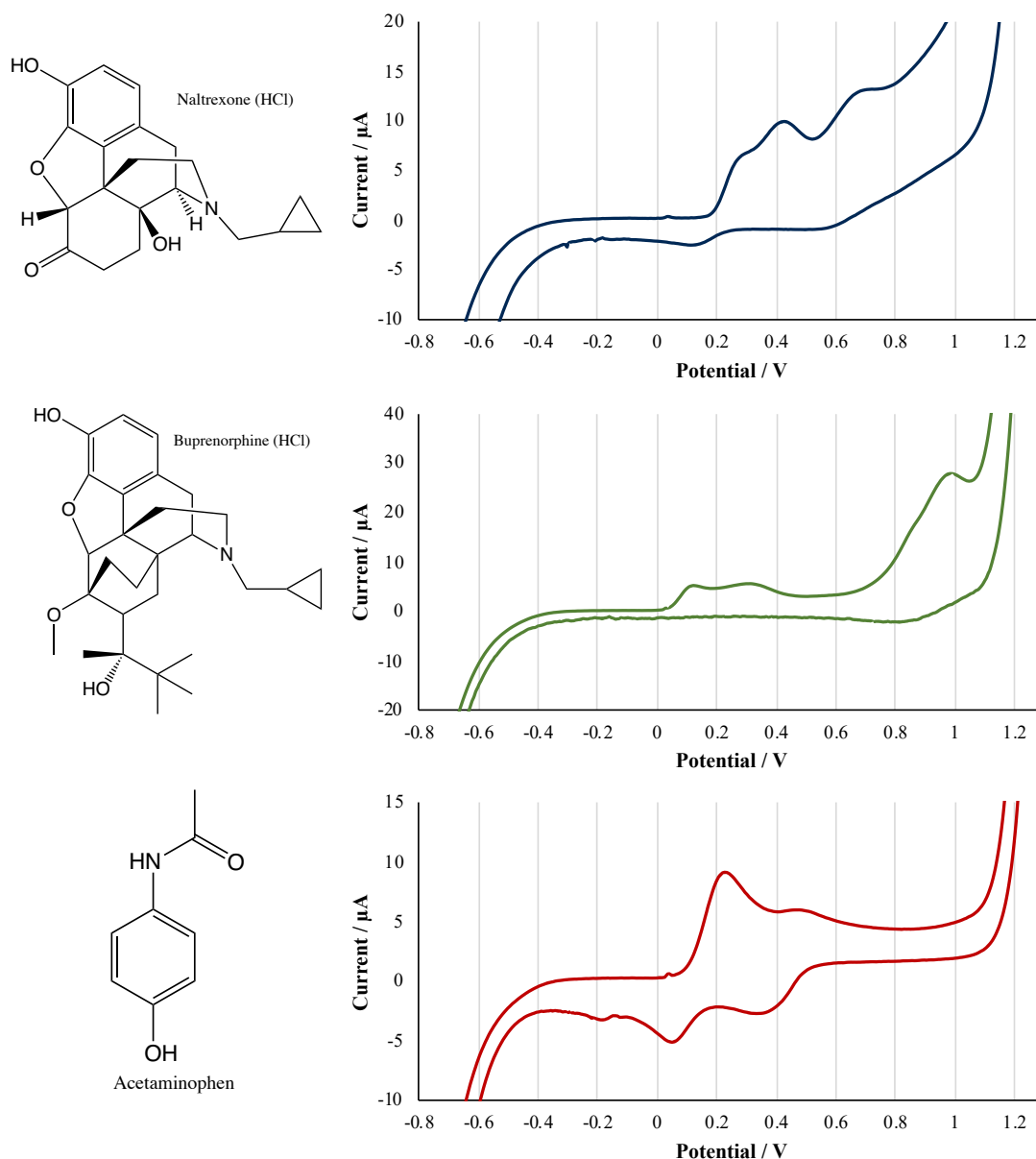


Figure 12. Cyclic voltammograms and the molecular structure for three examples of more complex redox behavior in selected analytes. Cyclic voltammograms were collected for naltrexone (blue, 1000 ppm), buprenorphine (green, 220.5 ppm), and acetaminophen (red, 50 ppm) analyzed with 0.1 M KCl supporting electrolyte.

The two CV procedures tested demonstrated how the starting potential can influence redox behavior. By starting the analysis at -0.8 V, the analyte of interest immediately experiences a reduction potential that could cause a reduction of the analyte, where later oxidation behavior could result either from this product or the original analytes. Therefore, a CV procedure was also tested that started at 0 V. **Figure 13** demonstrates several examples of how the oxidation peak is shifted based on the starting potential.

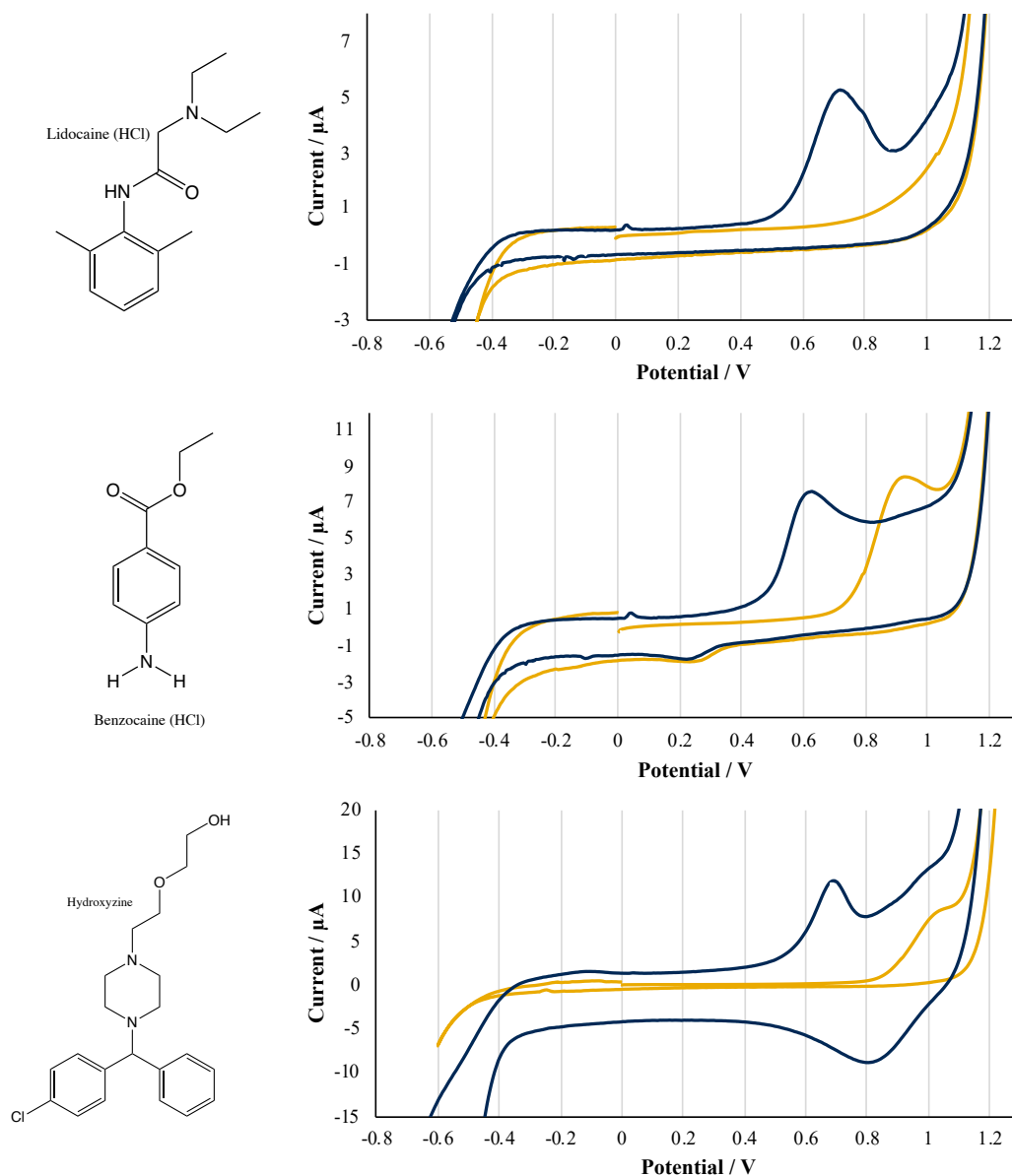


Figure 13. Cyclic voltammograms for three analytes demonstrating the difference in oxidation behavior based on the starting potential of the CV for lidocaine HCl (top), benzocaine HCl (middle), and hydroxyzine (bottom). The blue voltammograms represent CVs starting at -0.8 V and the yellow voltammograms represent CVs starting at 0 V.

Finally, the investigation into using a dibasic sodium phosphate pH 9.5 electrolyte and differential pulse voltammetry was briefly investigated to examine any changes in the oxidation potential of analytes. **Table 15** demonstrates the observed oxidation potentials of those analytes that were tested.

Table 15. Oxidation potentials observed for analysis of selected analytes by differential pulse voltammetry in a supporting electrolyte of dibasic sodium phosphate pH 9.5 solution.

Drug	Oxidation (V)	Diluent	Oxidation (V)
4-MMC	–	Acetaminophen	0.13
4-MEC	–	Benzocaine	0.65
Alprazolam	–	Boric acid	–
Buprenorphine	–	Caffeine	–
Codeine	–	Corn starch	–
Cocaine	–	Diltiazem	–
Fentanyl	–	Hydroxyzine	0.63, 0.75, 0.86
Heroin	0.72	Levamisole	1.03
Methamphetamine	–	Lidocaine	0.7
Mitragynine	–	Maltose	–
Morphine	0.15, 0.70	Myo-Inositol	–
Naltrexone	–	Phenacetin	0.65
PB-22	–	Phenolphthalein	0.50, 0.60
Sufentanil	–	Procaine	0.67
THC	–	Sorbitol	–

Electrochemical oxidation potentials of low concentration analytes in pH 9.5 dibasic sodium phosphate using differential pulse voltammetry

3.1.3. Assessment of Simulated Samples

Prior to the analysis of the mixtures directly, 50 ppm mixtures were prepared in 0.1 M KCl and analyzed to gain an understanding of how sample interactions might affect the observed oxidation and reduction behavior of the analytes. **Figure 14** demonstrates several of these mixtures of interest for cocaine/levamisole, fentanyl/methamphetamine, and heroin/acetaminophen. In the case of the cocaine and levamisole mixture, an overlap of the oxidation peaks of cocaine and levamisole did not allow differentiation of the oxidation peak; however, the reduction peak of levamisole can be observed. A different occurrence is observed in the fentanyl and methamphetamine mixture, where a clear oxidation peak can be seen in the region corresponding to fentanyl. The methamphetamine peak shows up as a small shoulder, demonstrating the difference in sensitivity of the two compounds for the electrochemical method. Lastly, several different oxidation and reduction peaks can be seen in the heroin and acetaminophen voltammogram. Identification of individual peaks is difficult since there is an overlap in the oxidation potentials of the two analytes. However, other peaks could still be identified. Finally, several of the mixtures were tested using by taking a small sample and dissolving it in the electrolyte for testing. Similarly, three of these samples are shown in **Figure 15**. It is important to understand that the electrochemical steps outlined here are meant to provide information regarding the electrochemical behavior of a set of analytes of interest and serve to inform the method development of the Spectro electrochemical methods described later. Additionally, electrochemistry can serve as a screening method that can be applied quickly and easily.

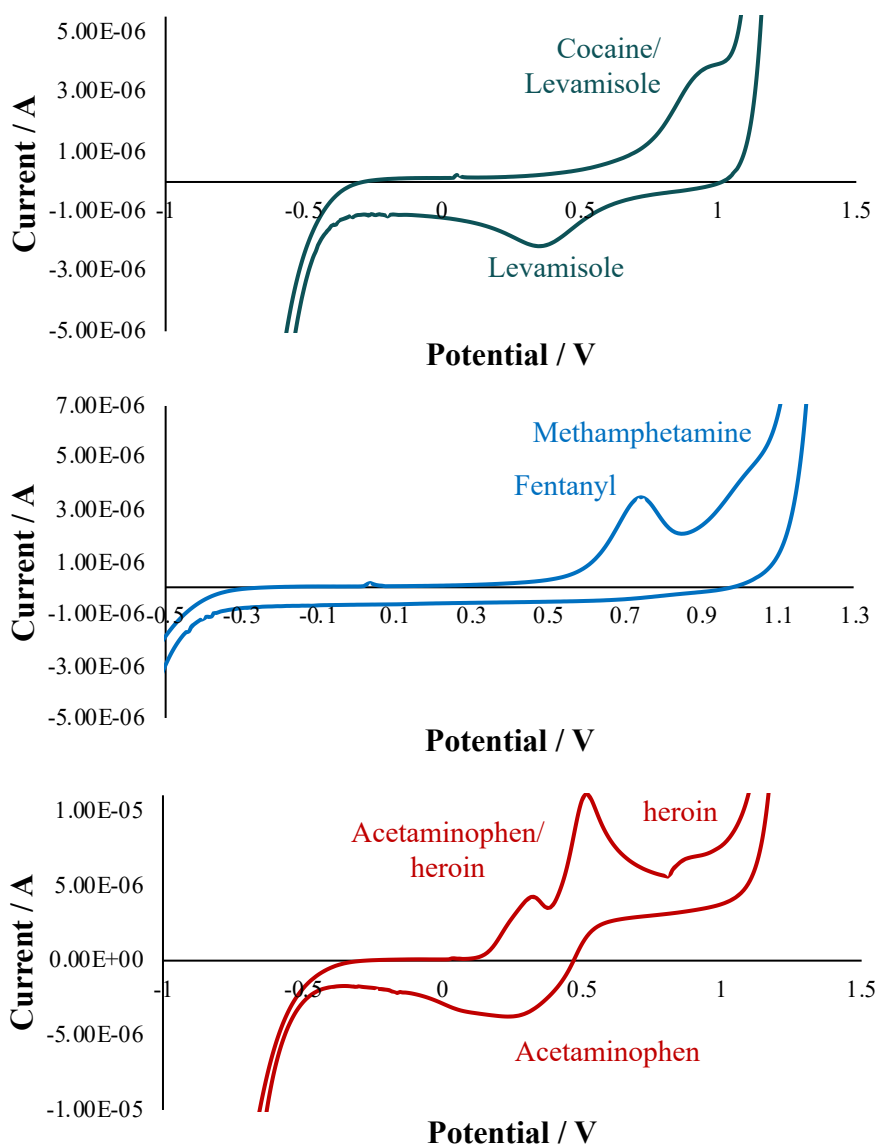


Figure 14. Cyclic voltammograms for 50 ppm mixtures in 0.1 M KCl for cocaine and levamisole (top), fentanyl and methamphetamine (middle), and heroin and acetaminophen (bottom).

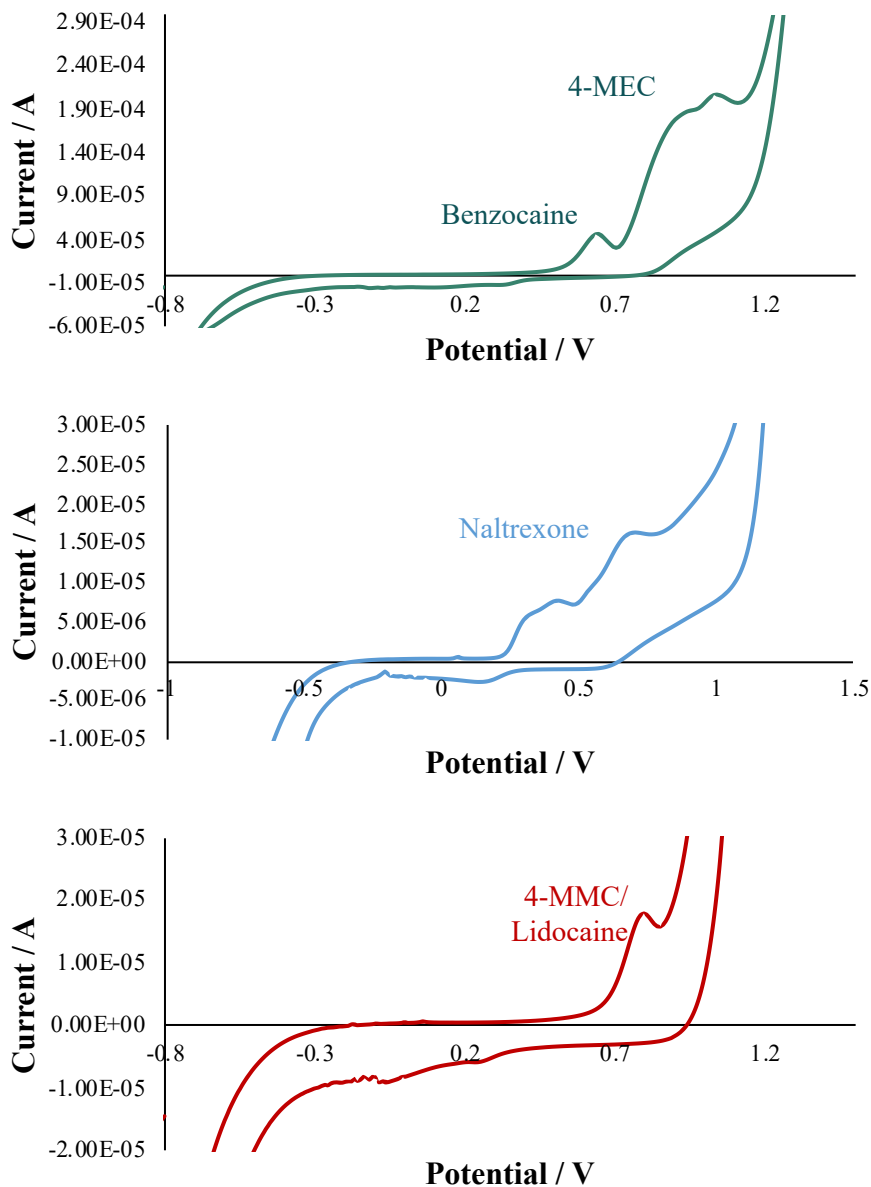


Figure 15. Cyclic voltammograms of simulated mixtures in 0.1 M KCl for a 1:7 mixture of 4-MEC to benzocaine (top), a 1:4 mixture of naltrexone to maltose (middle), and a 1:7 mixture of 4-MMC to lidocaine (bottom).

In summary, electrochemical characterization of the panel of analytes was carried out to understand the electroactivity of the compounds. The majority of the compounds were determined to be electroactive, with several exceptions on screen-printed carbon electrodes with a supporting electrolyte of 0.1 M potassium chloride. The oxidation and reduction potentials were recorded and assessed for analyte overlap and identification. The ability of electrochemistry to serve as a simple and rapid preliminary identification of analytes present in a sample. In addition, these potentials could be studied and used as part of method development in future applications and set the stage for the development of Spectro electrochemical methods that will be described later in this report.

2.5. Results and Findings for Task 2a: Raman Spectra using Tactic ID Instrument. Integration of Raman Data with Mass Spectrometry using DART-MS.

Raman spectra were obtained using a TacticID portable 785 nm laser Raman instrument from B&W Tek (Newark, DE). The unit was operated at either 20 %, 60 %, or 90 % laser power. Spectra were acquired between the range of 176 cm^{-1} and 2900 cm^{-1} with 9 cm^{-1} resolution. Spectra were automatically compared with the stored instrument library, as well as an in-house library created using the same instrument. A more detailed explanation can be found in the following publication. A summary of major findings is described in the following sections. Figures presented in this report are copyright of the respective Journal and have been added here for illustration purposes.

Travon Cooman, Colby Ott, Kourtney Dalzell, Amber Burns, Edward Sisco, Luis E. Arroyo. Screening of Seized Drugs Utilizing Potable Raman Spectroscopy and Direct Analysis in Real Time-Mass Spectrometry (DART-MS). *Forensic Chemistry*. 100352. August 2021 <https://doi.org/10.1016/j.forc.2021.100352>

2.5.1.1. Establishing Bias, Precision, & Reproducibility for the Portable Raman

Establishment of bias, precision, and reproducibility of the portable Raman instrument was performed following ASTM E1683-02,¹¹ ASTM E1840-96,¹² and United Nations Office on Drugs and Crime (UNODC) guidelines¹³ by investigating interference from different types of packaging, variability between analysts, mixture analysis, and verification of libraries within the instrument. For these studies, only a diluent panel was used for testing. Pure diluents were analyzed inside glass vials and 2 mil plastic bags. The point-and-shoot adapter was used for analysis through plastic bags, and no adaptor was used for analysis through glass. Spectra were acquired in triplicate at both 60 % and 90 % laser power. Reproducibility and repeatability were established through triplicate analysis performed by a total of three different operators. Analysis of variance (ANOVA) was used to evaluate within and between operator variability. The instrument's accuracy when analyzing pure drugs and diluents was reported.

2.5.1.2. Assessment of Mixtures

A total of 64 mixtures of target drugs and common diluents were created to simulate street samples and are shown in **Table 16**. Mixtures and ratios were selected based on published literature.¹⁴⁻¹⁹ As an example, a 1:4 ratio was prepared by mixing 10 mg of the target drug with 40 mg of diluent. All mixtures were analyzed via Raman through the plastic bags in triplicate at different areas to account for variability in the sample. The mixture analysis set was used for all mixtures, to allow for the identification of multiple compounds, with the number of hits—high spectrally correlated compounds set to 5 and the ratio threshold set to 15 %. Previous studies have shown that DART-MS is an established technique for drug abuse analysis.²⁰⁻²³ Therefore, a subset of 25 samples of the original 64 mixtures, highlighted in **Table 16**, was selected to demonstrate the applicability of DART-MS for mixture analysis. The accuracy of DART-MS, the TacticID instrument, and the orthogonal combination of both techniques were determined. The combined accuracy was determined when the compounds were correctly reported by either DART-MS or Raman. For example, if the drug was only reported from the DART-MS results and the diluent reported with Raman, a correct identification of both drug and diluent resulted for that particular mixture.

Table 16. Mixtures of drugs and diluents investigated in this study. Ratios with a checkmark were analyzed using the portable Raman system (n = 64). Samples with an asterisk (*) were also analyzed using DART-MS (n = 25).

Mixture	Mass Ratio (Drug : Diluent)			
	1:4	1:7	1:10	1:20
Heroin HCl / acetaminophen	✓*	✓		✓
Fentanyl HCl / caffeine				✓
Fentanyl HCl / methamphetamine HCl	✓			
Cocaine HCl / levamisole	✓*			
Fentanyl HCl / cocaine HCl	✓			
Methamphetamine HCl / levamisole	✓*	✓		
Methamphetamine HCl / caffeine	✓*			
Cocaine HCl / benzocaine	✓*			
Alprazolam / caffeine	✓*	✓*		
Alprazolam / levamisole	✓	✓		
4-MMC HCl / maltose	✓*			✓
4-MMC HCl / lidocaine		✓*	✓	
4-MEC HCl / maltose	✓*	✓		
4-MEC HCl / benzocaine		✓*	✓	
PB-22 / lidocaine	✓			
Sufentanil / caffeine	✓			
Codeine / acetaminophen	✓	✓	✓	✓
Codeine / maltose	✓*	✓*	✓*	✓*
Morphine / maltose	✓*	✓*	✓*	✓
Naltrexone HCl / maltose	✓*	✓*	✓*	✓*
Buprenorphine HCl / starch	✓*	✓*	✓*	✓
Cocaine HCl / caffeine	✓	✓	✓	✓
Cocaine HCl / diltiazem	✓	✓	✓	✓
Cocaine HCl / hydroxyzine	✓		✓	
Cocaine HCl / lidocaine	✓	✓		✓
Cocaine HCl / maltose		✓		✓
Cocaine HCl / procaine	✓	✓	✓	
Cocaine HCl / boric acid			✓	

2.5.1.3. Authentic Samples

Fifteen adjudicated case samples were provided by the Maryland State Police Forensic Sciences Division and analyzed via both the portable Raman system and DART-MS. Samples were assessed in triplicate using both methods and compared against their respective libraries. The Raman laser power was altered based on the color of the test material—20 % or 60 % for colored samples and 90 % power for white powders. Analysis of the authentic samples by DART was performed as described previously in **Table 16**. Samples were prepared following MSP-FSD protocols by dissolving 1 mg to 2 mg of powder in \approx 1 mL of methanol. The averaged mass spectrum was obtained for each sample from the triplicate analyses and used for identification in Mass Mountaineer with a tolerance of \pm 0.005 Da and threshold of 5 %, which was lowered to 1 % for differentiation of isomers. A multi-point drift compensation with tetracaine was used for calibration to serve as a positive control.

2.5.1.4. TacticID Results

The prevalence of portable Raman instruments in seized drug analysis has caused the forensic community to rely on standards and guidelines to address the limitations of these instruments. ASTM E1683-02 outlines guidelines to assess the performance of the Raman spectrometer,²⁴ whereas E1840-96 provides a guide for calibrating the spectrometer.²⁵ NIST also supplies reference materials to correct the relative intensity of the spectrometers.²⁶ Instrument manufacturers also provide reference standards to verify the instrument's performance. For example, Metrohm provides an integrated ASTM-standard polystyrene used for calibration and assessment of the TacticID portable Raman. The United Nations Office on Drugs and Crime (UNODC) guidelines for portable Raman devices were followed in this study by assessing interference from different types of packaging, variability between analysts, mixture analysis, and verification of libraries within the instrument.²⁷

An HQI is a measure of the spectral correlation between the known library spectrum and the unknown test spectrum. Rodriguez *et al.* described HQI by Equation 3.²⁸ The TacticID Raman reports the HQI as a percentage where a value closer to 100% means higher similarity, and a value closer to 0% means poor similarity. Validation of the instrument was performed with diluents only as a cost-saving option. **Figure 16** shows the distribution of the HQI for the diluents at 60% and 90% power for three operators. All HQI values were greater than 90%, although there was higher variation with operator 3. ANOVA results in **Table 17** showed myo inositol with the highest variation in the HQI value—2.0% CV observed between and within operators. The percent CV for all other compounds was less than 2%.

$$HQI = \frac{(Library*Test)^2}{(Library * Library)(Test*Test)} \quad \text{Equation (3)}$$

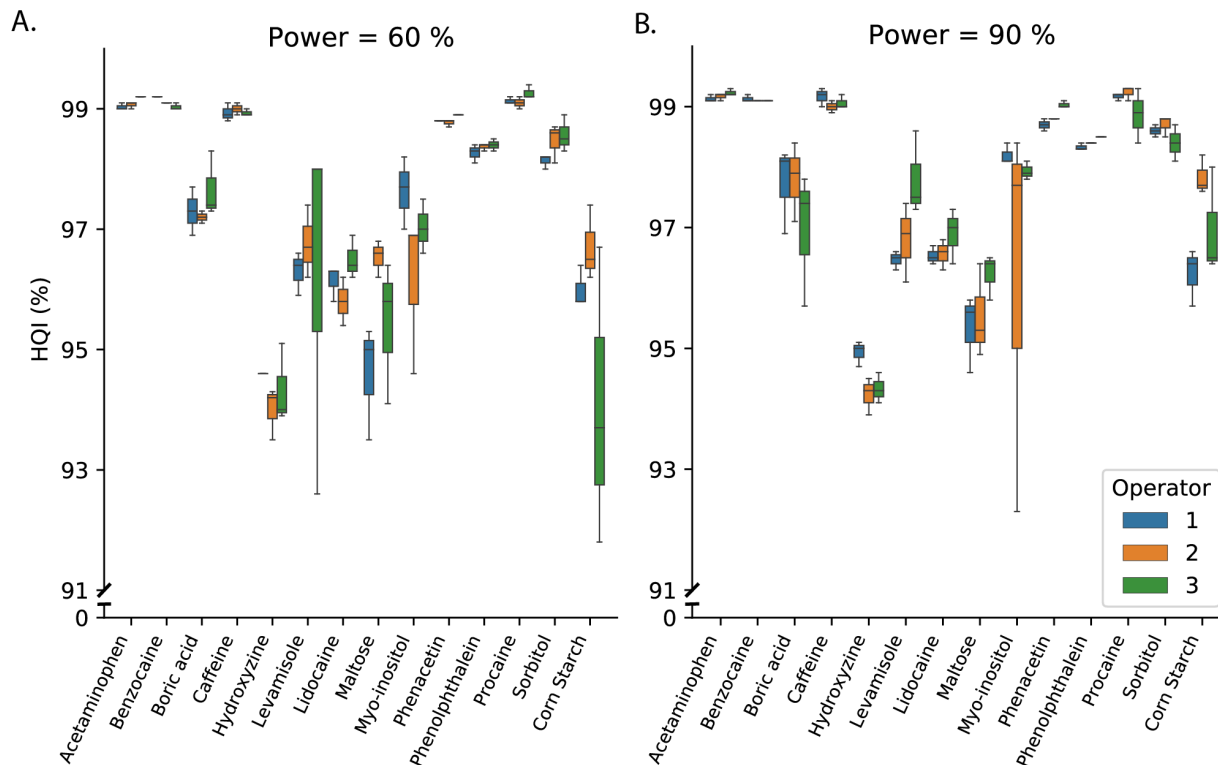


Figure 16. Boxplots showing the distribution of the HQI (%) between three operators when the TacticID was operated at 60% and 90% power. All diluents were powders and analyzed through plastic. Image obtained from reference 9.

Table 17. Precision results within and between operators for diluents.

Compounds	Between Operators CV(%)	Within Operators CV(%)
Acetaminophen	0.1	0.1
Benzocaine	0.0	0.0
Boric acid	0.9	0.9
Caffeine	0.1	0.1
Corn starch	1.0	0.6
D-(+)-Maltose monohydrate	0.7	0.6
Hydroxyzine 2HCl	0.5	0.3
Levamisole	0.9	0.6
Lidocaine HCl monohydrate	0.3	0.3
Myo inositol	2.0	2.0
Phenacetin	0.2	0.1
Phenolphthalein	0.1	0.0
Procaine HCl	0.3	0.3
Sorbitol	0.2	0.2

Figure 17 showed the distribution of HQI when the diluents were measured through glass and plastic at 60% and 90% power. Although all HQI values were greater than 85%, there was higher variation when the packaging material was glass at both laser powers. The laser power selected for the remainder of the study was 90%. A result for corn starch analyzed through the glass was only observed using the mixture setting on the instrument; therefore, it was not included in Figure 17 as a spectral weight, and

no HQI was reported. However, the portable Raman instrument returned all the pure diluents tested as the top hit.

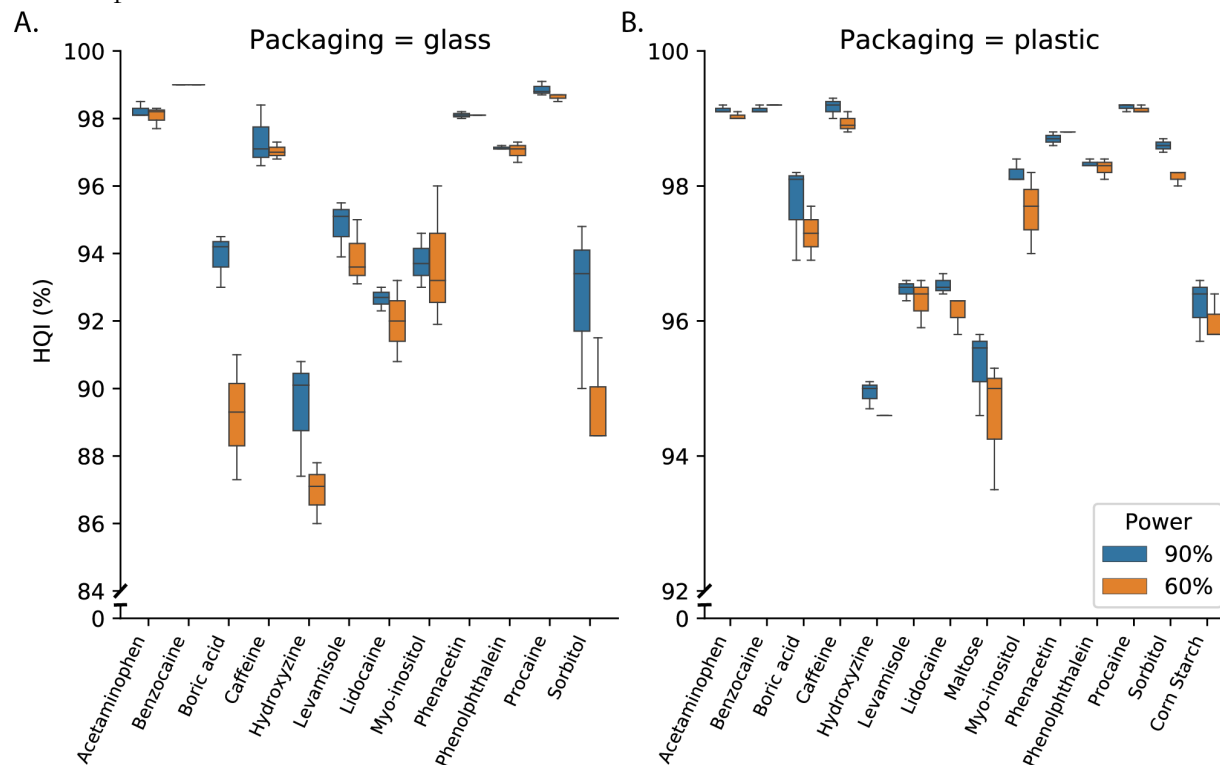


Figure 17. Boxplot comparing the type of packaging through which the diluents were analyzed when the instrument was operated at 60% and 90% power. Diltiazem is not plotted as it was not present in the instrument's library and returned a "no match" result. Corn starch is not shown for glass since the mixture setting was used to get a hit and the mixture setting provides a spectral weight percentage instead of a HQI. Image obtained from reference 9.

2.5.1.5. Performance Measures.

The performance of an instrument in relation to a particular purpose is important to understand its false identification rate. False identifications may result in erroneous incarcerations or fines which can severely impact the livelihood of citizens. The portable Raman's performance, which will be used for field applications or casework, was evaluated for its identification rate when glass or plastic was used as the packaging material. A True positive (TP) results when the instrument correctly predicts the spectrum of the drug when the drug is in the library; a True negative (TN) occurs when the instrument returns a "no match" result when the drug is absent from the library; a False positive (FP) occurs when the instrument erroneously returns a match for a drug, and a False negative (FN) occurs when the instrument returns a "no match" result when the drug is present in the library. Equations 4– 7 were used to calculate the instrument's accuracy, sensitivity, specificity, and precision. When 29 compounds were analyzed through plastic, the accuracy was 89%, TPR- 100%, TNR- 23%, and precision- 88%. When the analysis was performed through glass, the accuracy was 91%, TPR- 100%, TNR- 38%, and precision- 90%.

$$Accuracy = \frac{(TP+TN)}{(TP+FN+FP+TN)} \quad \text{Eq. (4)}$$

$$Sensitivity(TPR) = \frac{TP}{(TP+FN)} \quad \text{Eq. (5)}$$

$$Specificity(TNR) = \frac{TN}{(TN+FP)} \quad \text{Eq. (6)}$$

$$Precision = \frac{TP}{(TP+FP)} \quad \text{Eq. (7)}$$

Although the portable Raman instrument demonstrated high accuracy and TPR, the high false positive rate is one reason it is regarded as a preliminary method. For this reason, we explored the potential of combining the portable Raman technique with DART-MS.

2.5.1.6. Orthogonal Detection

Analytical schemes which leverage orthogonal techniques to provide complementary identification data have demonstrated improved reliability and accuracy, and therefore the data from the portable Raman and DART-MS were combined to compare the performance rates of the orthogonal approach. It is important to note that although Raman spectroscopy and mass spectrometry are considered SWGDRUG category A techniques, these instruments are being assessed as rapid screening techniques. Although the portable Raman initially struggled to identify the drug analyte in dilute mixture ratios, the diluent was correctly identified 100 % of the time in the subset of mixtures used for the orthogonal detection study. In contrast, DART-MS excelled at detecting both drug and diluent compounds; however, many diluents were not identified due to analysis in positive mode. Therefore, the combination of both techniques yielded high accuracy for both drug and diluent compounds in all the analyzed samples, demonstrating the combined strength and enhanced reliability through orthogonal combination. **Table 18** presents the comparison of overall performance rates for the samples assessed orthogonally, first by portable Raman and followed by DART-MS analysis. Specificity does not apply because the instruments always returned a match based on the library search. Performance measures were determined using **Equations 4-7**. Accuracy for both analytes (drug + diluent) was determined by the sum of the samples producing identifications for both the drug and diluent divided by the total number of samples. Lastly, the accuracy of the combination of the two instruments was assessed as the sum of the samples producing the respective identifications by either portable Raman and/or DART-MS divided by the total number of samples (**Table 18**).

Table 18. Comparison of accuracy between Raman, DART-MS, and the orthogonal combination when mixtures were analyzed. The accuracy of the Raman shown below is only for the 25 mixtures that were also analyzed by DART-MS. Specificity is not applicable as there were no True negatives in this study.

	Raman		DART-MS			Combined	
	Drug	Diluent	Both Analytes	Drug	Diluent*	Both Analytes*	Both Analytes
Accuracy	48 %	100 %	56 %	85 %	33 %	26 %	96 %
Sensitivity	56 %	100 %	56 %	92 %	36 %	28 %	96 %
Specificity	NA	NA	NA	NA	NA	NA	NA
Precision	78 %	100 %	100 %	92 %	82 %	78 %	100 %

* Diluents measured by DART-MS were acetaminophen, benzocaine, caffeine, levamisole, lidocaine, maltose, and starch.

2.5.1.7. Authentic Sample Results

To investigate how the orthogonal approach worked for real samples, fifteen authentic adjudicated case samples were obtained from the Maryland State Police Forensic Sciences Division. The majority of the samples were white powders or white crystalline samples, and several samples were off-white to gray-brown. All samples were analyzed by portable Raman through plastic bags or through capsules. **Table 19** provides the accuracy results of the portable Raman and DART-MS analyses along with the ground-truth results, which were obtained using GC-MS analysis. Accuracy was defined as the ability of the instrument to detect those compounds assigned as ground truth for each respective group (drug, diluent, or all analytes). For example, if the ground truth contained two diluents, both needed to be detected for a positive result for diluent accuracy. In this manner, the detection of all ground truth compounds was required. The overall accuracy of the portable Raman was 44 % for all analytes, whereas the accuracy of the DART-MS analysis was 74 % for all analytes. The failure of the portable Raman instrument to detect some controlled substances, due to their low proportion, was compensated for with DART-MS, as the combination of the two techniques resulted in 83 % accuracy in the detection of all ground truth compounds for the authentic samples. It is important to note that while both instruments performed well, in one instance, both instruments were needed to yield a full profile of the unknown substance, as demonstrated by case #1. Some diluents can foul the GC-MS source; therefore, most drug chemistry laboratories screen samples for controlled substances but do not always report diluents. In one case, #3, a diluent was detected by both Raman and DART-MS but not observed by GC-MS. Given that the diluent was mannitol, it is expected as GC-MS is not sensitive to sugar alcohols.

Table 19. The accuracy results for the authentic case samples. The calculation of the accuracy was performed in similar fashion as described above in section 1.3.5. Sample #9 was not included since it was a true negative sample.

Performance Measure	Raman	DART-MS	Combined
Drug Accuracy	41 %	82 %	82 %
Diluent Accuracy	45 %	68 %	83 %
Accuracy for All Analytes	44 %	74 %	83 %

In summary, in this study, a portable Raman spectrometer was validated according to the UNODC guidelines on a panel of 15 commonly encountered drugs of abuse and 15 diluent compounds. The HQI for pure diluents through plastic was higher than that for glass, >90 % and >86 %, respectively. The between-operator precision was low at ≤ 2 %. Analysis through plastic resulted in an accuracy of 89 % and precision of 88 %, while analysis through glass resulted in an accuracy of 91 % and precision of 90 %. The system excelled at the identification of analytes in their pure form and in higher percent ratio but demonstrated some difficulty in detecting the analyte at low concentrations. In comparison, DART-MS demonstrated high accuracy and sensitivity for the drug analytes of interest and many of the diluent compounds. However, DART-MS struggled with diluent compounds that perform better in negative mode (only positive mode was used). Although these techniques are strong on their own, the combination of both instruments resulted in a drug accuracy of 96 %, diluent accuracy of 100 %, and overall accuracy for two-part mixtures of 96 %. Analysis of authentic case samples using both techniques resulted in 44 % accuracy by Raman, 74 % by DART-MS, and 83 % accuracy when both techniques were combined. This combination of orthogonal data demonstrates the improved

reliability and accuracy possible when both techniques are used in screening. The ability to detect both drug and diluent analytes provides useful information for drug intelligence operations that can be performed rapidly for improved investigative leads and real-time decision-making.

2.6. Results and findings for tasks 2a and 3b: Raman and Multivariate Analysis.

2.6.1.1. *Machine Learning for Drug Identification in Portable Instruments*

The limitations of portable Raman instruments continue to make it a challenge in forensic science. Some limitations include its low sensitivity to drugs in small concentrations, fluorescence from samples interfering with signals, unsuitable for dark samples and complex matrices, fluctuation from the laser source, and its limited use for qualitative analysis.¹³ Chemometrics and machine learning have sought to improve some of these challenges, especially the analysis of multicomponent mixtures. Guirguis used principal component analysis (PCA)—a data reduction and exploratory technique as a classification method for the analysis of NPS using a hand-held Raman with a 1064 nm laser and reported 89% correct classification.¹⁹ Omar et al also used PCA to distinguish fentanyl, cathinone, and synthetic cannabinoids in seized Customs samples by comparing three hand-held Raman instruments—Progeny (1064 nm laser), Cora 5600 (1064 nm laser) and Bravo (785- 1000 nm laser) but did not provide classification rates although each drug class formed separate clusters²⁹. Weng et al used PCA followed by discriminant algorithms to classify methamphetamine and 3,4-methylenedioxy methamphetamine with an accuracy of >95% using a surface-enhanced Raman spectroscopy.³⁰ Although the selected algorithm can affect misclassification rates, preprocessing of the data is important as spectral peak overlap, fluorescence, and variable Raman intensities can influence this process. O'Connell et al reported correct classification rates of about 90% after using the first derivative of the Raman spectrum as a preprocessing technique.³¹ Simple methods such as PCA or linear discriminant analysis do not perform as well with mixtures that are commonly encountered in seized materials.

Therefore, we will focus in this section on describing methods that can improve the detection of compounds by portable Raman instruments. A database was created containing simulated binary, ternary, and quaternary mixtures. This data was used to explore machine learning algorithms to classify compounds by their drug class and drug name. The models improved the correct classification of binary mixtures from 19% using the instrument's hit quality index algorithm to 64% using convolutional neural networks. Therefore, incorporating machine learning algorithms in portable instruments can improve the detection of unknown substances with high accuracy.

In this study, we evaluate the accuracy of six machine learning algorithms— k-nearest neighbors (kNN), naïve bayes (NB), support vector machine (SVM), random forest (RF), neural network (NN), and convolutional neural network (CNN), on pure drug spectra, binary, ternary, and quaternary mixtures and compare their accuracy to a recently validated portable Raman instrument which uses an HQI algorithm.⁹ The findings presented here can be easily adapted to many other materials and applications. A more detailed explanation can be found in the following publication, and a summary is presented in the following sections. Figures presented in this report are copyright of the respective Journal and have been added here for illustration purposes.

Travon Cooman, Tatiana Trejos, Aldo Romero, Luis E. Arroyo. *Implementing Machine Learning for the Identification and Classification of Compounds and Mixtures in Portable Raman Instruments. Chemical Physics Letters.* 139283. 2022.[https://doi.org/ 10.1016/j.cplett.2021.139283](https://doi.org/10.1016/j.cplett.2021.139283)

2.6.1.2. Spectra Acquisition

Spectra were acquired using a TacticID portable Raman spectrometer with a 300 mW, 785 nm laser, and 9 cm⁻¹ resolution (B&W Tek, Newark, DE). As previously described,⁹ spectra were measured for 14 drugs—4-methylethcathinone (4-MEC), 4-methylmethcathinone (4-MMC), alprazolam, buprenorphine, cocaine, codeine, fentanyl, heroin, methamphetamine, mitragynine, morphine, naltrexone, PB-22, sufentanil and 15 diluents—acetaminophen, benzocaine, boric acid, caffeine, diltiazem, hydroxyzine, levamisole, lidocaine, maltose, Myo-inositol, phenacetin, phenolphthalein, procaine, sorbitol, starch, using a laser power of 60% and 90%. The powder samples were measured through glass vials and 2 mil plastic bags. A total of 444 pure spectra were collected.

The spectra were baseline corrected and truncated to include Raman shifts from 176 to 2000 cm⁻¹. A Savitsky-Golay filter³² was applied to smooth the spectra with a 5-point window length and third-order polynomial.

2.6.1.3. Spectral Comparison

The cosine similarity and Pearson's correlation were used to compare an authentic test set of pure compounds (referred to as authentic, pure set). These compounds included acetaminophen, benzocaine, boric acid, caffeine, diphenhydramine, levamisole, lidocaine, maltose, mannitol, Myo-inositol, phenacetin, and procaine. Spectra were acquired in triplicate through 2 mil plastic bags, and the instrument was operated at 90% power. A second database was created comprising the first derivative of the spectra from **section 2.6.1**, and comparisons to the test spectra are reported.

2.6.1.4. Pure Spectra Algorithms

To increase the number of spectra used for training and testing the algorithms, 444,000 spectra were created by multiplying each spectrum by 1000 random numbers between 0 and 1. This introduced variation in the spectra and simulated instances where there might be suppression of signals, hence training the algorithms under the worst-case scenario. Data augmentation is common when spectra are limited for training machine learning algorithms (MLA).³³⁻³⁵ Each spectrum was normalized to its maximum intensity.

Six machine learning algorithms, including kNN, NB, SVM, RF, NN, and CNN were explored. *Scikit-learn v 0.24.1*³⁶ in python was used for kNN, NB, SVM and RF classifiers. NN and CNN were based on *Keras v 2.4.0* with *Tensorflow v 2.4.1* backend.³⁷ Two models were created for each algorithm—one based on the compounds (n = 29), where the output is the compounds listed in **Table 20** and the second based on the compounds' class (n = 17), also listed in **Table 20**. The training was performed on 80% of the data in each class and testing on 20% using the *stratify* argument in the *train_test_split* function in *Scikit-learn*. The optimized parameters selected for the algorithms included *neighbors = 2* for kNN, RF—*estimators = 1000*, *max_depth = 20*, and SVM—*kernel = linear*, regularization parameter *-C = 0.09*.

Table 20. The compounds and their designated class used for training the pure spectra algorithms.

Compounds	Class
4-MEC	Cathinone
4-MMC	Cathinone
Acetaminophen	Analgesic
Alprazolam	Benzodiazepine
Benzocaine	Anesthetic
Boric acid	Acid
Buprenorphine	Opioid
Caffeine	Stimulant
Cocaine	Cocaine
Codeine	Opioid
Diltiazem	Calcium channel blocker
Fentanyl	Opioid
Hydroxyzine	Antihistamine
Levamisole	Anthelmintic
Lidocaine	Anesthetic
Maltose	Sugar
Methamphetamine	Amphetamine
Mitragynine	Opioid
Morphine	Opioid
Myo-inositol	Sugar
Naltrexone	Opiate antagonist
PB-22	Cannabinoid
Phenacetin	Analgesic
Phenolphthalein	Dye
Procaine	Anesthetic
Sorbitol	Sugar
Starch	Carbohydrate
Sufentanil	Opioid

The CNN architecture was the same for the compound model and compound class model. The entire spectrum of shape 457x1 was used as the input with 200 3x1 filters in the first convolutional layer, followed by a 2x1 *MaxPooling* layer, a second convolutional layer with 100 3x1 filters, a 2x1 *MaxPooling* layer, a *Flatten* layer and an output layer with 29 units for the compound model and 17 units for the compound class model. The *ReLU* activation function was used in the convolutional layers whereas the *softmax* function was used in the output layer. The model was compiled using the *categorical cross entropy* loss function and the *adam* optimizer function. Early stopping was implemented and the *batch size* for the fitted models was 5.

Two fully connected NN models were created—one for compound, and another for compound class prediction. The compound model contained 457 neurons in the first hidden layer, 20% *dropout* to prevent overfitting,³⁸ 128 and 114 neurons in the second and third hidden layers, respectively, with 10% *dropout* in both layers, the output layer contained 29 units. The compound class model contained 457 neurons in the first hidden layer with 20% *dropout*, 100 neurons in the second, third and fourth layers with 20% *dropout* in the second layer, and 10% in the third and fourth layers. The output layer contained 17 units. Both models used the *sigmoid* activation function in the output

layer, the *ReLU* activation function in the hidden layers, a *batch size* of 32 for fitting the model, and implemented early stopping.

The authentic pure set was used to evaluate the models. Two drugs—diphenhydramine (antihistamine), and mannitol (sugar) were not included in the training data and misclassification of these substances were expected with the models trained based on the compounds. However, we evaluated their classification based on the drug class.

A summary of the methods is shown in figure 18.

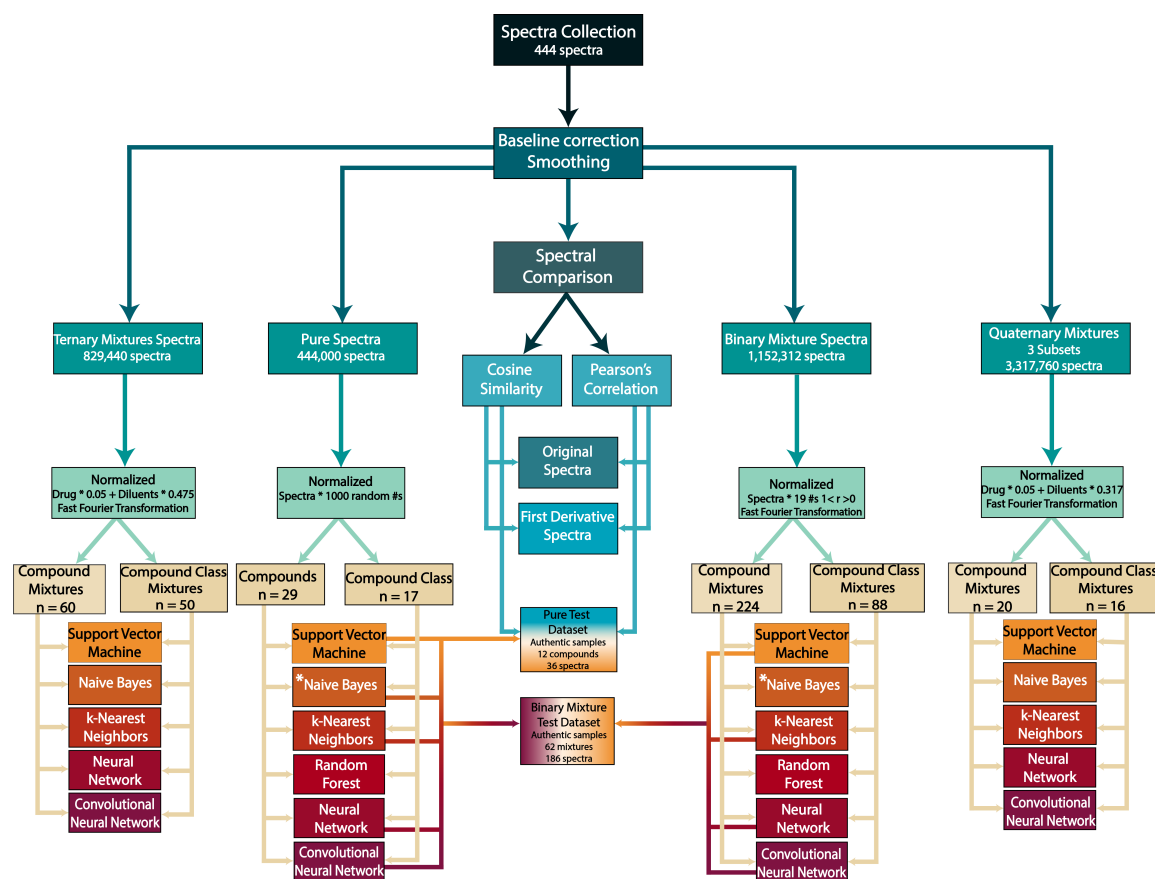


Figure 18. Summary of the workflow used in this study. *— The Naïve Bayes algorithm was not used to evaluate the authentic, pure test and authentic binary mixture datasets. All simulated datasets, excluding the pure spectra dataset, included Fast Fourier transformed data. The Quaternary mixture dataset contained a total of 3,317,760 spectra and was divided into three subsets: subset 1 contained 663,552 spectra with 4 compound mixtures and 4 compound class mixtures; subset 2 contained 1,327,104 spectra with 8 compound mixtures and 8 compound class mixtures; and subset 3 contained 1,327,104 spectra with 8 compound mixtures and 4 compound class mixtures. Image obtained from Reference 8.

A comparison of the effect of training with the mixture models or pure models to predict the compounds in the test mixtures demonstrated the importance of having the appropriate model in the library. For example, if ternary mixtures are being tested, the models should be trained on ternary mixtures. If the pure model, which returns a single compound, is used on mixtures, a result for the compound most representative of the spectrum will result. Additionally, the algorithms detected differences in spectra of ternary and quaternary mixtures, that would otherwise be challenging to observe by inspection, with high accuracies (~ 83-100%). Depending on the application, if the number of component mixtures is known, algorithms can be designed to meet this expectation. For example, if the number of mixtures in street drugs does not typically exceed five compounds, then training algorithms to detect more than four components would not be necessary.

We propose the use of models created to report single compounds, single compound classes, and binary, ternary, and quaternary mixtures using the CNN algorithm due to the high correct identification rates and accuracy reported in this study. Instead of implementing these classification techniques post-processing, they can be incorporated into portable instruments and, depending on the application, provide spectral correlation information using the HQI, cosine similarity, or Pearson's correlation, and classification as demonstrated by the proposed workflow in **Figure 19**. One advantage of this classification and reporting workflow is the gain of feedback to the end-user. When the identity of a compound is unknown and misclassified by the conventional HQI, having a built-in CNN algorithm can provide additional information about drug classes and potential mixtures. For example, when pure PB-22 was analyzed using the portable Raman instrument, it was reported as BB22 using the HQI due to the similarity between their spectra. Nonetheless, using the machine learning algorithm for compound class classified it as a synthetic cannabinoid even though it was absent from the library.

It should be noted that depending on the application, the proposed approach still has some limitations. For example, in the pharmaceutical industry, where purer compounds are encountered, and Raman is the primary technique used, instead of using the top three hits, the top hit might be more important. On the other hand, in forensic science, where portable Raman is used as a screening method, it might be acceptable to consider the top three hits as potential compounds since confirmation using a secondary technique would be required before reporting components of seized materials. One of the drawbacks of using machine learning algorithms on large datasets is that it requires high computing capabilities, as observed with Random Forests in this study. However, given that portable instruments such as the TacticID have Wi-Fi capabilities, access to a server can be used to train the algorithms on new data and be used to perform searches. In future studies, other data augmentation parameters, such as Raman shift offset, can be used in training the models to increase their robustness. Additionally, authentic ternary and quaternary mixtures can be created to demonstrate the capability of the algorithms as more complex drugs: diluent mixtures have previously been reported in casework.³⁹

Machine learning, which detects minor differences in spectra of complex mixtures, outperformed the HQI algorithm incorporated in a portable Raman system. Implementing machine learning algorithms that detect single compounds, mixtures, and their classes can provide useful screening information about unknown compounds or molecules. Although our proposed approach provides a probability for each hit, a spectral correlation technique can be used when needed. Furthermore, building these methods into the instrument eliminates the need to export the data for post-processing. It does not require separate libraries to be installed on the instrument as models can be trained offline and then transferred to the device.

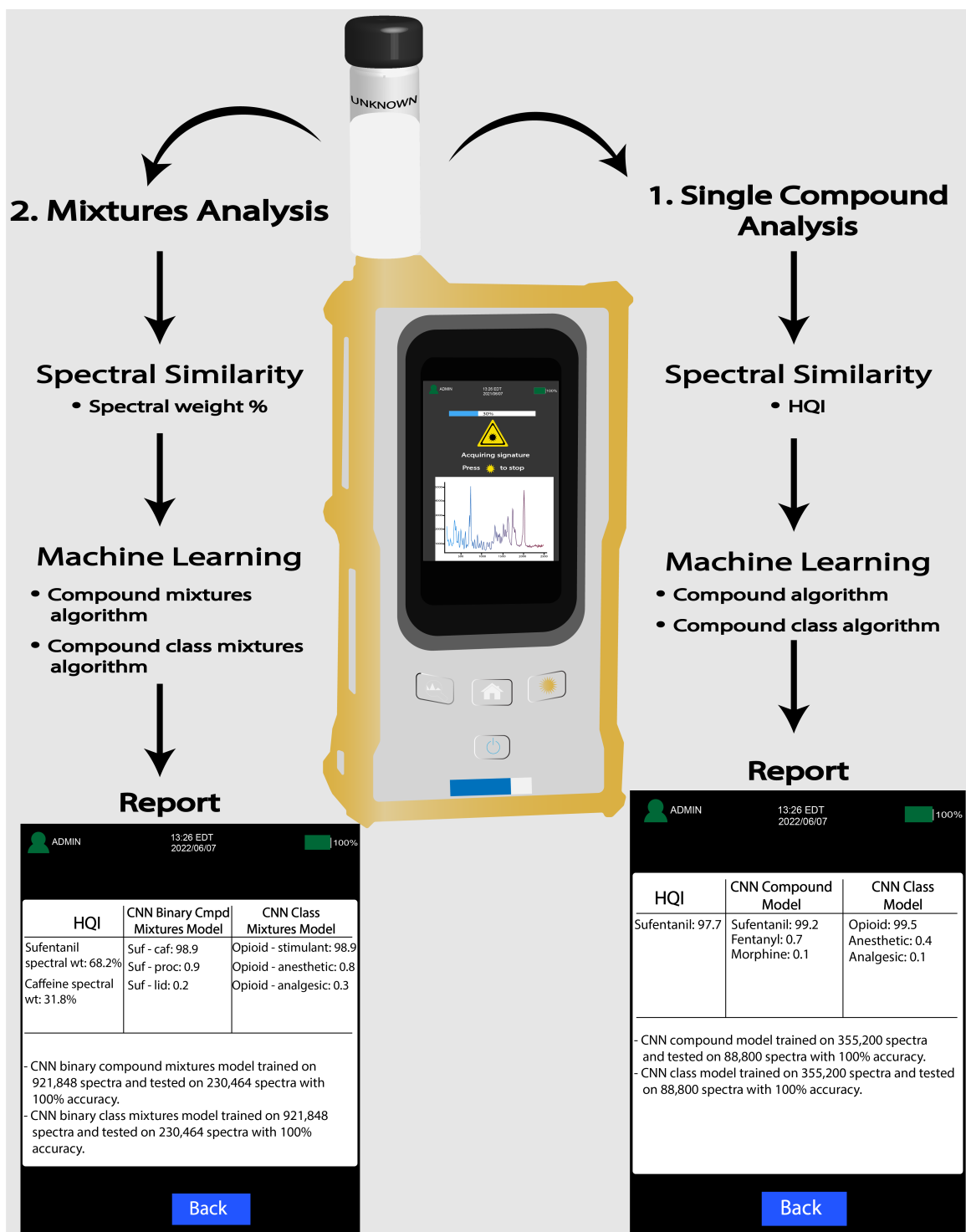


Figure 19. An example of a workflow that can be implemented in portable Raman instruments. If the intended application requires a numerical value for spectral correlation, a similarity metric can provide an HQI for pure compounds and spectral weight for mixtures. Machine learning algorithms can also be incorporated to identify the compounds and their classes. In the final report, a summary of the potential bits and their respective class probabilities is reported. Imaged obtained from Reference 8.

Reporting the accuracy of the models, as shown in **Figure 19**, the size of the training, and testing data results in more transparent reporting of results. The concept proposed in this study will therefore benefit applications where portable Raman instruments are used for compound screening, including forensic science, medicine, and pharmaceutical industries.

In summary, six machine learning algorithms—kNN, NB, RF, SVM, NN, and CNN were investigated and compared to a portable Raman instrument's accuracy in detecting pure powders, binary, ternary, and quaternary mixtures in this study. The CNN performed better than all algorithms with 100% correct identification for pure substances by compound and class. Both the NN and CNN resulted in superior correct identification on the authentic binary mixture data— 65% and 64%, respectively in detecting both compounds in comparison to 19% observed in the portable Raman instrument. Improved accuracy in the binary simulated mixtures was observed, ranging from 83 to 100%, depending on the model and algorithm used, with superior performance observed for CNN. The CNN also provided the highest accuracy on the ternary and quaternary mixtures—100%, demonstrating its ability to provide compound and class information on samples that simulate common seized drug formulations.

We propose the use of the HQI for spectral correlation and CNN models in portable Raman instruments to provide preliminary information about the identity of a compound and its class. Incorporating machine learning algorithms into portable Raman systems can enhance the response and feedback provided to law enforcement and scientists at the laboratory and onsite, facilitating more efficient and safer decision-making during sampling and investigative stages. The methods proposed here are broadly applicable to other materials and disciplines that use Raman spectroscopy as a rapid method for point-of-contact analysis.

2.7. Results and Findings for tasks 2b-c and 3a: SPELEC Raman and Performance measures.

2.7.1.1. Surface-Enhanced Raman Spectroscopy (SERS).

One method for improving the Raman response is through the use of surface-enhanced Raman spectroscopy (SERS). The SERS effect generally occurs when the analyte of interest is near a metal surface. This process can increase the Raman effect with an enhancement in the signal generally between 10^5 - 10^8 , with some enhancements reported as 10^{11} or higher.^{41,42} The SERS effect occurs for several reasons. The first is through changes to the electromagnetic field. Metals exhibit a large electromagnetic field when the incident wavelength of radiation is similar to the metal's plasma wavelength. This results in the excitation of electrons within the conduction band to an excited state termed a surface plasmon resonance. Proximity to this excited state increases and enhances the vibrational modes of the molecule. The second reason for the SERS effect is the formation of charge-transfer complexes with transitions within the visible wavelengths of light, allowing resonance enhancement. In general, lone pairs and pi-cloud molecules will exhibit the strongest SERS effect along with other electron-rich groups.^{40,43} **Figure 20** demonstrates the SERS effect on a simulated spectrum.

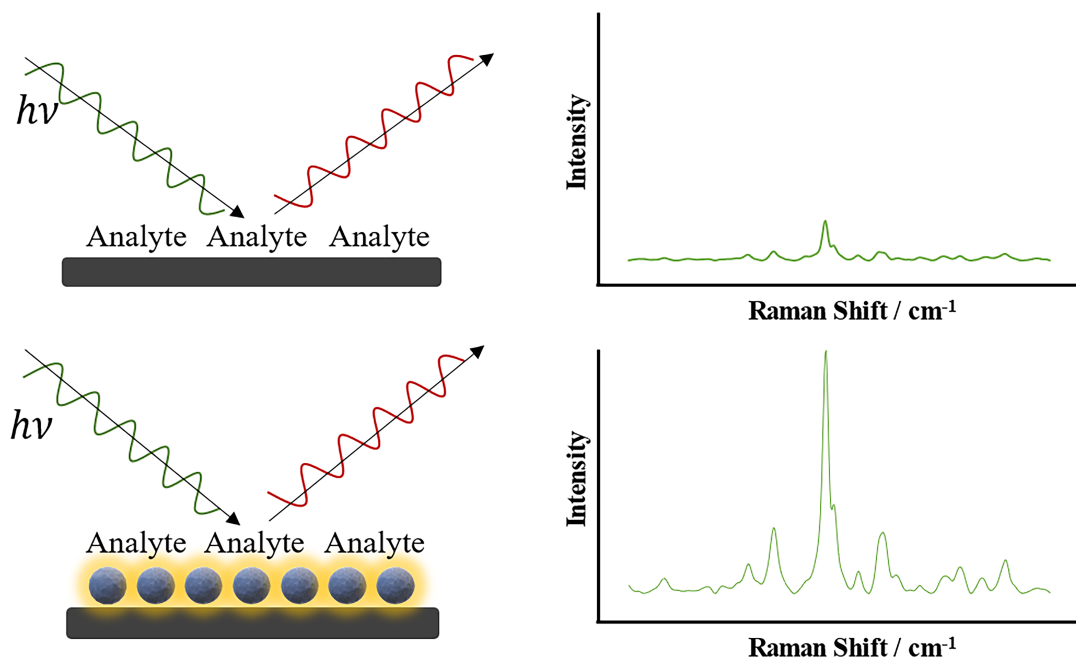


Figure 20. Demonstration of signal enhancement from the presence of metal nanoparticles on electrode surface to induce the SERS effect.

The SERS effect demonstrates the potential for the analysis of drugs on modified electrode surfaces. Although the SERS effect can be utilized in a variety of Raman applications, of interest to this report is achieving the SERS effect in tandem with electrochemistry, which will be described in more detail later. Electrode modifications using metals such as silver and gold is a common

electrochemical technique that can be accomplished within the laboratory, or electrodes can be purchased from a variety of vendors. Therefore, the combination of electrochemistry with Raman spectroscopy can prove a valuable technique for the spectroelectrochemical analysis of drugs of abuse. Other benefits of the use of SERS include limited or no sample preparation, rapid and portable methods, and instrumentation, and, as stated, there are many multiplexing capabilities.⁴³ Furthermore, it is possible to add a solution of metal nanoparticles to liquid samples and analyze the sample directly to achieve the SERS effect.⁴⁴

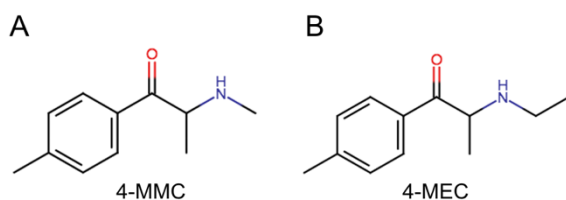
2.7.1.2. EC-SERS Experiment

Spectroelectrochemistry refers to the combination of electrochemistry and spectroscopy used within a single experiment. While these experiments can be done separately, in most cases, the two techniques are combined in a tandem fashion. Traditionally, spectroelectrochemical applications have involved the analysis of electron transfer mechanisms and electrochemical intermediates.^{43,45} Recently however, spectroelectrochemistry has been utilized as a novel SERS platform termed EC-SERS or electrochemical-surface-enhanced Raman spectroscopy.^{6,46} The combination of two techniques provides the opportunity for orthogonal analytical information and, in the case of EC-SERS, provides a method of generating a SERS-active substrate. While many of the previously described SERS methods rely on *ex situ* nanoparticle preparations using various synthesis and deposition methods, EC-SERS methods have demonstrated the ability to generate a SERS-active substrate *in situ* using electrochemistry during the Raman measurement. This approach utilizes the redox properties of a metal electrode surface and a proper electrolyte to produce metal nanostructures on the electrode surface through the oxidation and subsequent reduction of the metal.

This report will provide examples of the use of EC-SERS in the detection and identification of drugs. The first example presents a time-resolved spectroelectrochemical method for detecting two synthetic cathinones 4-MMC and 4-MEC- using a gold SPE electrode as SERS substrate (AuSPE). A more detailed explanation is provided in the following publication, and a summary of major findings is presented in the following sections. Some figures presented in this report are copyright of the respective Journal and have been added here for illustration purposes.

Jerson Gonzalez-Hernandez, Colby Edward Ott, Maria Julia Arcos-Martinez, Alvaro Colina, Maria Aranzazu Heras-Vidaurre, Ana Lorena Alvarado-Gamez, Roberto Urcuyo, Luis E. Arroyo-Mora. "Rapid determination of the 'legal highs' 4MMC and 4MEC by spectroelectrochemistry: simultaneous cyclic voltammetry and *in situ* surface-enhanced Raman spectroscopy". *Sensors* 2022, 22(1), 295.
<https://doi.org/10.3390/s22010295>

These two cathinones (Scheme 1) are structurally similar, differing only by a CH₂ group, which challenges their identification when they are present as mixtures in diluents or other drugs.



Scheme 1. Chemical structures of synthetic stimulant drugs. **(A)** (R/S)-2-(methylamino)-1-(4-methylphenyl)propan-1-one (4-MMC) and **(B)** (R/S)- 2-(ethylamino)-1-(4-methylphenyl)propan-1-one (4-MEC).

All the EC-SERS experiments are run in the SPELEC Raman system which combines a potentiostat and Raman. This instrument uses a laser with a wavelength of 785 nm. The two synthetic stimulant drugs studied are classified as secondary amines with a calculated pKa around 8.1.⁴⁷ The electrochemical potential of these weak bases is influenced by the pH of the medium in which the measurement is performed. Sulfuric acid at a pH of 1.8 made it possible to work with a wider electrochemical window when gold electrodes were used.⁴⁸ These conditions enabled the separation of the two oxidation waves corresponding to the analyte and the substrate.

2.7.1.3. Determination of the electro-activity

The electro-activity of the target drugs shown in scheme 1 was determined via cyclic voltammetry (CV). The experiment was conducted in the positive direction, starting the sweep at +0.60 V, which allowed the resolution of the peaks to the gold's oxidation wave used as the working electrode. The electrochemical process of 4-MMC and 4-MEC using AuSPE is outlined in **Figure 21**, where the average of the three measurements for each concentration is plotted. The electro-oxidation of both substances occurs at a potential of around +0.91 V (peak I), as suggested by the growth of the current peak when increasing the concentration from 50 $\mu\text{g/mL}$ to 100 $\mu\text{g/mL}$, while gold oxidizes around +1.1 V (peak II). The prominent cathodic peak at +0.62 V for drug samples (peak III) or +0.52 V for the blank, corresponds to the reduction of the gold compounds previously formed in the positive scan. Both oxidation and reduction peaks are shifted towards less positive potentials for the blank. The voltammograms demonstrate the common hysteresis of the oxide formation-reduction behavior that some metals, such as gold, undergo in electron transfer reactions.⁴⁹

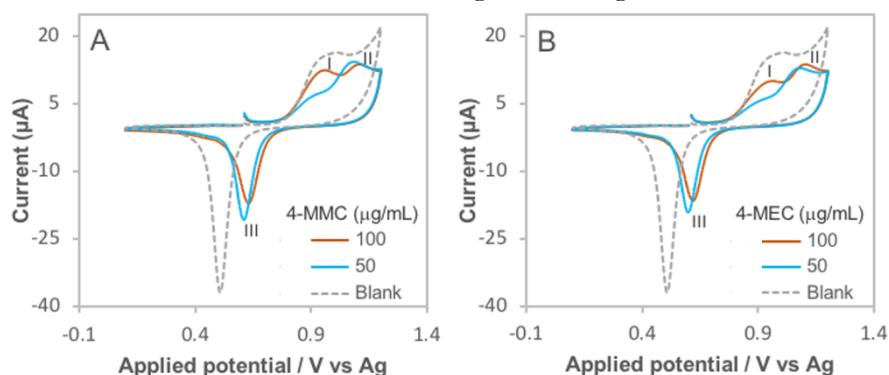


Figure 21. Cyclic voltammograms of the target drugs. (A) 4-MMC and (B) 4-MEC, both in 0.01 M H_2SO_4 at a AuSPE starting at +0.6 V in the positive direction. Scan rate: 50 mV/s. Image source: see Reference 7.

During spectroelectrochemical analysis, voltammetric scanning has the dual role of tentatively determining the amount of analyte in the sample while performing in situ pretreatment on the electrode surface. The developed nanostructures using this approach serve as a substrate for the acquisition of Raman spectra. **Figure 22** shows the construction of calibration curves for both analytes, which demonstrate potential use for quantitative analysis. These curves corresponded to peak height vs. analyte concentration and were obtained using cyclic voltammetry (CV) on the AuSPE. One of the limitations of using CV is the overall low sensitivity offered, mainly due to the susceptibility to residual currents encountered.⁵⁰ Therefore, at low concentrations, the shape of the analyte peaks is more difficult to recognize from the gold oxidation peak, as shown in **Figure 22B**. The corresponding calibration plots show a linear response: $I_p = 0.064 \cdot C - 0.532$ for 4-MMC (**Figure 22A**) and $I_p = 0.119 \cdot C - 3.92$ for 4-MEC (**Figure 22B**) with regression coefficients (R^2) of 0.997 and 0.999, respectively. The limit of detection (LOD) was estimated at three times the standard

deviation of the linear regression divided by the slope of the linear curve ($3\sigma/S$). The method for 4-MMC exhibited an LOD of $6.6 \mu\text{g/mL}$ and $2.4 \mu\text{g/mL}$ for 4-MEC. Finally, time-resolved electrochemical and spectroscopic information provides the necessary methodology to perform the selective determination of these two designer drugs.

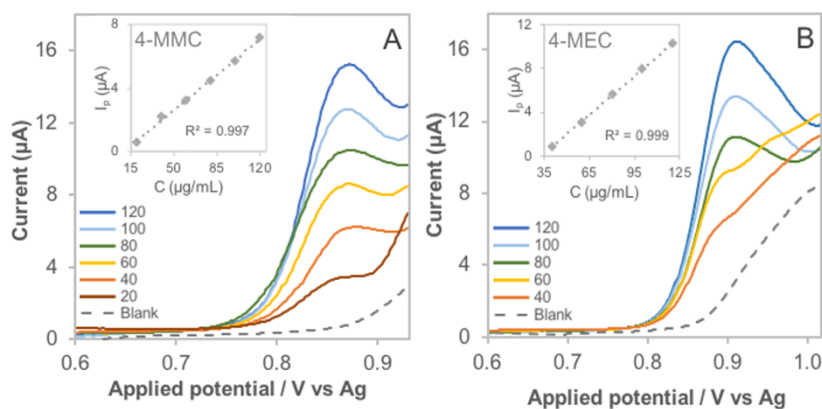


Figure 22. Partial CV profile recorded on a AuSPE for different concentrations of the drugs in $0.01 \text{ M H}_2\text{SO}_4$. (A) 4-MMC [$20 - 120$] $\mu\text{g/mL}$. (B) 4-MEC [$40 - 120$] $\mu\text{g/mL}$. Insert shows the calibration curve: peak height vs analyte concentration. Scan rate: 50 mV/s . Image source: see reference 7.

Despite the mentioned similarity of the drugs studied, it is possible to discriminate the chemical structures accurately by EC-SERS. **Figure 23B** depicts EC-SERS spectra of both substances in an acid solution. The most significant difference between the two spectra is in the region of the gray dashed rectangle [$1150 - 1225$] cm^{-1} . The spectrum of 4-MMC shows a triplet with signals at 1161 cm^{-1} , 1185 cm^{-1} , and 1213 cm^{-1} , which could be attributed to aromatic $\delta(\text{CH})$ in-plane deformation vibrations,^{51,52} while for 4-MEC, only one doublet is distinguished with the signals at 1185 cm^{-1} and 1213 cm^{-1} . The absence of the band at 1161 cm^{-1} in the 4-MEC EC-SERS spectrum agrees with the results in **Figure 23C** for the spectra acquired from substances in the form of crystalline powder, allowing for the correct identification of each of the stimulants studied, as it has been reported.^{53,54}

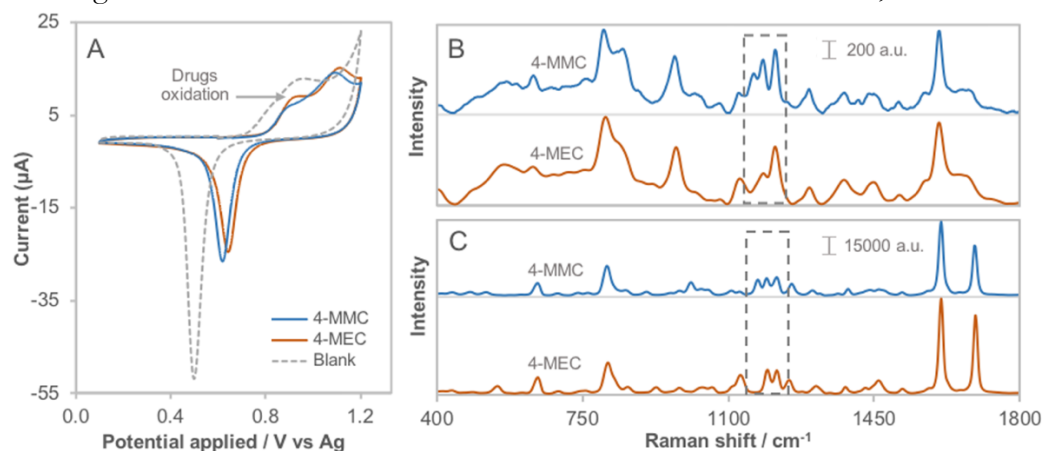


Figure 23. Comparison of the spectroelectrochemical results of 4-MMC and 4-MEC obtained in solution at $50 \mu\text{g/mL}$ in $0.01 \text{ M H}_2\text{SO}_4$ and the spectra from the crystalline powders using the SPELEC instrument. (A) Overlay of cyclic voltammetry recorded on a AuSPE at 50 mV/s starting at 0.6 V in the positive direction. (B) EC-SERS spectra, laser power of 379.1 mW and integration time of 3 s . (c) Raman spectra of the drugs as solid powders. Image source: See reference 7.

According to the results, the advantage of activating an optimal surface morphology to induce the SERS effect is its ability to analyze a very low concentration of the analyte. In comparison, these low concentrations may not be detected using non-SERS Raman due to a decrease in sensitivity, and, therefore, a loss in peak resolution compared to SERS. The possibility to identify and quantify low concentrations of the target drugs gives the technique a potential use for testing both seizure samples and biological matrices⁵⁵ or even in instances where the fluorescence overwhelms the Raman signals.⁵⁶ Furthermore, *in situ* SERS substrate activation provides some benefits to overcoming a possible time-dependent decrease of the surface and plasmonic properties, which could affect the reproducibility and reliability of the measurements.⁵⁷

In summary, the spectroelectrochemical sensing and comparison of the results for 4-MMC and 4-MEC were explored for the first time using a portable instrument. Both drugs were found to be electro-active on a gold electrode at pH 1.8 by the CV technique. This electrochemical sweep allows a simultaneous *in situ* activation of the SPE surface to induce the SERS effect. The CV vs SERS spectroelectrochemical process enables a rapid and reliable analysis technique in which both synthetic cathinones can be selectively analyzed or detected through the characteristic bands of the EC-SERS spectrum that provide a real fingerprint of the molecule, even for molecules as similar as those studied in this work.

2.7.1.4. EC-SERS Electrode and Surface Characterization.

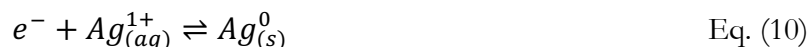
This section will focus on the development of the mechanisms involving the EC-SERS analysis of seized materials using silver or gold screen-printed electrodes. Understanding the processes involved in the formation of nanostructures at the surface of the electrode and their characterization is an integral part of understanding the SERS phenomenon within the context of the EC-SERS technique. As described previously, there are many ways of synthesizing and formulating nanoparticles from and in solutions and other substrates, but the EC-SERS method differs in that the fundamental process occurs *in situ* on the metal substrate. In some cases, the electrochemical method applied serves only in the preparation of the substrate, while in other methods, the electrochemical signal may also be used analytically. Utilizing the silver electrode as an example, the preparation of the surface occurs as follows: 1) An anodic (oxidizing) potential is applied to the electrode in the presence of the supporting electrolyte. This potential results in the oxidation of the surface of the metal working electrode, as shown in **Equation 8**,



where the silver ion now exists within the electrolyte solution at the electrode: solution interface. 2) The positively charged silver ions may interact with chloride in solution, forming silver chloride (**Equation 9**)



and/or 3) application of a suitable cathodic (reducing) potential can be applied to the working electrode, resulting in the reduction of the silver ions to silver metal nanostructures on the surface of the electrode, resembling a “plating-out” effect (**Equation 10**).



In practice, a mix of silver chloride cubes and silver nanostructures should now exist on the surface of the working electrode, providing regions capable of providing the SERS effect. A description of some of the properties and characterization of this type of system has been described in the literature.^{58,59}

This process was carried out within these experiments by two different methods: cyclic voltammetry and multi-pulse amperometric detection (MPD). While the description above describes the MPD approach, a similar result is achieved with CV. The only difference is that the applied potentials are swept, meaning that the electrode and the solution will feel all potentials between the oxidation and reduction steps, possibly altering the formation of the nanostructures, favoring the pure metal or silver chloride, or having an effect on the size and distribution of the structures.

Cyclic voltammetry was initially used to study the changes to the electrode surface. Cyclic voltammograms were scanned from +0.3 V in the cathodic direction to approximately -0.3 V. **Figure 24** demonstrates an example voltammogram for a silver electrode in 0.1 M HClO₄ + 0.01 M KCl. The electroreduction of the silver surface occurs between -0.10 V and -0.15 V. It is important to note that two different reduction peaks are seen (-0.11 V and -0.14 V) to make up the overall reduction wave, suggesting that two different processes are occurring in this situation. These two processes may be attributed to the direct oxidation and reduction of pure silver ions in solution and back to the electrode surface and reduction related to the silver chloride structures.

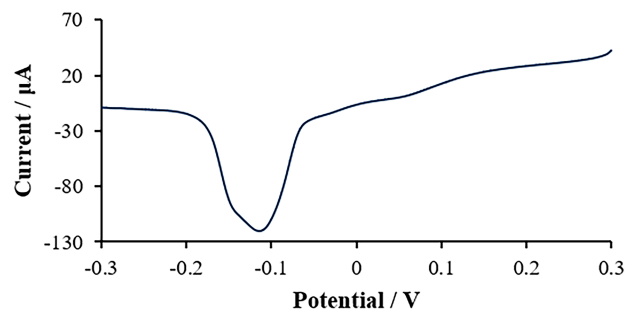


Figure 24. Voltammogram representing the generation of the SERS substrate in situ through application of potentials starting at +0.30 V and scanned using a cyclic voltammetry method until -0.30 V. Only the portion of the CV voltammogram in the cathodic direction is shown. The supporting electrolyte utilized was 0.1M HClO₄ + 0.01M KCl as a drop on a DRP-C013 SPE.

The described CV *in situ* approach was used during the investigation of the surface characteristics of the electrodes and the generation of nanostructures on the surface. Several experiments were tested to determine the effect of electrolytes and multiple treatments. **Figure 25** provides SEM comparisons at varying magnifications for the pristine silver SPE versus the various roughening approaches. The following comparisons and order are shown in the figure:

- A) Pristine silver screen-printed electrode, DRP-C013
- B) Reduced silver screen-printed electrode in 0.1M HClO₄ + 0.01M KCl, 1 cycle
- C) Reduced silver screen-printed electrode in 0.1M HClO₄ + 0.01M KCl, 2 cycles
- D) Reduced silver screen-printed electrode in 0.1M KCl, 1 cycle

The top left image demonstrates the silver working electrode of interest for the other images. It can be seen that the pristine silver electrode is generally smooth and appears plate-like. A few defects and debris can be seen in the images; however, the surface is mostly devoid of any topographical features of interest. The SEM images in set B demonstrate that a single scan is sufficient to produce silver nanostructures on the surface of the electrode. These structures appeared to resemble a middle state between a cube and a sphere and were generally similar in size. Some aggregation can be noted, with typical clusters containing about three particles. A marked difference is seen when considering two consecutive CV scans (seen in the panel set C). Due to the addition of a 2nd cycle, anodic potentials were applied for a second time and over a longer period than the first scan. This would be expected to result in the oxidation of the silver surface for a second time and, potentially, of the nanostructures. This could also result in more opportunity for the formation of silver chloride, which may be evidenced by the presence of more cubic structures in the SEM images.

Additionally, great aggregation of the larger nanoparticles is evident, creating groupings of many nanoparticles along with more debris-like structures, although the generation of these nanostructures seems to be mostly homogenous across the electrode surface. Of note, the second scan produced more SERS response than the single scan, suggesting an effect from either the size of the nanoparticles produced, which appear larger with two scans than with one, or due to the presence of a high number of nanostructures. Finally, the SEM image set in the D panels corresponds to the use of different electrolytes during the *in-situ* generation, 0.1M KCl. This electrolyte does not contain acid, meaning a more neutral pH was achieved. Also, the concentration of potassium chloride was 10X higher than that of the other experiments. It is clear that this was not ideal, resulting in large accumulations of silver chloride and aggregation.

Similar studies were conducted with gold screen-printed electrodes. Two types of electrodes were included, although only the 220BT was assessed for nanoparticles because separate experiments demonstrated that the 220BT gold electrodes (which are cured at low temperature, *BT* for *baja temperatura*) were superior for electrochemical measurements, while the 220AT electrodes (which are cured at high temperature, *AT* for *alta temperatura*) were superior for Raman measurements. These experiments were conducted as part of this project following the development of an EC-SERS method demonstrating electrochemical identification and SERS identification of two cathinones: mephedrone (4-MMC, 4-methylmethcathinone) and 4-MEC (4-methylethcathinone) as described in **section 6.1**. Although a SERS phenomenon was achieved in the experiment from the use of the applied CV and sulfuric acid electrolyte, minimal differences were observed in the SEM images between the pristine gold 220BT electrode and the generated SERS substrate electrode.

To this end, a similar set of steps was followed. Cyclic voltammetry was again used as the electrochemical method to generate the SERS substrate. The potential was started at either +1.0 V or +0.6 V versus the pseudo silver reference electrode and scanned in anodic direction to +1.4 V at the vertex and then in the cathodic direction to approximately +0.1 V. The supporting electrolyte for these measurements was 0.01 M H₂SO₄. The resulting voltammogram from a blank sample for the generation of the SERS substrate can be seen in **Figure 26**.

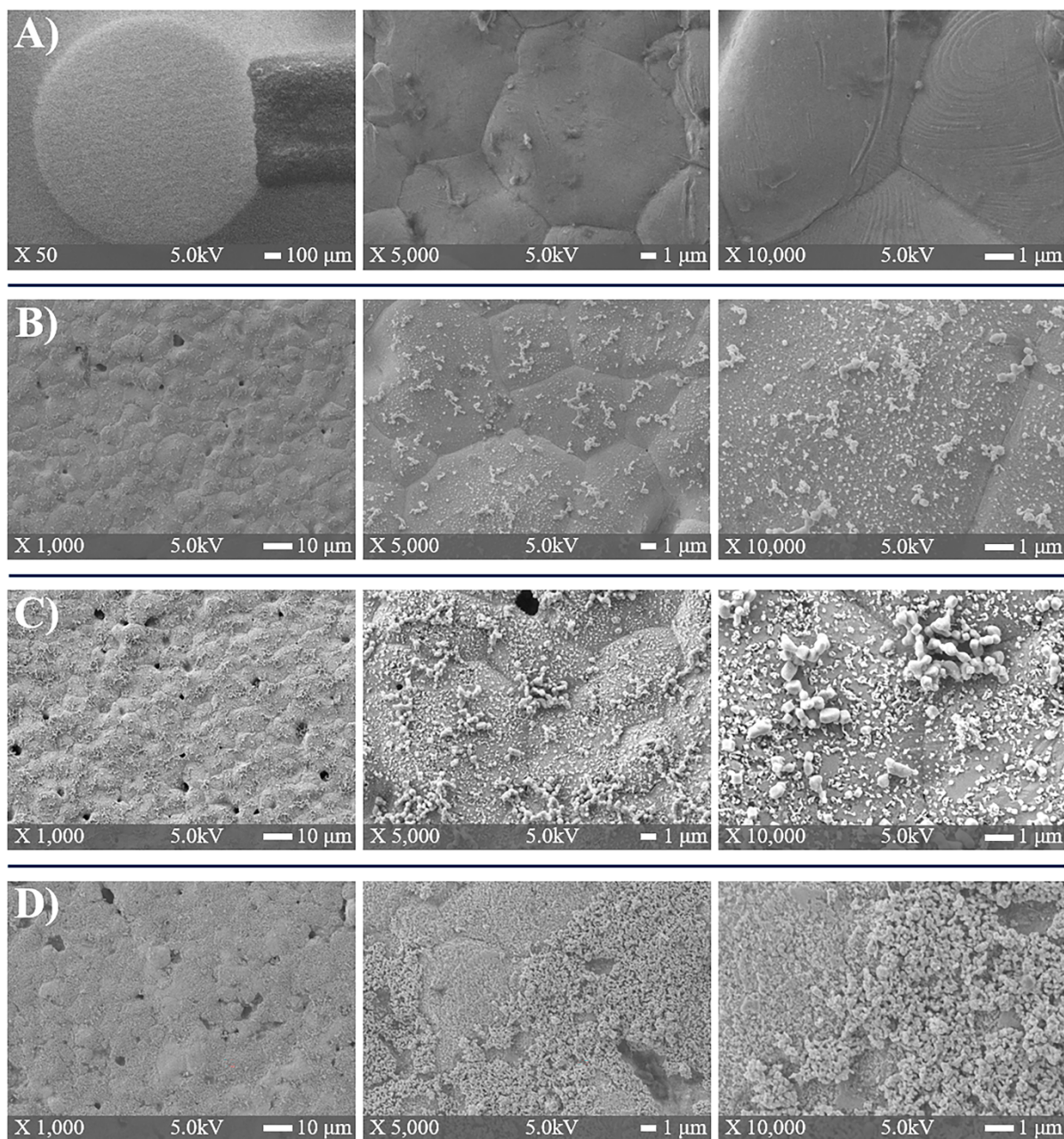


Figure 25. Scanning electron microscopy images of A) pristine silver SPE, B) silver SPE with CV generation of nanostructures with 1 cycle in 0.1M HClO_4 + 0.01M KCl , C) silver SPE with CV generation of nanostructures with 2 cycles in 0.1M HClO_4 + 0.01M KCl , and D) silver SPE with CV generation of nanostructures with 1 cycle in 0.1M KCl . SEM images were obtained from the WVU Shared Research Facility.

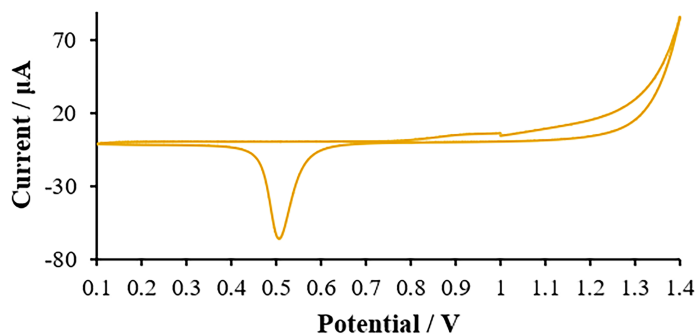


Figure 26. Cyclic voltammogram for the generation of a SERS substrate on a gold 220BT screen-printed electrode performed in 0.01M sulfuric acid with the initial potential of +1.0 V, upper vertex of +1.4 V, and lower vertex of +0.1 V.

In a similar fashion to the silver electrodes, the initial oxidation of the gold surface may be a critical step in the generation of the gold nanoparticles following the similar mechanism described previously. The electrode remained in these oxidative potentials until reaching the reduction wave of the gold at approximately +0.5 V. The shape of this reduction was well-defined with a single peak. Following the return signal in the anodic direction, an oxidative peak occurring between +0.9 V and +1.0 V is evident, demonstrating the oxidation of the gold surface/gold nanostructure. The following SEM comparisons are provided and can be seen in **Figure 27**:

- A) Pristine gold 220BT screen-printed electrode
- B) Reduced gold 220BT electrode in 0.01M H₂SO₄, starting at 0.6 V
- C) Reduced gold 220BT electrode in 0.01M H₂SO₄, starting at 1.0 V
- D) Pristine gold 220AT screen-printed electrode

A significant difference between the pristine gold 220BT electrode (A) and the pristine gold 220AT electrode (D) can be seen in the SEM images. While the 220BT electrode is made of several layers of gold nanoparticles plated out as an electrode, the 220AT electrode is a much smoother and more consistent surface. These characteristics may explain their performance characteristics; since the 220BT electrodes demonstrate a higher surface area, the electrochemical performance may be enhanced. Meanwhile, the 220AT electrodes appear to have a more homogenous surface, suggesting a potential “purity” of the electrode paste that supports less background response to the Raman laser.

Considering the 220BT electrodes as SERS substrates, minimal differences can be seen when the CV procedure was applied in the sulfuric acid solution. Although difficult to determine, the SERS gold surface may exhibit more roughness and possible small formations of nanoparticles on the larger particles themselves. Although the visual differences are far less than those seen with the silver electrodes, a SERS response was evident in the experiments, suggesting some change to the electrode surface, enabling the SERS phenomenon to be achieved.

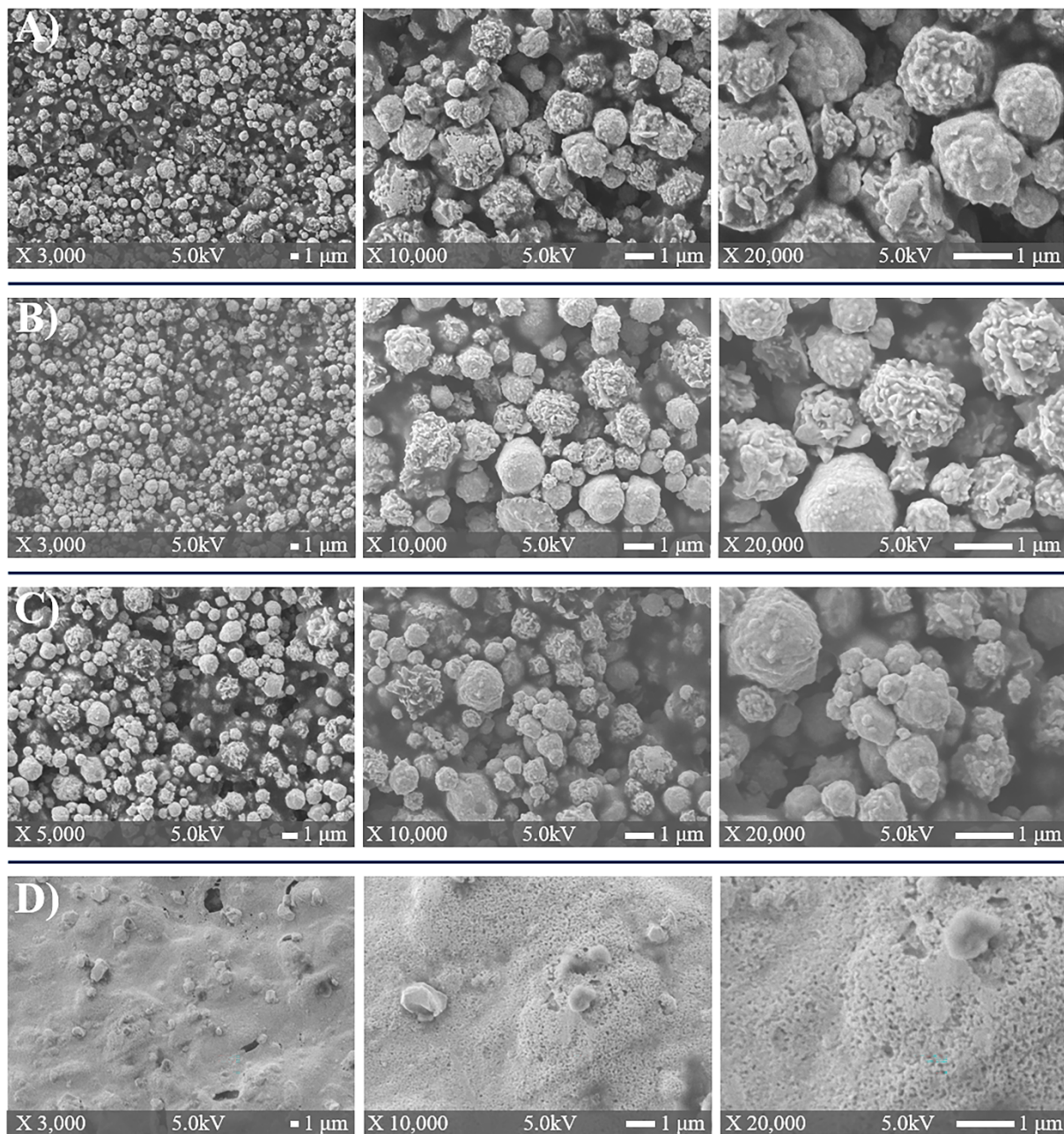


Figure 27. Scanning electron microscopy images of A) pristine gold 220BT SPE, B) gold 220BT SPE with CV generation of nanostructures at a starting potential of +0.6 V in 0.01M H₂SO₄, C) gold 220BT SPE with CV generation of nanostructures at a starting potential of +1.0 V in 0.01M H₂SO₄, and D) pristine gold 220AT SPE. SEM images were obtained from the WVU Shared Research Facility.

Characterization of a select group of these electrode surfaces was also conducted using atomic force microscopy (AFM). AFM is a scanning probe technique that can provide topographical information using a probe that interacts with the surface under investigation. Generally, the deflection of the probe is measured extremely accurately to provide the topographical information, often on the nanometer scale. This data can then be analyzed and represented through the generation of 3D topographical maps of the surface area analyzed to provide a visual representation of what the surface looks like on the micro/nanometer scale. The free software WSXM was used for the generation of the 3D images. As done previously, the silver electrodes will be discussed first, followed by a short discussion of the results for the gold electrodes. Not all the electrodes were selected for AFM analysis due to the cost and time of the instrument. The following silver electrodes were assessed via AFM:

- A) Pristine C013 screen-printed electrode
- B) Reduced silver screen-printed electrode in 0.1M HClO₄ + 0.01M KCl, 1 cycle

Based on the SEM images described previously, it is unsurprising that the AFM analysis showed drastic differences between the pristine silver C013 screen-printed electrode and the silver electrode that was reduced in the perchloric acid and potassium chloride electrolyte (**Figure 28**). While the SEM images provided an excellent visual representation of the nanostructures on the electrode surface, the AFM images are an excellent addition of information, really demonstrating the change that occurs to the electrode surface and the presence of the nanostructures that are responsible for eliciting the SERS response. Additionally, fairly even distribution and change to the electrode surface can be observed. Although several measurements from different areas of the working electrode were recorded, only a single area result is shown here for each electrode for brevity.

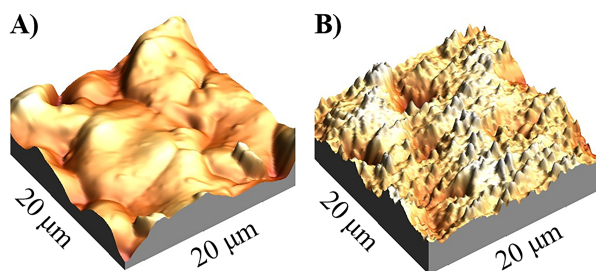


Figure 28. 3-Dimensional representation of the surface topography of a A) pristine silver C013 screen-printed electrode and B) reduced silver screen-printed electrode in 0.1M HClO₄ + 0.01M KCl obtained using atomic force microscopy (AFM). The analysis area was 20 µm by 20 µm. AFM images were obtained with the use of the WVU Shared Research Facility.

Following the SEM and AFM characterization, the corresponding SEM electrodes to the AFM electrodes were chosen for more in-depth analysis of the nanostructures, namely the distribution and size of the particles. For this process, ImageJ was used for measuring the nanoparticles and counting. **Figure 29** shows the SEM image under consideration again, along with the resulting distribution and descriptive statistics. Although some distribution in the size of the nanoparticles was observed, their size was centered around 150 nm, with an average particle size of 163 nm ± 81 nm. The minimum nanoparticle size observed was 54 nm and the maximum size was 666 nm, with a total of 304 particles counted in the 12 µm by 9 µm SEM image.

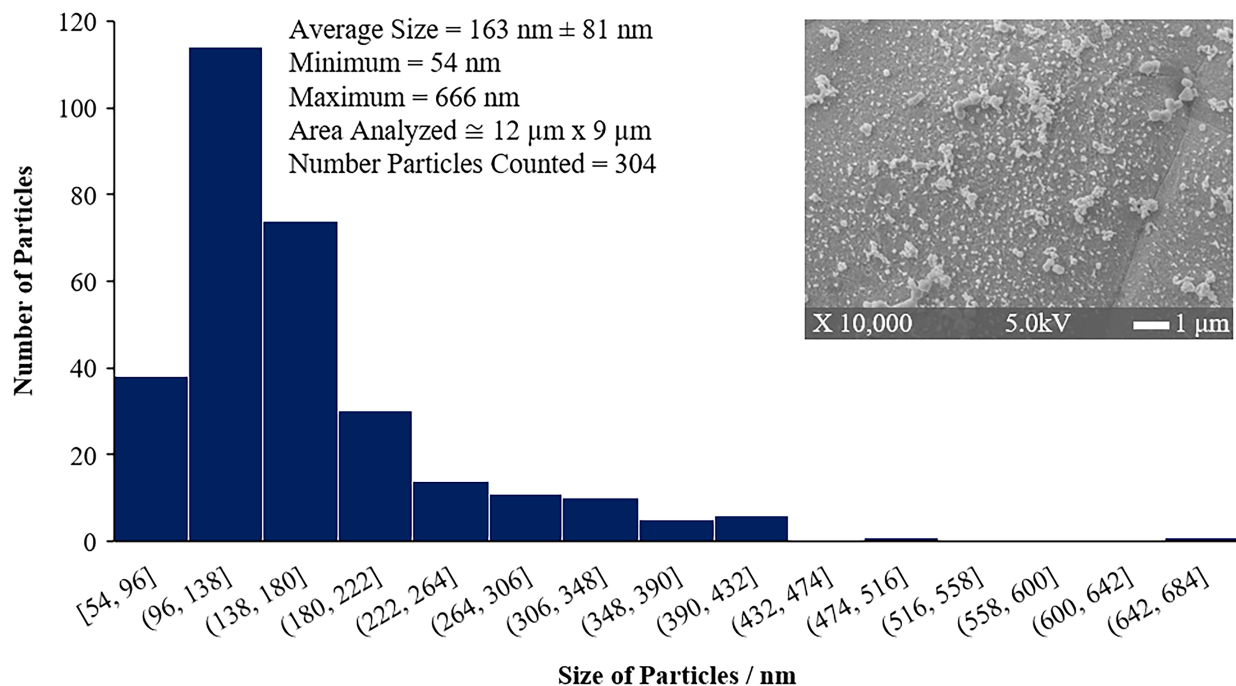


Figure 29. Histogram distribution of the nanoparticles found in the 10,000X SEM image of the reduced silver electrode surface along with the descriptive statistics for the distribution. Particle counts and measurements were done in ImageJ.

The following gold electrodes were then analyzed via AFM:

- A) Pristine gold 220BT screen-printed electrode
- B) Reduced gold 220BT electrode in 0.01M H₂SO₄, starting at 0.6 V
- C) Reduced gold 220BT electrode in 0.01M H₂SO₄, starting at 1.0 V

In a similar fashion, the results from the AFM study of the gold electrodes could be predicted from the SEM images. As discussed previously, there was little visual difference between the pristine gold electrodes and the reduced gold electrodes that produced SERS response (**Figure 30**). Some variance in the surface morphology can be observed, particularly in the set of AFM images in pane B, where one area of the electrode demonstrated more “roughness” than another area. However, this was generally the case with all the gold electrodes tested, including the pristine electrode. Due to the high similarity between the AFM images for the gold electrodes, no conclusions could be made regarding the generation of nanoparticles from the CV procedure.

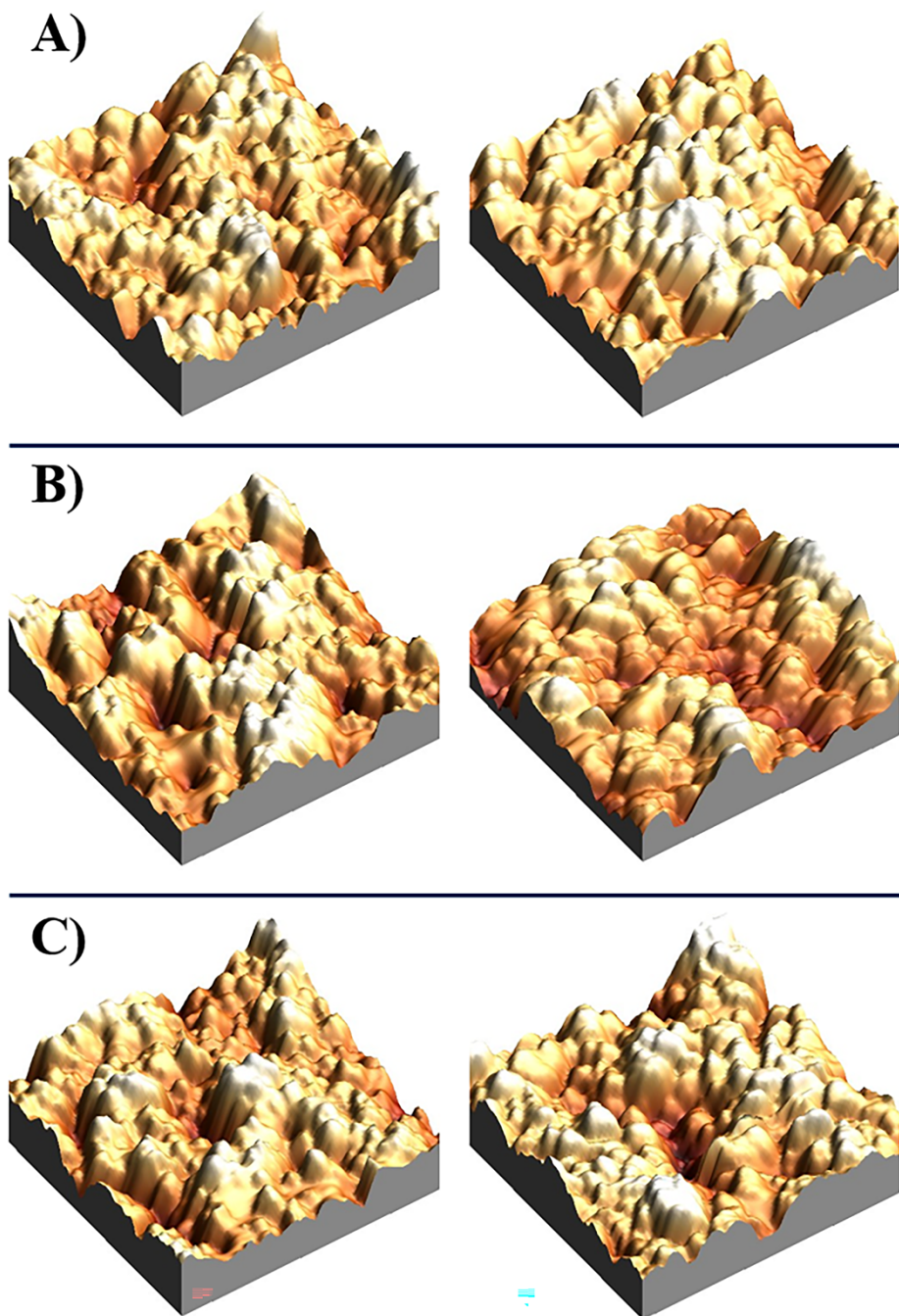


Figure 30. 3-Dimensional representation of the surface topography of A) pristine gold 220BT screen-printed electrode, B) reduced gold 220BT electrode starting the CV procedure at +0.6 V, and C) reduced gold 220BT electrode starting the CV procedure at +1.0 V. Reduction was performed in 0.01M sulfuric acid. Two different areas of the same electrode are shown in each set with 20 μm by 20 μm analysis area. AFM images were obtained with the use of the WVU Shared Research Facility.

Again, it is important to note that the SERS effect was observed in the experiments even though a difference in the electrode could not be visually distinguished.

The characterization of the electrode surfaces provided valuable insights into the processes occurring during an electrochemical generation of a SERS substrate on a metal working electrode. Specifically, the silver electrode demonstrated clear generation of nanostructures on the working electrode, which could be altered based on the number of oxidation/reduction steps or the supporting electrolyte. These nanostructures are responsible for the observation of the SERS phenomenon in these EC-SERS applications.

2.7.1.5. Targeting the identification of fentanyl and fentanyl analogs: MPD

After demonstrating the ability of electrochemical methods to generate SERS-capable substrates using the C013 silver screen-printed electrodes, these electrodes were chosen for the development of an EC-SERS screening approach for fentanyl and then extended to fentanyl analogs.

MPD is an amperometric method, meaning that potentials are held constant for some amount of time rather than being scanned like in a voltammetric method. However, MPD makes use of multiple different potentials and allows control over the time that these potentials are held constant, allowing the user to quickly switch the applied potential between oxidizing and reducing potentials for a target analyte. For the sake of simplicity, one can generally think of positive potentials as oxidizing potentials and negative potentials as reducing potentials, although this depends on the analyte of interest. Looking at **Figure 31** as an example, the first step in the MPD procedure prepares the surface by applying a high oxidizing potential. During this step, the current values have a curve from positive currents toward negative currents, indicating that oxidation is occurring. The next step in the process is the application of a reduction potential that can be identified by the rapid decrease in the current, signifying a change in potential and negative currents signaling reduction. This is similar to the third step, which is also a reduction; however, the change in potential did not result in a large current response like the first step in the process.

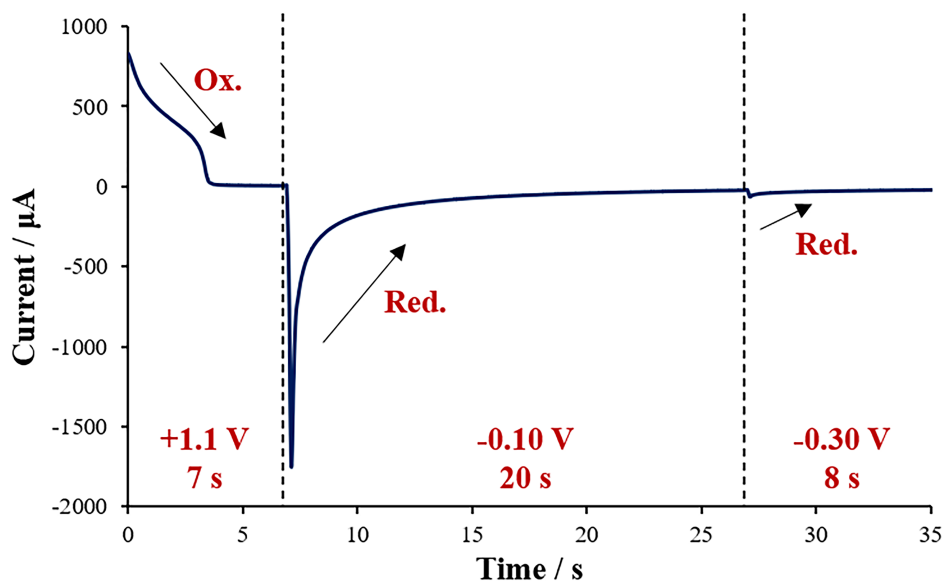


Figure 31. Multi-pulse amperogram for 21 $\mu\text{g}/\text{mL}$ cocaine in 100 mM KCl on a 220BT gold electrode. A three-step MPD method was employed, although for the diagram the third step was shortened for illustration purposes.

These processes can be visualized better by viewing the optimized MPD method for a sample containing 15 μM fentanyl analyzed on a silver electrode. **Figure 32** shows the resulting amperogram from the MPD procedure. This MPD procedure is a five-step process with two oxidation and reduction cycles. Recall that the oxidation step is required to provide the metal ion into the solution from the electrode surface. In contrast, the reduction step reduces that metal back to the electrode surface as a nanostructure. In this case, a short oxidation pulse is applied before the reduction phase for 30 seconds. In the case of this procedure for fentanyl, the OCP (open circuit potential) is hypothesized to allow the fentanyl molecule to adsorb and come in contact with the surface of the nanostructures and the working electrode. Finally, the second cycle of oxidation and reduction can be seen to be enhanced compared to the first cycle, indicating more current flowing, and by association, more redox processes occurring. It is this second cycle of oxidation and reduction that contributes to a very large increase in the SERS signal for fentanyl, as will be seen later. Additionally, since close proximity is a requirement for the SERS process to occur, the adsorption at OCP concentrated the fentanyl molecule in the region of the newly developed nanoparticles, also serving to increase the signal. It is also important to note the stabilization of the current following the initial application of the reduction current and OCP.

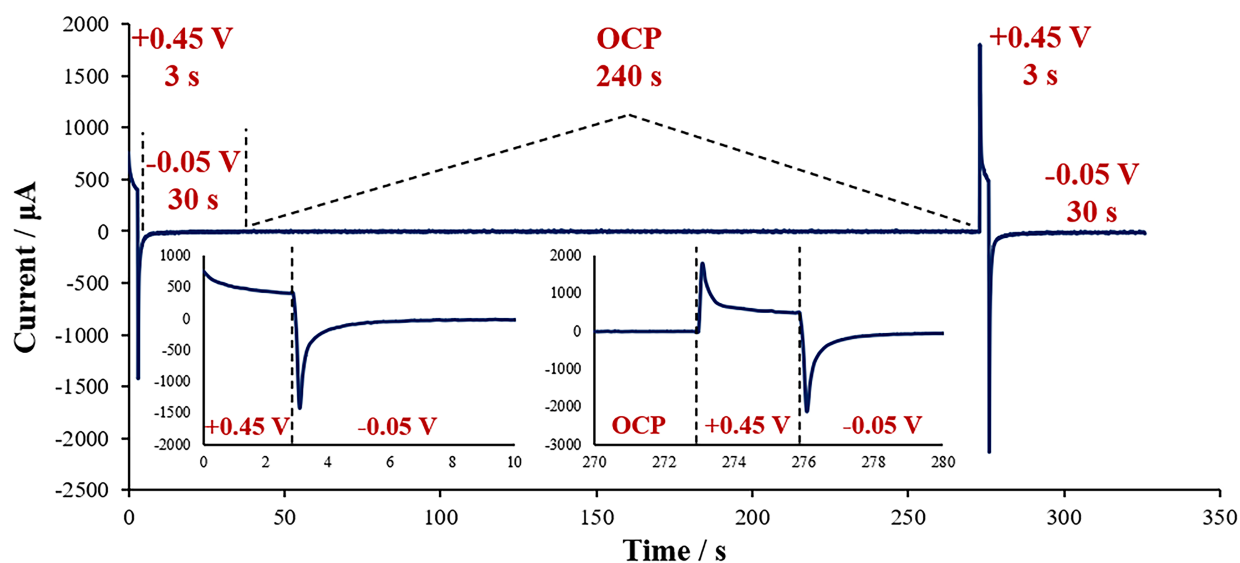


Figure 32. Multi-pulse amperogram for 15 μM fentanyl analyzed in supporting electrolyte of 0.1 M perchloric acid supplemented with 0.01 M potassium chloride. Insets provide a focused view of the two oxidation and reduction regions within the MPD procedure, demonstrating the change in current values and increased current flow upon the second cycle.

Before diving deeper into the data for fentanyl, a description of the optimization process for the applied potentials will be discussed briefly. As stated above, the first experiment is to conduct cyclic voltammetry in the electrolyte of choice with the drug and electrode material of interest. Several of these cyclic voltammetry experiments were conducted and investigated to choose several different potentials of interest related to any oxidation and reduction processes occurring within the voltammogram. A typical MPD procedure can be built using just the list of suspected potentials of interest and assessing the effect of adding or removing potentials or changing the amount of time as potential is applied by comparison of the intensity of the Raman bands for the analyte molecule. As an example, **Figure 33** demonstrates the importance of the OCP step in the analysis procedure for achieving detection of low-concentration samples. Without the OCP step in the MPD procedure, the

Raman intensities for the bands of interest are quite low; however, when the OCP stage is incorporated, the intensity of the bands increases by about seven times.

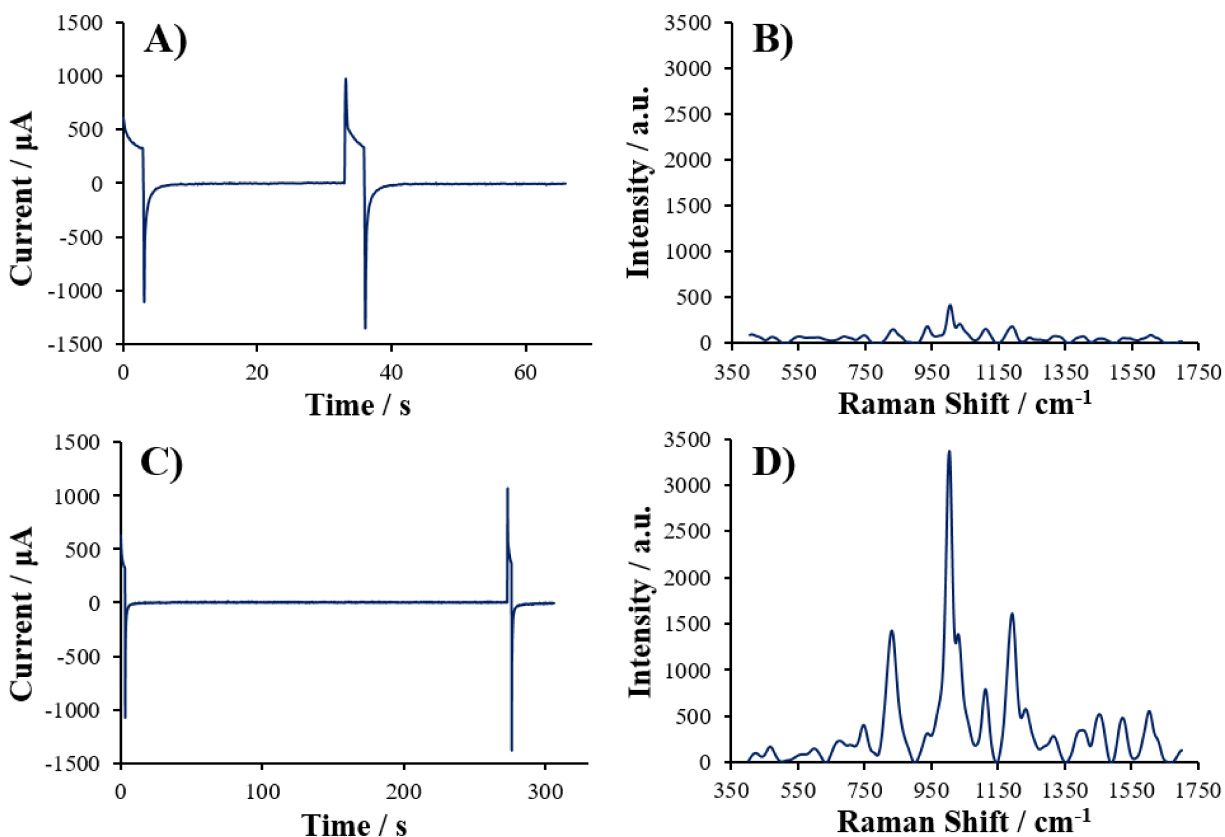


Figure 33. Comparison of 1.5 μM Fentanyl samples analyzed using **A)** an MPD procedure without the inclusion of OCP and **C)** an MPD procedure with the inclusion of OCP along with the Raman response recorded from these OCP methods in **B** and **D** with an integration time of 1000 ms and laser power of 379.1 mW with a 785 nm laser.

2.7.1.6. Differentiation of Analogs and Limits of Detection

Following the optimization of the amperometric and Raman parameters for analysis, the characterization of the model analyte could be completed. For this report, fentanyl served as the model drug for analysis and assessment of the strength of the method. As such, fentanyl was characterized via the optimized method at a high concentration to establish the known Raman shift bands and characteristics of the drug. **Figure 34** demonstrates what is termed an amperoRamagram, the Raman intensity for a chosen band plotted against the time axis of the applied multi-pulse method overlaid with the current response of that MPD method. In this case, the band chosen was the one with the greatest intensity and occurred at 1004 cm^{-1} . By displaying the data like this, one can clearly see how the electrochemical potentials are directly related to the enhancement of the Raman signal and differentiate at what point the largest signal occurs on the amperogram. In order to understand this process more, the Raman spectra from various points along the amperogram have also been shown. Looking at the spectrum collected initially, this represents what the Raman spectrum would look like if only analyzed using Raman alone with no electrochemical method applied. Clearly, this spectrum provides no information regarding the analyte(s) present in the sample. However, following this

oxidation with a reduction step, the spectrum collected at 31 seconds demonstrates the initial enhancement of the Raman scattering and corresponds to the generation of the silver nanostructures on the surface. However, the initial enhancement is minimal. Next, the blue spectrum corresponds to the Raman spectrum from the OCP step of the MPD procedures, while the purple is from the second oxidation stage. Again, both demonstrate no enhancement of the Raman signal and the inability to detect the fentanyl molecule. As mentioned previously, this OCP step was essential for increasing the Raman signal by allowing time for the fentanyl molecule to adsorb close to the surface of the working electrode and nanostructures prior to the last oxidation/reduction step. The effect of the final reduction step can be seen in the green spectrum, demonstrating significant enhancement of the signal and resolution between the Raman bands. This large increase in intensity is also observed in the amperoRamagram, with the largest enhancement around 295 seconds at a potential of -0.05 V.

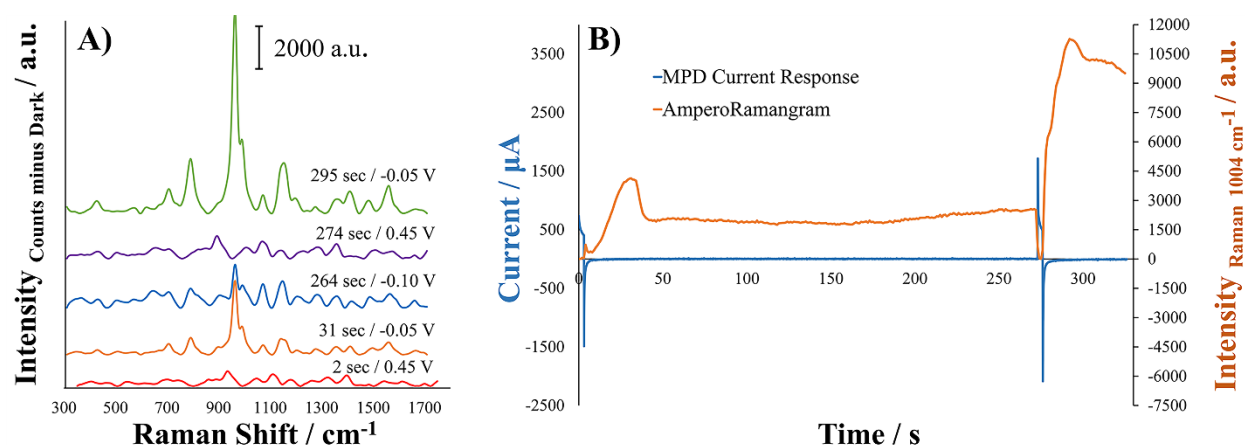


Figure 34. Analysis of a 5 μM solution of fentanyl in 0.1 M perchloric acid + 0.01 M KCl for (A) overlay of EC-SERS spectra on the same y-axis scale for the evolution of the Raman spectrum of Fentanyl during the MPD method and (B) MPD current response generated from the applied potential at different times and evolution of the Raman signal during the in-situ preparation of the electrode SERS substrate. A large increase in the Raman signal can be noted around 295 seconds following the second reduction potential. Spectra were collected with a 1 second integration time at a laser power of 379.1 mW.

Now with an understanding of the behavior of the fentanyl molecule with the optimized MPD method, the characteristic Raman bands for the molecule could be determined. **Figure 35** provides the EC-SERS spectrum for fentanyl, along with labels for the bands of interest corresponding to the identification of the fentanyl structure with the functional groups identified and outlined in **Table 21**. Focusing first on the Raman bands of greatest intensity, the band at 1004 cm^{-1} was attributed to C-C-C trigonal bending related to the presence of aromatic rings in combination with 1030 cm^{-1} for C-C stretch and/or CH in plane bending. Other bands of significant interest include 1237 cm^{-1} (C-N piperidine stretch) and 612 cm^{-1} (R-CO-NR₂ in plane bending). The other bands can be attributed as follows 619 cm^{-1} (-C-C symmetric in plane ring bending), 654 cm^{-1} (C-H rocking), 746 cm^{-1} and 830 cm^{-1} (symmetric C-H bending), 1179 cm^{-1} (C-C stretching and CH in plane bending), 1200 cm^{-1} (symmetric C-C stretching), 1285 cm^{-1} (C-H twisting), 1447 cm^{-1} (CH₃ and CH₂ bending), and 1583 cm^{-1} and 1600 cm^{-1} (C-C symmetrical stretch).

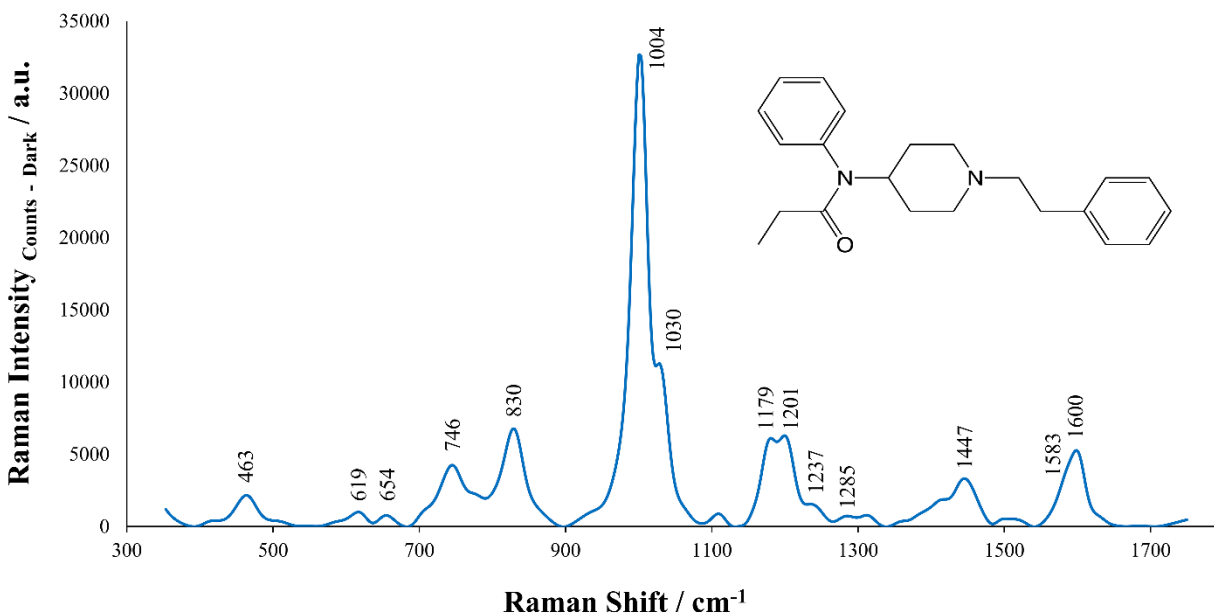


Figure 35. EC-SERS spectrum for a 25 µg/mL fentanyl sample with Raman bands of interest labeled.

Table 21. Raman shift values and their corresponding vibrational descriptions. Descriptions based on literature sources [117–119].

EC-SERS Raman Shifts/ cm ⁻¹	Vibrational Description
619	C-C-C sym in plane ring bend R-CO-NR ₂ in plane bending
654	C-H rocking
746	symmetric C-H bending
830	asymmetric C-H bending
1004	C-C-C trigonal bend
1030	C-C stretch CH in plane bending
1179	C-C stretch CH in plane bending
1200	symmetric C-C stretch
1237	C-N piperidine stretch, C-H wag
1285	C-H twist
1447	CH ₃ and CH ₂ bending
1583	C-C sym stretch
1600	C-C sym stretch

Keeping this fentanyl spectrum in mind, the rise of fentanyl within the drug landscape has prompted many other compounds to be synthesized and distributed throughout the market, both for licit and illicit purposes. What makes fentanyl so interesting is that an extreme number of analog compounds have been synthesized. As a reminder, an analog compound is a compound that is structurally related

and similar to another compound that is currently in existence. That is to say, part of the original molecule's structure is retained in the analog's structure. It has been estimated that there may be 2,000 or more possible analog combinations for fentanyl. While it may be impossible to analyze and assess all these analogs with this method due to time and cost, assessing a subset of analogs is important to determine their sensitivity to an EC-SERS type of method. Indeed, it was important to assess if this method could differentiate analogs that were extremely similar in structure. As a reminder, **Figure 36** demonstrates the areas of interest in the core fentanyl structure. For this part of the study, the amide moiety (highlighted in a red box in **Figure 36**) was chosen to test the EC-SERS method. Therefore, only fentanyl analogs with substitutions to this area of the molecule were considered for comparison.

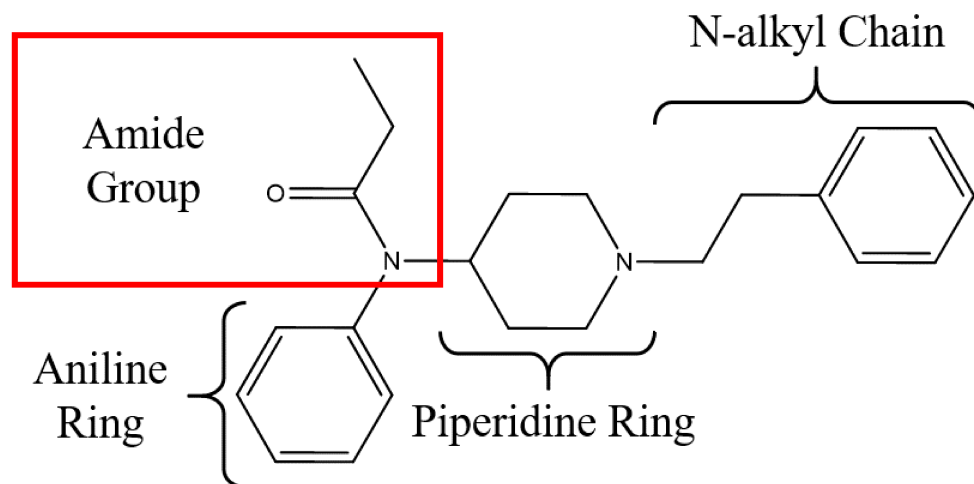


Figure 36. Fentanyl core structure outlining the areas of interest for modification to generate fentanyl analog structures through substitutions. The amide moiety is highlighted in red and was the area of interest for this part of the study.

Although other fentanyl analogs were chosen for study, substitutions to the amide group will be the initial focus. Brief results for other analogs of interest will be provided at the end of this section as supporting data from additional experiments. To this end, six different fentanyl amide-group analogs were assessed, including: acetyl fentanyl, methoxyacetyl fentanyl, furanyl fentanyl, acryl fentanyl, valeryl fentanyl, and 4-ANPP (despropionyl fentanyl). **Figure 37** provides the individual structures and Raman spectra for each fentanyl analog, as well as highlights for the differences between these analogs. One can see a large amount of similarity in these structures and in the Raman spectra themselves, making this a difficult task. However, the EC-SERS method demonstrated an ability to differentiate most of the analytes with ease at higher concentrations. Differences in the presence and absence of certain bands, as well as changes in the ratios of some bands, could be observed. One difficulty seen for these analogs was in the case of differences within the alkyl chain of the amide group. For example, acetyl fentanyl contains one carbon, fentanyl contains two carbons, and valeryl fentanyl contains four carbons within this chain. The spectra for these three analytes are especially similar to each other and differ only slightly, making their differentiation difficult and tricky, although it may be possible.

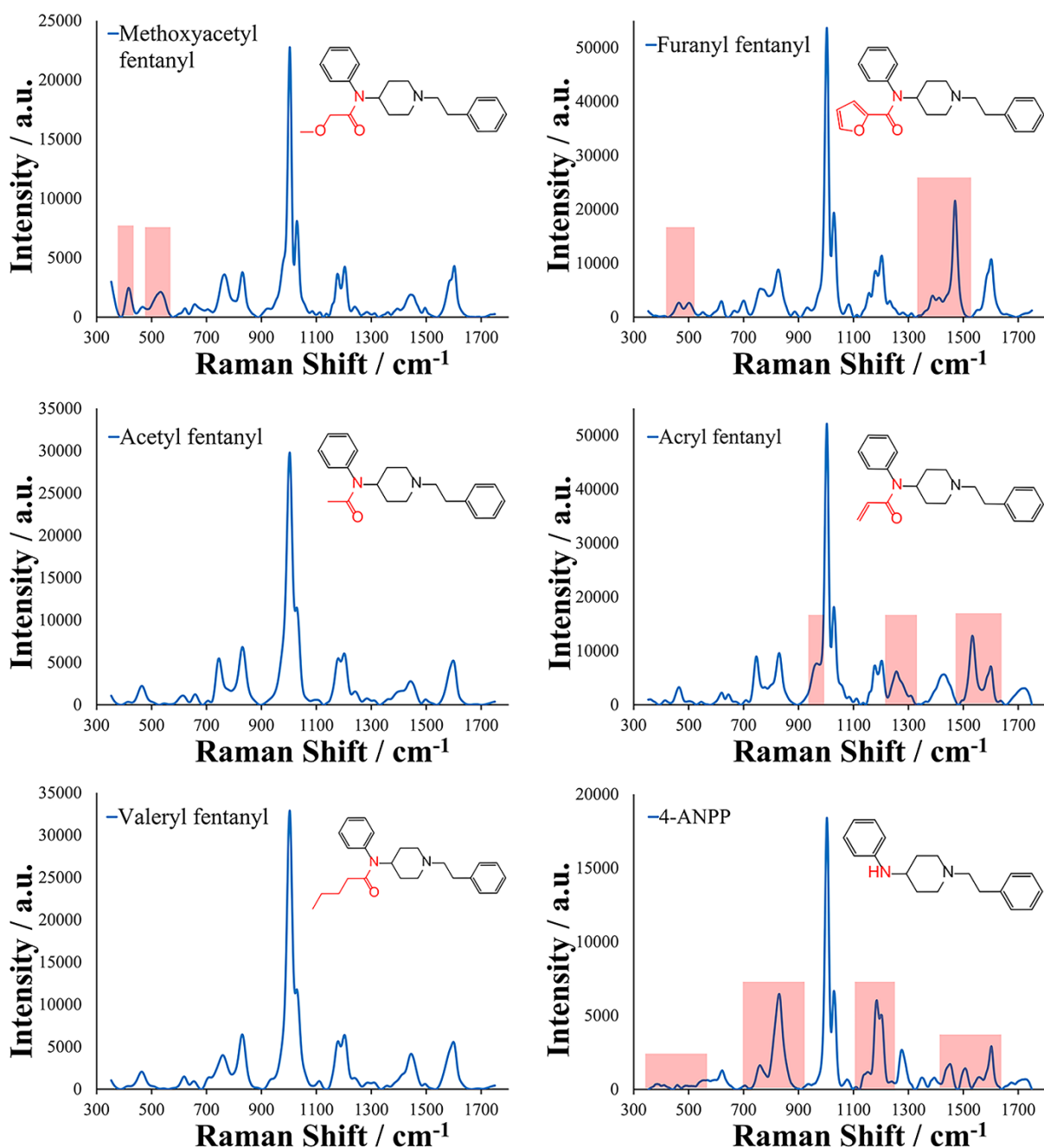


Figure 37. EC-SERS spectra were collected for fentanyl analogs with substitutions made at the amide group (highlighted in red) of the core structure for methoxyacetyl fentanyl, furanyl fentanyl, acetyl fentanyl, acryl fentanyl, valeryl fentanyl, and 4-ANPP. Raman shifts related to the amide group substitution are highlighted in light red in the spectra.

With concern for the other analogs of interest, more noticeable differences are apparent. Methoxy acetyl fentanyl demonstrates the presence of two Raman bands early in the spectrum and shift values around 400 cm⁻¹ and 500 cm⁻¹, which are absent in the other analogs. In the case of furanyl fentanyl, a large difference in the spectrum can be observed at approximately 1460 cm⁻¹. It is important to note

that this structure is the most different out of the six analogs. The twin shifts at the start of the spectrum were also unique to this analog. Acryl fentanyl contains an additional double bond, a location of π electrons, suggesting good Raman activity. Several differences can be seen in its spectrum, including the most obvious difference at a Raman shift of approximately 1530 cm^{-1} . The last analog but of great interest was 4-ANPP, which demonstrated multiple differences in Raman shifts, including the absence of intense peaks at the beginning of the spectrum, a change in the ratios for the shifts at 760 cm^{-1} and 830 cm^{-1} , a change in the ratio of the shifts at 1190 cm^{-1} , and several differences in the Raman shift area between 1400 cm^{-1} and 1700 cm^{-1} .

This analog was of interest because instead of a substitution to the amide group, the amide is removed completely for this compound and represents a precursor for fentanyl synthesis as well as a major metabolite of fentanyl in the body. This molecule demonstrated heightened sensitivity to the EC-SERS approach leading to the discussion on the establishment of the limit of detection (LOD) for each of these compounds. The LOD was established experimentally through the analysis of samples of decreasing concentration and assessed as the ability to detect the main peak of the spectrum at three times the response of the blank samples. For this approach, both the height and area of the main band at 1004 cm^{-1} were determined. This same process was performed for four blank samples, where the height and area response for anything within this region was recorded and averaged together ($n = 4$) for the blank response before comparison with the analog samples. The following limits of detection were determined for the analogs and were in the low to the mid-parts-per-billion range:

4-ANPP (despropionyl fentanyl)	= 10 ng/mL
Acetyl fentanyl	= 100 ng/mL
Fentanyl	= 100 ng/mL
Methoxyacetyl fentanyl	= 100 ng/mL
Valeryl fentanyl	= 100 ng/mL
Furanyl fentanyl	= 300 ng/mL
Acryl fentanyl	= 500 ng/mL

As stated earlier, 4-ANPP had an LOD of 10 ng/mL, a full order of magnitude (10 times) lower than the other analog compounds. This enhancement in the sensitivity should be directly related to the structure of the molecule, which completely lacks the amide moiety. The absence of this functional group provides a structure that can be thought of as more linear and with less steric hindrance than the other fentanyl analogs. This may allow this molecule better access to the electrode surface and the nanostructures, improving the absorption to the generated nanostructures, possibly due to free nitrogen and an improved molecular orientation on the surface of the electrode. **Figure 38** provides the Raman spectra obtained for 4-ANPP, demonstrating the sensitivity.

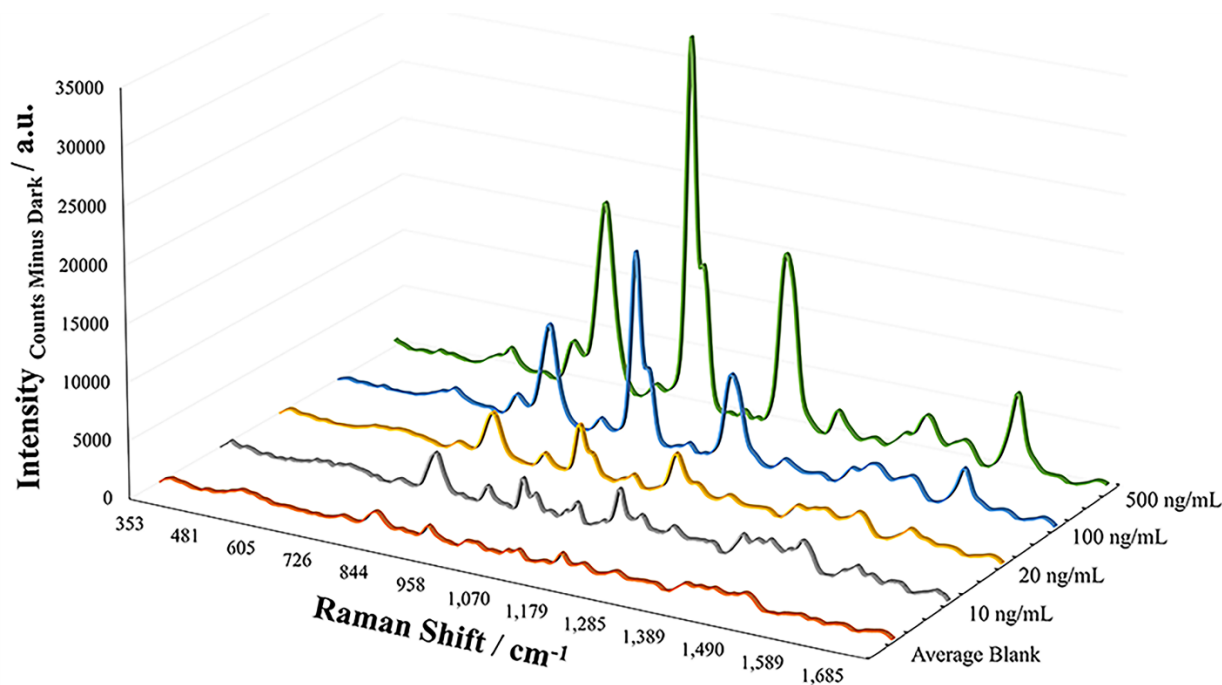


Figure 38. EC-SERS spectral overlays demonstrating the LOD studies for 4-ANPP, showing an LOD of 10 ng/mL.

The opposite effect was seen for the two fentanyl analogs with the most difference in the amide groups (furanly and acryl fentanyl). While these groups, especially the double bonds, may have initially been thought to provide an electron-rich environment, it is possible that these additions to the moiety served to inhibit either orientation or adsorption characteristics of the molecule, leading to high limits of detection. Although furanly fentanyl contains one more double bond than acryl fentanyl, it still demonstrated a lower LOD. This may be due to the slight “conjugation” of the five-member ring structure, allowing for sufficient enhancement of the Raman signal in comparison to the single, double bond in acryl fentanyl.

2.7.1.7. Quantitative Capabilities

Following the assessment of the limits of detection and ability to differentiate various analog compounds, it was of interest to determine if the EC-SERS method was amenable to quantitative analysis scenarios. Historically, Raman and SERS measurements have suffered from the difficulty in obtaining quantitative data due to the nature of the SERS and Raman phenomenon being linked to more than just the concentration of the analyte within the sample like the orientation of the molecules. Therefore, fentanyl was again chosen to investigate the reproducibility and quantitative character of the EC-SERS method, which also provides a measure of the reproducibility of the *in situ* generation of the SERS substrate. To this end, a calibration curve was established spanning the low/mid-parts-per-billion range to the low parts-per-million range for a final analytical measurement range of 0.170 $\mu\text{g/mL}$ to 3.4 $\mu\text{g/mL}$ with a 5-point curve. Each calibration measurement was repeated in triplicate with new electrodes for each sample for a total of 15 different measurements. **Figure 39** provides the calibration curve.

Excellent linearity was achieved for this approach with an R^2 of 0.9939. To assess the ability and accuracy of this calibration curve, water samples were chosen for analysis since it is not unlikely that fentanyl may enter waterways and water treatment plants due to the high prevalence of this molecule in the entirety of the United States. For this, tap water was spiked with fentanyl at two different concentrations: a high of 2.5 $\mu\text{g}/\text{mL}$ and a low of 0.47 $\mu\text{g}/\text{mL}$, and measured in triplicate again. Good accuracy was demonstrated by the curve and provided a concentration of 2.77 $\mu\text{g}/\text{mL}$ and 0.53 $\mu\text{g}/\text{mL}$ for the high and low and resulting in an error of 9.7% and 12.9%, respectively. This demonstrated the reproducible character of the nanostructures that could be prepared in-situ using electrochemical methods and applied for quantitative applications.

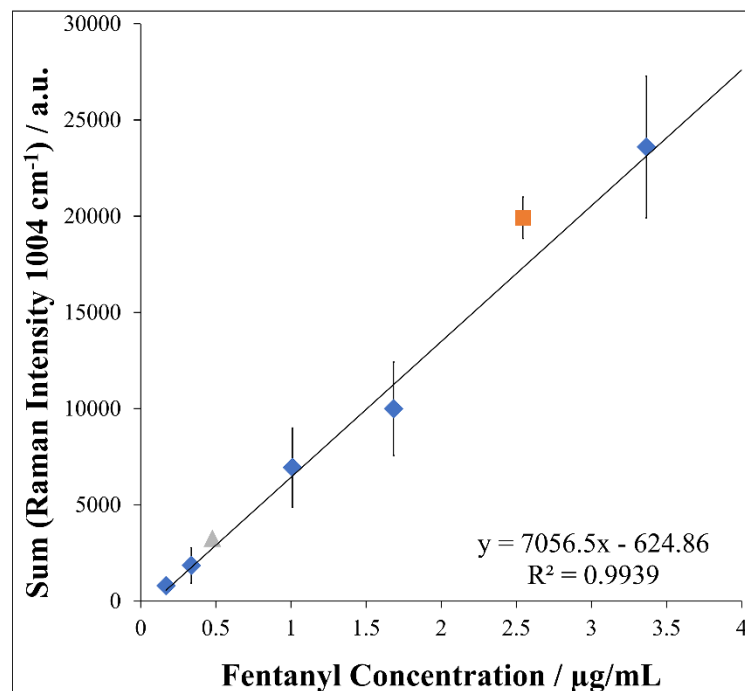


Figure 39. Calibration curve and test samples for EC-SERS quantitative analysis of fentanyl in tap water ($n=3$) with test samples assessed at both a high and low concentration within the calibration curve. The diamond points represent the concentration levels of the calibration curve, while the triangle and square points represent the spiked samples compared to the curve for the low and high concentration spikes, respectively.

2.7.1.8. Interference Studies

This EC-SERS method demonstrated the capacity for detecting fentanyl and fentanyl analogs in a reproducible and sensitive manner. However, for applications pertaining to the screening of seized drugs of abuse and other forensic applications, it is important to understand the selectivity of the technique through the assessment of potentially interfering compounds. While normal Raman can measure just about any pure compound with high accuracy and Raman intensity, the use of EC-SERS may not. In fact, this was a principle that was relied upon to increase the selectivity of this method. Specifically, due to the optimization of the electrochemical potentials applied, their order, and the times of application, the development method contains inherent selective steps, preventing the enhancement of some target molecules. In addition, not all substances are amenable to SERS, and not

all will exhibit the same level of enhancement. For this reason, other analytes of interest were assessed using EC-SERS to determine the specificity of the method for the fentanyl molecule/core structure.

In fact, many of the tested samples did not experience appreciable EC-SERS signal or enhancement, suggesting that when paired with fentanyl, it would not produce any Raman bands that could interfere with the accurate identification of the fentanyl compound in the sample. Analytes that demonstrated this lack of signal were acetaminophen, buprenorphine, caffeine, heroin, mephedrone (4-MMC), methamphetamine, and naloxone.

Figures 40 and **41** demonstrate the Raman signals in comparison to the average blank for the above-mentioned compounds. It is important to note, that while methamphetamine was included in this group, at high concentrations, some enhancement of the Raman signal can be seen for the molecule, which could provide some confusion as to the identity of fentanyl compounds. However, close investigation typically shows differences from that of fentanyl. The low signal enhancement makes the identification of methamphetamine challenging when using this approach. Additionally, the incorporation of naloxone and buprenorphine testing with the method was performed due to their relationship with fentanyl and other opioids. Buprenorphine is a partial agonist of the mu-opioid receptor and is currently used as a treatment for patients who are addicted to opioids in order to wean the patient off of the opioid easier and with fewer withdrawal problems. Naloxone, on the other hand, is a mu-opioid antagonist and is used for the quick reversal of opioid overdose as a rescue medication. Therefore, these medications are often found in combination with fentanyl in patient samples related to toxicology analysis. The absence of response for these medications is important in allowing the detection of fentanyl, which is likely to be at much lower concentrations. The analytes presented generally followed the background blank sample in their response, demonstrating no appreciable enhancement in the Raman signal and no interference with the fentanyl molecule signal.

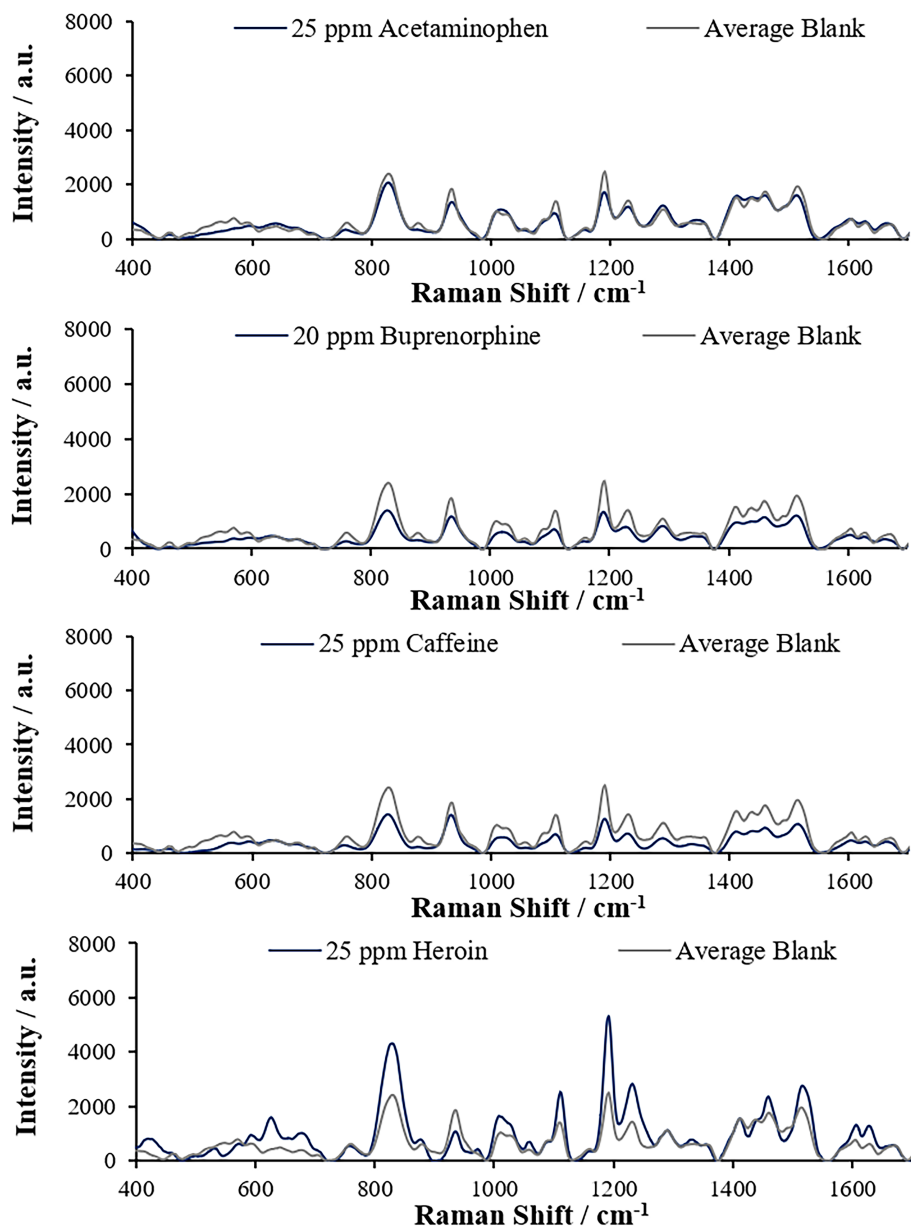


Figure 40. Raman spectra for non-interfering compounds in comparison to the average blank signal ($n=4$) for acetaminophen, buprenorphine, caffeine, and heroin.

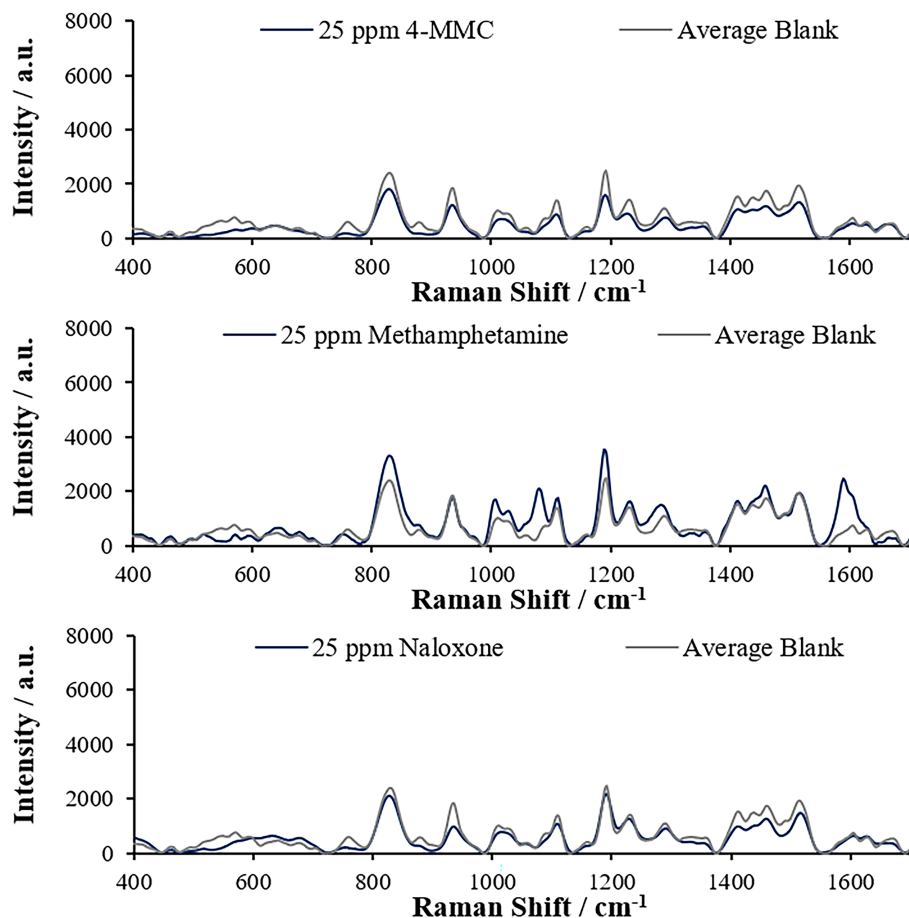


Figure 41. Raman spectra for non-interfering compounds in comparison to the average blank signal ($n=4$) for 4-MMC (mephedrone), methamphetamine, and naloxone.

This low-level response demonstrates some of the selective ability of the method. Using normal Raman, these analytes demonstrate Raman scattering response but not with this EC-SERS method. Several other analytes of interest were studied using EC-SERS, including alprazolam, cocaine, levamisole, naltrexone, and quinine.

These drugs represent a diverse group of drug classes that may be commonly encountered. Alprazolam is a prototypical benzodiazepine, and cocaine is a stimulant and one of the most encountered drugs of abuse. On the other hand, both levamisole and quinine are used as cutting agents in the preparation of street drugs. Levamisole is more commonly used in the treatment of parasitic worms in veterinary care, while quinine is used in the treatment of malaria. Lastly, naltrexone is another mu-opioid antagonist used for the treatment of opioid addiction; however, it is not generally used as rescue treatment like naloxone but is more often provided to help reduce the addictive nature of opioids in addicts.

Unlike the previous group of analytes, these compounds did demonstrate activity with the EC-SERS method. **Figure 42** shows the Raman spectra of these compounds in comparison to the average blank signal again. It is important to note the signal for cocaine. While some enhancement of the Raman

signal occurred, that signal appeared highly correlated with the signal for the blank, suggesting very weak Raman scattering activity and very limited potential interference with fentanyl detection. However, the other analytes demonstrated appreciable enhancement of the Raman scattering and the appearance of important Raman bands for identification purposes. The signal associated with quinine is presented in a separate figure in **Figure 43**, as quinine will be discussed in further detail later.

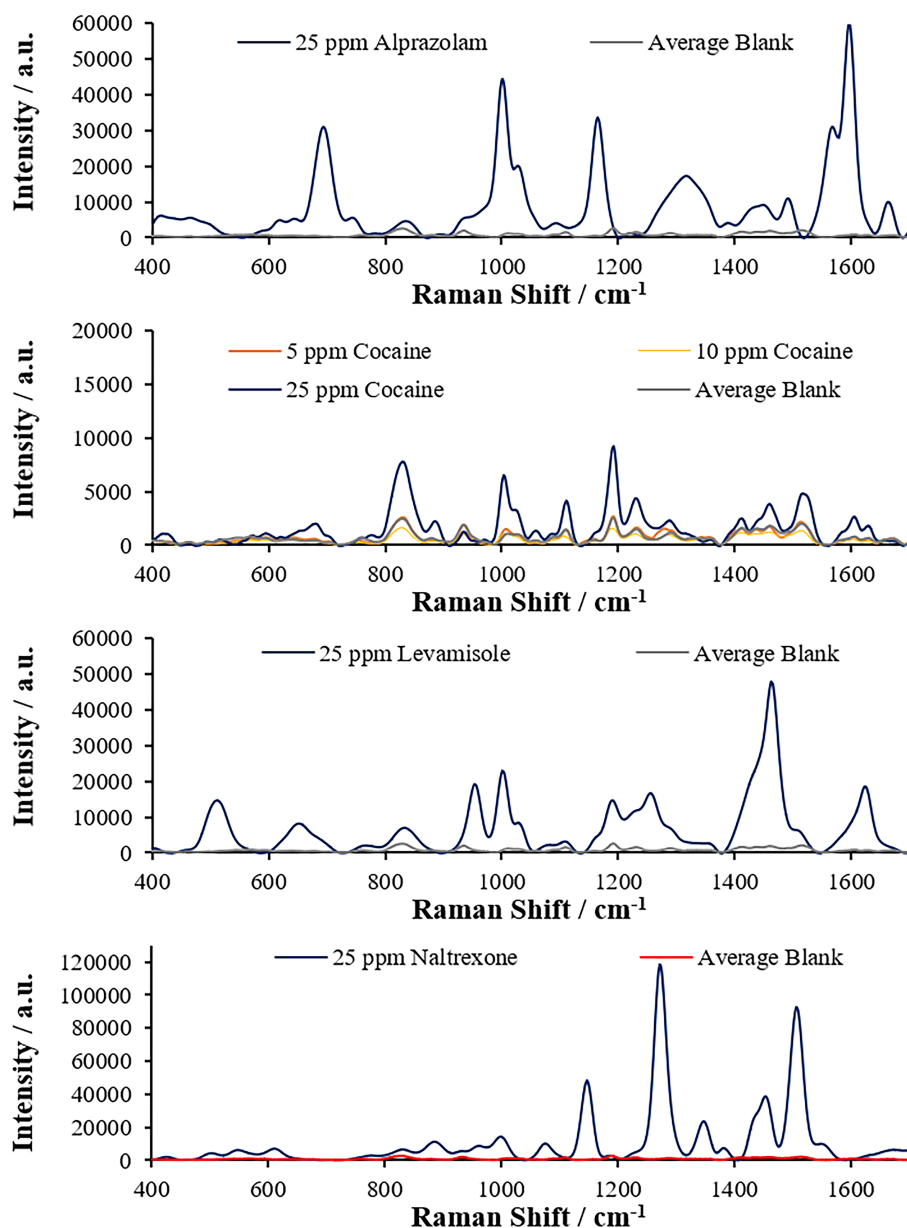


Figure 42. Raman spectra for potentially interfering compounds that present Raman signal using the EC-SERS method in comparison to the average blank signal ($n=4$) for alprazolam, cocaine, levamisole, and naltrexone.

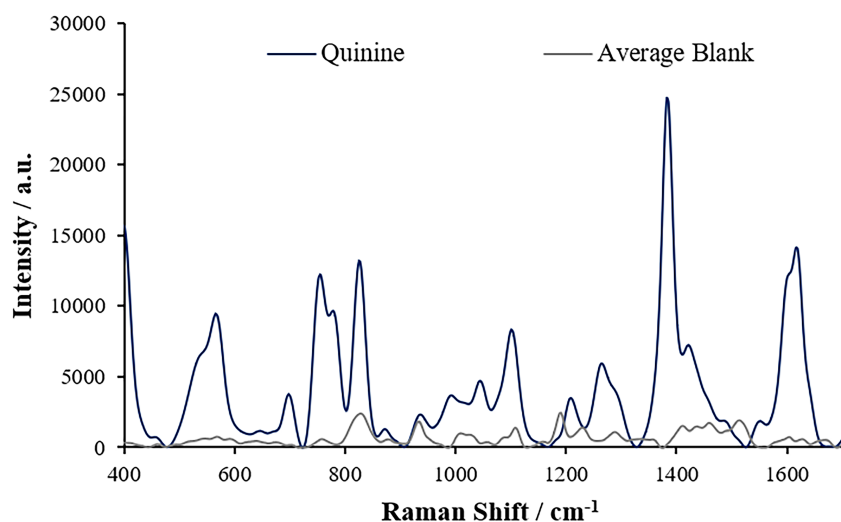


Figure 43. Raman spectrum of quinine generated using EC-SERS compared to the average blank signal ($n=4$).

2.7.1.9. Assessment of Simulated Samples

Since Raman spectroscopy is classified by SWGDRUG as a category A technique, the highly discriminating characteristics obtained from the unique presentation of the Raman bands to each compound generally allow the differentiation of one substance from others. Therefore, the individual analytes assessed above that demonstrated signal would not be expected to interfere with the identification of fentanyl. However, when present in the same sample, such as in mixtures, which are commonly encountered in seized drugs, the presence of Raman bands from multiple analytes may obscure the spectrum for each compound individually. Therefore, it was of interest to study these compounds in combination with fentanyl to determine if the mixture of analytes interfered with identification. To this end, mixture samples were prepared to replicate potential casework samples to contain fentanyl with other diluents (adulterants and other drugs of abuse) at various ratios. The binary mixtures were prepared as previously described by Cooman et al.⁴ Briefly, for a 1:4 ratio mixture samples, 10 mg of the first compound was combined with 40 mg of the second compound within a plastic baggie. The simulated powder samples were prepared in this way as solid mixtures. However, due to the absence of analytes in powder form or limited solid samples, some mixtures were prepared as liquid mixtures. To this end, each analyte was prepared to the same concentration as its pair for the mixture and then added in the appropriate ratio, in the case of a 1:4 ratio: 10 μ L and 40 μ L. **Table 22** shows the binary mixtures that were assessed.

Table 22. Binary mixtures and their ratios tested by the EC-SERS MPD method.

Binary Mixture	Ratio
Fentanyl:Cocaine	1:4
Fentanyl:Heroin	1:4, 1:20, 1:100
Fentanyl:Methamphetamine	1:4
Fentanyl:Caffeine	1:20
Fentanyl:Naltrexone	1:1, 1:4, 1:10

Since fentanyl is commonly encountered with other drugs of abuse to its high potency and relatively cheap cost, making it an exceptional cutting agent, mixtures of fentanyl with other drugs of abuse were assessed, including cocaine, methamphetamine, and heroin. While it is well known that mixtures of fentanyl and heroin have been a predominant problem in society as part of the opioid epidemic, mixtures with cocaine and methamphetamine have become more common. The results for these studies were generally as expected based on the individual drug analysis performed first. Since these analytes produced little to no Raman response, interference was not expected to occur. **Figure 44** demonstrates these three mixture analyses via EC-SERS and compares them to the Raman spectra of the pure compounds. Raman bands related to the fentanyl molecule can be clearly observed and differentiated from the background, allowing for simple and accurate detection.

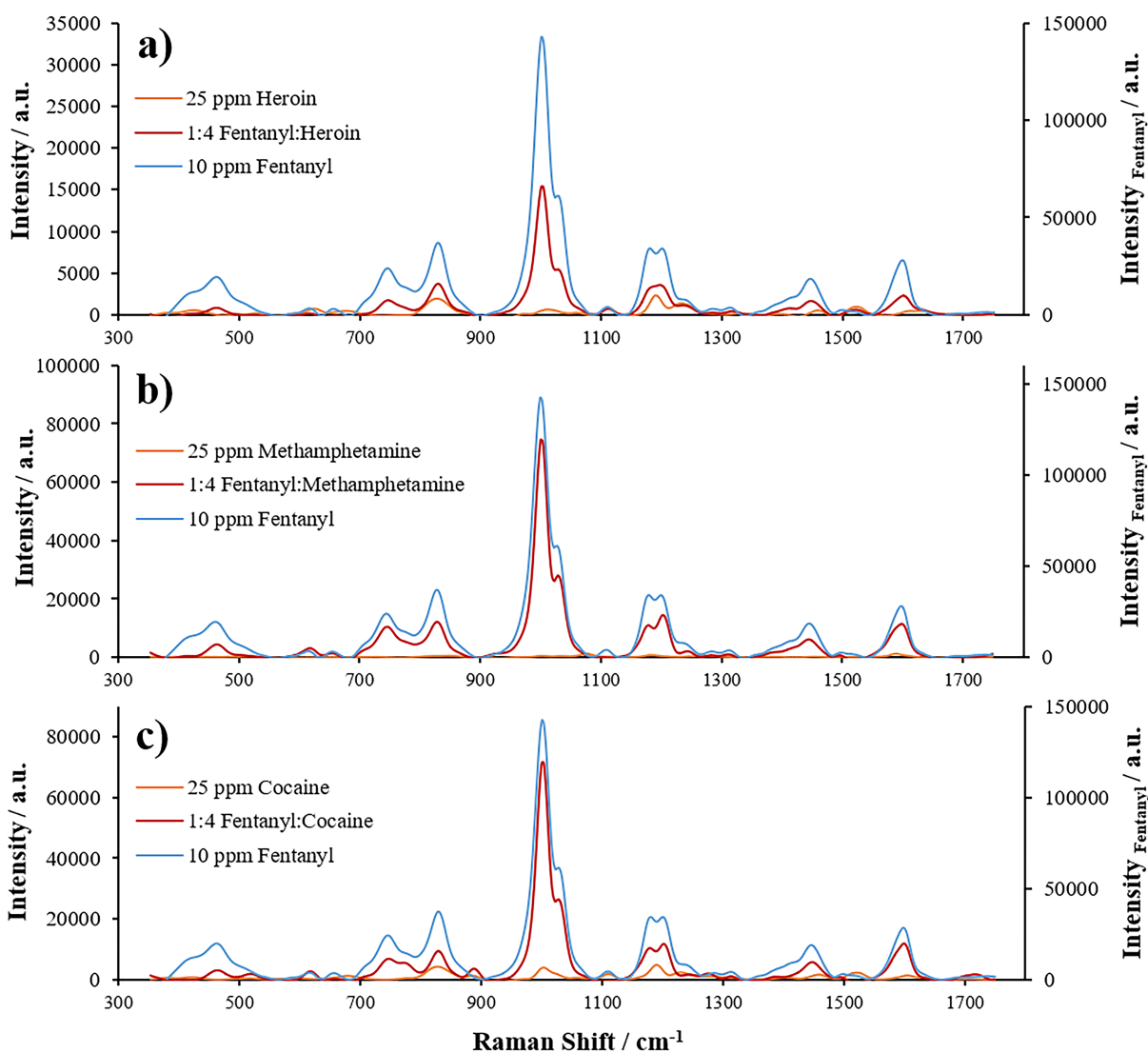


Figure 44. EC-SERS analysis of simulated seized drug samples and different mixture ratios by weight for (A) 1:4 fentanyl to heroin, (B) 1:4 fentanyl to Methamphetamine, and (C) 1:4 fentanyl to cocaine. Note that the secondary axis is for fentanyl, demonstrating higher sensitivity than the other analytes. Spectra have been background subtracted with the blank.

Additionally, drugs of abuse also contain various other cutting agents and adulterants in addition to fentanyl. One example of a commonly used substance is caffeine. **Figure 45** provides the Raman spectrum of an EC-SERS analysis of a fentanyl and caffeine mixture. Cutting agents such as caffeine can be present at much higher concentrations than their respective drugs of abuse. In relationship to fentanyl, fentanyl is typically found at very low concentrations with other compounds. In order to test this relationship with caffeine, a low contribution of fentanyl in a mixture was prepared for a 1:20 fentanyl-to-caffeine mixture ratio. This represents an approximate 5% fentanyl contribution. **Figure 46** demonstrates that even at such a low concentration of fentanyl, the EC-SERS method was easily able to enhance the signal from the fentanyl molecule. However, some differences can be noted, including a change in the band ratios between 700 cm^{-1} and 900 cm^{-1} and the appearance of two additional peaks that may have arisen from the interaction between the two analytes. However, fentanyl can be easily identified in this sample, demonstrating the strength of this EC-SERS method.

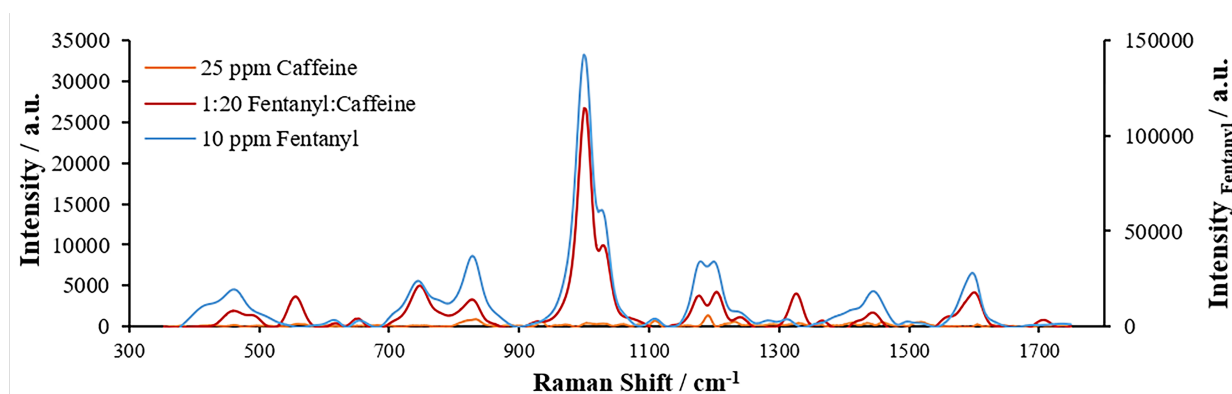


Figure 45. EC-SERS analysis of simulated seized drug sample containing a 1:20 mixture ratio of fentanyl to caffeine (5% fentanyl). Note that the secondary axis is for fentanyl, demonstrating higher sensitivity than the other analytes. Spectra have been background subtracted with the blank.

Following a similar idea, lower ratios were prepared for the fentanyl and heroin mixtures to assess the sensitivity in the presence of heroin. Although heroin did not demonstrate appreciable SERS response in the individual tests, it did appear that the presence of the molecule along with fentanyl served to suppress the Raman scattering of fentanyl, resulting in lower intensity signals compared to the Raman spectra in **Figure 46**. However, fentanyl could still be detected at these low ratios consisting of 1:20 and 1:100 fentanyl-to-heroin mixture ratios, as demonstrated in **Figure 46**.

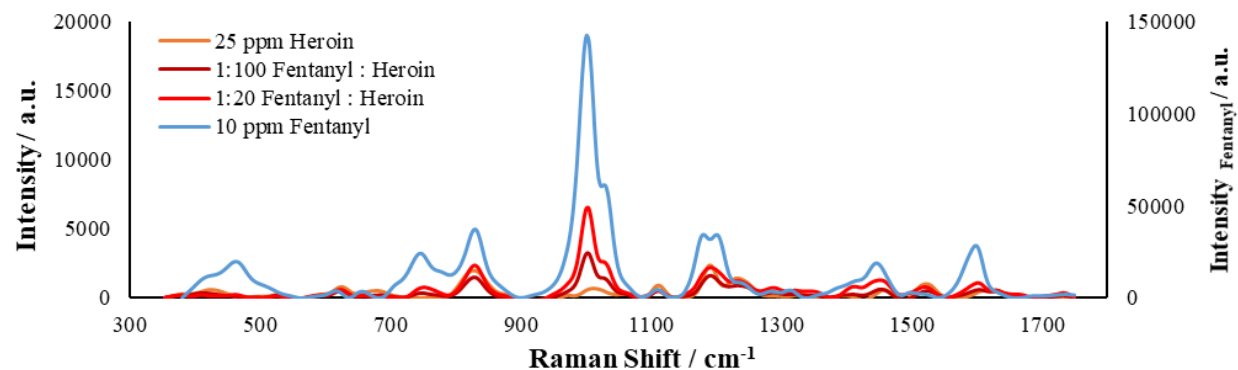


Figure 46. EC-SERS analysis of a 1:20 and 1:100 mixture of fentanyl to heroin, demonstrating accurate and visually observable identification of fentanyl at low percent contribution (1%).

Lastly, since buprenorphine and naloxone did not demonstrate EC-SERS enhancement, they were not investigated in mixtures. However, since naltrexone did demonstrate the response to the method, various mixture ratios of fentanyl and naltrexone were prepared for 1:1, 1:4, and 1:10 mixture ratios. **Figure 47** demonstrates the comparison of these mixtures with the pure compounds and includes the remainder of the individual analytes in panel 'a'. Recall that the Raman bands differ drastically between naltrexone and fentanyl. Also, recall that for the SERS effect to occur, the analyte of interest must be in close proximity to the SERS substrate or adsorbed to the SERS substrate. Looking at panel 'b' for the 1:1 mixture ratio of fentanyl and naltrexone, the spectrum for the mixture cannot be differentiated from that of the pure fentanyl spectrum, including the ratio of split peak bands to each other and relative intensity. However, upon decreasing the amount of fentanyl to a 1:4 mixture, some contribution from naltrexone begins to become visible, as highlighted by the dashed lines in the figure. It is important to note that the majority of the spectrum is still highly correlated with the pure fentanyl spectrum, although some new Raman bands begin to be seen as shoulders and very small peaks. Finally, upon decreasing the fentanyl contribution to a 1:10 mixture ratio, Raman bands related to the naltrexone molecule can be observed. While some of these new additions to the mixture spectrum correlate directly with the naltrexone molecule, some of the new bands do not. These changes to the spectrum are evident at 1114 cm^{-1} , 1195 cm^{-1} , 1234 cm^{-1} , 1527 cm^{-1} , and 1630 cm^{-1} . However, when considering the requirements for SERS, these differences can be explained. First, the selective enhancement of the fentanyl molecule over another EC-SERS active analyte demonstrates the preferential adsorption of the fentanyl molecule to the SERS substrate over that of naltrexone, a touted benefit and aid to selectivity of the EC-SERS method, shown in real time in this figure. In addition, it is most likely a competitive adsorption process, where fentanyl can outcompete naltrexone for sites on the SERS substrate. Additionally, the seemingly uncorrelated peaks may result from the proximity of the two molecules to each other, altering the geometry of the molecules adsorbed or a result of adsorption of molecules on top of each other. Regardless, the high preference for the fentanyl molecule is clear and provides evidence for the selectivity of the method.

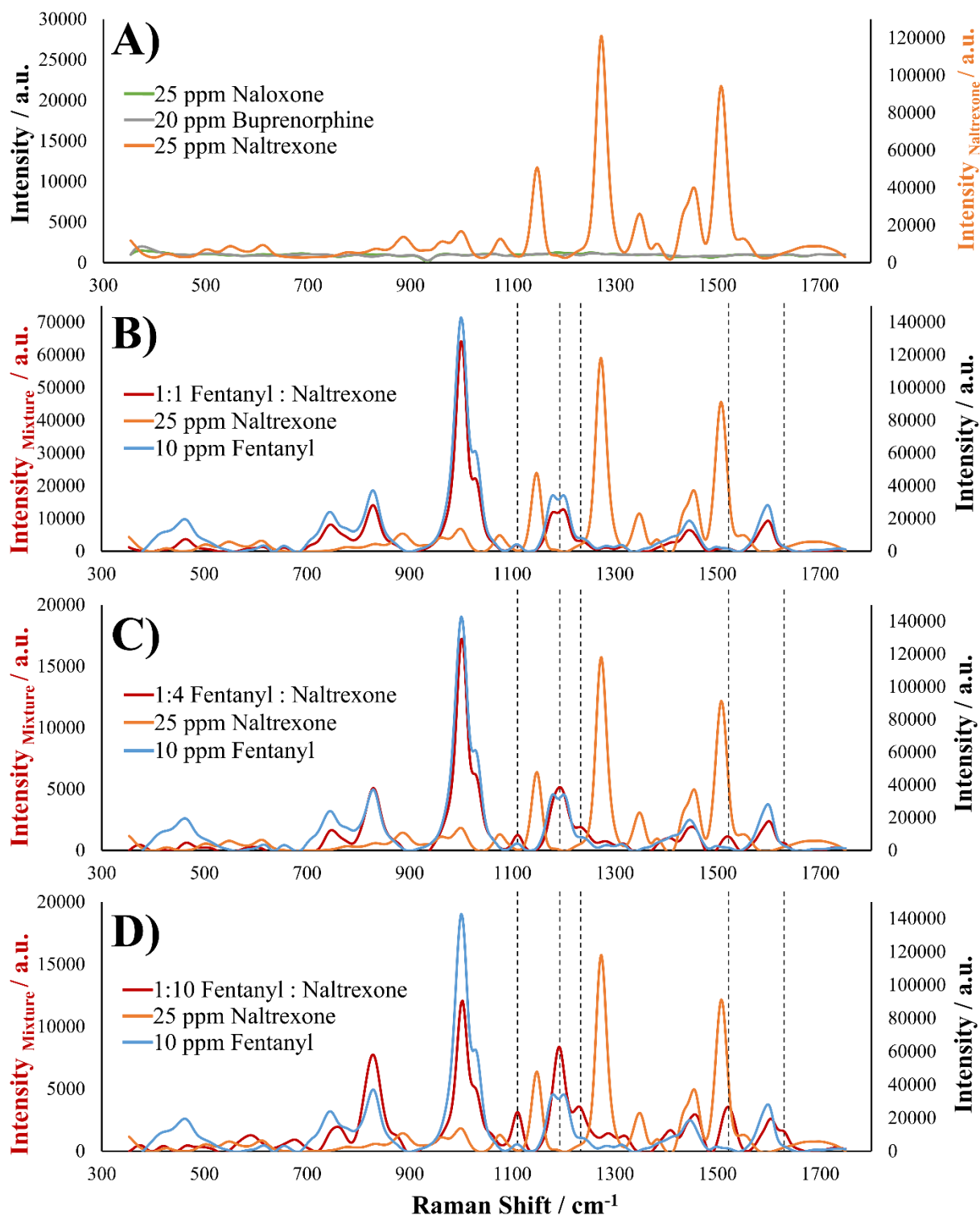


Figure 47. EC-SERS analysis of a) Naloxone, Buprenorphine, and Naltrexone as potential interfering compounds and simulated mixture samples of fentanyl and naltrexone containing b) 1:1 Fentanyl to Naltrexone, c) 1:4 Fentanyl to Naltrexone, and d) 1:10 Fentanyl to Naltrexone compared to the pure compounds. Note the differences in the primary and secondary axes between (a) and (b,c,d).

2.7.1.10. Performance on Authentic Samples

While the EC-SERS method demonstrated excellent selectivity and sensitivity on the test sample population and simulated binary mixtures, the true measure of the ability of the method is its fit-for-purpose, which can be assessed using authentic samples. Several problems may be presented by authentic seized drug samples, including the incorporation of many different types of analogs and the inclusion of many different compounds in the mixture. As such, this method has been proposed as a screening method for fentanyl compounds in drug samples, meaning that identification of any fentanyl analog/fentanyl-like compound is the goal, with specific identification of the fentanyl analog as a secondary outcome.

For this goal, collaboration with the Maryland State Police Forensic Sciences Division provided access for authentic adjudicated seized drug specimens. In total, 24 samples were tested using the developed EC-SERS method with ground-truth results provided by GC-MS analysis. Following these analyses, LC-MS/MS was performed on a subset of the samples as additional ground truth and to provide quantitative analysis. The authentic samples represented an extremely difficult sample set, as multiple compounds were present in most of the samples. **Table 23** provides an overview of the number of compounds in a single sample and how many of the authentic samples contained that number of compounds, as confirmed by GC-MS. For the authentic samples, it is important to remember that the EC-SERS method serves as a screening tool for fentanyl and fentanyl analogs and is not touted as a replacement for confirmatory analytical methods but rather a tool to provide informed decision-making regarding analyst safety and what confirmatory methods to use.

Table 23. Number of compounds contained in each authentic sample.

Number of Compounds in the Sample	Number of Authentic Samples
1	10
2	5
3	0
4	5
5	1
6	2
7	1

2.7.1.11. Comparison to Chemical Color Tests

Current screening protocols commonly utilize chemical color tests, but these tests may struggle with the presence of multiple compounds in the same sample, may be subjective, and may be problematic considering the prevalence of novel psychoactive substances in the drug landscape, including fentanyl analogs.⁶⁰⁻⁶⁴ Subjectivity may be introduced in these tests, where results could depend on the experience of the chemist in interpreting colors, especially those colors where the shade may denote differences. One example is the Marquis test, where an orange color may indicate methamphetamine or fentanyl, while a salmon color may indicate cocaine, and a range of yellows to oranges to reds may indicate a number of drugs.⁶⁵⁻⁶⁸ Generally, a color testing scheme is utilized with multiple color tests to overcome these challenges and provide discrimination between drugs and drug classes since a series of identical results may be more unlikely. Although the number of tests must be considered in terms of time, sample size limitations, and solvent/waste issues. As such, color will generally only provide a class of drug or tentative identification of a single drug or group of drugs.

As a comparison, the results of chemical color tests performed at the MSP forensic laboratory are also shown in **Figure 48** for the majority of samples, along with presumptive identifications and remarks. Due to the subjective and presumptive nature of the color tests, it is difficult to provide an accurate assessment of the results as there were multiple instances where several analytes could have been the correct conclusion. However, there was one instance (5 %) of a false positive for heroin when no heroin was detected via GC-MS or LC-MS/MS. There were multiple instances (30 %) where the results of the testing scheme were not as expected for the target compounds, and these were categorized as inconclusive without providing a suggested identification for the purposes of this paper. Finally, 65 % of the samples were correctly identified presumptively for at least one controlled compound or samples with no controlled substance, with the caveat that more than one compound may produce the observed result, lowering the analytical significance. Similar results were observed in the literature.⁶⁹

This targeted EC-SERS method provides an opportunity to selectively monitor and screen samples for fentanyl-like compounds with the possibility of analog differentiation and identification. The benefit of this approach is increased analytical significance added from the addition of a vibrational spectroscopic technique providing structural information. Therefore, the EC-SERS method provides an improvement over the current chemical color test schemes, allowing improved differentiation between fentanyl/fentanyl analogs and other drugs of abuse. Another point of comparison is chemical consumption and waste. Preparation of the color test reagents used here required cobalt thiocyanate, concentrated sulfuric acid and formaldehyde (Marquis), mercuric chloride, and potassium iodide (Mayer's).^{65,70} Aside from the preparation and chemical waste generated from these tests, these compounds also include many hazards, including targeting lung, thyroid, eyes, and kidneys, toxicity, corrosivity, carcinogenicity, heritable genetic damage, reproductive toxicity, and long-lasting aquatic environmental impact.^{65,71} This EC-SERS method uses only dilute perchloric acid and water as the solvent for analysis, reducing waste and improving on safety hazards; although perchloric acid still has its own hazards to be aware of, including corrosivity and targeting the thyroid on repeated exposure, these hazards are reduced in diluted form. Additionally, EC-SERS requires interaction with a powdered sample one time versus multiple times for color testing. Finally, the time required to complete presumptive testing should be considered. This color testing scheme was previously reported by Sisco et al. and took 18.6 min for a set of five samples.⁶⁹ The targeted EC-SERS method is versatile in the fact that there are two enhancement regions for the SERS effect. The first occurs within the first 30 s, and the second is near the end of the experiment, around 300 s. In this way, samples with higher concentrations of target analyte can be easily observed and enhanced in the first 30 s, while samples with very low percent contributions will demonstrate increased sensitivity during the second enhancement. Therefore, a set of five samples could take between 5 min and 30 min to be screened, including sample preparation. As such, the time requirement is similar between the color testing scheme and the EC-SERS method.

	Fentanyl	Quinine	Heroin	Cocaine	Caffeine	Acetyl codeine	Acetyl fentanyl	Carfentanyl	Chlorisobutryl fentanyl	Cyclopropyl fentanyl	FIBF	Furanyl fentanyl	Methamphetamine	Methoxyacetyl fentanyl	Morphine	Tramadol	U-47700	Acetaminophen	Mannitol	Noscapine	Procaine	Cobalt Thiocyanate	Marquis	Mayer's	Presumptive ID	
Unknown 1*																						-	-	-	-	
Unknown 2																										Fent/Meth
Unknown 3																										Heroin
Unknown 4																										Heroin
Unknown 5																										Fent/Meth
Unknown 6																										Fent/Meth
Unknown 7																										Inconclusive
Unknown 8																										Fent/Meth
Unknown 9																										-
Unknown 10																										Inconclusive/Coc/Quin
Unknown 11																										Fent/Meth
Unknown 12																										Inconclusive/Her
Unknown 13																										Fent/Meth
Unknown 14																										Inconclusive/Quin
Unknown 15*																										-
Unknown 16*																										-
Unknown 17*																										Coc
Unknown 18																										Fent/Meth
Unknown 19																										Inconclusive/Quin
Unknown 20																										Inconclusive/Quin
Unknown 21																										Inconclusive/Quin
Unknown 22*																										Fent/Meth
Unknown 23*																										Fent/Meth
Unknown 24*																										Inconclusive
	Top 5 Analytes				Drugs of Abuse												Diluents			Chemical Color Tests						

Figure 48. Graphical comparison between identifications provided by GC-MS (gold/yellow), LC-MS/MS (blue), and chemical color tests. Solid, gold-colored squares and asterisk indicate samples not analyzed via LC-MS/MS. For chemical color tests, square color corresponds to the color change result of the test. Color test legend: blue circles = blue specs, two colors = mix of the colors, 'NR' = no reaction, 'E' = effervescence, and for Mayer's: all yellow = yellow precipitate, large white circle = white precipitate, yellow gradient to medium white circle = yellowish-white precipitate. Presumptive identification is provided based on the color test with the following abbreviations: Fent = fentanyl, Meth = methamphetamine, Quin = quinine, Coc = cocaine.

2.7.1.12. Targeted Fentanyl EC-SERS Performance

As noted earlier, this multipulse amperometric detection (MAD) EC-SERS method was employed onsite at the MSP laboratory to rapidly analyze the authentic samples. **Figure 49** provides the Raman spectra from the EC-SERS analysis for six authentic samples of interest, including single compound and multi-drug samples. These spectra are compared to a known fentanyl standard and analyzed using the same method. Unknown 7 was confirmed to be fentanyl by GC-MS and provided excellent correlation to the fentanyl standard by EC-SERS, providing a positive identification. Unknown 1 demonstrated a very different type of sample due to the identification of six compounds in the sample by GC-MS.

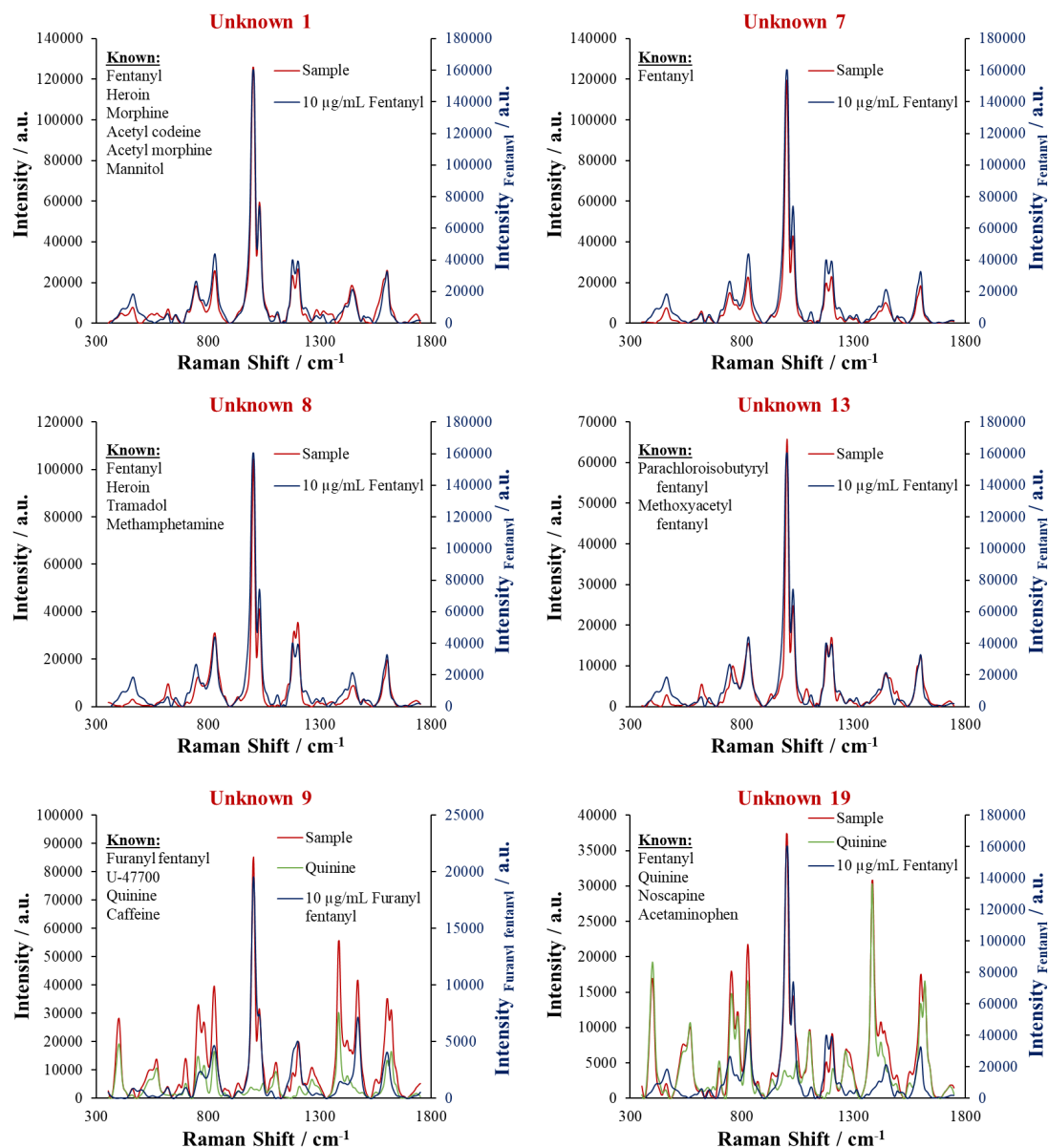


Figure 49. Targeted EC-SERS spectra for the analysis of authentic seized drug samples demonstrating the correlation and identification of fentanyl and fentanyl-like compounds within the samples providing evidence toward the screening capabilities of EC-SERS.

Despite a large number of compounds in this sample, the targeted EC-SERS method demonstrated excellent selectivity, preferentially amplifying the fentanyl signal, allowing identification through the correlation of major Raman bands with the fentanyl standard. Similar results are seen for Unknowns 8 and 13. During the development of the MAD method, quinine was found to be the most significant interfering compound, demonstrating enhancement of the Raman signals. Unknowns 9 and 19 demonstrate this interference from quinine. However, these samples still allowed tentative identification of a fentanyl compound in the sample. It is also interesting to note that Unknown 9 demonstrated a large Raman band around 1467 cm^{-1} , correlating with furanyl fentanyl. This, along with the largest Raman band provided a tentative identification of furanyl fentanyl. It is worth noting another sample with interesting results, Unknown 12. Analysis of this sample via GC-MS did not provide sufficient signal for the identification of fentanyl but did identify heroin. However, analysis by the targeted EC-SERS method provided a presumptive identification of fentanyl. This was confirmed via the LC-MS/MS analysis of the sample. This provides an excellent demonstration of the increased sensitivity and reliability of this targeted EC-SERS method for the screening of seized substances. **Figure 50** demonstrates the EC-SERS spectrum for Unknown 12.

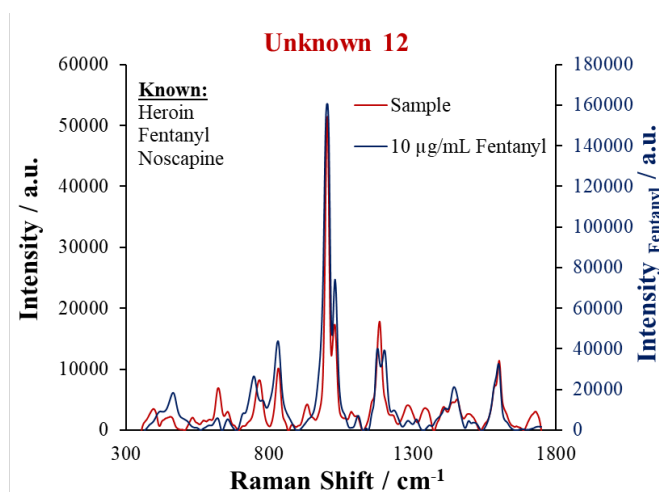


Figure 50. Screening identification of fentanyl in an authentic seized drug sample that was approximately 4 % fentanyl by weight according to LC-MS/MS analysis, demonstrating the sensitivity of the EC-SERS approach.

While interference from quinine was demonstrated previously, it is important to present examples where this interference resulted in a false negative conclusion. **Figure 51** demonstrates two examples of authentic samples where the quinine signal overwhelmed the signal from fentanyl, although the main Raman band for fentanyl can still be observed. Unknown 3 provides an excellent opportunity to observe this effect since this sample contained only fentanyl and quinine. The LC-MS/MS data was used to determine the ratio of fentanyl to quinine that may prevent successful identification. The ratio of fentanyl to quinine in Unknown 3 was 1:29 and in Unknown 20 was 1:9. In general, the ratio in samples that still afforded identification of fentanyl was 1:3.

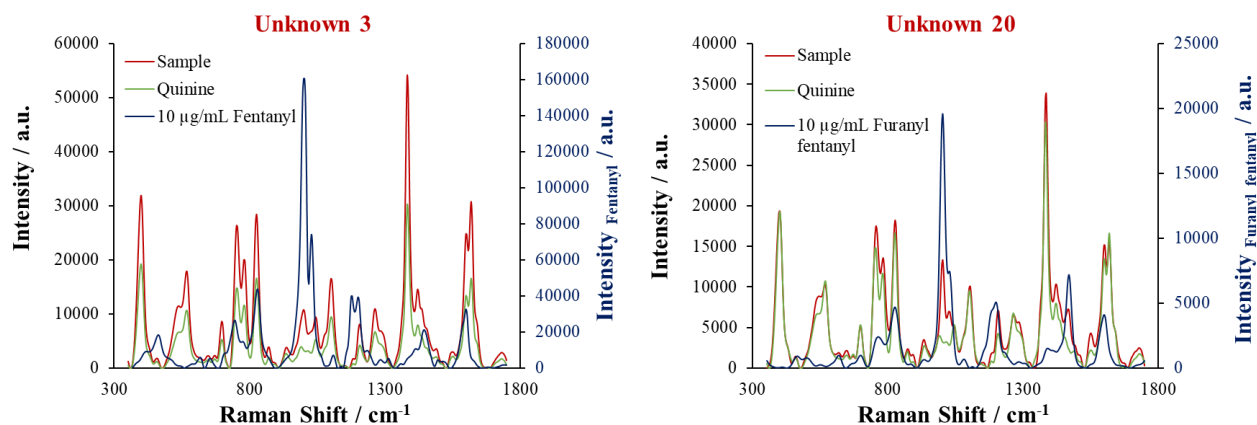


Figure 51. Targeted EC-SERS spectra for authentic samples containing quinine, demonstrating the interference exhibited by this molecule when present in the seized samples. Ground truth identifications were as follows: Unknown 3 contained fentanyl and quinine and Unknown 20 contained furanyl fentanyl, U-47700, and quinine.

Although this *in situ* EC-SERS method was targeted toward fentanyl, high concentrations of other analytes may still present some Raman signal due to the enhancement from the SERS substrate. However, it is important to note that the signal from these other molecules is significantly smaller than that seen for fentanyl.

Using the ground-truth data from the GC-MS analysis, the performance of the *in situ* targeted EC-SERS method was assessed based on correct identification of fentanyl or a fentanyl-like substance in the authentic data set. Out of the 24 authentic seized samples, there were no false positives for fentanyl. However, there were several false negatives, which were all a result of interference from quinine in the sample. It is important to note that the LC-MS/MS data provided an opportunity to assess the relative percent contribution of fentanyl or fentanyl analogs to the overall sampled mass from the seized specimens.

As demonstrated in our previous work, identification of fentanyl was possible at low percent contributions, a significant advantage to this type of screening method. When considering fentanyl, the average weight percent of fentanyl in this data set was approximately 6 %. When taking into account all fentanyl and fentanyl analogs individually, the average weight percent of these was also approximately 6 %; however, when considering the total contribution of fentanyl-like compounds in a sample, the average weight percent increased to approximately 9 % due to some samples containing multiple fentanyl-like compounds. **Table 24** provides the performance measures of the targeted fentanyl EC-SERS method for screening authentic seized samples, demonstrating the effectiveness of this screening approach.

Table 24. Performance rates calculated based on the authentic seized samples. A total of 14 of the samples were identified as containing fentanyl or a fentanyl analog, 7 samples did not contain a fentanyl-like substances, and 3 samples contained a fentanyl-like substances but were not identified by the EC-SERS screening.

$FP = \frac{100 * FP}{TN + FP}$	False Positive	0 %
$FN = \frac{100 * FN}{TP + FN}$	False Negative	17.6 %
$TN = \frac{100 * TN}{TN + FP}$	True Negative	100 %
$TP = \frac{100 * TP}{TP + FN}$	True Positive	82.4 %
$Accuracy = \frac{100 * (TP + TN)}{TP + TN + FP + FN}$	Accuracy	87.5 %

In summary, a Spectro electrochemical approach such as this electrochemical surface-enhanced Raman spectroscopy (EC-SERS) screening method provides several advantages over traditional color testing, including improved selectivity, reduced chemical waste and hazards, and the ability for targeted approaches. Unlike other SERS applications that require many synthesis steps and materials, EC-SERS utilizes a simple and effective electrochemical generation of the SERS substrate, improving reproducibility for a fast, simple, and inexpensive method. The EC-SERS approach presented here represents a targeted screening for fentanyl-like substances that is rapid and effective, providing a powerful technique with high discrimination ability for seized drugs. Using a screen-printed electrode platform allows this methodology to be portable for laboratory or field operation, increasing the usefulness and ability of the EC-SERS method. In addition, a simple sampling approach using just the tip of a spatula was implemented, allowing for a small amount of the seized sample to be tested easily. This screening approach, previously developed by our group, was applied to authentic samples from the Maryland State Police. Excellent detection capabilities were demonstrated with positive fentanyl identifications on samples that averaged 6 % to 9 % fentanyl or fentanyl-like substances. This targeted method was selective, demonstrating preferential enhancement of the fentanyl signal compared to other drug analytes, allowing for the exclusion of cocaine and methamphetamine, as well as other analytes. Quinine was identified as the major interfering compound, solely leading to the false negative results of approximately 18 % (3 samples) in the authentic samples. The overall accuracy for screening for fentanyl-like substances in the authentic data set was approximately 87 %, an increase from the color test results. This EC-SERS method represents one of the first demonstrations of EC-SERS applications toward forensic drug analysis and represents a step forward in developing novel screening methods for drugs of abuse that can improve the reliability of analysis, the safety of first responders, and selectivity in a changing drug landscape while helping to streamline further confirmatory testing. A summary of major EC-SERS database is compiled as monograph Appendix B. A more detailed explanation is provided in the following publication for the fentanyl analogs, and an upcoming publication, where the targeted method will be explained in more detail.

Colby E Ott, Martin Perez-Estebanez, Sheila Hernandez, Kendra Kelly, Kourtney A Dalzell, M Julia Arcos-Martinez, Aranzazu Heras, Colina Alvaro, Luis E. Arroyo. Forensic Identification of Fentanyl and its Analogs by Electrochemical-Surface Enhanced Raman Spectroscopy (EC-SERS) for the Screening of Seized Drugs of Abuse. *Front. Anal. Sci.*, 10 February 2022 <https://doi.org/10.3389/frans.2022.834820>

2.8. PARTICIPANTS AND OTHER COLLABORATING ORGANIZATIONS

This research has provided a robust platform for training the next generations of forensic scientists in current and emerging technologies aiming for future adoption in forensic laboratories. A comprehensive plan was designed to evaluate Raman and Spectro electrochemical tools as an emerging technology for seized-drug detection. Direct cooperation with a forensic science laboratory, along with the partnership of a private business enterprise, and logistically supported via three external collaborators, provide a robust framework to evaluate the novel technology. Our proposal provided unique training and education to several students to become better prepared for the future workforce. The graduate and undergraduate students will have the opportunity to learn about experimental design, operate state-of-the-art instrumentation (GC/MS and LC/MS, Raman and Electrochemical devices), collect data with portable instruments, and perform statistical interpretation of the data. Also, they will gain entrepreneurship skills while interacting with a private business collaborator in developing sensors as a potential solution to tackle drug identification. The interaction with crime laboratories and law enforcement will enhance their understanding of needs in the judiciary system. All of these active learning skills will help them to boost their future careers in forensic science.

Moreover, this project's resources and research settings have provided all undergraduate and graduate students the unique opportunity to present their results at scientific venues. The opportunities provided to undergraduate researchers, some of them first-generation university students or minority students, have served as an essential foundation for their professional development. Four of our undergraduate researchers joined the graduate school (three of them continue in my research group and the other one at another institution), and the remaining joined the workforce. These students' achievements and STEM professional preparation are, in our opinion, the most valuable product of NIJ-funded efforts like this one.

Table 25. List of main participants and collaborating organizations

Participant Name	Affiliation	Role	Funding support	Contributions
Luis E. Arroyo	West Virginia University	Principal investigator	Yes	Managed the project and directly supervised students on the analysis by EC, EC-SERS, GC/MS, LC-MS and statistical interpretation of the data. Supervised management plans.
Maria Julia Arcos Martinez, Alvaro Colina, Aranzazu Heras	Universidad de Burgos	EC Consultant	Yes, Only Maria Julia Arcos (subaward)	Collaborated as an expert in electrochemistry in drug analysis. Dr. Arcos-Martinez provided key support to our students and also assisted with the interpretation of the data. She was co-author of manuscripts.

Participant Name	Affiliation	Role	Funding support	Contributions
Aldo Romero	West Virginia University	Computational material science	No	Aided in the application of machine learning algorithms to the identification and classification of drugs of abuse using Raman Spectroscopy and other sensors data.
Colby Ott	West Virginia University	Graduate Student (PhD)	No	Colby worked in Dr. Arroyo's group. His main contribution was in the development and optimization of electrochemical sensors for the of drugs as well as the development of EC-SERS targeted and non-targeted method. He also participated in the machine learning work.
Kylea Mathison	West Virginia University	Graduate Student (MSFS)	Yes	Kylea was an undergraduate student who joined the Arroyo group in Fall 2019. She joined the group as a graduate MS student in Fall 2020 and contributed to the implementation and validation of LC/MS analysis and application in alternative matrices to increase scope of application.
Travon Cooman	West Virginia University	Graduate Student (PhD)	Yes	Travon was a PhD student. He contributed to the GC/MS method validation for the target drugs and materials, Tactic ID Raman and DART-MS data acquisition. Also, he was responsible for the development of neural networks work.
Sara Kuberski	West Virginia University	Undergraduate student	No	Sara worked during the Spring of 2021 as part of fulfillment of RAP forensic chemistry program. Her most important contribution was analysis of buprenorphine, naltrexone via

Participant Name	Affiliation	Role	Funding support	Contributions
				EC as well as fentanyl. She joined graduate education at another institution.
Erika Heyhurst	West Virginia University	Undergraduate Student	No	Erika received training in EC and contributed to the creation of drug database, chemical information and structures during Spring 2020.
Kendra Kelly	West Virginia University	Undergraduate student	No	Kendra's main contribution was assisting Colby's work in EC.
Alexis Wilcox	West Virginia University	Graduate student	No	Alexis was an undergraduate student who joined the Arroyo's group in Summer 2021. She joined the group as a graduate MS student in Fall 2021 and contributed to Raman data using the Tactic ID.
Kourtney Dalzell	West Virginia University	Graduate student	No	Kourtney was an undergraduate student who joined the Arroyo's group in fall 2019. She joined the group as graduate MS student in Fall 2020 and contributed to EC work on several drugs.
Sean McIntosh	Foothold Labs	Industry Collaborator	No	Foothold and WVU signed a MOA from March 2019 until December 2020 to cooperate on development on sensors and handheld deployable electrochemical devices. In this MOA Foothold Labs provided an in kind portable electrochemical unit called FLStat, controlled by Microsoft Surface Go.
Edward Colihan, Kia Williams, Michael Kubisko, Michael Allen	Metrohm, USA Inc.	Industry Collaborator	No	Metrohm provided support by in kind loan of a portable Raman 1064 nm, electrodes and sponsor a webinar to help in the dissemination of Spectroelectrochemistry in USA.

Participant Name	Affiliation	Role	Funding support	Contributions
Edward Sisco	National Institute of Standards and Technology (NIST)	Industry Collaborator	No	Dr. Sisco assisted with training on DART-MS technology for graduate students and also actively participated with our crime lab collaborator (Amber Burns) with casework specimens. He is a co-author in manuscripts
Amber Burns	Maryland State Police Forensic Science Division	Crime Lab Collaborator	No	The laboratory provided training in conjunction with Dr. Sisco to the graduate students, Travon, Colby, and Alexis on using the DART-MS and the analysis of evidence for forensic casework. They also provide support in the form of processing adjudicated casework samples for testing our portable units and helped in dissemination in scientific conferences in the form of co-authoring posters.
Sheri Lemons	West Virginia State Police Forensic Laboratory	Crime Lab Collaborator	No	The WV crime lab agreed to provide authentic adjudicated specimens and to measure them onsite in the near future.
Ana Lorena Alvarado, Miriam Barquero-Quiros and Jerson Gonzalez-Hernandez	University of Costa Rica, Center of Electrochemistry and Chemical Energy (CELEQ)	Academia Collaborator	No	UCR/CELEQ provided funding to one master's student, Jerson Gonzalez, to complete a technical exchange visit at WVU. Jerson's expertise in electrochemistry has been useful to our project as he trained our students on modern techniques for the modification of electrode surfaces with nanoparticles and was instrumental in one of the initial applications of EC-SERS.

2.9. CHANGES IN APPROACH.

Nothing to report.

2.10. LIMITATIONS.

Two main limitations were encountered in this study. First, the COVID pandemic prevented regular access to research labs, and partner institutions and caused delays in the acquisition of materials. Second, a planned technical visit to our partner collaborator in Spain was delayed for the same situation. These combined external factors required the solicitation of a no-cost extension to complete the totality of the proposed tasks.

III. ARTIFACTS. LIST OF PRODUCTS, DISSEMINATION ACTIVITIES, AND DATASETS GENERATED

Publication List

Reference: NIJ award # 2019-DU-BX-0030 (NIJ R&D Award)

Project Title: Fast On-site Screening of Seized Drugs y Electrochemical and Spectroscopic Tools: Identification of Fentanyl and Novel Psychoactive Substances.

01/2020-12/2022

\$267,438.00

West Virginia University, Luis Arroyo (PI)

Scholarly Products.

Scientific Manuscripts:

1. Colby E Ott, Martin Perez-Estebanez, Sheila Hernandez, Kendra Kelly, Kourtney A Dalzell, M Julia Arcos-Martinez, Aranzazu Heras, Colina Alvaro, Luis E. Arroyo. Forensic Identification of Fentanyl and its Analogs by Electrochemical-Surface Enhanced Raman Spectroscopy (EC-SERS) for the Screening of Seized Drugs of Abuse. *Front. Anal. Sci.*, 10 February 2022
<https://doi.org/10.3389/frans.2022.834820>
2. Jerson Gonzalez-Hernandez, Colby Edward Ott, Maria Julia Arcos-Martinez, Alvaro Colina, Maria Aranzazu Heras-Vidaurre, Ana Lorena Alvarado-Gamez, Roberto Urcuyo, Luis E. Arroyo-Mora. “Rapid determination of the ‘legal highs’ 4MMC and 4MEC by spectroelectrochemistry: simultaneous cyclic voltammetry and in situ surface-enhanced Raman spectroscopy”. *Sensors* 2022, 22(1), 295.
<https://doi.org/10.3390/s22010295>



3. Travon Cooman, Tatiana Trejos, Aldo Romero, Luis E. Arroyo. Implementing Machine Learning for the Identification and Classification of Compound and Mixtures in Portable Raman Instruments. *Chemical Physics Letters*. 139283. 2022.
<https://doi.org/10.1016/j.cplett.2021.139283>
4. Travon Cooman, Colby Ott, Kourtney Dalzell, Amber Burns, Edward Sisco, Luis E. Arroyo. Screening of Seized Drugs Utilizing Potable Raman Spectroscopy and Direct Analysis in Real Time-Mass Spectrometry (DART-MS). *Forensic Chemistry*. 100352. August 2021
<https://doi.org/10.1016/j.forc.2021.100352>
5. Ott, Colby E.; Cunha-Silva, Hugo; Kuberski, Sara L.; Cox, Joseph A.; Arcos-Martínez, M. Julia; Arroyo, Luis E. Electrochemical detection of fentanyl with screen-printed carbon electrodes using squarewave adsorptive stripping voltammetry for forensic applications. *Journal of Electroanalytical Chemistry*. Vol 873, 2020.
<https://doi.org/10.1016/j.jelechem.2020.114425>

Manuscripts under review:

1. ***"Transition of surface-enhanced Raman spectroscopy to the forensic drug chemistry and toxicology laboratory: Current and future perspectives"***. WIRE Wiley Review Article. Submitted (Article ID # FORSCI-256).
2. ***"Targeted Forensic Drug Screening Utilizing Electrochemical Surface-Enhanced Raman Spectroscopy (EC-SERS) Applied to Authentic Seized Drug Casework Samples"*** The final draft of this manuscript is now under **NIST internal peer review # 935896**.
3. ***"Evaluation and Classification of Fentanyl-Related Compounds using EC-SERS and Machine Learning"*** Draft is completed. Submission Pending JFS Editorial Office to Open Special Edition link.

Presentations:

1. Korean National Police University Conference. (Virtual Meeting) "Electrochemical and Spectroscopic tools with portable solutions for Seized Drug and Gunshot Residue Detection". Colby Ott and Luis E. Arroyo. December 2022.
2. Metrohm Webinar: "Spectroelectrochemistry: Drug Identification in Forensic Applications". Colby Ott and Luis E. Arroyo. August 23, 2022.
3. 2022 European Academy of Forensic Science Conference (EAFS), Session Chair, Seized Drugs. Monday May 30, 2022.
4. Mid-Atlantic Association of Forensic Scientist (MAAFS) Annual Meeting. "Evaluation of the analytical performance of a portable 1064 nm Raman instrument on simulated drug mixtures and authentic case samples using deep learning. Alexis N. Wilcox, Colby E. Ott, Travon Cooman, Amber Burns, Edward Sisco, Luis Arroyo. Newport News, VA. May 10-13, 2022.
5. 2022 Midwest Association for Toxicology and Therapeutic Drug Monitoring (MATT) Meeting. "Screening of Fentanyl/Analogues and Drugs of Abuse Utilizing Electrochemical-Surface Enhanced Raman Spectroscopy (EC-SERS)". Colby Ott, Luis E. Arroyo. Kalamazoo, MI. April 6-8.

6. 2022 Online Forensic Symposium. The Center for Forensic Science Research and Education. (CFSRE) Platform Presentation. "The Use of Spectroelectrochemistry in Seized Drug Analysis". Luis Arroyo and Colby Ott. Friday January 28th, 2022.
7. 2022 Midwest Association for Toxicology and Therapeutic Drug Monitoring (MATI) Meeting. "Screening of Fentanyl/Analogues and Drugs of Abuse Utilizing Electrochemical-Surface Enhanced Raman Spectroscopy (EC-SERS)". Colby Ott, Luis E. Arroyo. Kalamazoo, MI. April 6-8.
8. 2022 Midwest Association for Toxicology and Therapeutic Drug Monitoring (MATI) Meeting. "Development and Validation of a Quantitative Method for the Analysis of 35 Analytes in Postmortem Oral Cavity Fluid using UPLC-MS-MS. Kylea Mathison, Luis E. Arroyo. Kalamazoo, MI. April 6-8.
9. 3rd Forensic Science Brazilian Winter School. "Spectroelectrochemistry in Forensic Science: A Powerful Technique for Acquiring Orthogonal Data and Enhanced Screening". Colby Ott and Luis E. Arroyo. Virtual Meeting Federal University of Rio Grande do Sul (UFRGS) and WVU. October 25-29, 2021.
10. 13th Annual Summer Undergraduate Research Symposium "Identification of Hydroxyzine hydrochloride Utilizing Electrochemistry and Time-Resolved Raman Spectroelectrochemistry on Screen-Printed Electrodes". Kendra Kelly, Alexis Wilcox, Colby Ott, Luis E. Arroyo. Morgantown, July 29, 2021 (online poster).
11. Current Trends in Electrochemistry, 41st Meeting of the Electrochemistry Group of the Spanish Royal Society of Chemistry. 1st French-Spanish Atelier/Workshop on Electrochemistry (online meeting) "Spectroelectrochemical screening of drugs of abuse for time-resolved electrochemical and SERS detection in forensic investigations" Paris, France. Colby E. Ott, Jerson González-Hernández, Sara L. Kuberski, Kourtney A. Dalzell, Travon Cooman, Ana L. Alvarado-Gámez, Roberto Urcuyo, M. Julia Arcos-Martínez, Aranzazu Heras, Alvaro Colina, and Luis E. Arroyo-Mora. (July 6 - July 9, 2021)
12. Current Trends in Electrochemistry, 41st Meeting of the Electrochemistry Group of the Spanish Royal Society of Chemistry. 1st French-Spanish Atelier/Workshop on Electrochemistry (online meeting) "Electrochemical detection of fentanyl using screen-printed carbon electrodes for seized drugs of abuse and forensic applications" Paris, France. Colby E. Ott, Hugo Cunha-Silva, Sara L. Kuberski, Kourtney A. Dalzell, Joseph A. Cox, M. Julia Arcos-Martínez, and Luis E. Arroyo-Mora (July 6 - July 9, 2021).
13. NIJ (National Institute of Justice) -Innovations in Forensic Examination of Seized Drugs and Forensic Toxicology. Session Number: G06 "Spectroelectrochemistry: An alternative tool for Drug Detection and Identification in seized drug scenarios". Invited speaker. Luis E. Arroyo, Colby Ott. Travon Cooman. Monday, March 08, 2021.
14. Pittcon Conference and Expo. Virtual Event. "Portable Raman Spectroscopy and Mass Spectrometry Techniques for the Analysis of Seized Drug: TacticID® and AccuTOF™-DART". Travon Cooman, Colby Ott, Kourtney Dalzell, Amber Burns, Edward Sisco, Luis E. Arroyo. March 8-12, 2021.
15. Pittcon Conference and Expo. Virtual Event. "Integration of Electrochemistry and Raman Spectroscopy for Detection of Drugs of Abuse". Colby E. Ott, Jerson González-Hernández, Travon Cooman, Kylea M. Mathison, Kourtney A. Dalzell, Sara L. Kuberski, William J. Feeney, Ana L. Alvarado-Gámez, Roberto Urcuyo, M. Julia Arcos-Martínez, Aranzazu Heras, Alvaro Colina, Luis E. Arroyo. March 8-12, 2021.
16. 18th Undergraduate Research Day at the Capitol (UGRD). "Rapid Electrochemical Sensing of Acetaminophen Utilizing Screen-Printed Carbon Electrodes in Forensic and

- Environmental Applications”. Sara Kuberski, Colby Ott, Luis E. Arroyo. Charleston, WV. March 5, 2021.
17. The American Society of Crime Lab Directors (ASCLD) Lighting Talk. “Electrochemical Methods for the Analysis of Fentanyl and Seized Drugs”. Emerging Techniques and Applications for Seized Drug Analysis. October 29, 2020. Colby Ott. (Dr. Arroyo, PI).
 18. 72nd Annual Scientific Meeting of the American Academy of Forensic Science (AAFS). “Determination of Synthetic Cannabinoids AB Pinaca and AB-Fubinaca with Disposable Screen-Printed Carbon Electrodes (SPCE) Modified with Nanoparticles and Enzymes”. Julian Portuguez, Miriam Barquero-Quirós, Luis E. Arroyo. Anaheim, CA, February 17-22, 2020.
 19. 72nd Annual Scientific Meeting of the American Academy of Forensic Science (AAFS). “Electrochemical Detection of Fentanyl Using Screen-Printed Carbon Electrodes with Confirmatory Analysis of Fentanyl and Its Analogs in Oral Fluid Using Liquid Chromatography/Tandem Mass Spectrometry (LC/MS/MS)”. Colby E. Ott, Hugo Cunha-Silva, Joseph A. Cox, Julia Arcos-Martínez, Luis E. Arroyo. Anaheim, CA, February 17-22, 2020.
 20. 72nd Annual Scientific Meeting of the American Academy of Forensic Science (AAFS). “Electrochemical Screening of Synthetic Cannabinoids”. Miriam Barquero Quirós, Mario Molina Porras, Jerson Gonzalez, Luis E. Arroyo. Anaheim, CA, February 17-22, 2020.
 21. Undergraduate Research Day at the Capitol (URDC). “Development of electrochemical sensors for Buprenorphine and Naltrexone using screen-printed carbon electrodes”. Sara Kuberski, Colby Ott, Luis E. Arroyo. Charleston, WV, February 7, 2020.

Databases available:

1. [GC/MS Mass Spectral Monograph for public access](#)
2. [EC-SERS Monograph for public access](#)

IV. REFERENCES

1. Head JM. Synthetic Drug Threats in the United States [Internet]. Webinar; **2016**. <https://ndews.umd.edu/sites/ndews.umd.edu/files/u1424/JillHeadNDEWSWebinarPresentation2016.pdf>
2. U.S. Customs and Border Protection. U.S. Customs and Border Protection CBP. United States. Drug Seizure Statistics 2021. <https://www.cbp.gov/newsroom/stats/drug-seizure-statistics>.
3. Speaker PJ. Project FORESIGHT Annual Report, 2016-2017. **2018** Jun pp. 1–92.
4. Fedchak S. Presumptive Field Testing Using Portable Raman Spectroscopy **2014** Jan pp. 1–100. Report No.: 244564
5. Spicher C, Yeatman T, Alford I, Waugh L. The Evaluation of Portable Handheld Raman Systems for the Presumptive Identification of Narcotics: Thermo Scientific TruNarc. **2016** Sep pp. 1–38.
6. Colby E Ott, Martin Perez-Estebanez, Sheila Hernandez, Kendra Kelly, Kourtney A Dalzell, M Julia Arcos-Martinez, Aranzazu Heras, Colina Alvaro, Luis E. Arroyo. Forensic Identification of Fentanyl and its Analogs by Electrochemical-Surface Enhanced Raman Spectroscopy (EC-SERS) for the Screening of Seized Drugs of Abuse. *Front. Anal. Sci.*, 10 February 2022. <https://doi.org/10.3389/frans.2022.834820>
7. Jerson Gonzalez-Hernandez, Colby Edward Ott, Maria Julia Arcos-Martinez, Alvaro Colina, Maria Aranzazu Heras-Vidaurre, Ana Lorena Alvarado-Gamez, Roberto Urcuyo, Luis E. Arroyo-Mora. “Rapid determination of the ‘legal highs’ 4MMC and 4MEC by spectroelectrochemistry: simultaneous cyclic voltammetry and in situ surface-enhanced Raman spectroscopy”. *Sensors* 2022, 22(1), 295. <https://doi.org/10.3390/s22010295>
8. Travon Cooman, Tatiana Trejos, Aldo Romero, Luis E. Arroyo. Implementing Machine Learning for the Identification and Classification of Compound and Mixtures in Portable Raman Instruments. *Chemical Physics Letters*. 139283. 2022. <https://doi.org/10.1016/j.cplett.2021.139283>
9. Travon Cooman, Colby Ott, Kourtney Dalzell, Amber Burns, Edward Sisco, Luis E. Arroyo. Screening of Seized Drugs Utilizing Potable Raman Spectroscopy and Direct Analysis in Real Time-Mass Spectrometry (DART-MS). *Forensic Chemistry*. 100352. August 2021 <https://doi.org/10.1016/j.forc.2021.100352>
10. Ott, Colby E.; Cunha-Silva, Hugo; Kuberski, Sara L.; Cox, Joseph A.; Arcos-Martínez, M. Julia; Arroyo, Luis E. Electrochemical detection of fentanyl with screen-printed carbon electrodes using squarewave adsorptive stripping voltammetry for forensic applications. *Journal of Electroanalytical Chemistry*. Vol 873, 2020. <https://doi.org/10.1016/j.jelechem.2020.114425>
11. ASTM International (2014) E1683-02 Standard Practice for Testing the Performance of Scanning Raman Spectrometers.
12. ASTM International (2014) E1840- 96 Standard Guide for Raman Shift Standards for Spectrometer Calibration.

13. UNODC (2017) Guidelines on handheld Raman field identification devices for seized material.
14. Fiorentin TR, Krotulski AJ, Martin DM, et al (2019) Detection of Cutting Agents in Drug-Positive Seized Exhibits within the United States. *J Forensic Sci* 64:888–896. <https://doi.org/10.1111/1556-4029.13968>
15. Administration DE (2018) National drug threat assessment (2018). US Department of Justice.
16. Administration DE (2019) National Drug Threat Assessment 2019.
17. Drug Enforcement Administration D.O.J (2018) 2016 Heroin Domestic Monitor Program.
18. Miserez B, Ayrton O, Ramsey J (2014) Analysis of purity and cutting agents in street mephedrone samples from South Wales. *Forensic Toxicol* 32:305–310. <https://doi.org/10.1007/s11419-014-0232-y>
19. Guirguis A, Corkery JM, Stair JL, et al (2017) Intended and unintended use of cathinone mixtures. *Hum Psychopharmacol Clin Exp* 32:e2598. <https://doi.org/10.1002/hup.2598>
20. Sisco E, Verkouteren J, Staymates J, Lawrence J (2017) Rapid detection of fentanyl, fentanyl analogues, and opioids for on-site or laboratory based drug seizure screening using thermal desorption DART-MS and ion mobility spectrometry. *Forensic Chem* 4:108–115. <https://doi.org/10.1016/j.forc.2017.04.001>
21. Sisco E, Robinson EL, Burns A, Mead R (2019) What's in the bag? Analysis of exterior drug packaging by TD-DART-MS to predict the contents. *Forensic Sci Int* 304:109939. <https://doi.org/10.1016/j.forsciint.2019.109939>
22. Lian R, Wu Z, Lv X, et al (2017) Rapid screening of abused drugs by direct analysis in real time (DART) coupled to time-of-flight mass spectrometry (TOF-MS) combined with ion mobility spectrometry (IMS). *Forensic Sci Int* 279:268–280. <https://doi.org/10.1016/j.forsciint.2017.07.010>
23. Gwak S, Almirall JR (2015) Rapid screening of 35 new psychoactive substances by ion mobility spectrometry (IMS) and direct analysis in real time (DART) coupled to quadrupole time-of-flight mass spectrometry (QTOF-MS). <https://doi.org/10.1002/dta.1783>
24. SWGDRUG (2016) Scientific Working Group for the Analysis of Seized Drugs (SWGDRUG) recommendations. United States Department of Justice Drug Enforcement Administration.
25. Kudelski A (2008) Analytical applications of Raman spectroscopy. *Talanta* 76:1–8. <https://doi.org/10.1016/j.talanta.2008.02.042>
26. Harvey SD, Vucelick ME, Lee RN, Wright BW (2002) Blind field test evaluation of Raman spectroscopy as a forensic tool. *Forensic Sci Int* 125:12–21. [https://doi.org/https://doi.org/10.1016/S0379-0738\(01\)00615-6](https://doi.org/https://doi.org/10.1016/S0379-0738(01)00615-6)
27. Hargreaves MD, Page K, Munshi T, et al (2008) Analysis of seized drugs using portable Raman spectroscopy in an airport environment—a proof of principle study. *J Raman Spectrosc* 39:873–880. <https://doi.org/10.1002/jrs.1926>
28. Rodriguez JD, Westenberger BJ, Buhse LF, Kauffman JF (2011) Standardization of Raman spectra for transfer of spectral libraries across different instruments. *Analyst* 136:4232. <https://doi.org/10.1039/c1an15636e>
29. Omar J, Slowikowski B, Guillou C, et al (2019) Identification of new psychoactive substances (NPS) by Raman spectroscopy. *J Raman Spectrosc* 50:41–51. <https://doi.org/10.1002/jrs.5496>
30. Weng S, Dong R, Zhu Z, et al (2018) Dynamic surface-enhanced Raman spectroscopy and Chemometric methods for fast detection and intelligent identification of methamphetamine

- and 3, 4-Methylenedioxy methamphetamine in human urine. *Spectrochim Acta Part A Mol Biomol Spectrosc* 189:1–7. <https://doi.org/10.1016/j.saa.2017.08.004>
31. O'Connell M-L, Ryder AG, Leger MN, Howley T (2010) Qualitative Analysis Using Raman Spectroscopy and Chemometrics: A Comprehensive Model System for Narcotics Analysis. *Appl Spectrosc* 64:1109–1121. <https://doi.org/10.1366/000370210792973541>
 32. Virtanen P, Gommers R, Oliphant TE, et al (2020) SciPy 1.0: fundamental algorithms for scientific computing in Python. *Nat Methods* 17:261–272.
 33. Mozaffari MH, Tay L-L (2021) Raman spectral analysis of mixtures with one-dimensional convolutional neural network. <https://doi.org/10.48550/arXiv.2106.05316>
 34. Bjerrum EJ, Glahder M, Skov T (2017) Data augmentation of spectral data for convolutional neural network (CNN) based deep chemometrics. <https://doi.org/10.48550/arXiv.1710.01927>
 35. Wahl J, Sjødahl M, Ramser K (2020) Single-Step Preprocessing of Raman Spectra Using Convolutional Neural Networks. *Appl Spectrosc* 74:427–438. <https://doi.org/10.1177/0003702819888949>
 36. Pedregosa, F., Varoquaux, G., Gramfort, A., Michel, V., Thirion, B., Grisel, O., Blondel, M., Prettenhofer, P., Weiss, R., Dubourg, V., Vanderplas, J., Passos, A., Cournapeau, D., Brucher, M., Perrot, M., Duchesnay E (2011) Scikit-learn: Machine Learning in Python. *J Mach Learn Res* 12:2825–2830
 37. Abadi M, Barham P, Chen J, et al (2016) Tensorflow: A system for large-scale machine learning. In: 12th symposium on operating systems design and implementation 16). pp 265–283.
 38. Srivastava N, Hinton G, Krizhevsky A, et al (2014) Dropout: a simple way to prevent neural networks from overfitting. *J Mach Learn Res* 15:1929–1958.
 39. Fiorentin TR, Krotulski AJ, Martin DM, et al (2019) Detection of Cutting Agents in Drug-Positive Seized Exhibits within the United States. *J Forensic Sci* 64:888–896. <https://doi.org/10.1111/1556-4029.13968>
 40. What are the Basic Principles of Raman Spectroscopy, Oxford Instruments ANDOR. (n.d.). <https://andor.oxinst.com/learning/view/article/raman-spectroscopy> (accessed March 27, 2020).
 41. E.C. Le Ru, P.G. Etchegoin, A quick overview of surface-enhanced Raman spectroscopy, in: *Princ. Surface-Enhanced Raman Spectrosc.*, 2009: pp. 1–27. <https://doi.org/10.1016/b978-0-444-52779-0.00007-6>.
 42. J. Langer, D.J. de Aberasturi, J. Aizpurua, R.A. Alvarez-Puebla, B. Auguie, J.J. Baumberg, G.C. Bazan, S.E.J. Bell, A. Boisen, A.G. Brolo, J. Choo, D. Ciialla-May, V. Deckert, L. Fabris, K. Faulds, F. Javier García de Abajo, R. Goodacre, D. Graham, A.J. Haes, C.L. Haynes, C. Huck, T. Itoh, M. Käll, J. Kneipp, N.A. Kotov, H. Kuang, E.C. Le Ru, H.K. Lee, J.F. Li, X.Y. Ling, S.A. Maier, T. Mayerhöfer, M. Moskovits, K. Murakoshi, J.M. Nam, S. Nie, Y. Ozaki, I. Pastoriza-Santos, J. Perez-Juste, J. Popp, A. Pucci, S. Reich, B. Ren, G.C. Schatz, T. Shegai, S. Schlücker, L.L. Tay, K. George Thomas, Z.Q. Tian, R.P. van Duyne, T. Vo-Dinh, Y. Wang, K.A. Willets, C. Xu, H. Xu, Y. Xu, Y.S. Yamamoto, B. Zhao, L.M. Liz-Marzán, Present and future of surface-enhanced Raman scattering, *ACS Nano*. 14 (2020) 28–117. <https://doi.org/10.1021/acsnano.9b04224>.
 43. A. Jaworska, S. Fornasaro, V. Sergo, A. Bonifacio, Potential of Surface Enhanced Raman Spectroscopy (SERS) in Therapeutic Drug Monitoring (TDM). A critical review, *Biosensors*. 6 (2016). <https://doi.org/10.3390/bios6030047>.

44. D.A. Skoog, F.J. Holler, S.R. Crouch, Principles of Instrumental Analysis, 6th ed., Thomson Brooks/Cole, 2007.
45. G.S. Bumbrah, R.M. Sharma, Raman spectroscopy – Basic principle, instrumentation and selected applications for the characterization of drugs of abuse, Egypt. J. Forensic Sci. 6 (2016) 209–215. <https://doi.org/10.1016/j.ejfs.2015.06.001>.
46. A.D. Burnett, H.G.M. Edwards, M.D. Hargreaves, T. Munshi, K. Page, A forensic case study: The detection of contraband drugs in carrier solutions by Raman spectroscopy, Drug Test. Anal. 3 (2011) 539–543. <https://doi.org/10.1002/dta.169>.
47. M.J. Menendez, V.W. Weedn, Collaboration in the Fight Against Fentanyl, in: Organized Crime Drug Enforcement Task Forces and George Washington University.
48. R.S. Vardanyan, V.J. Hruby, Fentanyl-related compounds and derivatives: current status and future prospects for pharmaceutical applications, Futur. Med Chem. 6 (2014) 385–412. <https://doi.org/10.4155/fmc.13.215.Fentanyl-related>.
49. Burke, L.D.; Nugent, P.F. The electrochemistry of gold: I the redox behaviour of the metal in aqueous media. *Gold Bull.* **1997**, *30*, 43–53.
50. Vilas-Boas, Â.; Valderrama, P.; Fontes, N.; Geraldo, D.; Bento, F. Evaluation of total polyphenol content of wines by means of voltammetric techniques: Cyclic voltammetry vs. differential pulse voltammetry. *Food Chem.* **2019**, *276*, 719–725.
51. Elie, L.; Elie, M.; Cave, G.; Vetter, M.; Croxton, R.; Baron, M. Microcrystalline testing used in combination with Raman micro-spectroscopy for absolute identification of novel psychoactive substances. *J. Raman Spectrosc.* **2016**, *47*, 1343–1350.
52. Farquharson, S.; Brouillette, C.; Smith, W.; Shende, C. A Surface-Enhanced Raman Spectral Library of Important Drugs Associated With Point-of-Care and Field Applications. *Front. Chem.* **2019**, *7*, 706.
53. Jones, L.E.; Stewart, A.; Peters, K.L.; McNaul, M.; Speers, S.J.; Fletcher, N.C.; Bell, S.E.J. Infrared and Raman screening of seized novel psychoactive substances: A large scale study of >200 samples. *Analyst* **2016**, *141*, 902–909.
54. Stewart, S.P.; Bell, S.E.; Fletcher, N.; Bouazzaoui, S.; Ho, Y.C.; Speers, S.; Peters, K.L. Raman spectroscopy for forensic examination of β -ketophenethylamine “legal highs”: Reference and seized samples of cathinone derivatives. *Anal. Chim. Acta* **2012**, *711*, 1–6.
55. Szaniawska, A.; Kudelski, A. Applications of Surface-Enhanced Raman Scattering in Biochemical and Medical Analysis. *Front. Chem.* **2021**, *9*, 296.
56. Chang, Y.-C.; Huang, B.-H.; Lin, T.-H. Surface-Enhanced Raman Scattering and Fluorescence on Gold Nanogratings. *Nanomaterials* **2020**, *10*, 776.
57. Sivashanmugan, K.; Squire, K.; Tan, A.; Zhao, Y.; Kraai, J.A.; Rorrer, G.L.; Wang, A.X. Trace Detection of Tetrahydrocannabinol in Body Fluid via Surface-Enhanced Raman Scattering and Principal Component Analysis. *ACS Sens.* **2019**, *4*, 1109–1117.
58. L. Dawei, W. Jian, X. Houwen, S. Xu, L. Fan-Chen, Enhancement origin of SERS from pyridine adsorbed on AgCl colloids, *Spectrochim. Acta - Part A Mol. Biomol. Spectrosc.* **43A** (1987) 379–382.
59. D. Martín-Yerga, A. Pérez-Junquera, M.B. González-García, J. V. Perales-Rondon, A. Heras, A. Colina, D. Hernández-Santos, P. Fanjul-Bolado, Quantitative Raman spectroelectrochemistry using silver screen-printed electrodes, *Electrochim. Acta.* **264** (2018) 183–190. <https://doi.org/10.1016/j.electacta.2018.01.060>.
60. M. Philp, S. Fu, A review of chemical “spot” tests: a presumptive illicit drug identification technique, *Drug Test Anal.* **10** (2018) 95–108. <http://mc.manuscriptcentral.com/dta>.

61. C.L. O'Neal, D.J. Crouch, A.A. Fatah, Validation of twelve chemical spot tests for the detection of drugs of abuse, *Forensic Sci Int.* 109 (2000) 189–201. [https://doi.org/10.1016/S0379-0738\(99\)00235-2](https://doi.org/10.1016/S0379-0738(99)00235-2).
62. P.A. Kosecki, P. Brooke, E. Canonico, Fentanyl as a potential false positive with color tests commonly used for presumptive cocaine identification, *J Forensic Sci.* 67 (2022) 2082–2088. <https://doi.org/10.1111/1556-4029.15090>.
63. B.C. Hauck, P.C. Riley, B.S. Ince, Effect of environmental conditions on the performance of fentanyl field detection tests, *Forensic Chemistry.* 27 (2022). <https://doi.org/10.1016/j.forc.2021.100394>.
64. E. Cuypers, A.J. Bonneure, J. Tytgat, The use of presumptive color tests for new psychoactive substances, *Drug Test Anal.* 8 (2016) 137–141. <https://doi.org/10.1002/dta.1847>.
65. Color Test Reagents/Kits for Preliminary Identification of Drugs of Abuse: NIJ Standard - 0604.01, 2000. <http://www.nlectc.org>.
66. [K.-A. Kovar, M. Laudszun, Chemistry and Reaction Mechanisms of Rapid Tests for Drugs of Abuse and Precursors Chemicals: Scientific and Technical Notes, 1989
67. L.J. Marinetti, B.J. Ehlers, A series of forensic toxicology and drug seizure cases involving illicit fentanyl alone and in combination with heroin, cocaine or heroin and cocaine, *J Anal Toxicol.* 38 (2014) 592–598. <https://doi.org/10.1093/jat/bku086>.
68. [FCS10-Procedure for Chemical Spot Tests, 2018.
69. E. Sisco, A. Burns, E. Schneider, C.R. Miller, L. Bobka, Comparing two seized drug workflows for the analysis of synthetic cannabinoids, cathinones, and opioids, *J Forensic Sci.* 67 (2022) 471–482. <https://doi.org/10.1111/1556-4029.14936>.
70. P.J. Houghton, A. Raman, *Laboratory Handbook for the Fractionation of Natural Extracts*, 1st ed., Springer US, Boston, MA, 1998. <https://doi.org/10.1007/978-1-4615-5809-5>.
71. Mayer's Reagent, Mercuric-Iodide TS Safety Data Sheet, 2017.

APPENDIX A

GC/MS Monographs

Forensic Drug Detection

**Reference Guide
2022**

Contents

Alprazolam	4
Buprenorphine	5
Cocaine	6
Codeine	7
Fentanyl	8
Heroin	9
Levamisole	10
Lidocaine	11
Methamphetamine	12
4-methylethcathinone	13
Mephedrone	14
Mitragynine	15
Morphine	16
Naltrexone	17
PB-22	18
Sufentanil	19
Delta-9-THC	20
Acetaminophen	21
Benzocaine	22
Boric acid	23
Caffeine	24
Corn Starch	25
Diltiazem	26
Hydroxyzine	27
Maltose	28
Myo-Inositol	29
Phenacetin	30

Phenolphthalein	31
Procaine	32
Sorbitol	33
NOTES.....	34

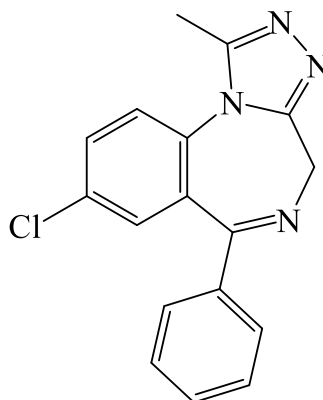
Alprazolam

1. General Information

IUPAC Name	8-chloro-1-methyl-6-phenyl-4 <i>H</i> -[1,2,4]triazolo[4,3- <i>a</i>][1,4]benzodiazepine
CAS #	28981-97-7
Source	Reference Standard

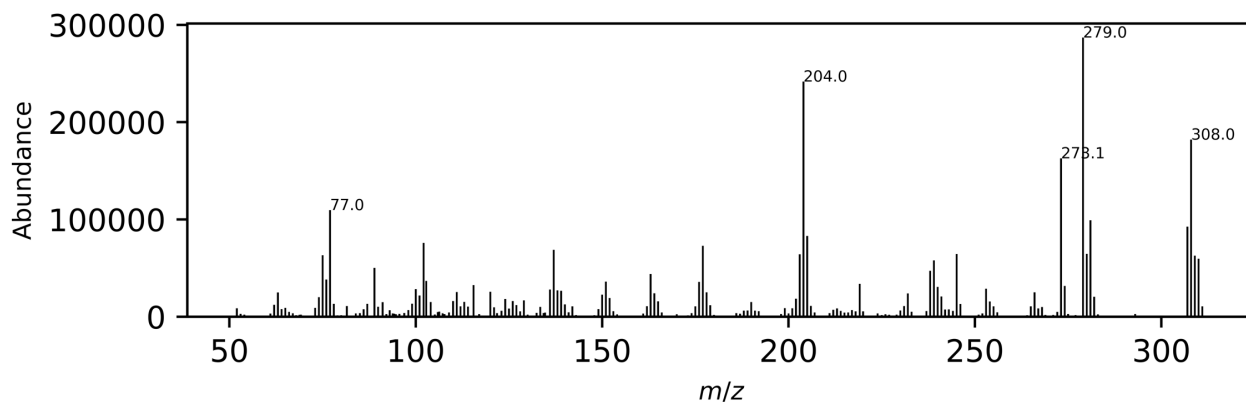
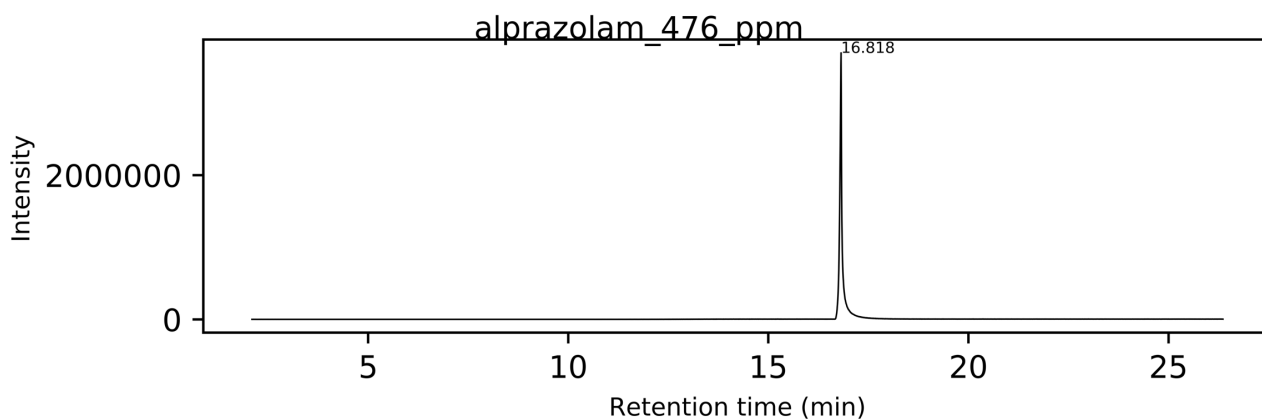
2. Chemical Data

Chemical Formula	C ₁₇ H ₁₃ ClN ₄
Molecular Weight	308.8 g/mol



3. Qualitative Data

- 3.1. GC/MS Full scan TIC and mass spectrum using an Agilent 5977 MSD with EI source (See notes for GC conditions, MS parameters, and retention indices).



Buprenorphine

1. General Information

IUPAC Name (1*S*,2*S*,6*R*,14*R*,15*R*,16*R*)-5-(cyclopropylmethyl)-16-[(2*S*)-2-hydroxy-3,3-dimethylbutan-2-yl]-15-methoxy-13-oxa-5-azahexacyclo[13.2.2.1^{2,8}.0^{1,6}.0^{2,14}.0^{12,20}]icosa-8(20),9,11-trien-11-ol

CAS # 52485-79-7

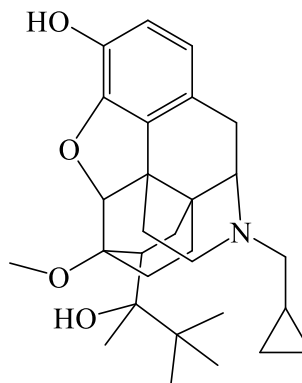
Source Reference Standard

2. Chemical Data

Chemical Formula C₂₉H₄₁NO₄

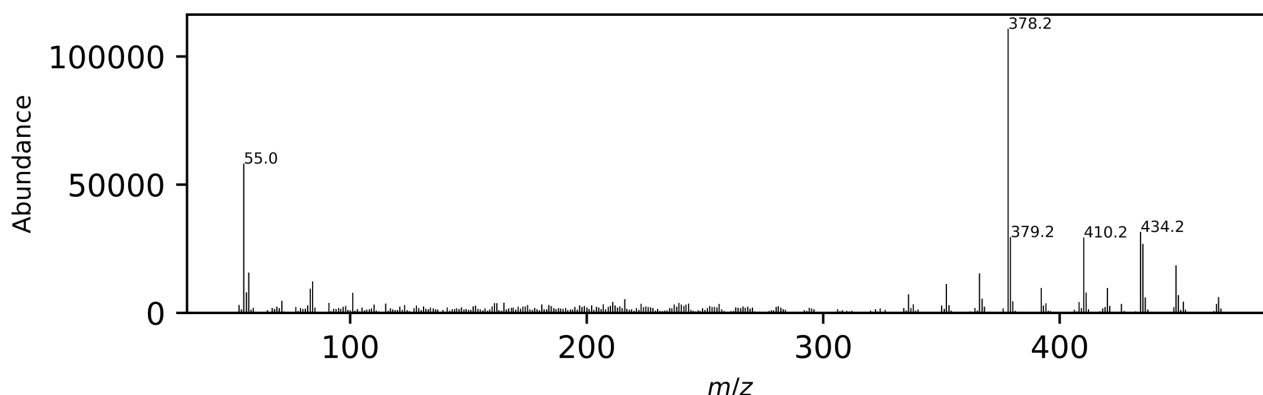
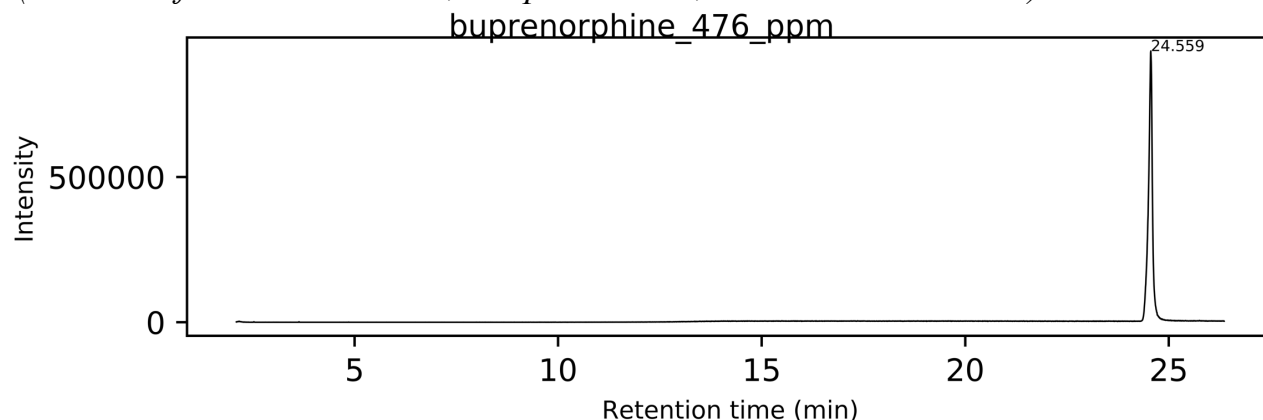
Molecular Weight 467.6 g/mol

pK_a 8.31



3. Qualitative Data

3.1. GC/MS Full scan TIC and mass spectrum using an Agilent 5977 MSD with EI source (See notes for GC conditions, MS parameters, and retention indices).



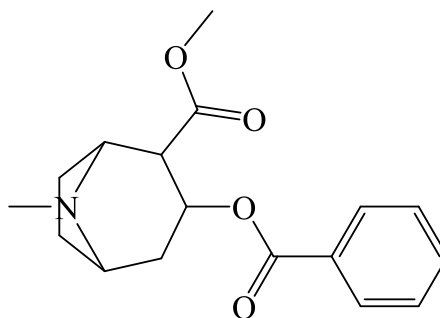
Cocaine

1. General Information

IUPAC Name	methyl (1 <i>R</i> ,2 <i>R</i> ,3 <i>S</i> ,5 <i>S</i>)-3-benzoyloxy-8-methyl-8-azabicyclo[3.2.1]octane-2-carboxylate
CAS #	50-36-2
Source	Reference Standard

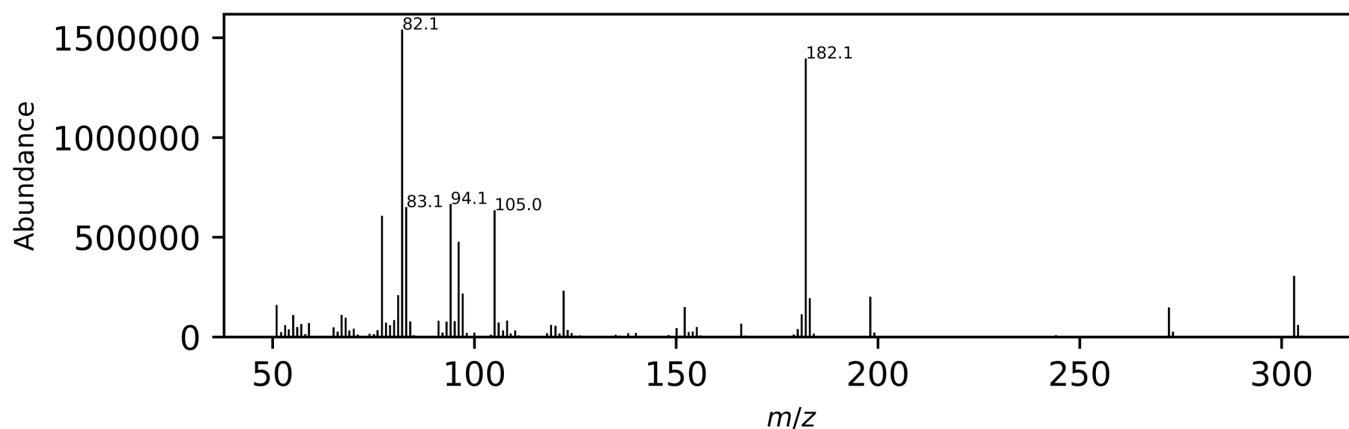
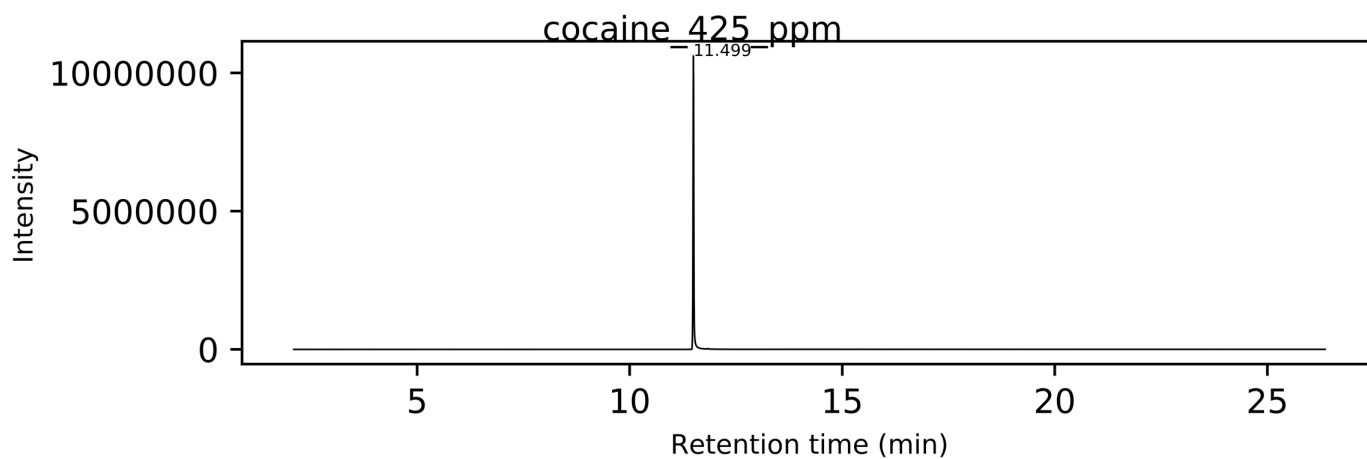
2. Chemical Data

Chemical Formula	C ₁₇ H ₂₁ NO ₄
Molecular Weight	303.35 g/mol
pK _a	8.7



3. Qualitative Data

3.1. GC/MS Full scan TIC and mass spectrum using an Agilent 5977 MSD with EI source (See notes for GC conditions, MS parameters, and retention indices).



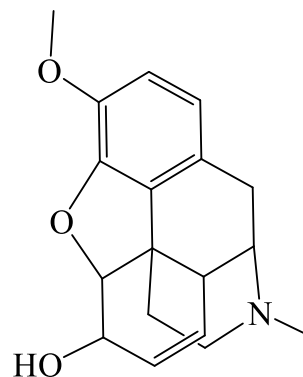
Codeine

1. General Information

IUPAC Name	(4 <i>R</i> ,4 <i>aR</i> ,7 <i>S</i> ,7 <i>aR</i> ,12 <i>bS</i>)-9-methoxy-3-methyl-2,4,4 <i>a</i> ,7,7 <i>a</i> ,13-hexahydro-1 <i>H</i> -4,12-methanobenzofuro[3,2- <i>e</i>]isoquinolin-7-ol
CAS #	76-57-3
Source	Reference Standard

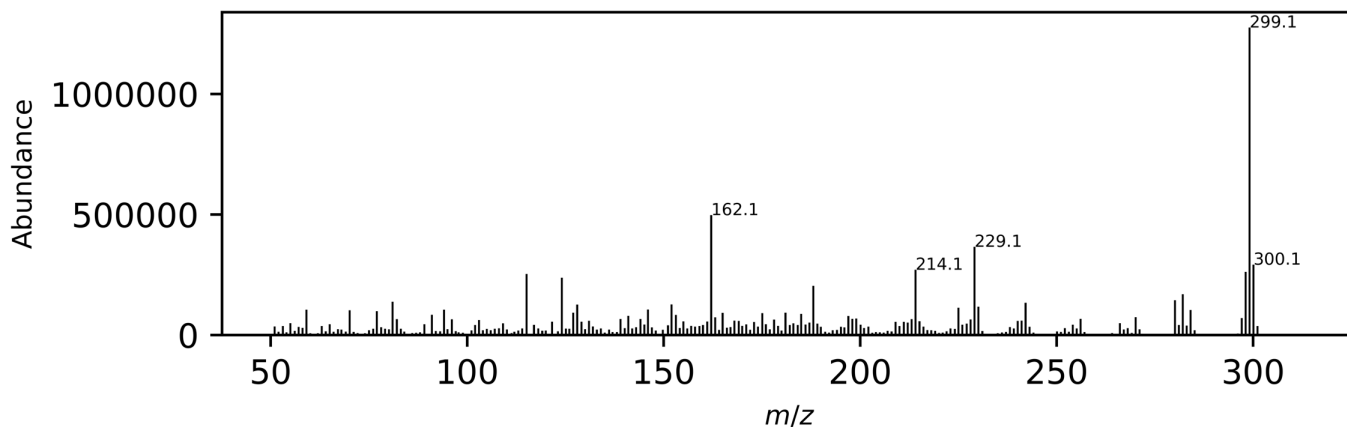
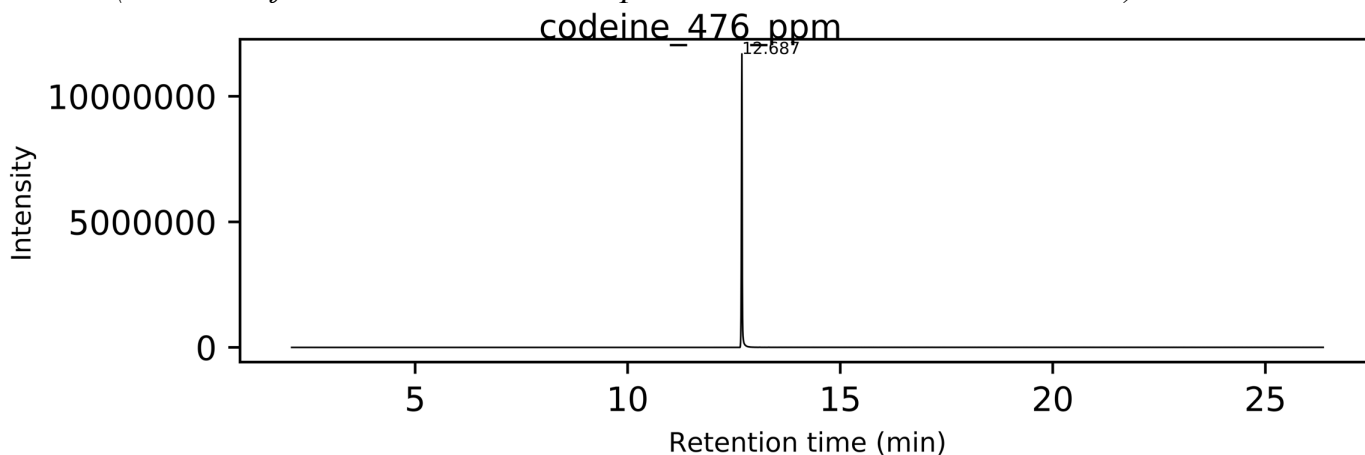
2. Chemical Data

Chemical Formula	C ₁₈ H ₂₁ NO ₃
Molecular Weight	299.4 g/mol
pK _a	8.2



3. Qualitative Data

3.1. GC/MS Full scan TIC and mass spectrum using an Agilent 5977 MSD with EI source (See notes for GC conditions, MS parameters, and retention indices).



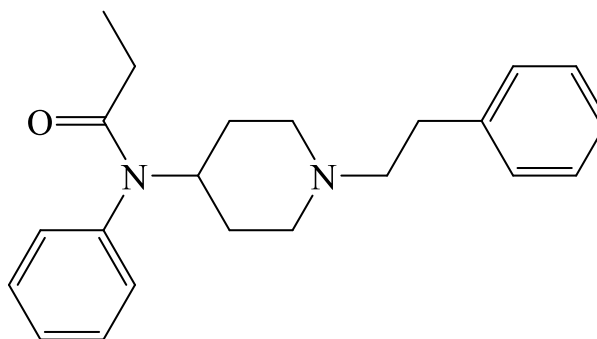
Fentanyl

1. General Information

IUPAC Name	<i>N</i> -phenyl- <i>N</i> -[1-(2-phenylethyl)piperidin-4-yl]8ropenamide
CAS #	437-38-7
Source	Reference Standard

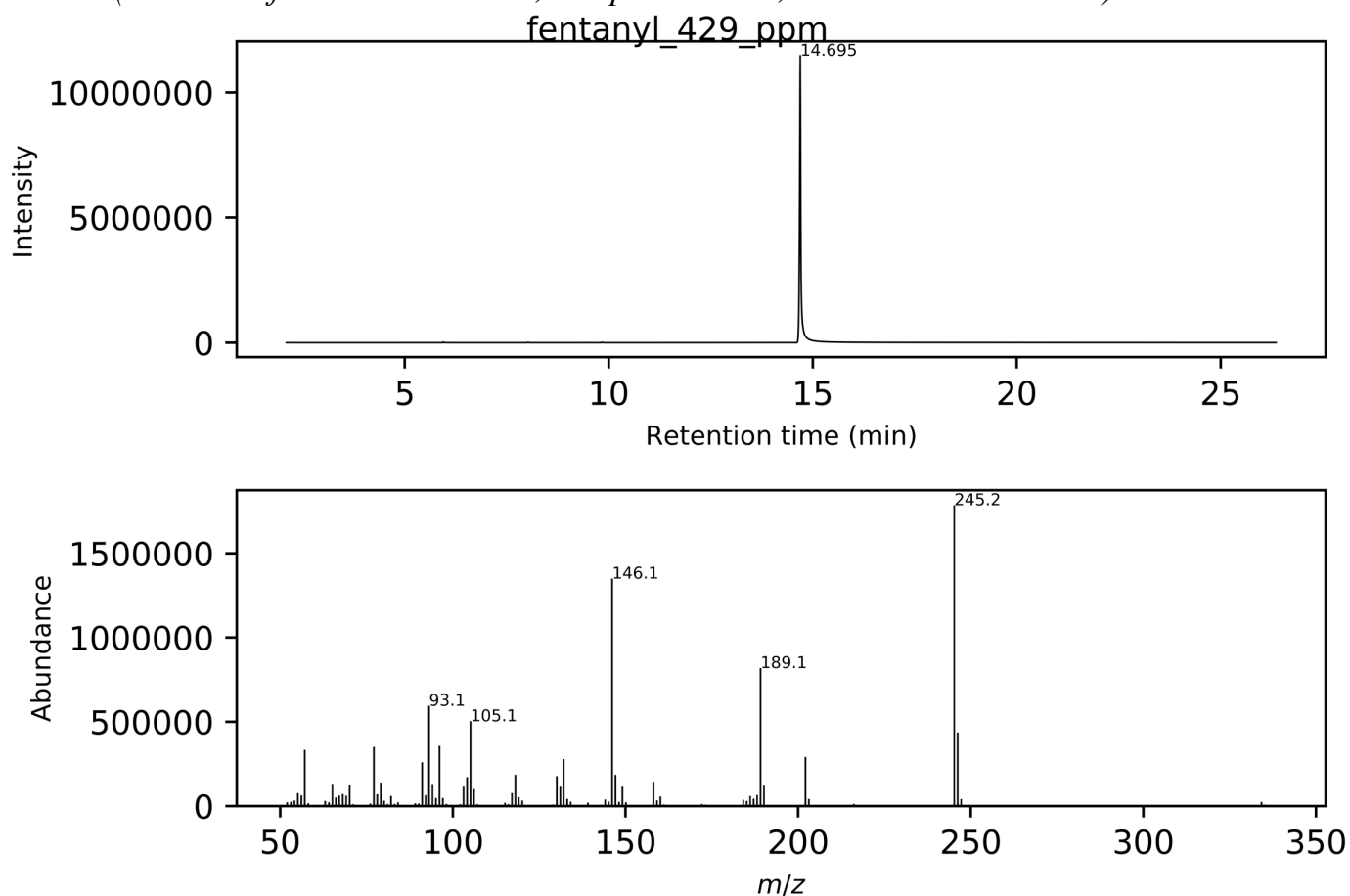
2. Chemical Data

Chemical Formula	C ₂₂ H ₂₈ N ₂ O
Molecular Weight	336.5 g/mol
pK _a	8.43



3. Qualitative Data

3.1. GC/MS Full scan TIC and mass spectrum using an Agilent 5977 MSD with EI source (See notes for GC conditions, MS parameters, and retention indices).



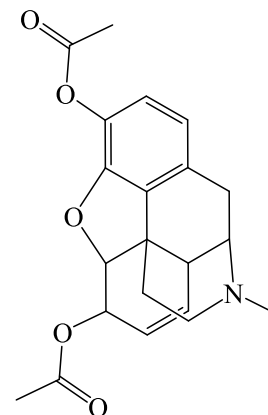
Heroin

1. General Information

IUPAC Name	[(4 <i>R</i> ,4 <i>aR</i> ,7 <i>S</i> ,7 <i>aR</i> ,12 <i>bS</i>)-9-acetyloxy-3-methyl-2,4,4 <i>a</i> ,7,7 <i>a</i> ,13-hexahydro-1 <i>H</i> -4,12-methanobenzofuro[3,2- <i>e</i>]isoquinolin-7-yl] acetate
CAS #	561-27-3
Source	Reference Standard

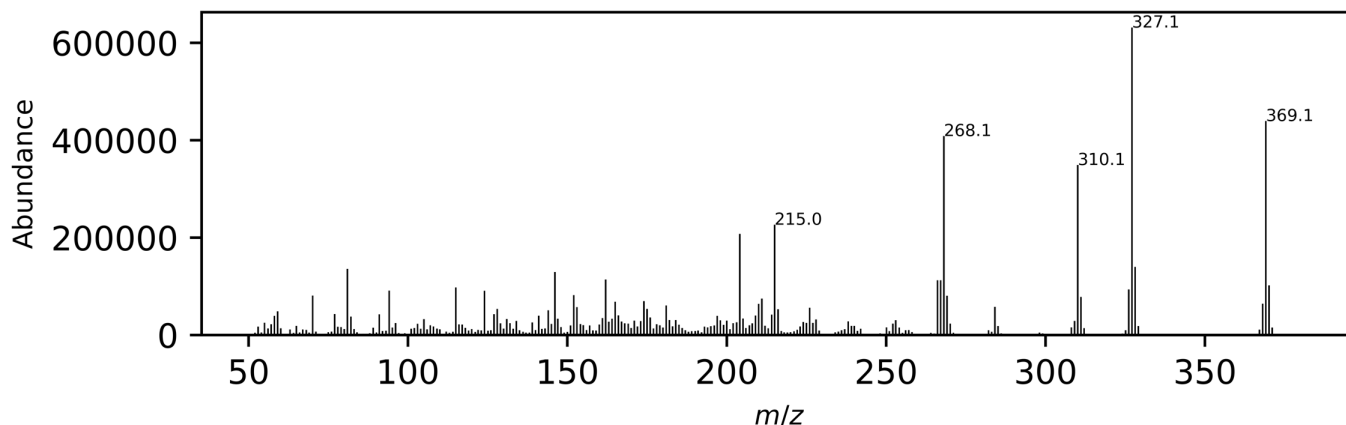
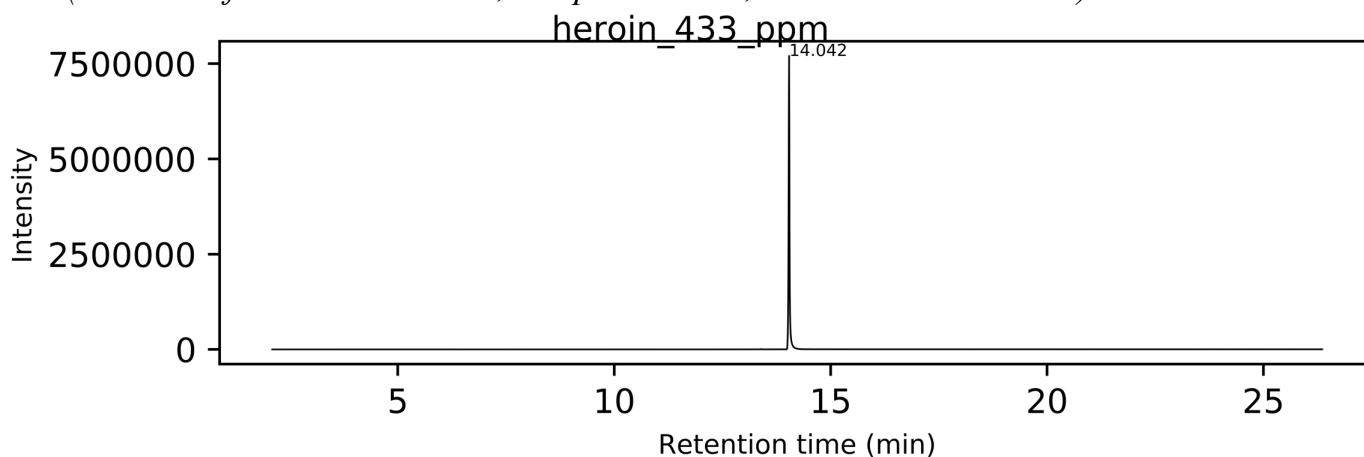
2. Chemical Data

Chemical Formula	C ₂₁ H ₂₃ NO ₅
Molecular Weight	369.4 g/mol
pK _a	7.96



3. Qualitative Data

3.1. GC/MS Full scan TIC and mass spectrum using an Agilent 5977 MSD with EI source (See notes for GC conditions, MS parameters, and retention indices).



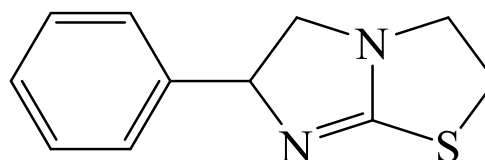
Levamisole

1. General Information

IUPAC Name (6*S*)-6-phenyl-2,3,5,6-tetrahydroimidazo[2,1-*b*][1,3]thiazole
CAS # 14769-73-4
Source Reference Standard

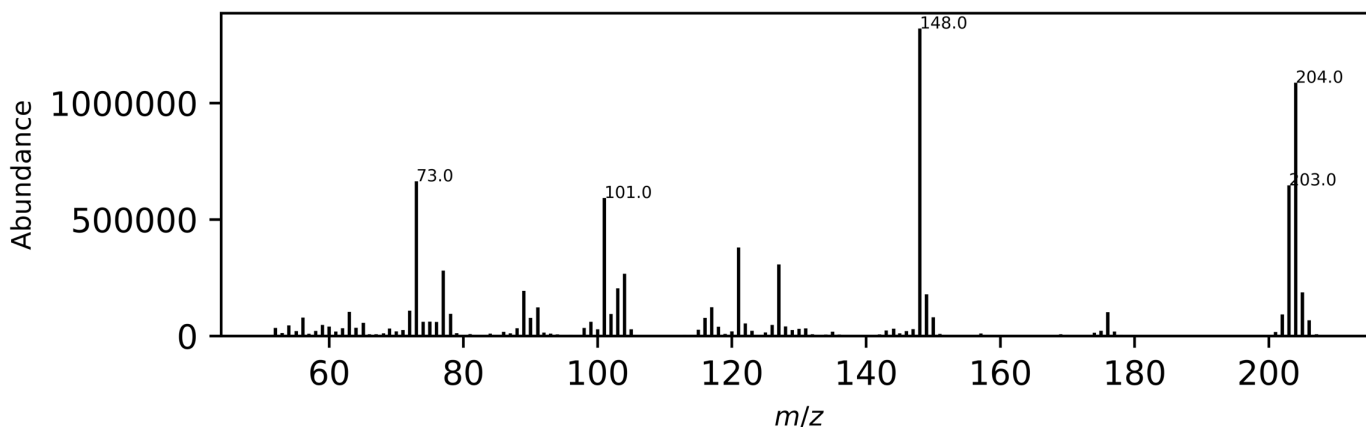
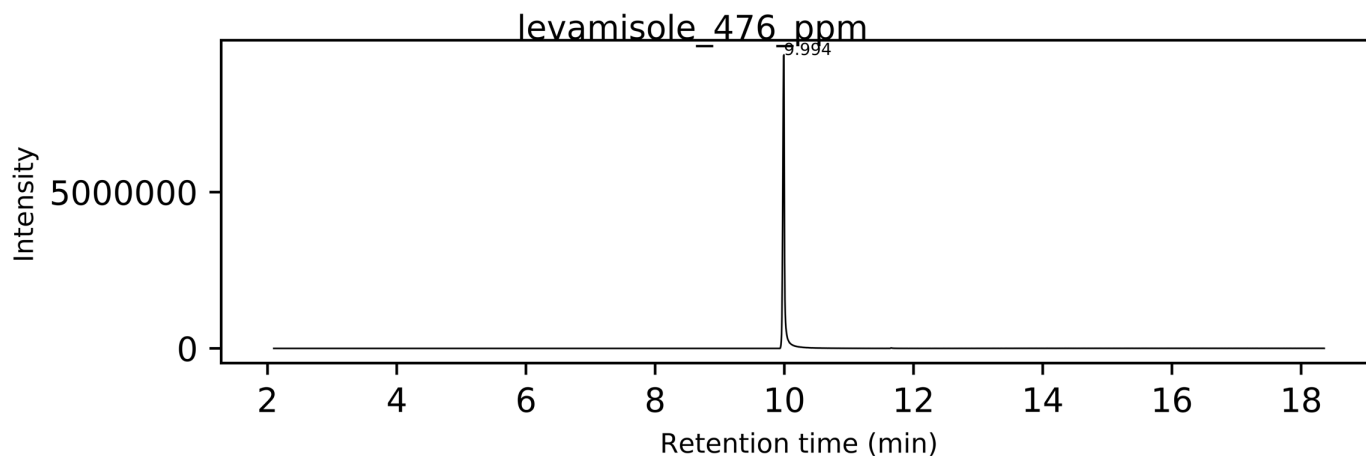
2. Chemical Data

Chemical Formula $C_{11}H_{12}N_2S$
Molecular Weight 204.29 g/mol
pK_a Not Available



3. Qualitative Data

3.1. GC/MS Full scan TIC and mass spectrum using an Agilent 5977 MSD with EI source (See notes for GC conditions, MS parameters, and retention indices).



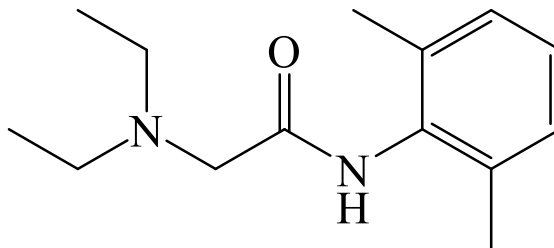
Lidocaine

1. General Information

IUPAC Name	2-(diethylamino)- <i>N</i> -(2,6-dimethylphenyl)acetamide
CAS #	137-58-6
Source	Reference Standard

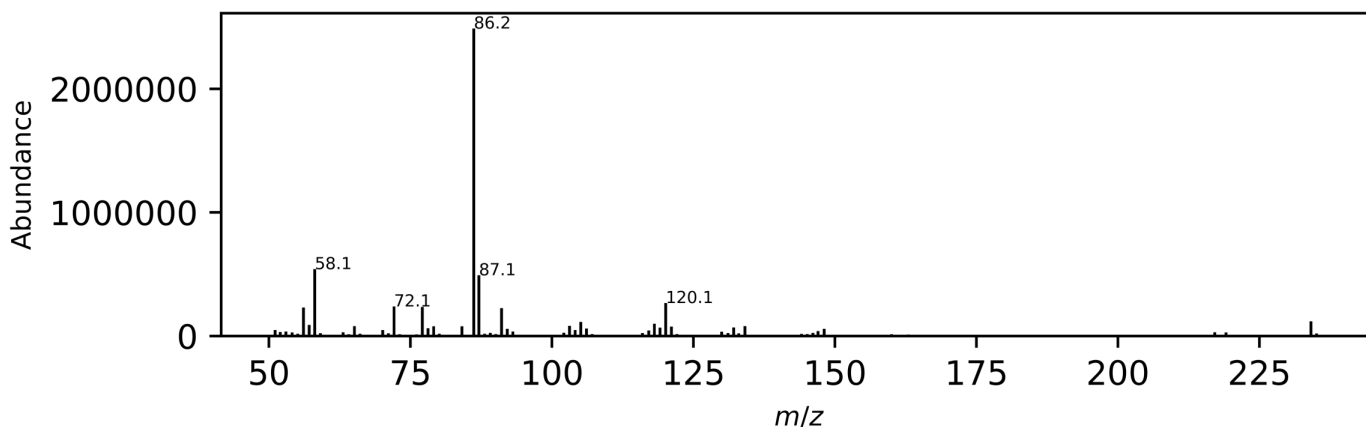
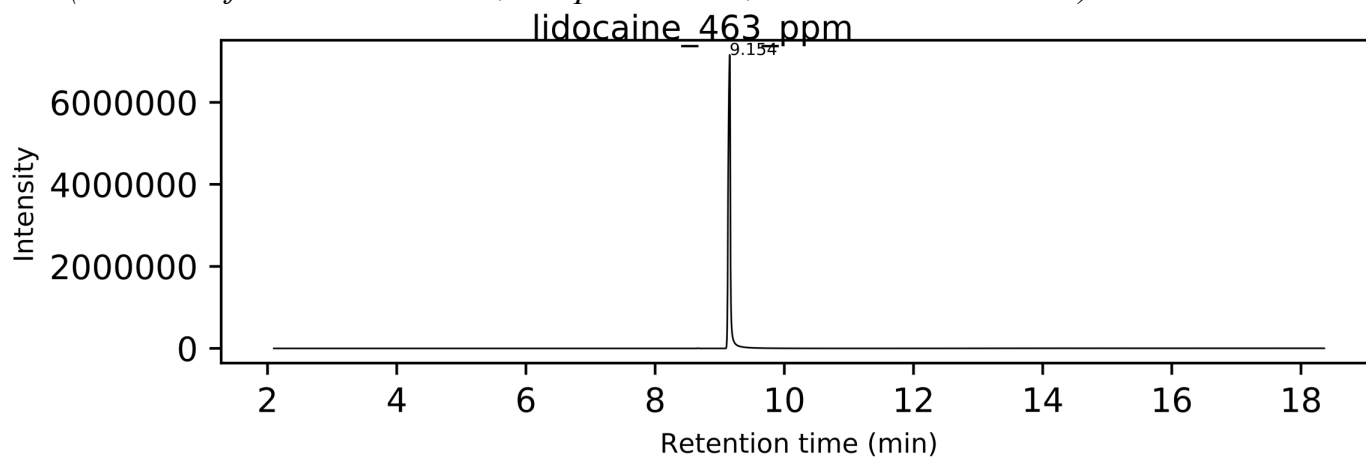
2. Chemical Data

Chemical Formula	C ₁₄ H ₂₂ N ₂ O
Molecular Weight	234.34 g/mol
pK _a	7.93



3. Qualitative Data

3.1. GC/MS Full scan TIC and mass spectrum using an Agilent 5977 MSD with EI source (See notes for GC conditions, MS parameters, and retention indices).



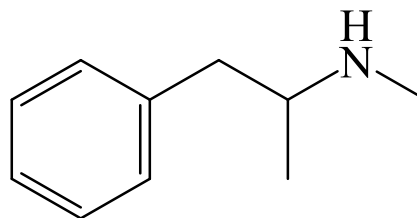
Methamphetamine

1. General Information

IUPAC Name (2*S*)-*N*-methyl-1-phenylpropan-2-amine
CAS # 537-46-2
Source Reference Standard

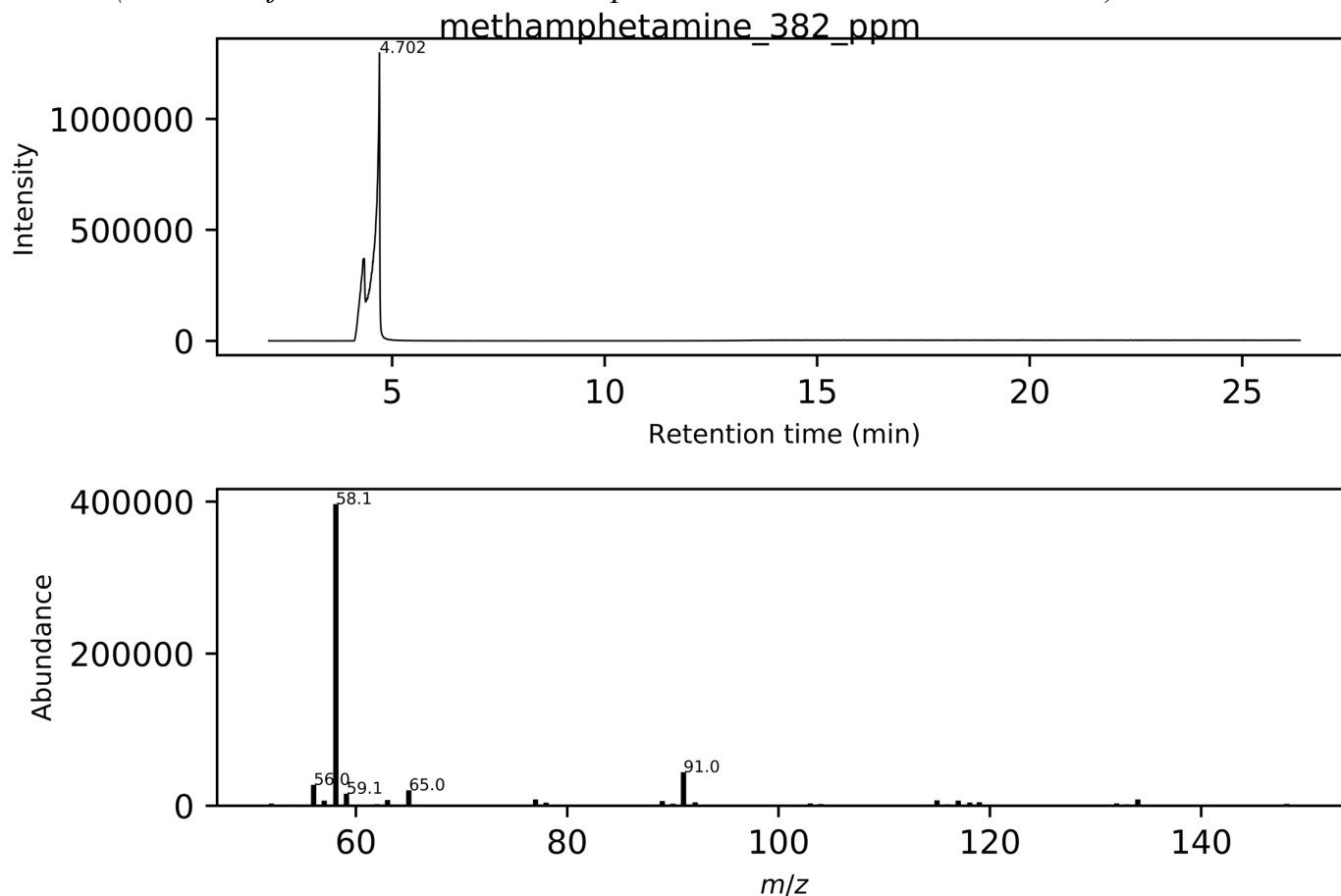
2. Chemical Data

Chemical Formula $C_{10}H_{15}N$
Molecular Weight 149.23 g/mol
pK_a 9.99



3. Qualitative Data

3.1. GC/MS Full scan TIC and mass spectrum using an Agilent 5977 MSD with EI source (See notes for GC conditions, MS parameters, and retention indices).



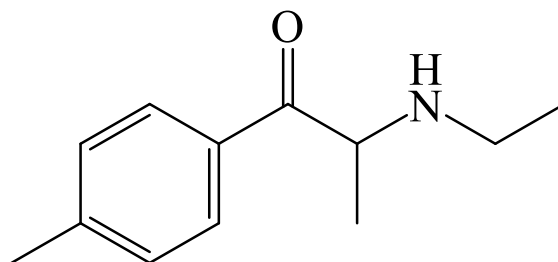
4-methylethcathinone

1. General Information

IUPAC Name 2-(ethylamino)-1-(4-methylphenyl)propan-1-one
CAS # 1225617-18-4
Source Reference Standard

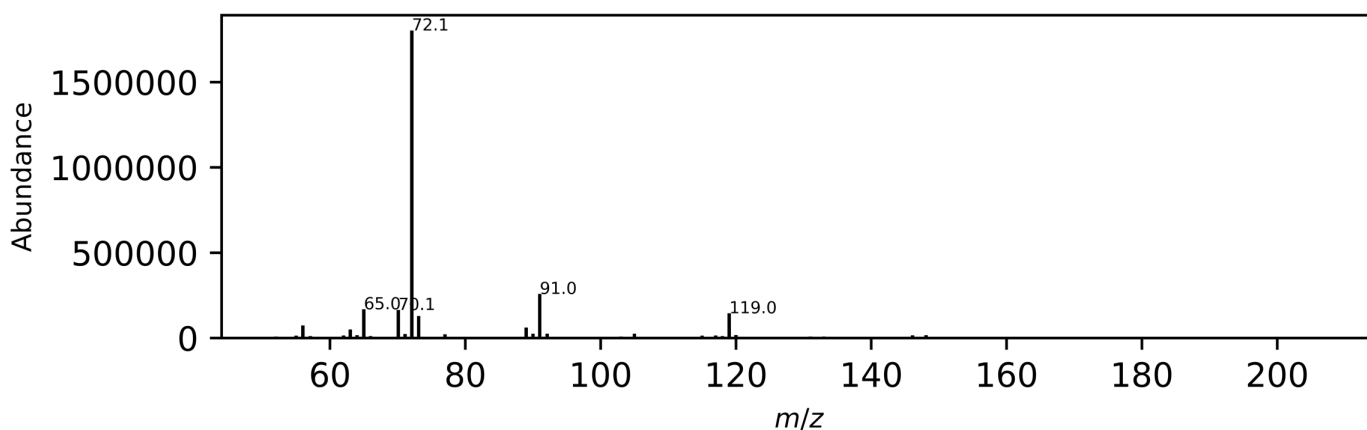
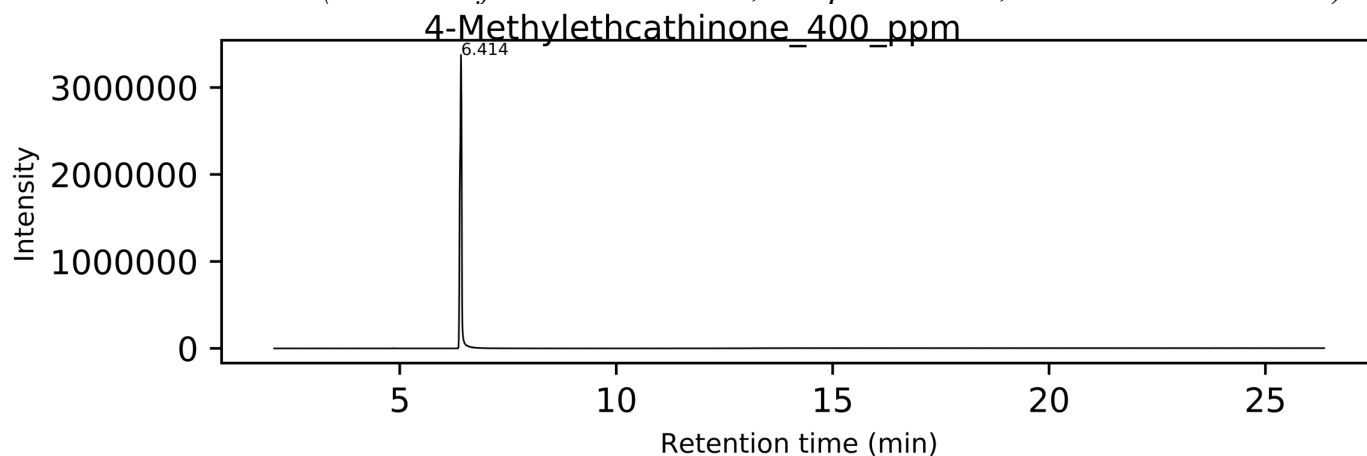
2. Chemical Data

Chemical Formula $C_{12}H_{17}NO$
Molecular Weight 191.27 g/mol
pK_a Not Available



3. Qualitative Data

3.1. GC/MS Full scan TIC and mass spectrum using an Agilent 5977 MSD with EI source (See notes for GC conditions, MS parameters, and retention indices).



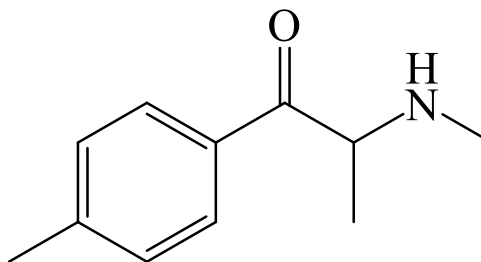
Mephedrone

1. General Information

IUPAC Name 2-(methylamino)-1-(4-methylphenyl)propan-1-one
CAS # 1189805-46-6
Source Reference Standard

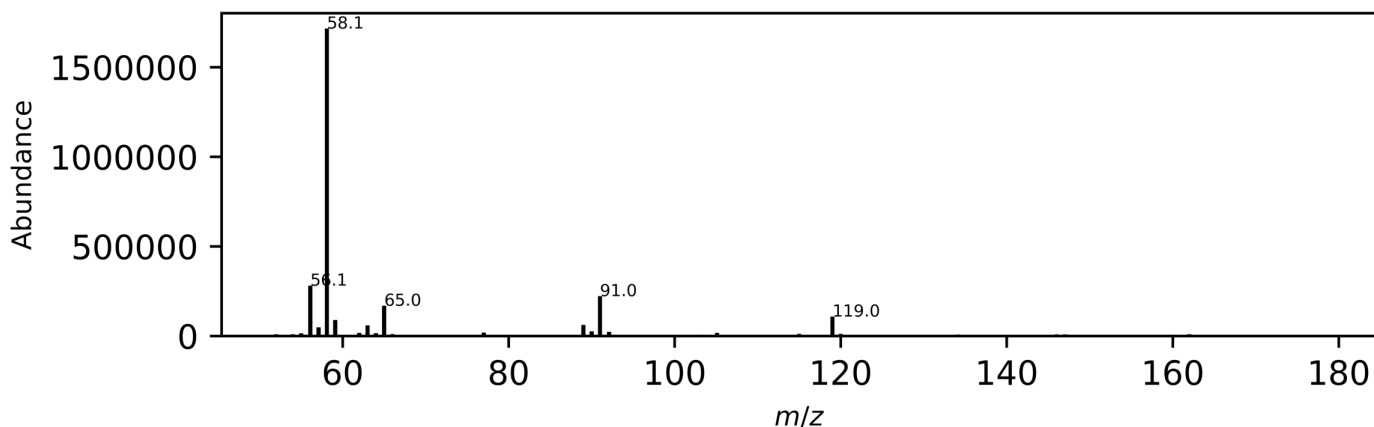
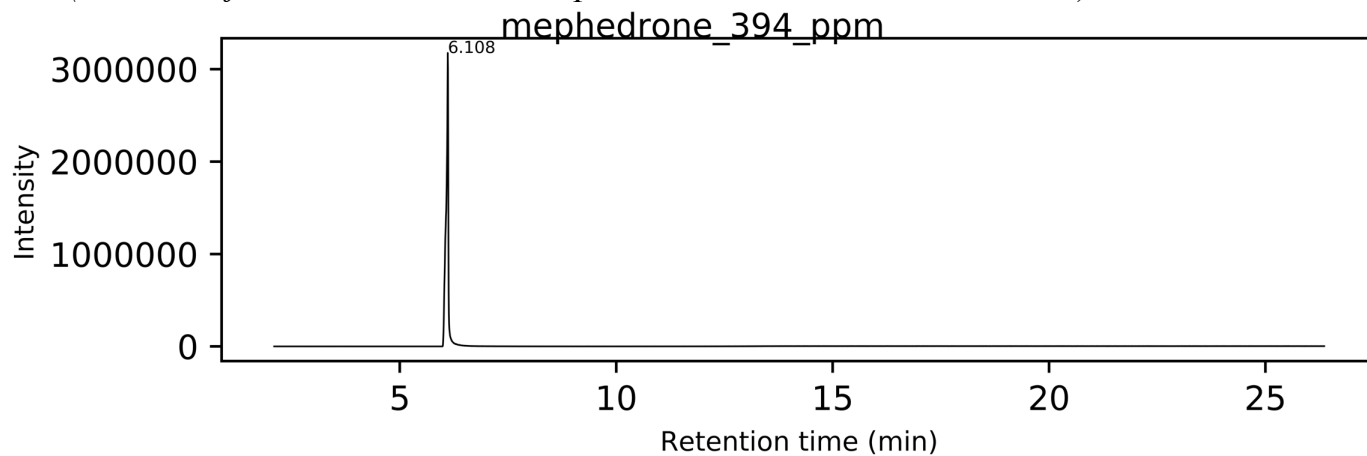
2. Chemical Data

Chemical Formula $C_{11}H_{15}NO$
Molecular Weight 177.24 g/mol
 pK_a Not Available



3. Qualitative Data

3.1. GC/MS Full scan TIC and mass spectrum using an Agilent 5977 MSD with EI source (See notes for GC conditions, MS parameters, and retention indices).



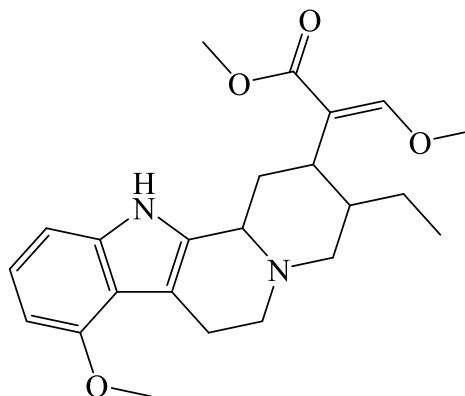
Mitragynine

1. General Information

IUPAC Name	methyl (<i>E</i>)-2-[(2 <i>S</i> ,3 <i>S</i> ,12 <i>bS</i>)-3-ethyl-8-methoxy-1,2,3,4,6,7,12,12 <i>b</i> -octahydroindolo[2,3- <i>a</i>]quinolizin-2-yl]-3-methoxyprop-2-enoate
CAS #	4098-40-2
Source	Reference Standard

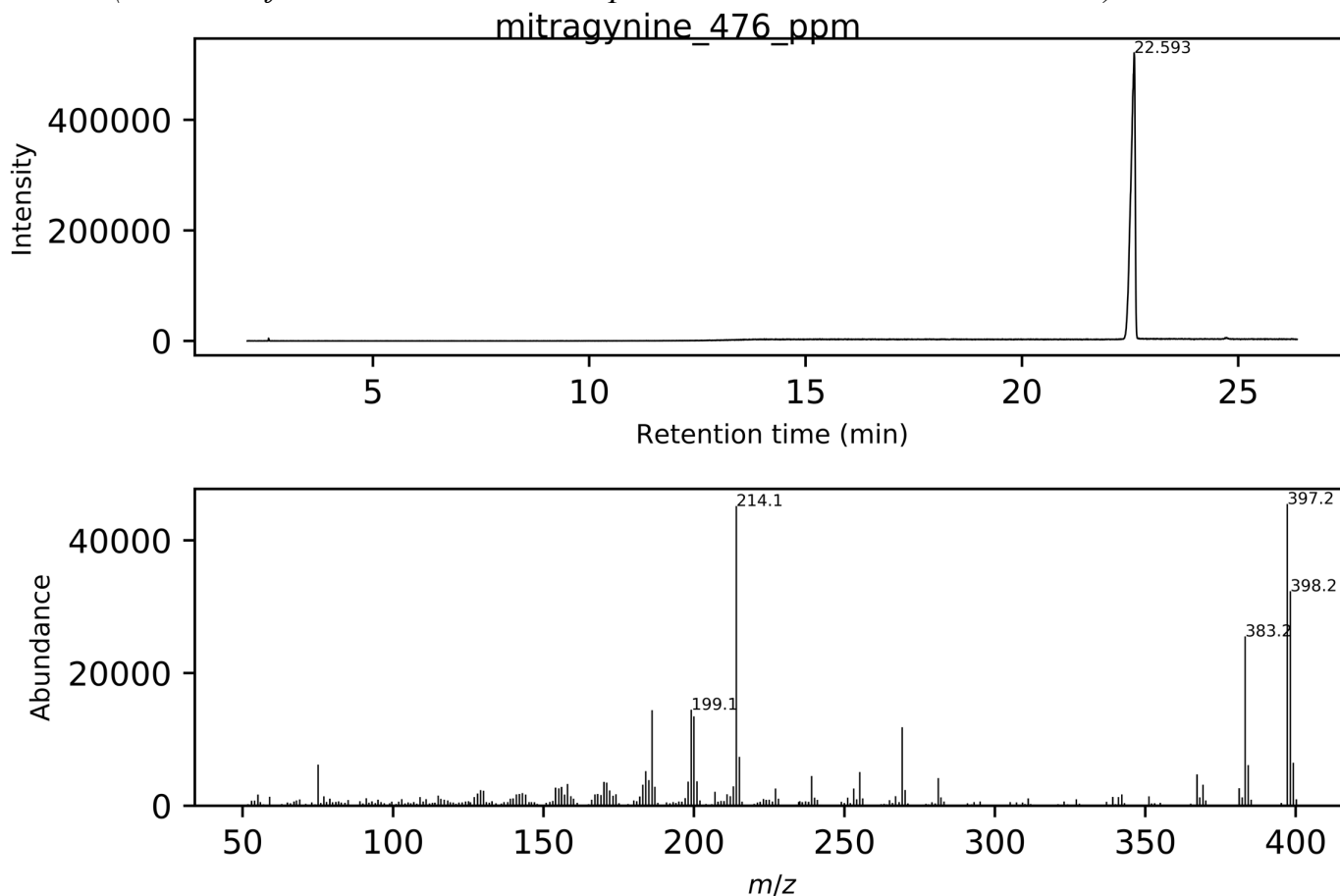
2. Chemical Data

Chemical Formula	C ₂₃ H ₃₀ N ₂ O ₄
Molecular Weight	398.5 g/mol



3. Qualitative Data

3.1. GC/MS Full scan TIC and mass spectrum using an Agilent 5977 MSD with EI source (See notes for GC conditions, MS parameters, and retention indices).



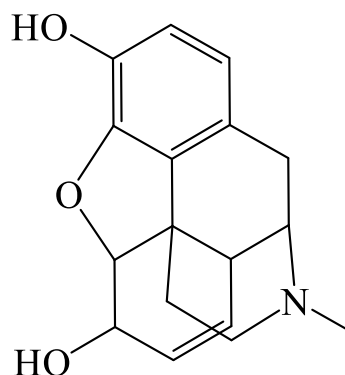
Morphine

1. General Information

IUPAC Name	(4 <i>R</i> ,4 <i>aR</i> ,7 <i>S</i> ,7 <i>aR</i> ,12 <i>bS</i>)-3-methyl-2,4,4 <i>a</i> ,7,7 <i>a</i> ,13-hexahydro-1 <i>H</i> -4,12-methanobenzofuro[3,2- <i>e</i>]isoquinoline-7,9-diol
CAS #	57-27-2
Source	Reference Standard

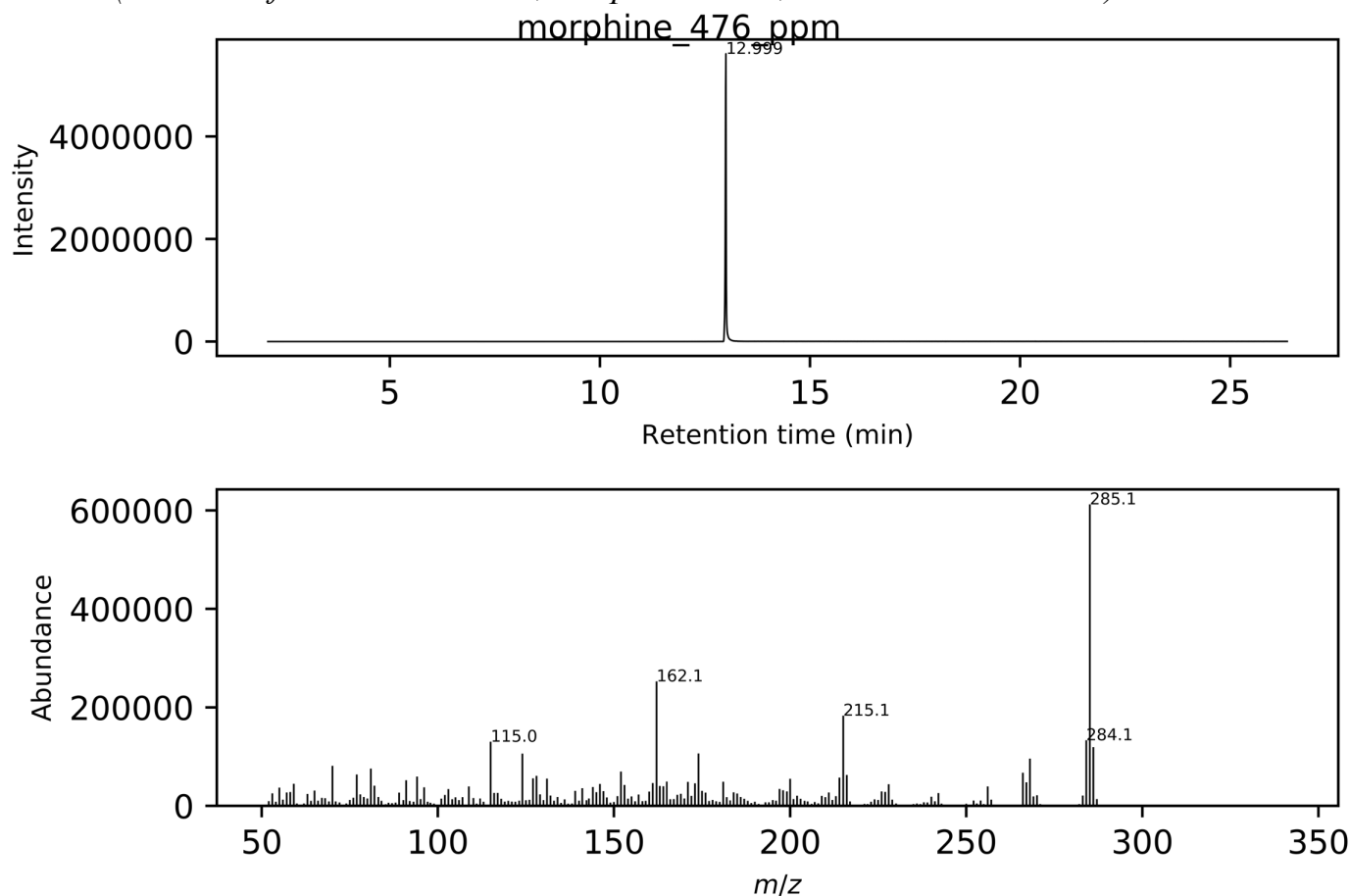
2. Chemical Data

Chemical Formula	C ₁₇ H ₁₉ NO ₃
Molecular Weight	285.34 g/mol
pK _a	8.18



3. Qualitative Data

3.1. GC/MS Full scan TIC and mass spectrum using an Agilent 5977 MSD with EI source (See notes for GC conditions, MS parameters, and retention indices).



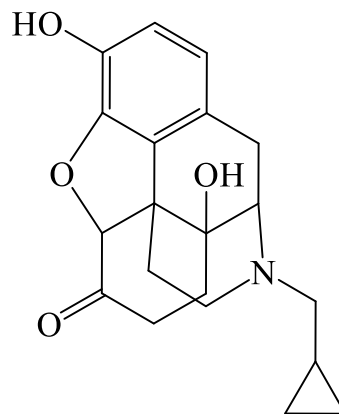
Naltrexone

1. General Information

IUPAC Name	(4 <i>R</i> ,4 <i>aS</i> ,7 <i>aR</i> ,12 <i>bS</i>)-3-(cyclopropylmethyl)-4 <i>a</i> ,9-dihydroxy-2,4,5,6,7 <i>a</i> ,13-hexahydro-1 <i>H</i> -4,12-methanobenzofuro[3,2- <i>e</i>]isoquinolin-7-one
CAS #	16590-41-3
Source	Reference Standard

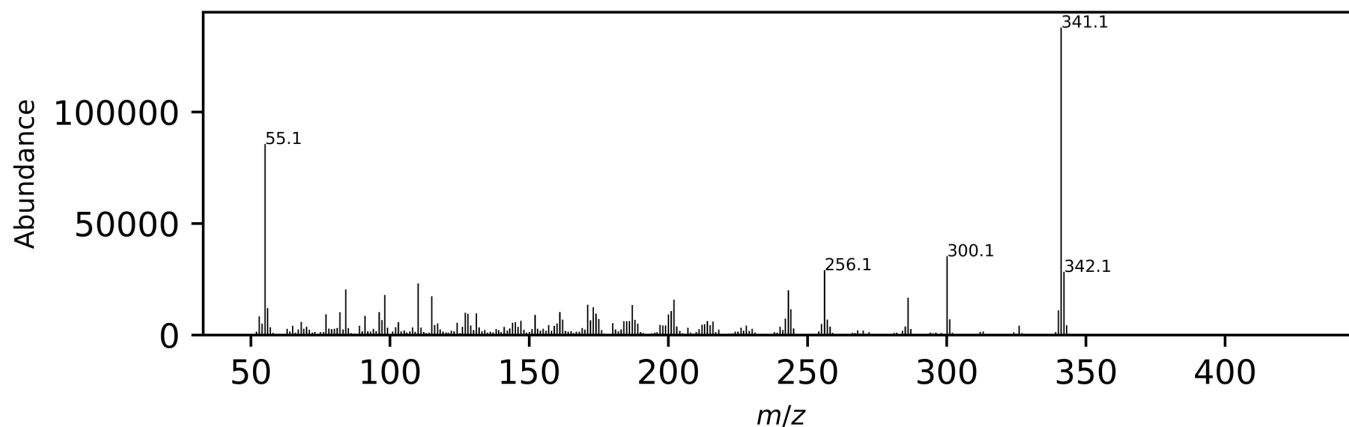
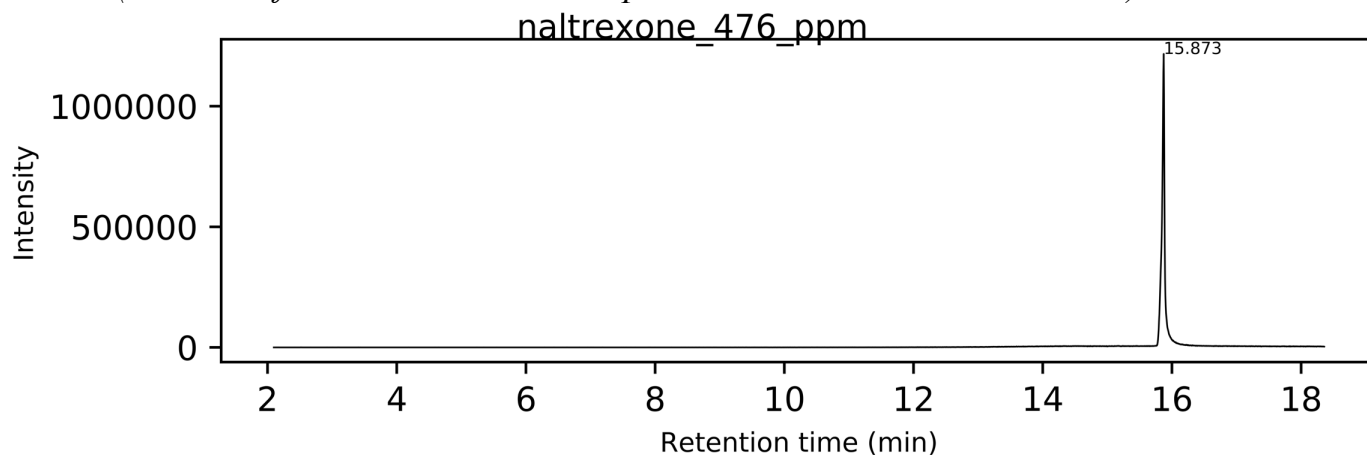
2. Chemical Data

Chemical Formula	C ₂₀ H ₂₃ NO ₄
Molecular Weight	341.4 g/mol
pK _a	8.38



3. Qualitative Data

3.1. GC/MS Full scan TIC and mass spectrum using an Agilent 5977 MSD with EI source (See notes for GC conditions, MS parameters, and retention indices).



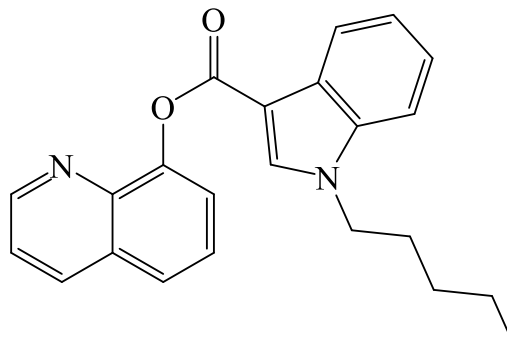
PB-22

1. General Information

IUPAC Name 1-pentyl-1*H*-indole-3-carboxylic acid, 8-quinolinyl ester
CAS # 1400742-17-7
Source Reference Standard

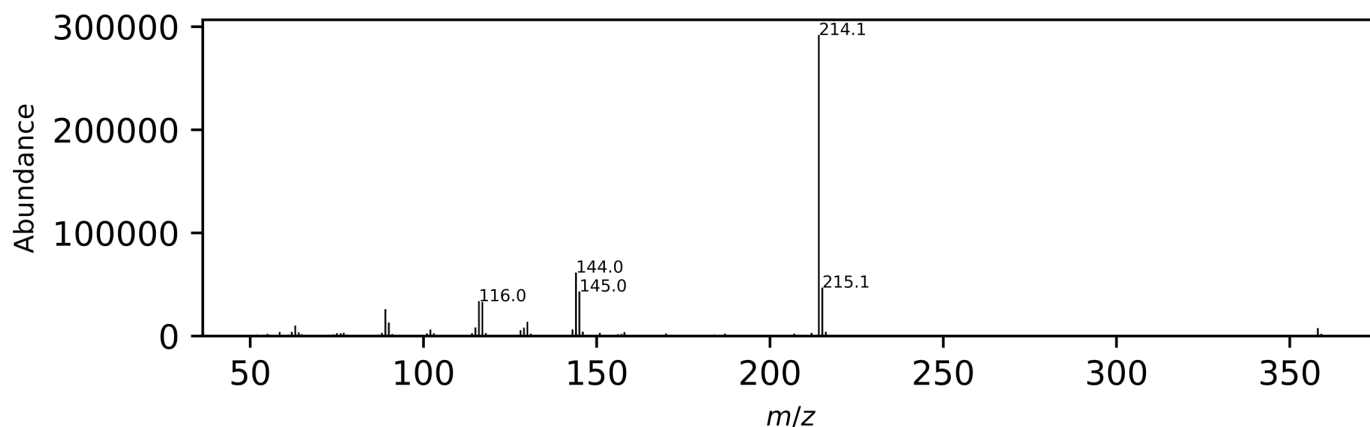
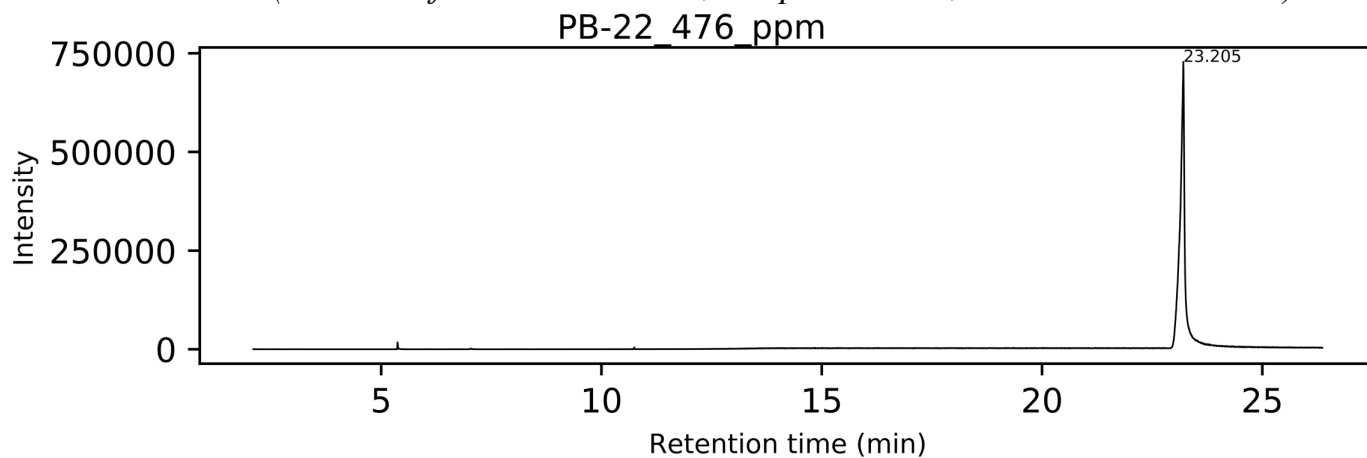
2. Chemical Data

Chemical Formula $C_{23}H_{22}N_2O_2$
Molecular Weight 358.4 g/mol
 pK_a Not Available



3. Qualitative Data

3.1. GC/MS Full scan TIC and mass spectrum using an Agilent 5977 MSD with EI source (See notes for GC conditions, MS parameters, and retention indices).



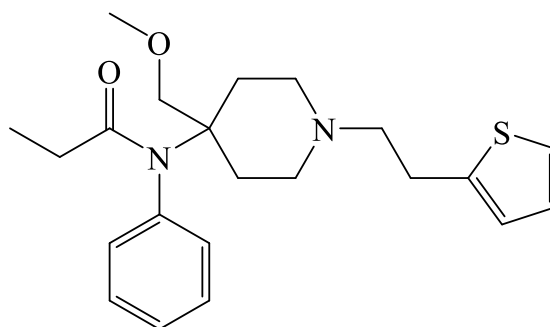
Sufentanil

1. General Information

IUPAC Name	<i>N</i> -[4-(methoxymethyl)-1-(2-thiophen-2-ylethyl)piperidin-4-yl]- <i>N</i> -phenylpropanamide
CAS #	56030-54-7
Source	Reference Standard

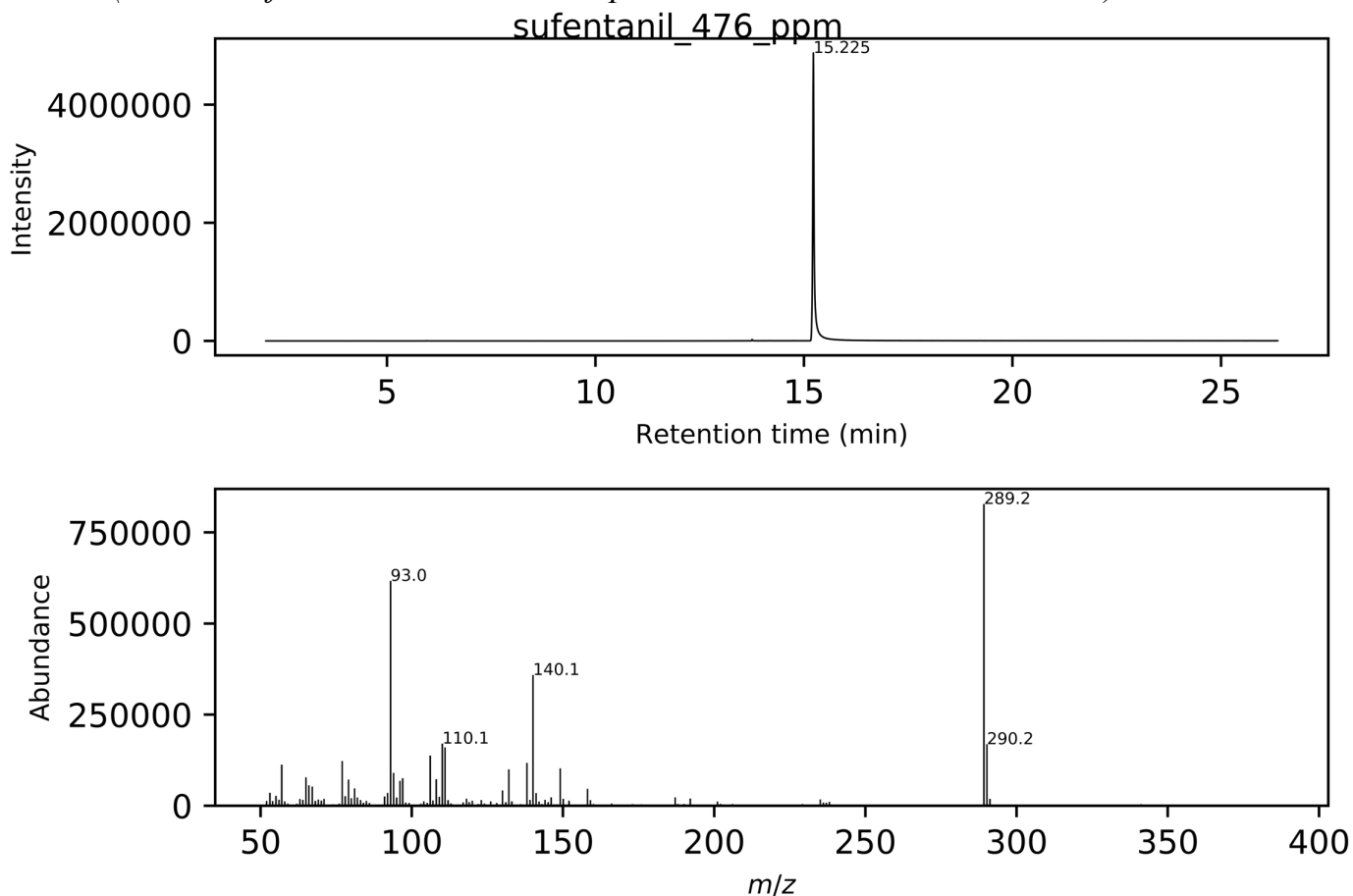
2. Chemical Data

Chemical Formula	C ₂₂ H ₃₀ N ₂ O ₂ S
Molecular Weight	386.6 g/mol
pK _a	7.85



3. Qualitative Data

3.1. GC/MS Full scan TIC and mass spectrum using an Agilent 5977 MSD with EI source (See notes for GC conditions, MS parameters, and retention indices).



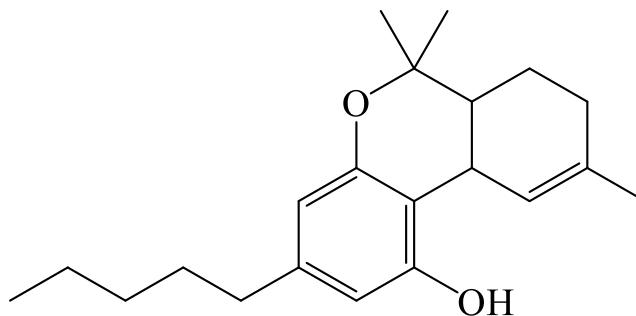
Delta-9-THC

1. General Information

IUPAC Name (6*aR*,10*aR*)-6,6,9-trimethyl-3-pentyl-6*a*,7,8,10*a*-tetrahydrobenzo[*c*]chromen-1-ol
CAS # 1972-08-3
Source Reference Standard

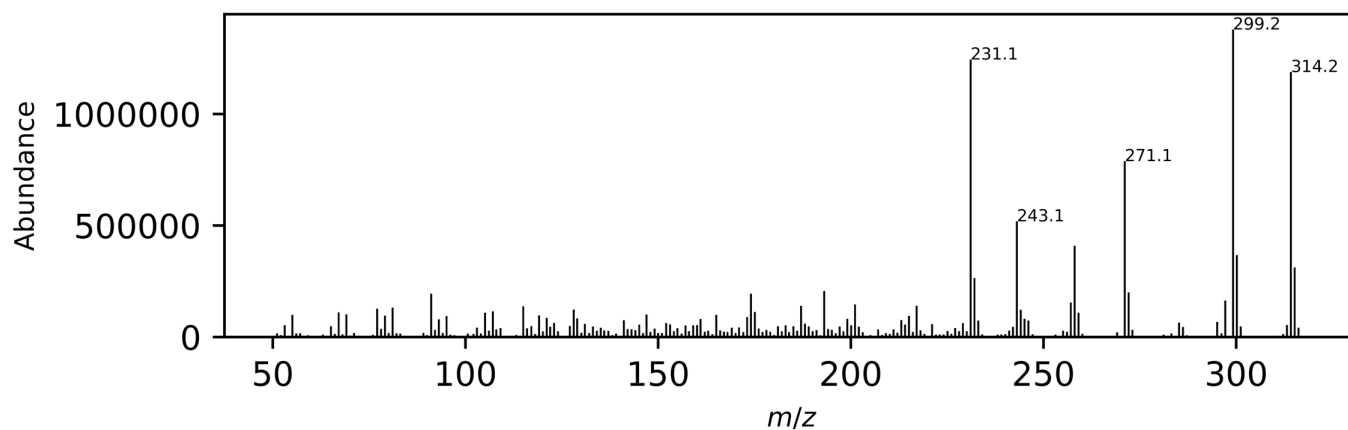
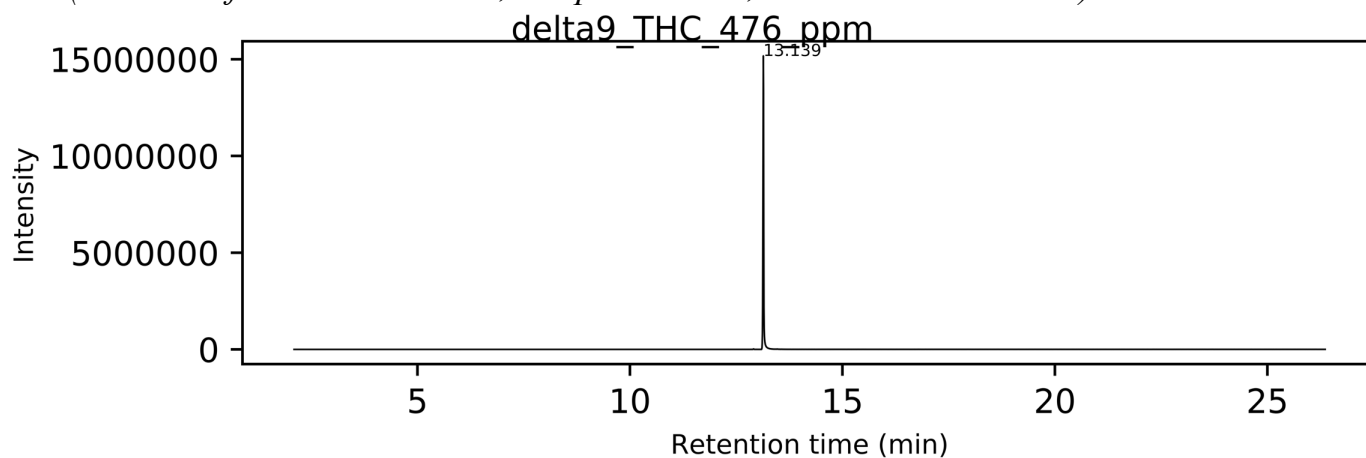
2. Chemical Data

Chemical Formula $C_{21}H_{30}O_2$
Molecular Weight 314.5 g/mol
pK_a 10.6



3. Qualitative Data

3.1. GC/MS Full scan TIC and mass spectrum using an Agilent 5977 MSD with EI source (See notes for GC conditions, MS parameters, and retention indices).



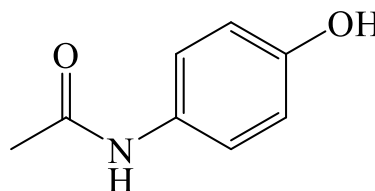
Acetaminophen

1. General Information

IUPAC Name N-(4-hydroxyphenyl)acetamide
CAS # 103-90-2
Source Reference Standard

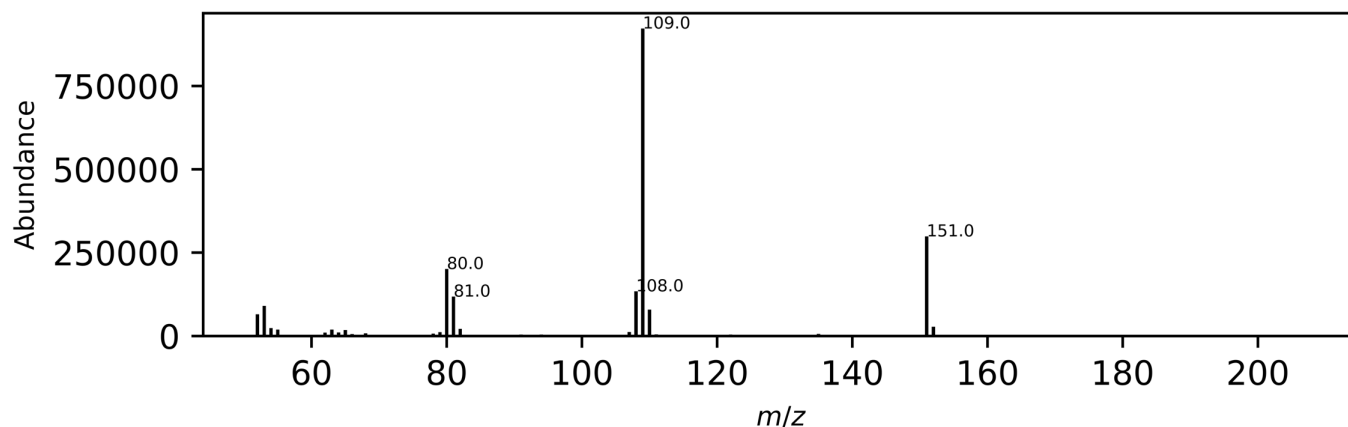
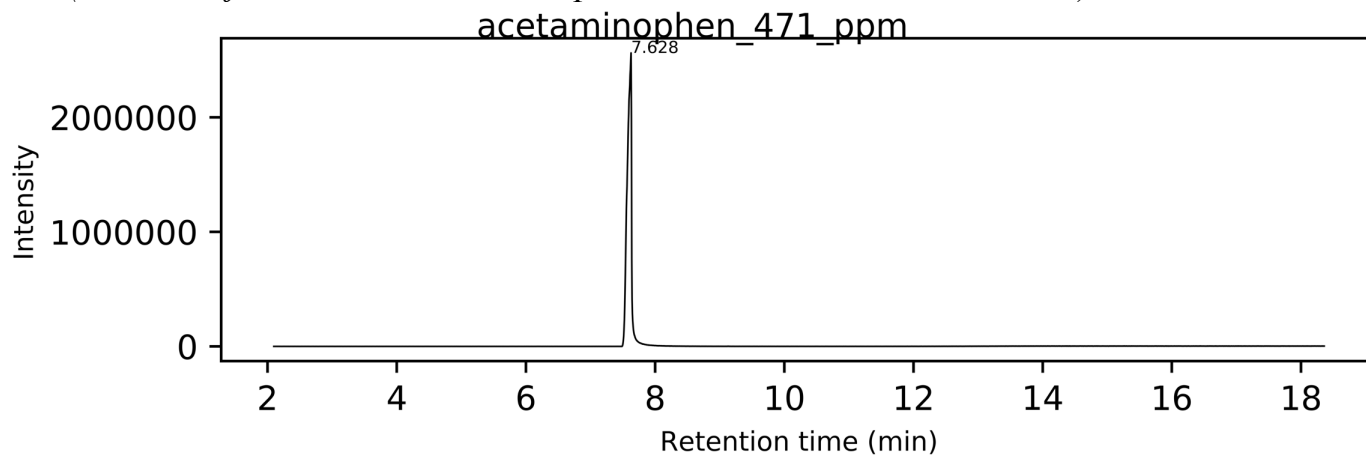
2. Chemical Data

Chemical Formula $C_8H_9NO_2$
Molecular Weight 151.16 g/mol
pK_a 9.38



3. Qualitative Data

3.1. GC/MS Full scan TIC and mass spectrum using an Agilent 5977 MSD with EI source (See notes for GC conditions, MS parameters, and retention indices).



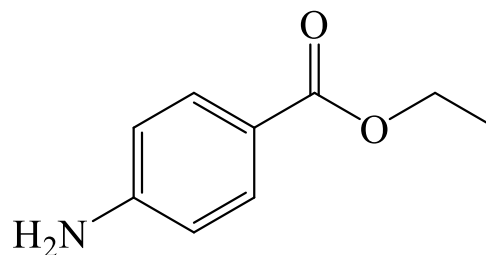
Benzocaine

1. General Information

IUPAC Name	ethyl 4-aminobenzoate
CAS #	94-09-7
Source	Reference Standard

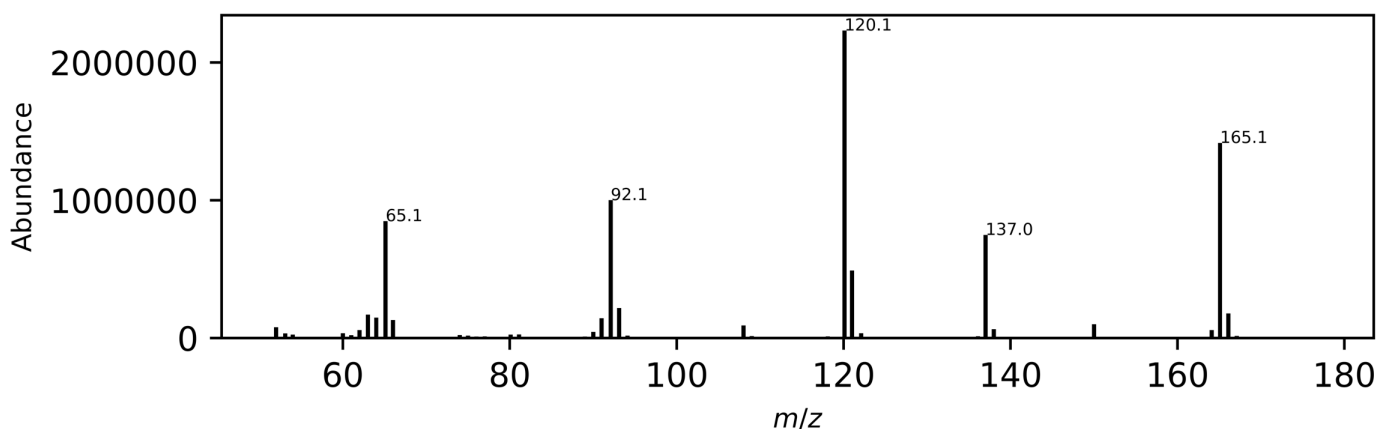
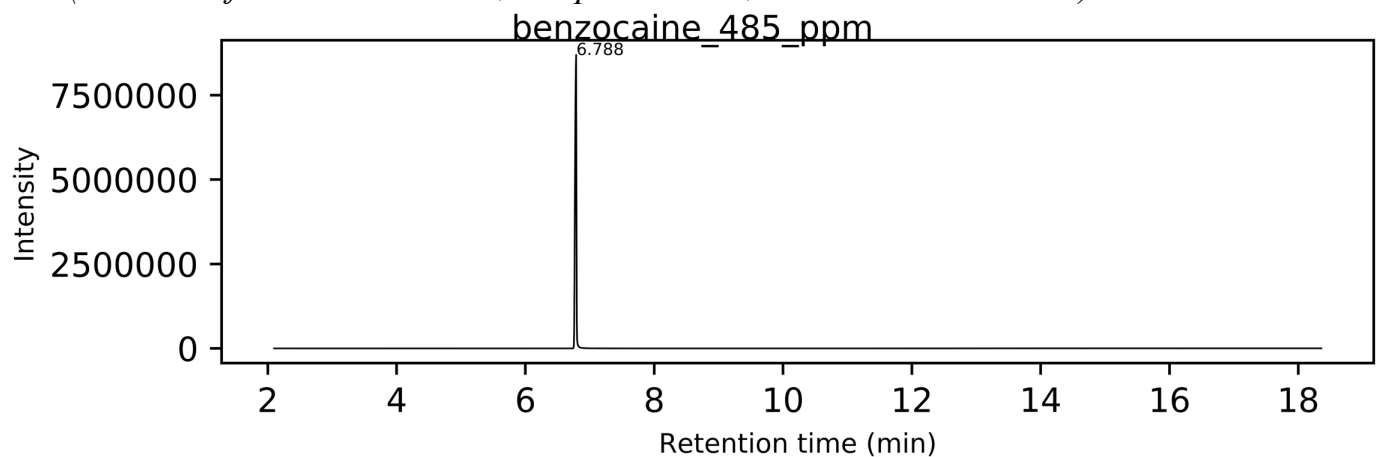
2. Chemical Data

Chemical Formula	C ₉ H ₁₁ NO ₂
Molecular Weight	165.19 g/mol
pK _a	2.51



3. Qualitative Data

3.1. GC/MS Full scan TIC and mass spectrum using an Agilent 5977 MSD with EI source (See notes for GC conditions, MS parameters, and retention indices).



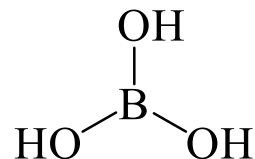
Boric acid

1. General Information

IUPAC Name	boric acid
CAS #	10043-35-3
Source	Reference Standard

2. Chemical Data

Chemical Formula	H ₃ BO ₃
Molecular Weight	61.84 g/mol
pK _a	9.24



3. Qualitative Data

- 3.1. *GC/MS Full scan TIC and mass spectrum using an Agilent 5977 MSD with EI source (See notes for GC conditions, MS parameters, and retention indices).*

NO SIGNAL UNDER TESTED CONDITIONS

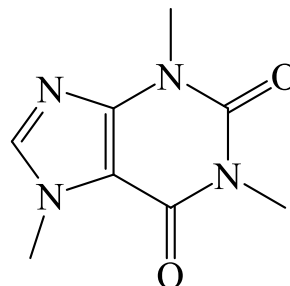
Caffeine

1. General Information

IUPAC Name 1,3,7-trimethylpurine-2,6-dione
CAS # 58-08-2
Source Reference Standard

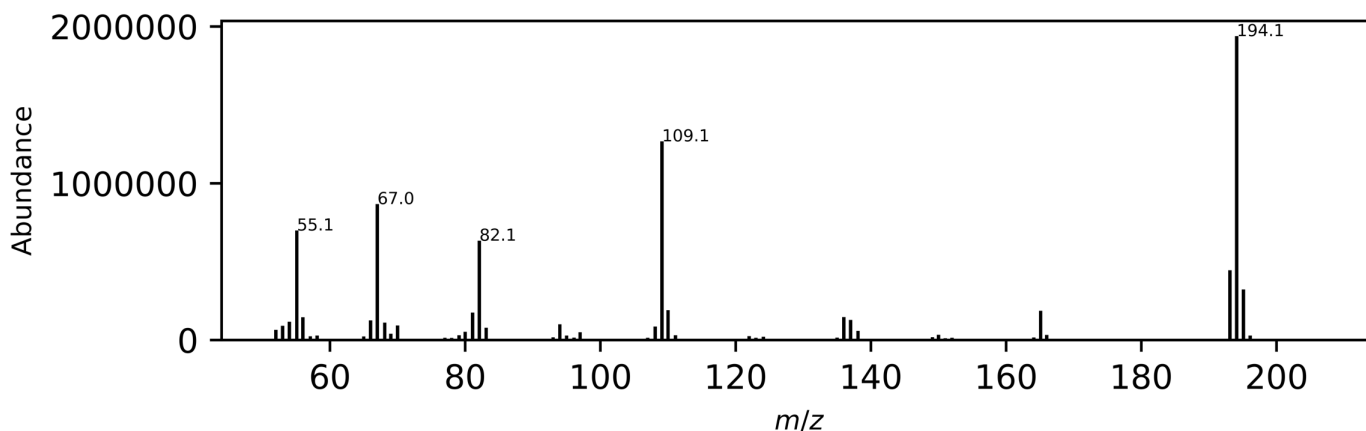
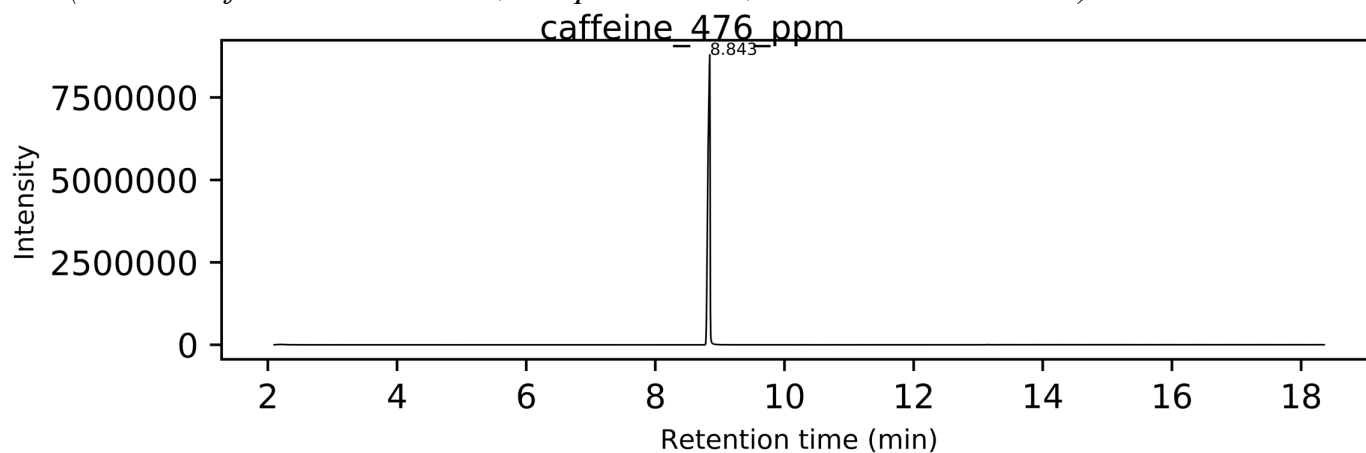
2. Chemical Data

Chemical Formula $C_8H_{10}N_4O_2$
Molecular Weight 194.19 g/mol
pK_a 14.0



3. Qualitative Data

3.1. GC/MS Full scan TIC and mass spectrum using an Agilent 5977 MSD with EI source (See notes for GC conditions, MS parameters, and retention indices).



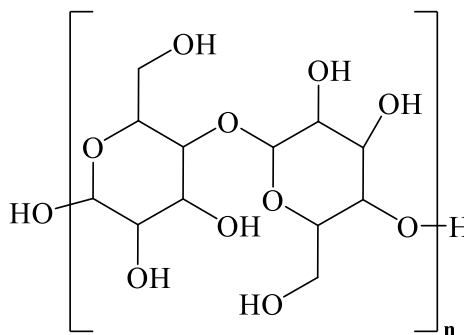
Corn Starch

1. General Information

IUPAC Name	2-(hydroxymethyl)-6- {[4,5,6-trihydroxy-2-(hydroxymethyl)oxan-3-yl]oxy}oxane-3,4,5-triol
CAS #	9005-25-8
Source	Reference Standard

2. Chemical Data

Chemical Formula	$(C_6H_{10}O_5)_n$
Molecular Weight	NA
pK _a	NA



3. Qualitative Data

- 3.1. *GC/MS Full scan TIC and mass spectrum using an Agilent 5977 MSD with EI source (See notes for GC conditions, MS parameters, and retention indices).*

NO SIGNAL UNDER TESTED CONDITIONS

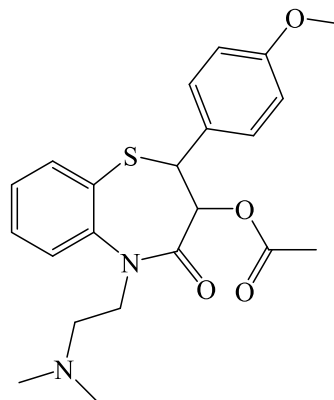
Diltiazem

1. General Information

IUPAC Name	[(2S,3S)-5-[2-(dimethylamino)ethyl]-2-(4-methoxyphenyl)-4-oxo-2,3-dihydro-1,5-benzothiazepin-3-yl] acetate
CAS #	56209-45-1
Source	Reference Standard

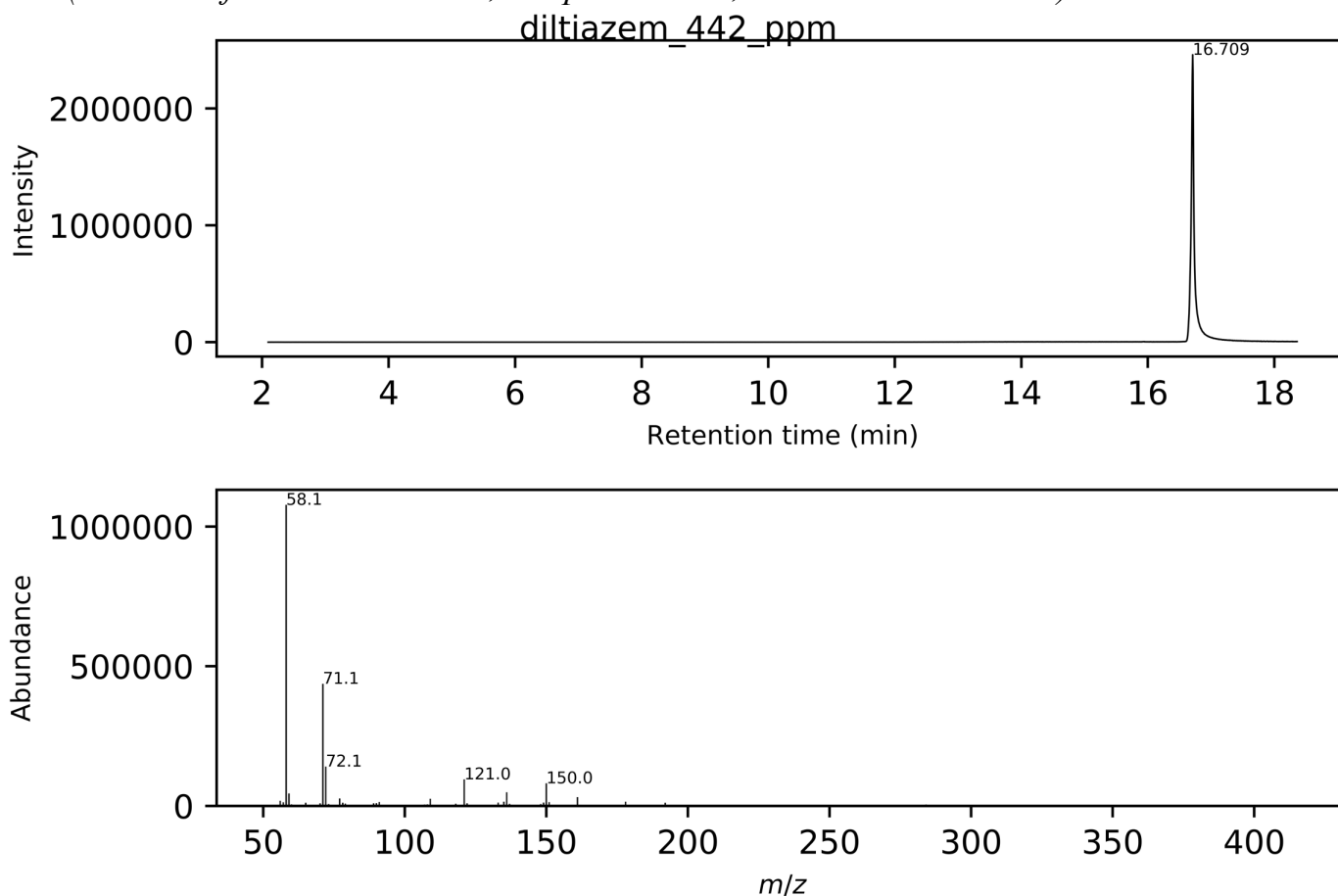
2. Chemical Data

Chemical Formula	C ₂₂ H ₂₆ N ₂ O ₄ S
Molecular Weight	414.5 g/mol
pK _a	8.06



3. Qualitative Data

3.1. GC/MS Full scan TIC and mass spectrum using an Agilent 5977 MSD with EI source (See notes for GC conditions, MS parameters, and retention indices).



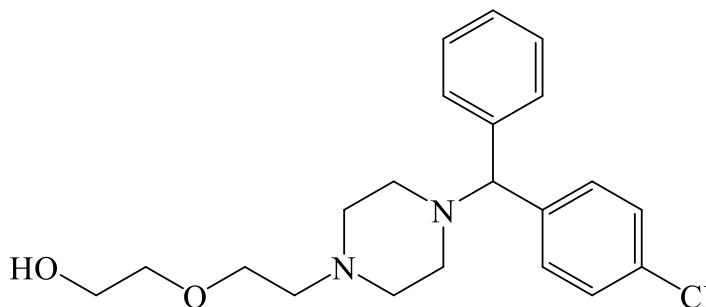
Hydroxyzine

1. General Information

IUPAC Name 2-[2-[4-[(4-chlorophenyl)-phenylmethyl]piperazin-1-yl]ethoxy]ethanol
CAS # 68-88-2
Source Reference Standard

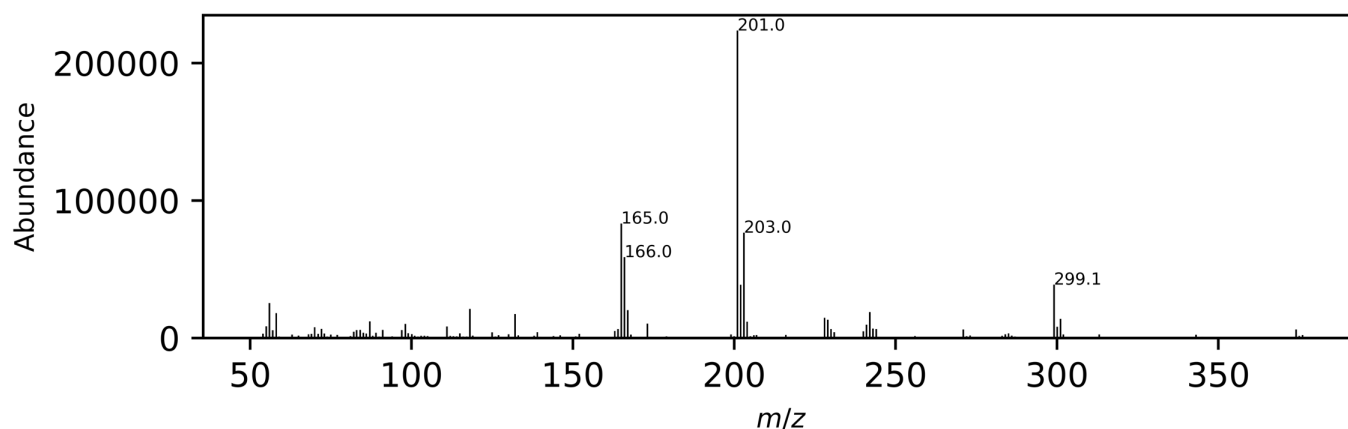
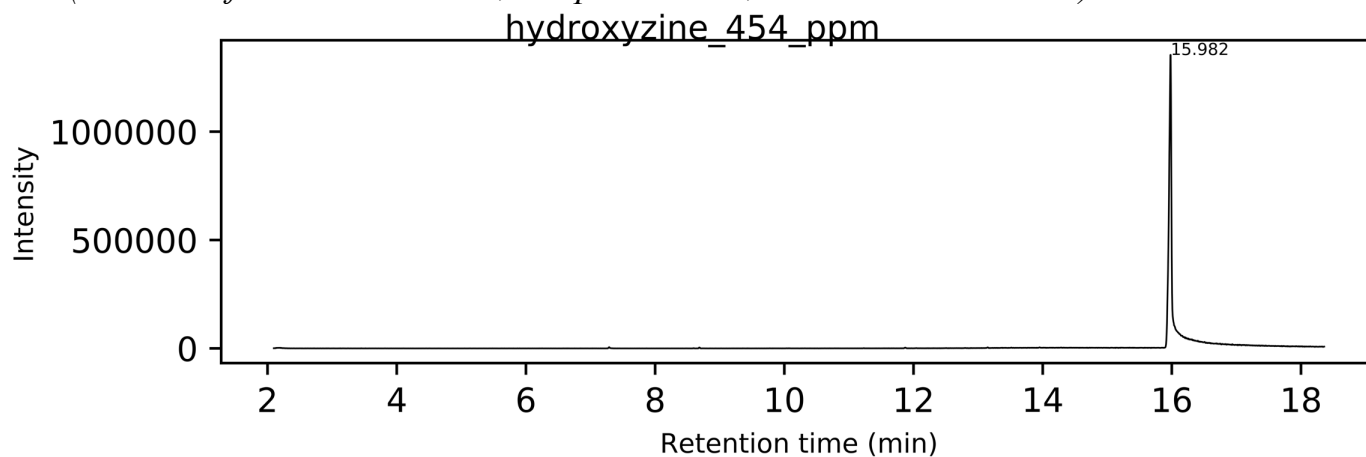
2. Chemical Data

Chemical Formula $C_{21}H_{27}ClN_2O_2$
Molecular Weight 374.9 g/mol
 pK_a 2.47



3. Qualitative Data

3.1. GC/MS Full scan TIC and mass spectrum using an Agilent 5977 MSD with EI source (See notes for GC conditions, MS parameters, and retention indices).



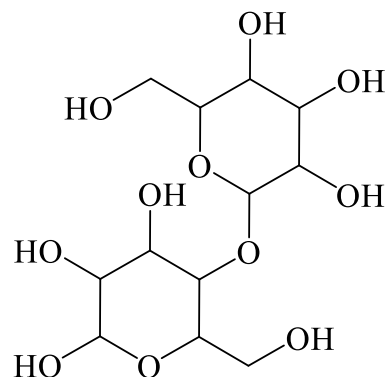
Maltose

1. General Information

IUPAC Name	(2R,3S,4S,5R,6R)-2-(hydroxymethyl)-6-[(2R,3S,4R,5R,6R)-4,5,6-trihydroxy-2-(hydroxymethyl)oxan-3-yl]oxyoxane-3,4,5-triol
CAS #	133-99-3
Source	Reference Standard

2. Chemical Data

Chemical Formula	C ₁₂ H ₂₂ O ₁₁
Molecular Weight	342.30 g/mol
pK _a	NA



3. Qualitative Data

- 3.1. *GC/MS Full scan TIC and mass spectrum using an Agilent 5977 MSD with EI source (See notes for GC conditions, MS parameters, and retention indices).*

NO SIGNAL UNDER TESTED CONDITIONS

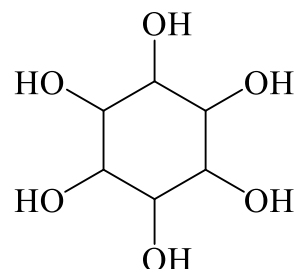
Myo-Inositol

1. General Information

IUPAC Name	cyclohexane-1,2,3,4,5,6-hexol
CAS #	551-72-4
Source	Reference Standard

2. Chemical Data

Chemical Formula	C ₆ H ₁₂ O ₆
Molecular Weight	180.16 g/mol
pK _a	NA



3. Qualitative Data

- 3.1. *GC/MS Full scan TIC and mass spectrum using an Agilent 5977 MSD with EI source (See notes for GC conditions, MS parameters, and retention indices).*

NO SIGNAL UNDER TESTED CONDITIONS

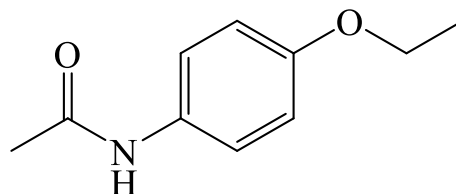
Phenacetin

1. General Information

IUPAC Name N-(4-ethoxyphenyl)acetamide
CAS # 62-44-2
Source Reference Standard

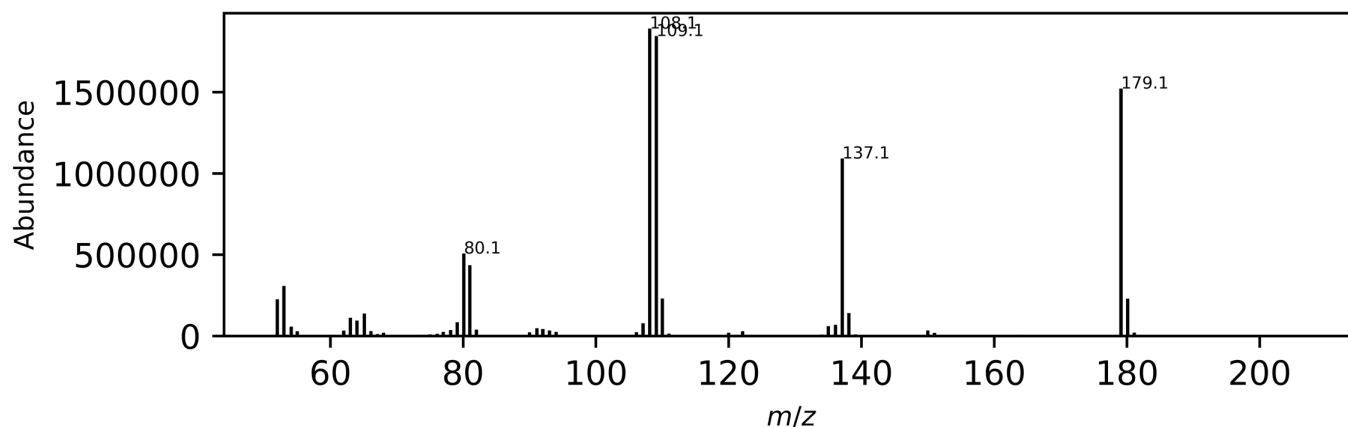
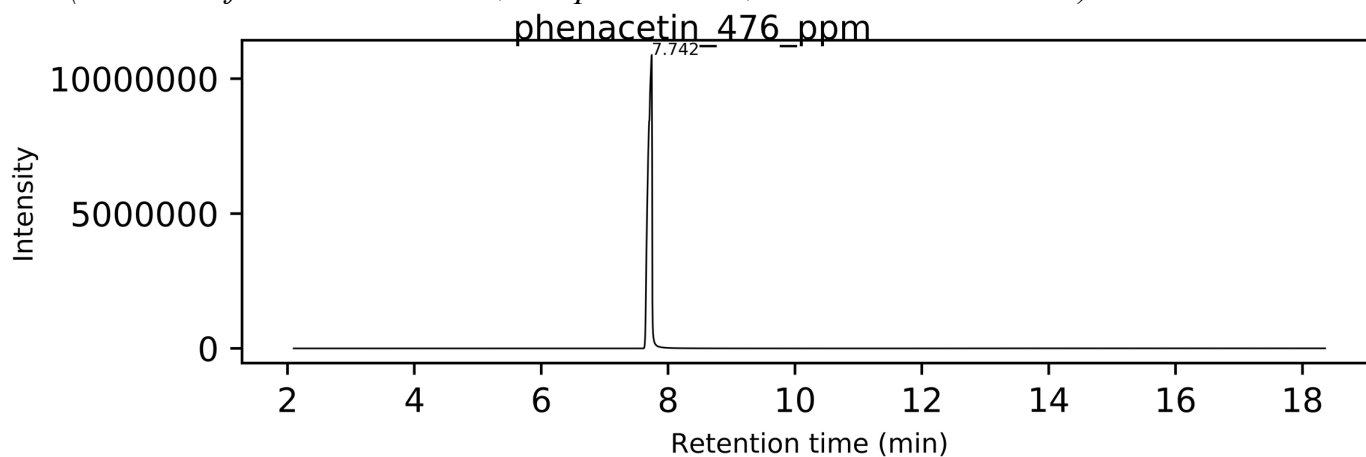
2. Chemical Data

Chemical Formula $C_{10}H_{13}NO_2$
Molecular Weight 179.22 g/mol
pK_a NA



3. Qualitative Data

3.1. GC/MS Full scan TIC and mass spectrum using an Agilent 5977 MSD with EI source (See notes for GC conditions, MS parameters, and retention indices).



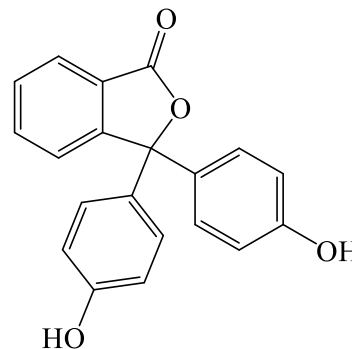
Phenolphthalein

1. General Information

IUPAC Name	3,3-bis(4-hydroxyphenyl)-2-benzofuran-1-one
CAS #	77-09-8
Source	Reference Standard

2. Chemical Data

Chemical Formula	C ₂₀ H ₁₄ O ₄
Molecular Weight	318.3 g/mol
pK _a	9.7



3. Qualitative Data

- 3.1. *GC/MS Full scan TIC and mass spectrum using an Agilent 5977 MSD with EI source (See notes for GC conditions, MS parameters, and retention indices).*

NO SIGNAL UNDER TESTED CONDITIONS

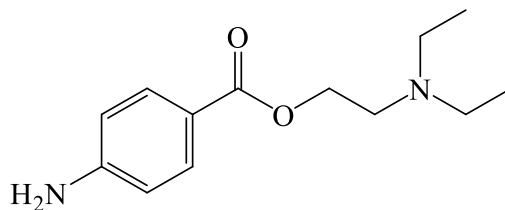
Procaine

1. General Information

IUPAC Name 2-(diethylamino)ethyl 4-aminobenzoate
CAS # 59-46-1
Source Reference Standard

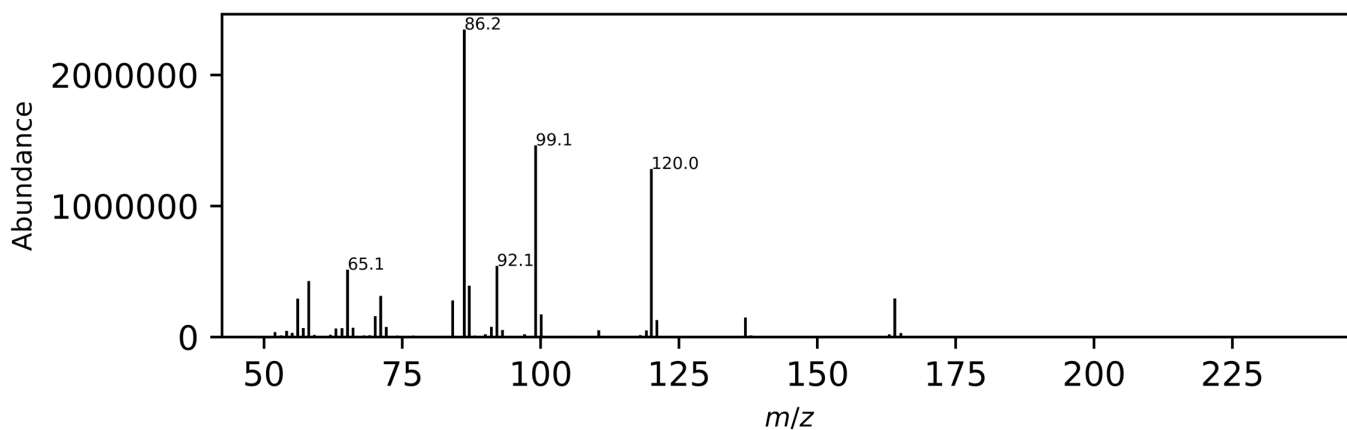
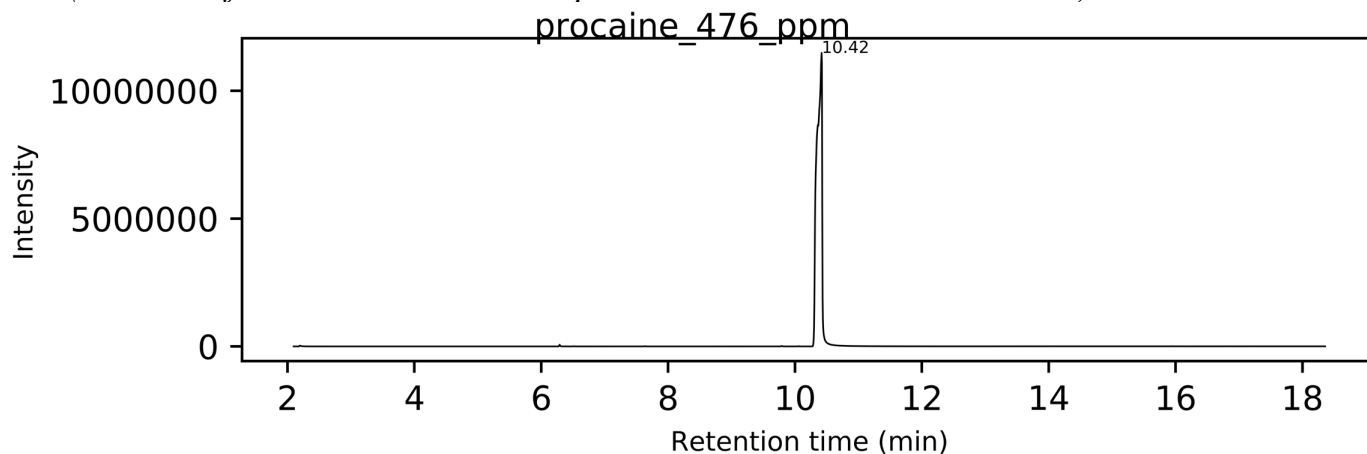
2. Chemical Data

Chemical Formula $C_{13}H_{20}N_2O_2$
Molecular Weight 236.31 g/mol
pK_a 9.04



3. Qualitative Data

3.1. GC/MS Full scan TIC and mass spectrum using an Agilent 5977 MSD with EI source (See notes for GC conditions, MS parameters, and retention indices).



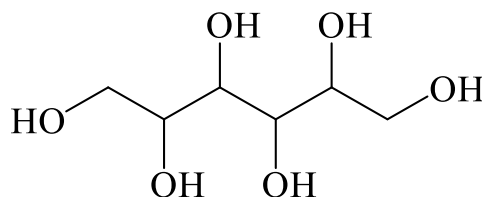
Sorbitol

1. General Information

IUPAC Name	(2R,3R,4R,5S)-hexane-1,2,3,4,5,6-hexol
CAS #	50-70-4
Source	Reference Standard

2. Chemical Data

Chemical Formula	C ₆ H ₁₄ O ₆
Molecular Weight	182.17 g/mol
pK _a	13.6



3. Qualitative Data

- 3.1. *GC/MS Full scan TIC and mass spectrum using an Agilent 5977 MSD with EI source (See notes for GC conditions, MS parameters, and retention indices).*

NO SIGNAL UNDER TESTED CONDITIONS

NOTES

The GC/MS system utilized is an Agilent 7890 coupled to 5977A MSD mass spectrometer with an electron ionization source operating @ 70 eV. The following parameters and conditions were utilized in the generation of the spectral library:

Analytical Column	Agilent J&W DB-5MS UI, 30 m x 0.25 x 0.25 μ m (5 %phenyl-methylpolysiloxane)
GC	Agilent 7890 B GC
Carrier Gas	Helium, constant flow mode, 1.5 mL/min
Sample Introduction	Split/Splitless Inlet, 1 μ L, 20:1 split ratio, 20 mL/min split flow, 22 mL/min total flow
Oven	60 °C (0 min); 20 °C/min to 188 °C for 0.15 min 5°C/min to 192°C for 0.15 min, 15°C/min to 280°C for 13 min Total Run time= 26.367
MSD	Agilent 5977 A MSD Mass Hunter GC/MS Rev B.07.00 SP.1549
Solvent Delay	2 min
MS Temperature	250 °C (source), 200 °C (quad)
Mass Range	50-500 m/z
Threshold	150
Scan Speed	1562 (N=2)
MS	EI, Full scan and SIM

Retention Indices Study

The retention index (RI) of selected compounds was evaluated by analyzing 100 ppm saturated alkanes before and after the compounds in triplicate over five days. The variability in retention time and RI were assessed. RI was calculated using the Equation shown below. The compounds' retention time is represented by $t_{r(x)}$, the retention time of the adjacent n-alkane with shorter retention time $t_{r(n)}$, the retention time of the adjacent n-alkane with longer retention time $t_{r(n+1)}$, and n is the number of carbon atoms in the n-alkane with longer retention time.

$$RI = 100n + 100 \left(\frac{t_{r(x)} - t_{r(n)}}{t_{r(n+1)} - t_{r(n)}} \right)$$

The retention indices (RI) of the compounds used in this study can be found in the Table below. No RI data was calculated for diltiazem, alprazolam, Mitragynine, PB22, and buprenorphine as these compounds eluted later than the longest n-alkane—one disadvantage of the RI method. As anticipated, the early eluting compounds had a lower RI than the later eluting ones. Methamphetamine eluted the earliest with a RI value of 1356, whereas hydroxyzine had the highest RI value, 3035. The figure below shows the chromatogram and the order of elution of the compounds. For compounds with RI values reported in the literature where a DB-5 column was

used, the values were comparable to the findings reported in Table 1 although the column conditions may not have been identical. The primary source for the RI values was the NIST Chemistry Webbook (www.webbook.nist.gov). Although the NIST Chemistry Webbook contains RI data on most of the compounds in Table 1, only RI data from a similar column was selected for comparison. When the precision of the RI values was assessed by ANOVA, only methamphetamine showed high within day (27.2% CV) and between-run (70.7% CV) variability. The variability for other compounds was less than 0%. One possible reason for the high variability observed from methamphetamine (HCl salt form) is due to the split peaks, which may have influenced how the peak was auto-integrated.

Table 1. Average retention times and retention indices.

Compound	Retention Time (mins)		Retention Index
	Avg \pm SD	CV(%)	Avg \pm SD
Methamphetamine	4.577 \pm 0.014	0.30	1356.0 \pm 1.99
4-Methylmethcathinone	6.048 \pm 0.004	0.07	1572.4 \pm 0.61
4-Methylethcathinone	6.374 \pm 0.002	0.02	1622.3 \pm 0.17
Benzocaine	6.761 \pm 0.002	0.02	1681.7 \pm 0.16
Acetaminophen	7.528 \pm 0.003	0.04	1786.5 \pm 0.19
Phenacetin	7.642 \pm 0.002	0.03	1801.6 \pm 0.19
Caffeine	8.790 \pm 0.002	0.02	1949.5 \pm 0.17
Lidocaine	9.126 \pm 0.002	0.02	1993.7 \pm 0.17
Levamisole	9.965 \pm 0.002	0.02	2110.1 \pm 0.21
Procaine	10.307 \pm 0.002	0.02	2160.0 \pm 0.19

Cocaine	11.483 ± 0.002	0.01	2341.7 ± 0.16
SKF 525A	12.124 ± 0.001	0.01	2448.6 ± 0.16
Codeine	12.670 ± 0.002	0.01	2544.3 ± 0.18
Morphine	12.970 ± 0.002	0.01	2598.4 ± 0.16
Δ ⁹ -THC	13.119 ± 0.002	0.01	2626.1 ± 0.15
Heroin	14.016 ± 0.002	0.01	2786.0 ± 0.21
Fentanyl	14.642 ± 0.002	0.01	2880.5 ± 0.20
Sufentanil	15.197 ± 0.002	0.02	2952.6 ± 0.26
Naltrexone	15.797 ± 0.005	0.03	3022.4 ± 0.27
Hydroxyzine	15.919 ± 0.003	0.02	3035.0 ± 0.19
Diltiazem	16.657 ± 0.003	0.02	--
Alprazolam	16.730 ± 0.004	0.02	--
Mitragynine	22.445 ± 0.010	0.05	--
PB22	22.949 ± 0.259	1.13	--
Buprenorphine	24.398 ± 0.011	0.04	--

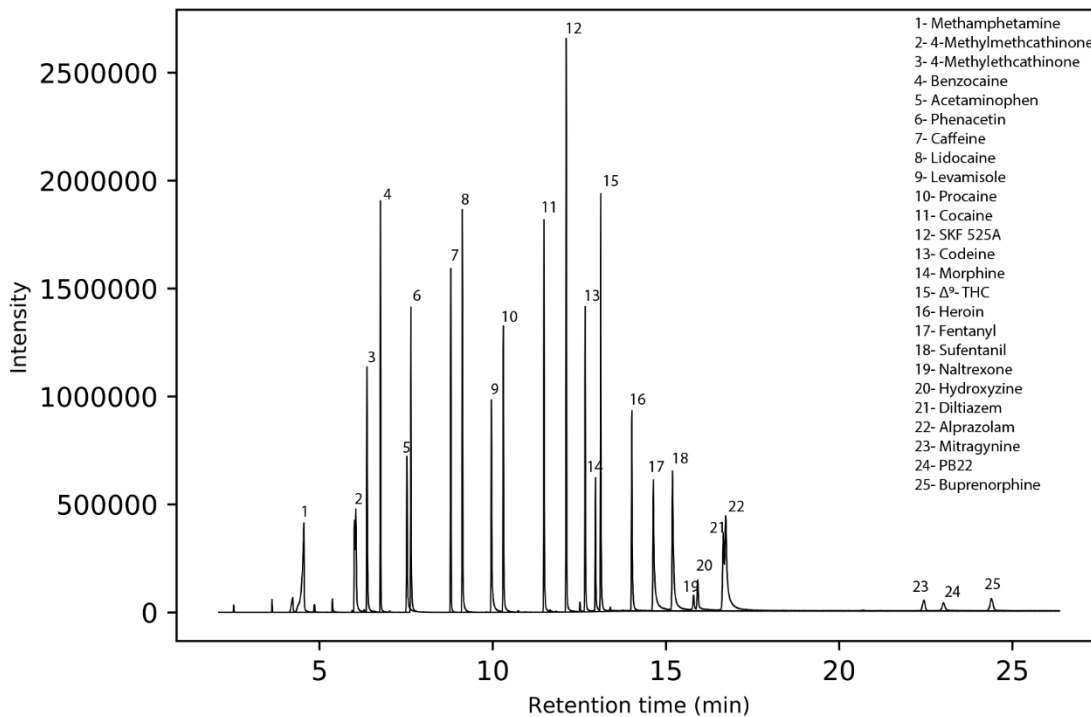


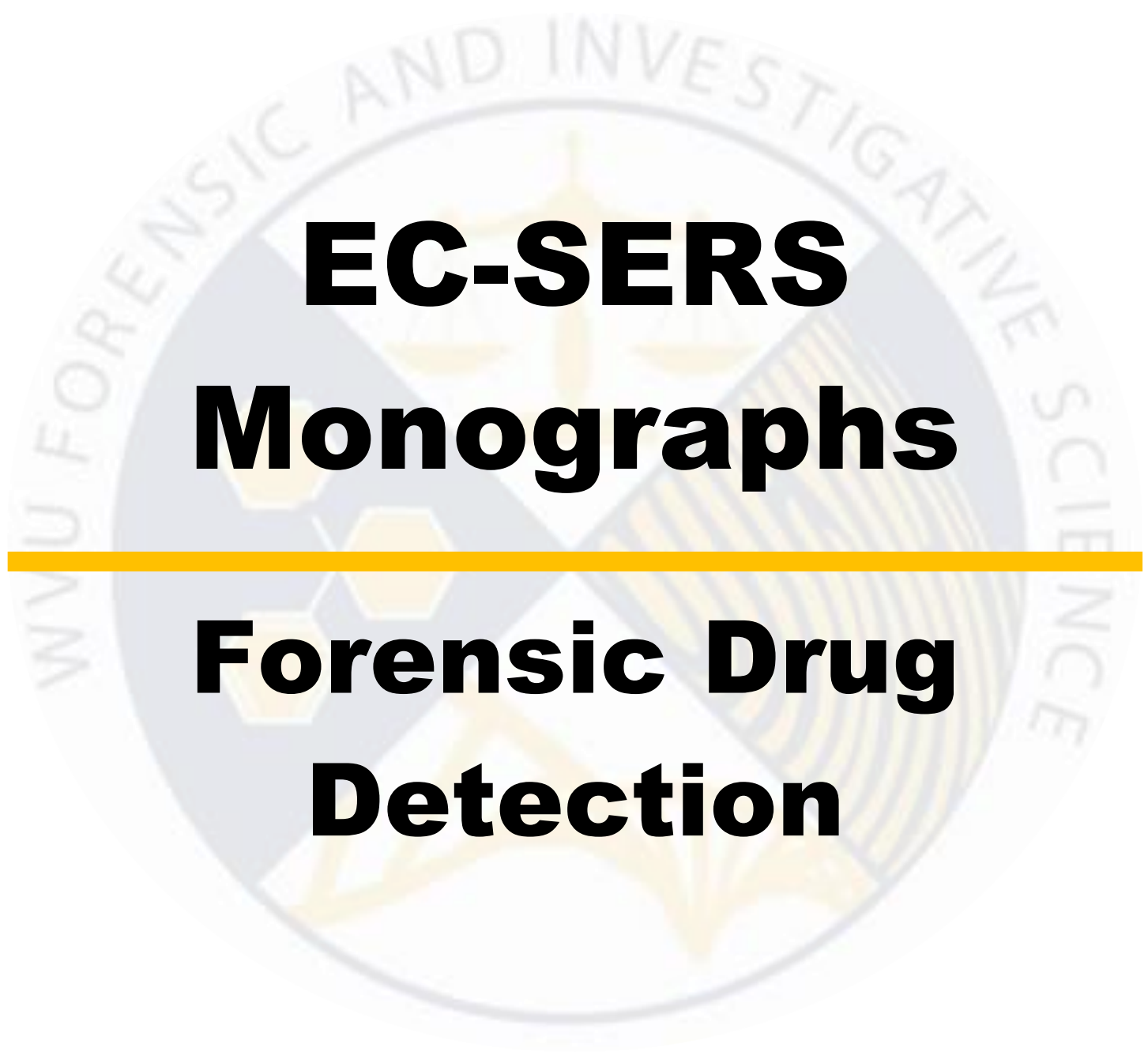
Figure 1. Full scan TIC Chromatogram of analyzed target compounds.

PubChem and/or Cayman Chemical were used as reference for relevant compound information.

ChemDraw Professional software version 21.0.0.28 was used for the generation of the chemical structures.

This data was collected in relation to National Institute of Justice Award # 2019-DU-BX-0030 to West Virginia University. The opinions, findings, and conclusions are those of the authors and do not necessarily reflect those of the department of justice.

APPENDIX B



EC-SERS Monographs

Forensic Drug Detection

Reference Guide
2022

Contents

Alprazolam	4
Buprenorphine	7
Cocaine.....	9
Codeine	13
Fentanyl	16
2'-fluoro <i>ortho</i> -Fluorofentanyl	20
4-ANPP	21
Acryl fentanyl.....	22
Furanyl fentanyl	23
Methoxyacetyl fentanyl.....	24
Valeryl fentanyl	25
Heroin	26
Levamisole.....	29
Lidocaine	32
Methamphetamine.....	34
4-methylethcathinone	37
Mephedrone	39
Mitragynine.....	41
Morphine	43
Naltrexone	45
PB-22.....	48
Quinine.....	50
Sufentanil.....	52
Delta-9-THC.....	54
Acetaminophen	56
Benzocaine.....	58
Boric acid.....	60

Caffeine	62
Corn Starch	64
Diltiazem	66
Hydroxyzine	68
Maltose	70
Myo-Inositol	72
Phenacetin	74
Phenolphthalein	76
Procaine	78
Sorbitol	80
NOTES	82

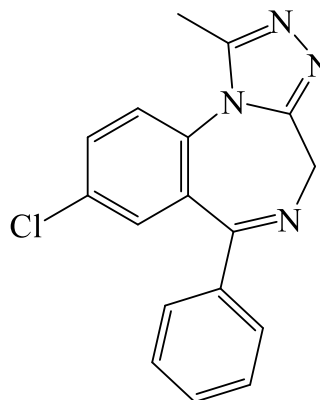
Alprazolam

1. General Information

IUPAC Name 8-chloro-1-methyl-6-phenyl-4*H*-[1,2,4]triazolo[4,3-*a*][1,4]benzodiazepine
CAS # 28981-97-7
Source Reference Standard

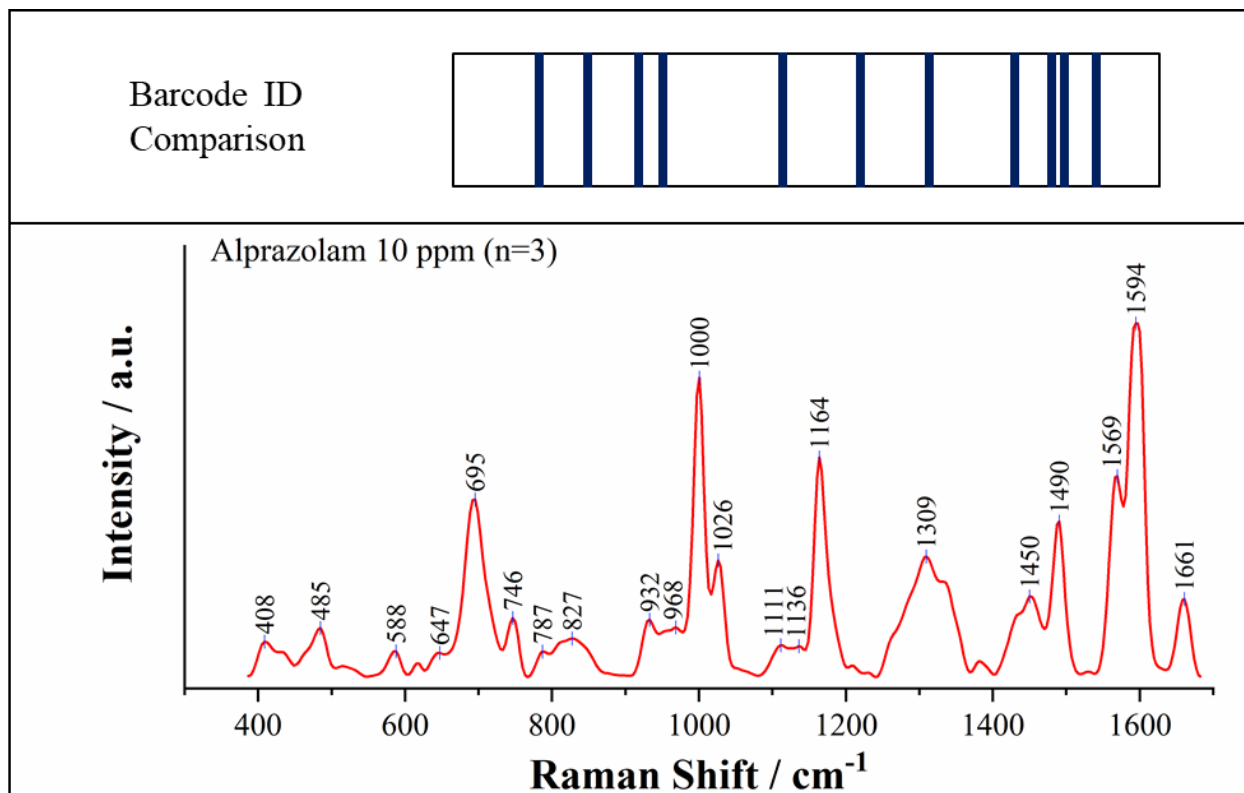
2. Chemical Data

Chemical Formula $C_{17}H_{13}ClN_4$
Molecular Weight 308.8 g/mol
pK_a Not Available

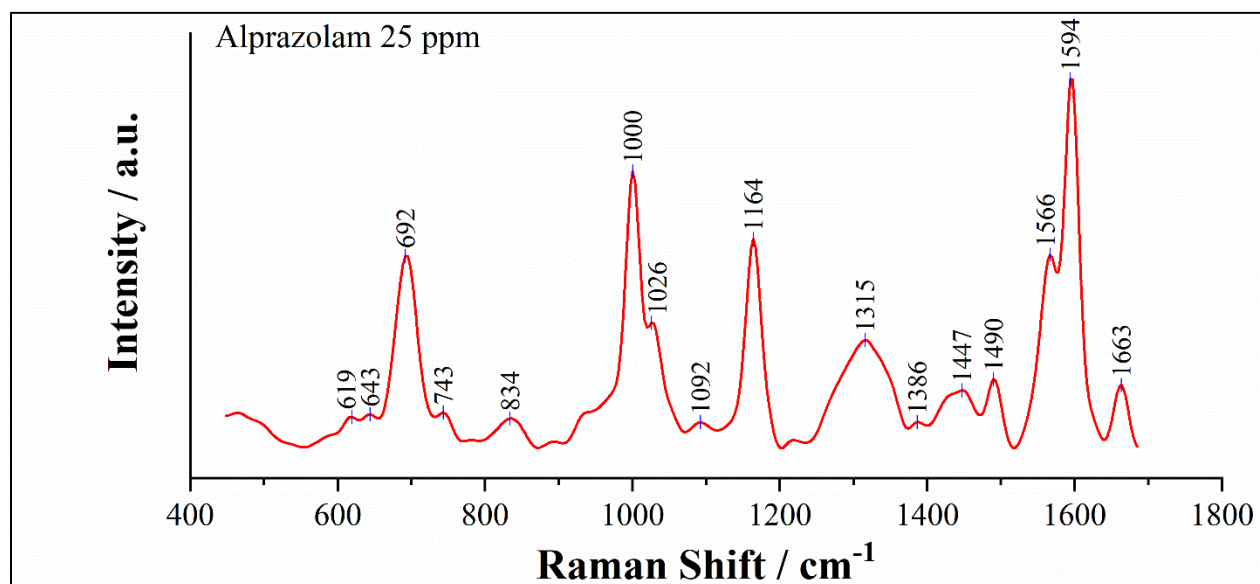


3. Qualitative Data

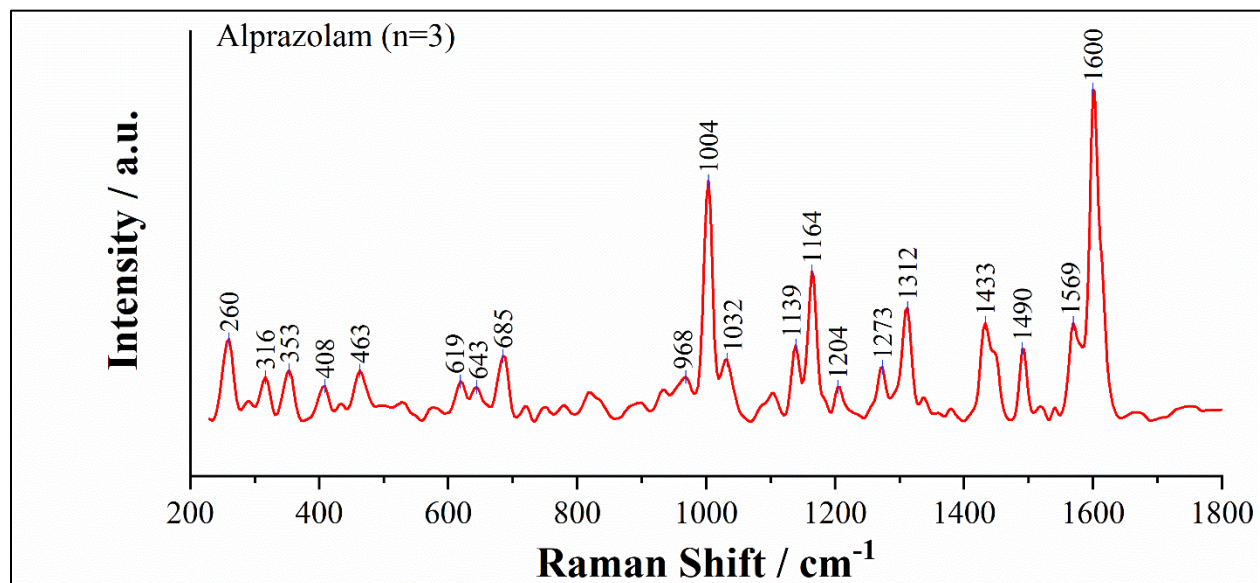
3.1. Nontargeted EC-SERS, 785-nm SPELEC Raman, Silver SPE

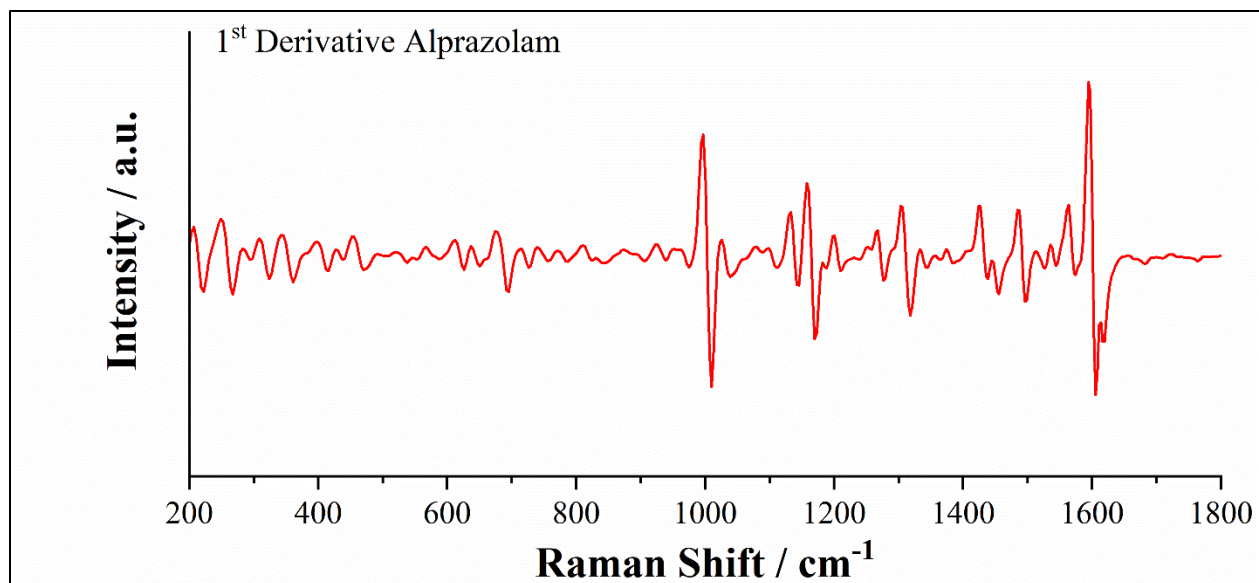


3.2. Fentanyl Targeted EC-SERS, 785-nm SPELEC Raman, Silver SPE

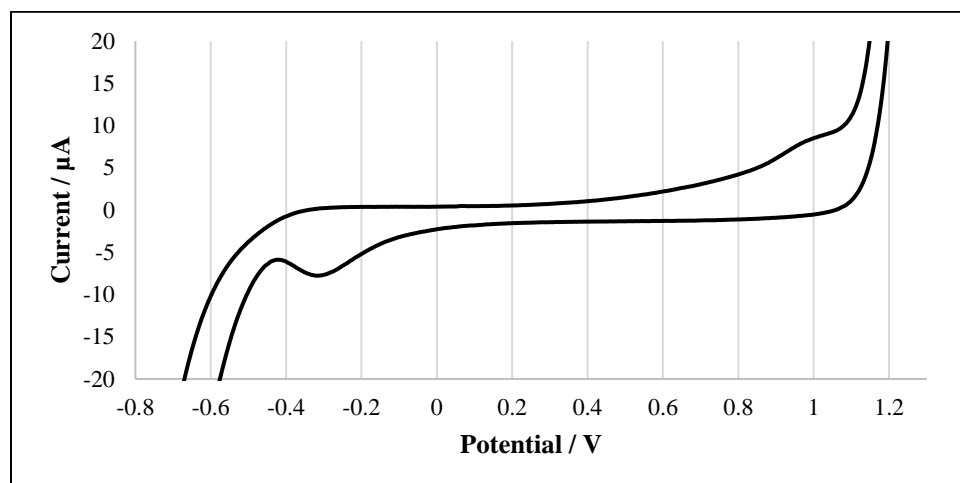


3.3. Normal Raman, 785-nm SPELEC Raman





3.4. Electrochemistry, SPCE, 0.1 M KCl



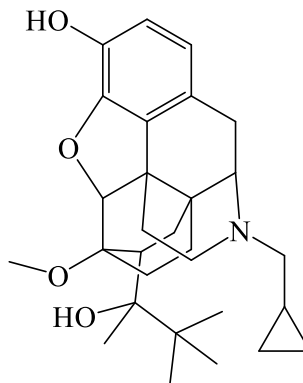
Buprenorphine

1. General Information

IUPAC Name	(1 <i>S</i> ,2 <i>S</i> ,6 <i>R</i> ,14 <i>R</i> ,15 <i>R</i> ,16 <i>R</i>)-5-(cyclopropylmethyl)-16-[(2 <i>S</i>)-2-hydroxy-3,3-dimethylbutan-2-yl]-15-methoxy-13-oxa-5-aza-hexacyclo[13.2.2.1 ^{2,8} .0 ^{1,6} .0 ^{2,14} .0 ^{12,20}]icosa-8(20),9,11-trien-11-ol
CAS #	52485-79-7
Source	Reference Standard

2. Chemical Data

Chemical Formula	C ₂₉ H ₄₁ NO ₄
Molecular Weight	467.6 g/mol
pK _a	8.31



3. Qualitative Data

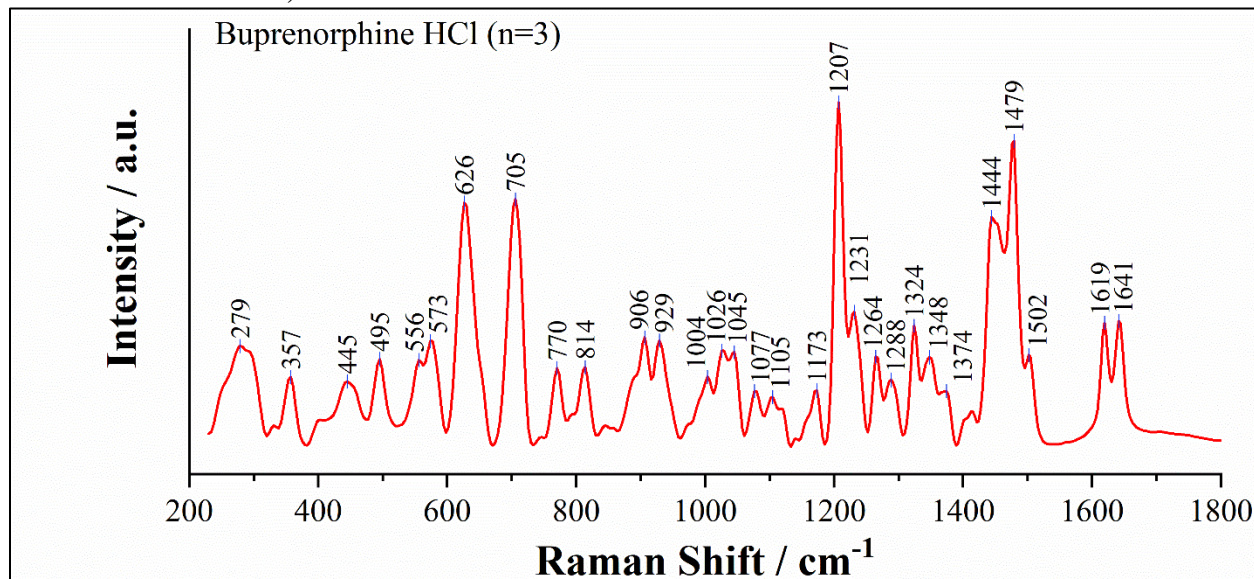
3.1. Nontargeted EC-SERS, 785-nm SPELEC Raman, Silver SPE

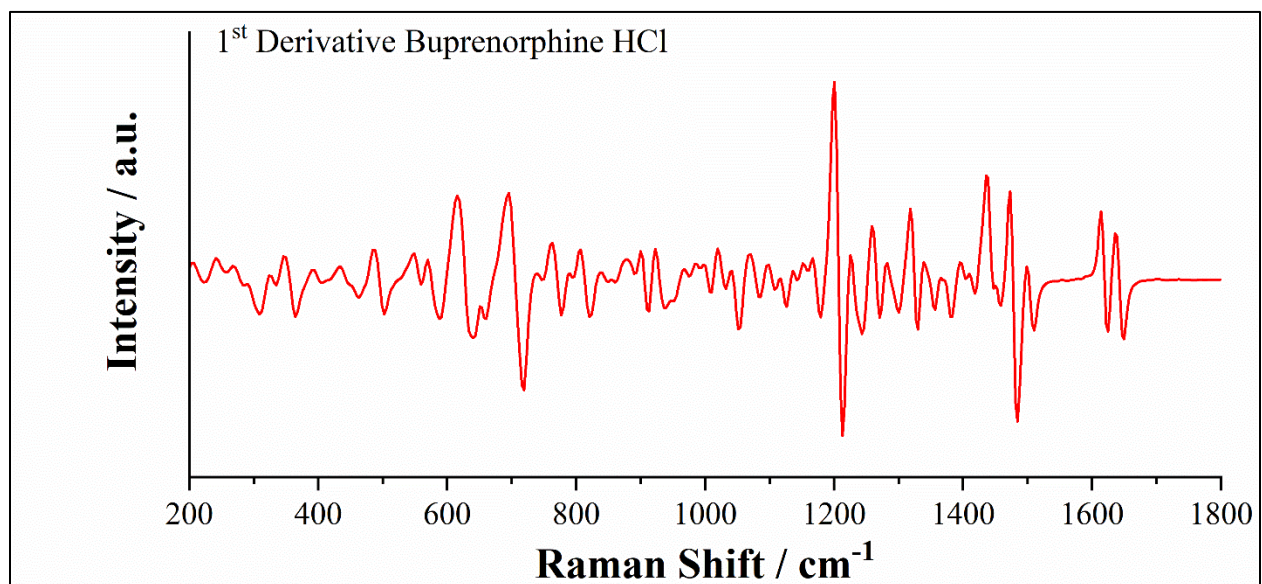
NO SIGNAL UNDER TESTED CONDITIONS

3.2. Fentanyl Targeted EC-SERS, 785-nm SPELEC Raman, Silver SPE

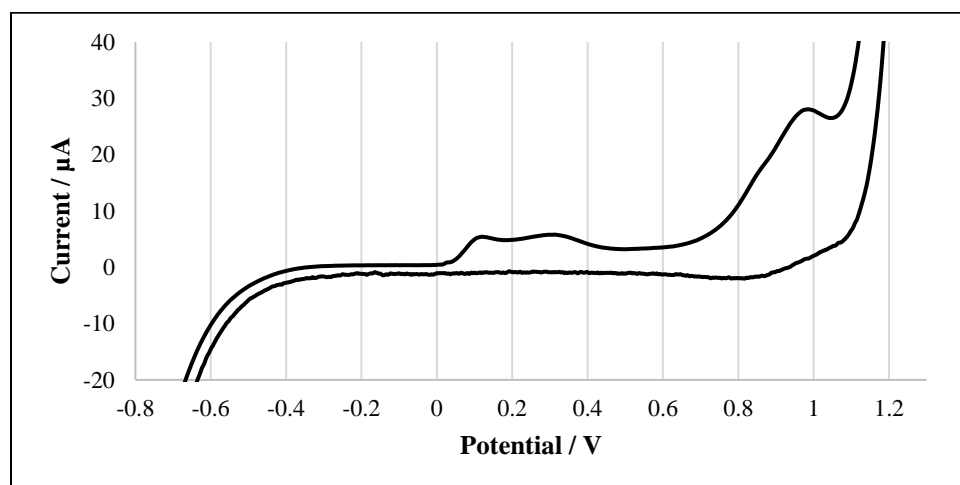
NO SIGNAL UNDER TESTED CONDITIONS

3.3. Normal Raman, 785-nm SPELEC Raman





3.4. Electrochemistry, SPCE, 0.1 M KCl



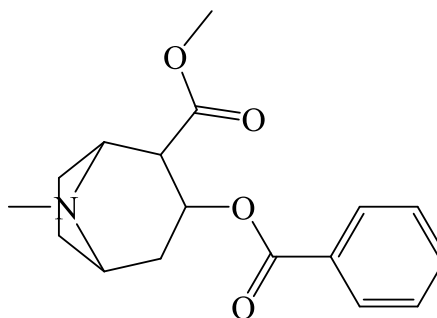
Cocaine

1. General Information

IUPAC Name	methyl (1 <i>R</i> ,2 <i>R</i> ,3 <i>S</i> ,5 <i>S</i>)-3-benzoyloxy-8-methyl-8-azabicyclo[3.2.1]octane-2-carboxylate
CAS #	50-36-2
Source	Reference Standard

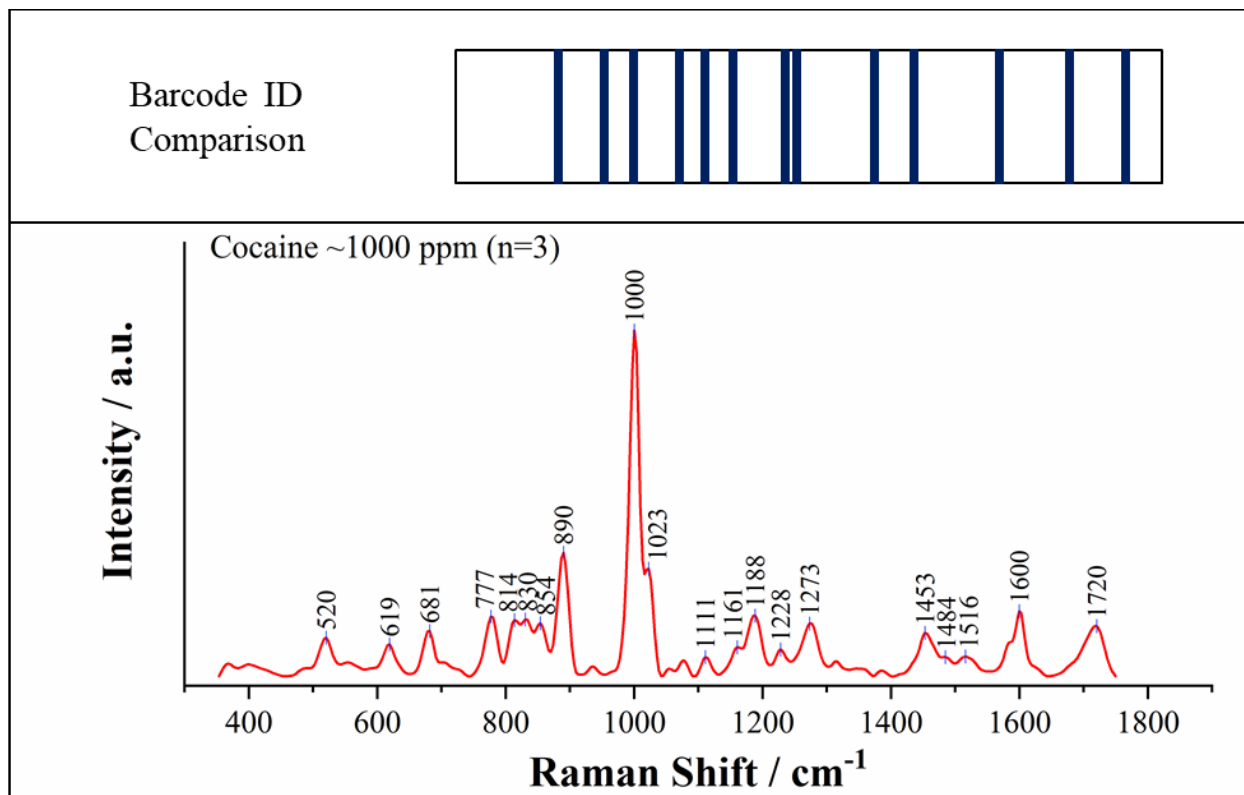
2. Chemical Data

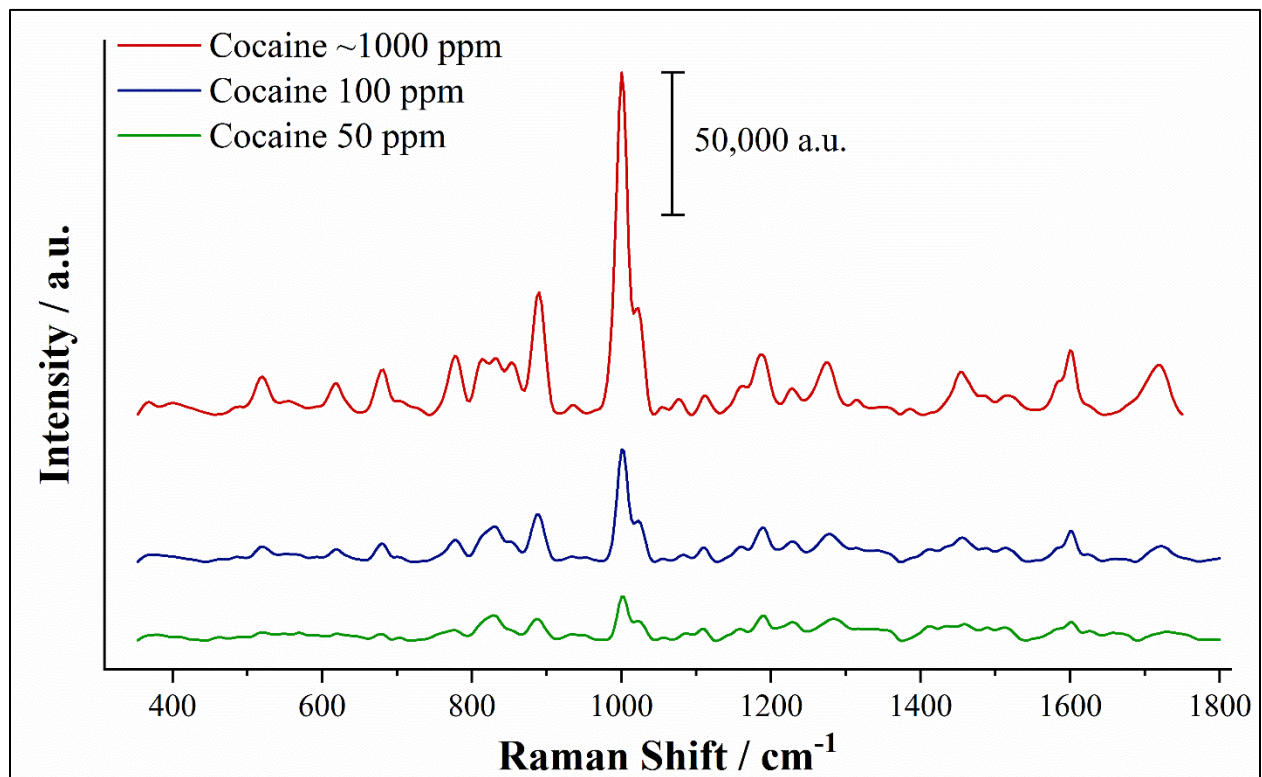
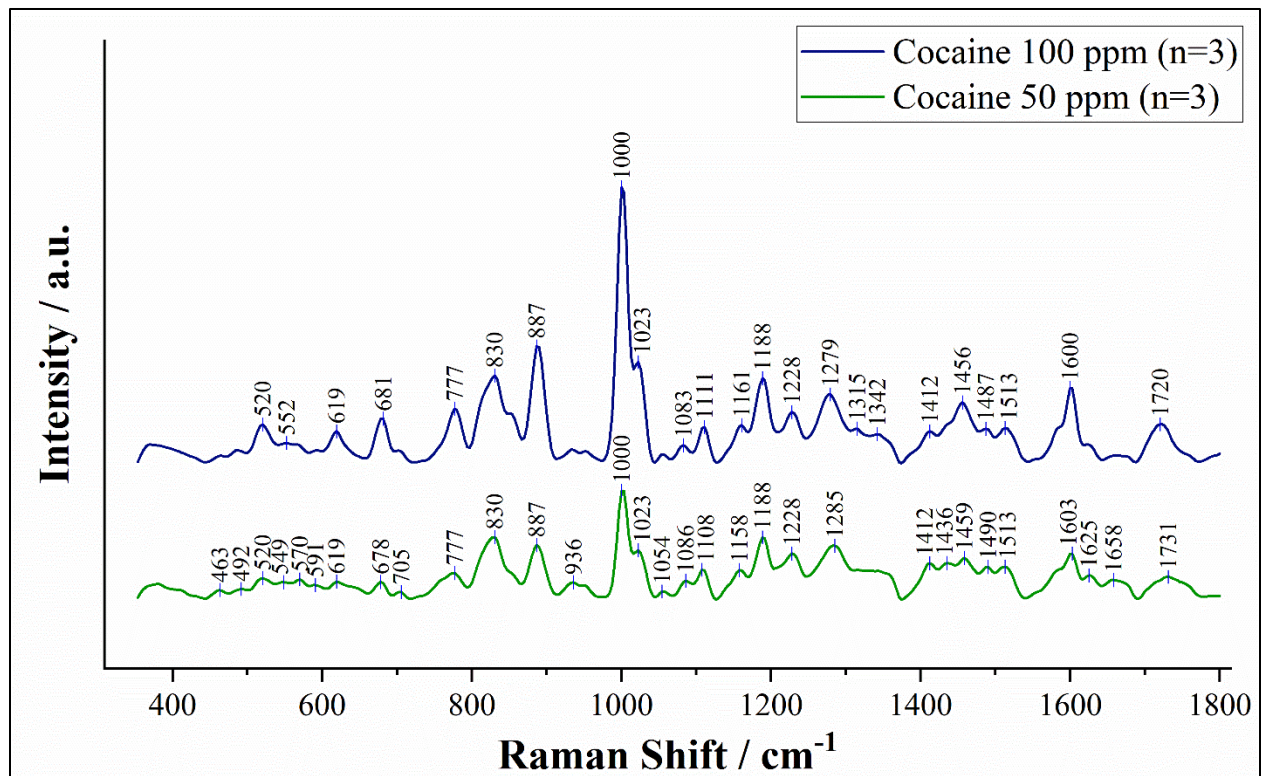
Chemical Formula	C ₁₇ H ₂₁ NO ₄
Molecular Weight	303.35 g/mol
pK _a	8.7



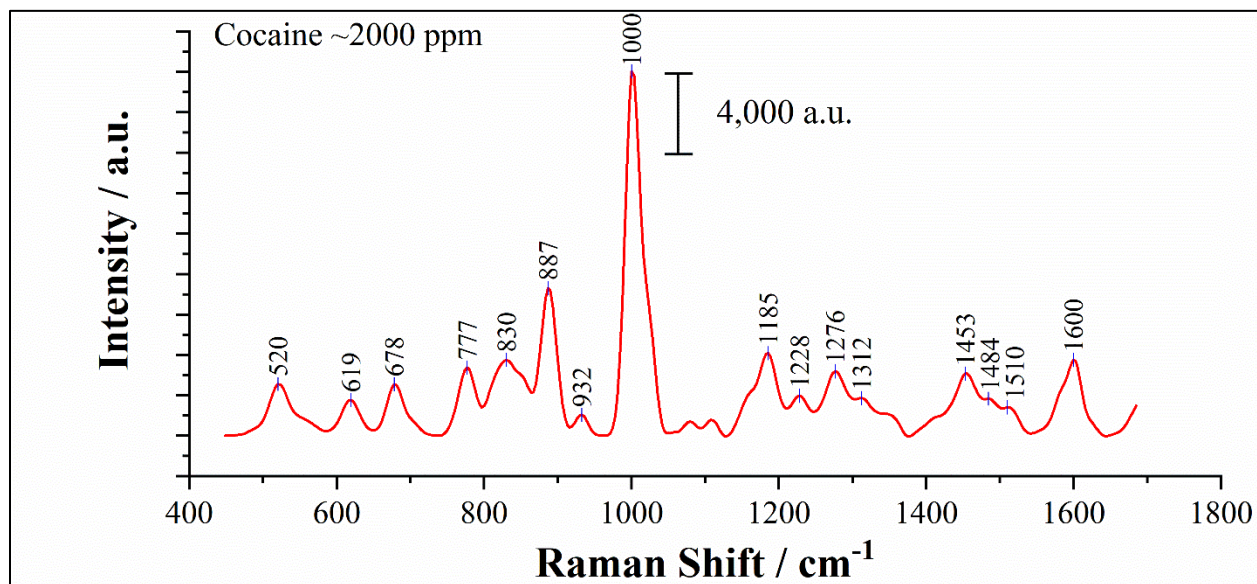
3. Qualitative Data

3.1. Nontargeted EC-SERS, 785-nm SPELEC Raman, Silver SPE

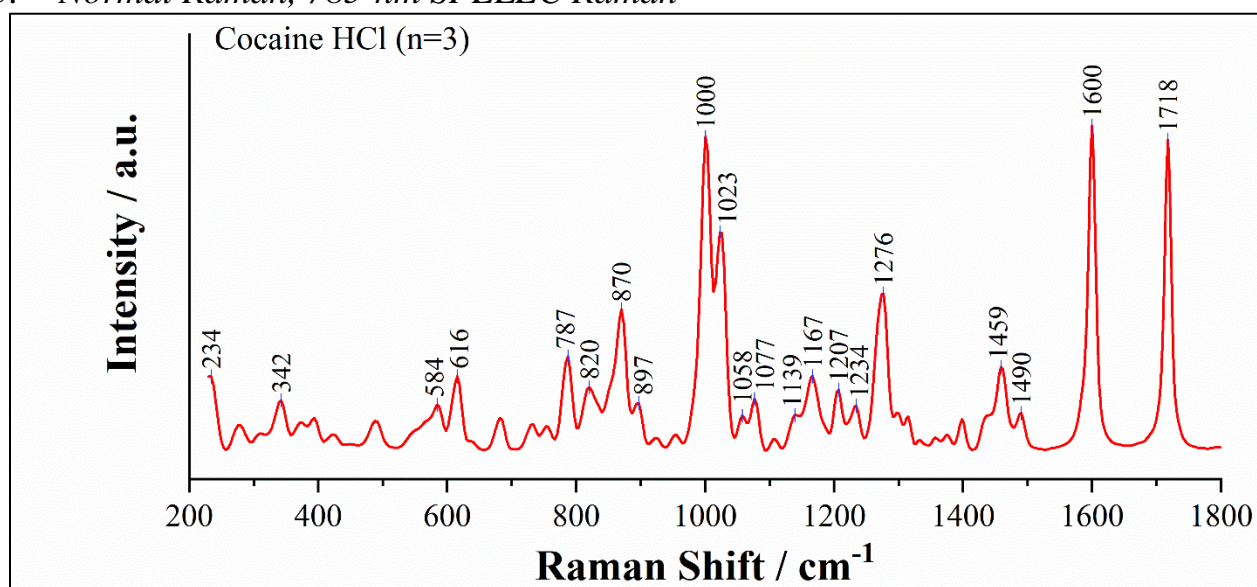


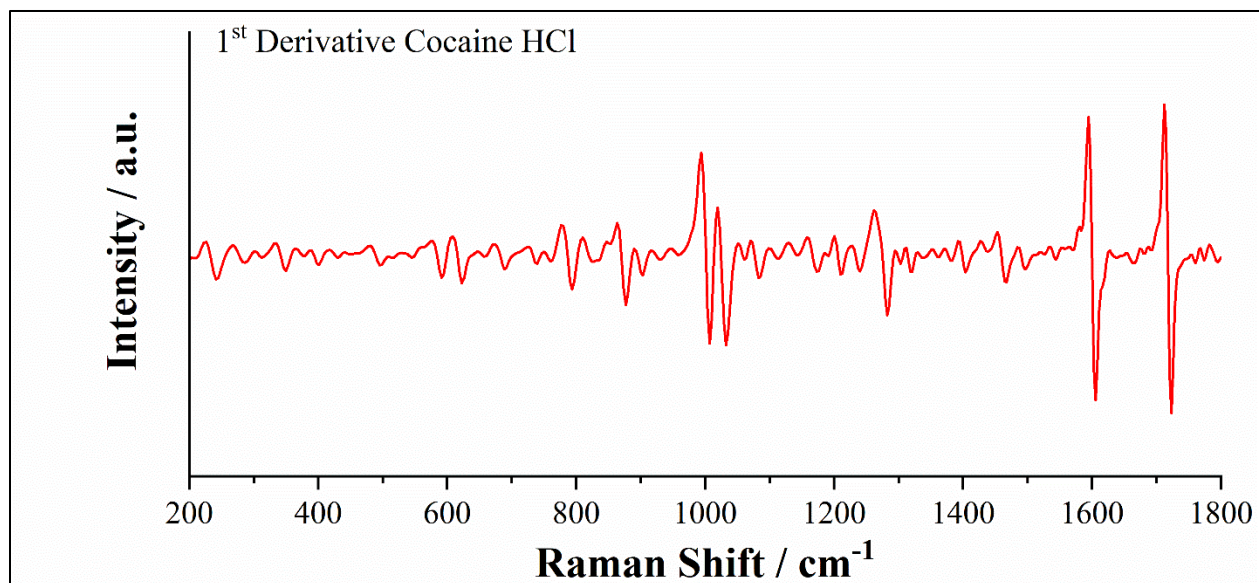


3.2. Fentanyl Targeted EC-SERS, 785-nm SPELEC Raman, Silver SPE

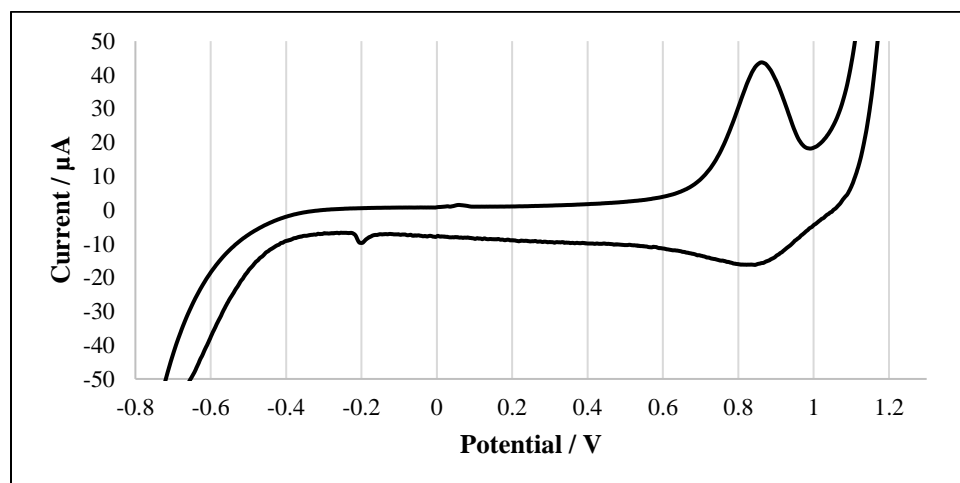


3.3. Normal Raman, 785-nm SPELEC Raman





3.4. Electrochemistry, SPCE, 0.1 M KCl



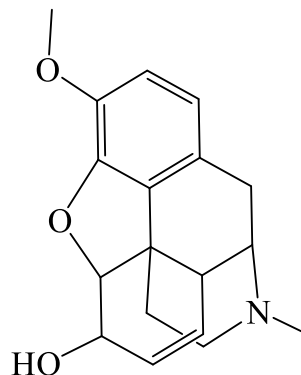
Codeine

1. General Information

IUPAC Name	(4 <i>R</i> ,4 <i>aR</i> ,7 <i>S</i> ,7 <i>aR</i> ,12 <i>bS</i>)-9-methoxy-3-methyl-2,4,4 <i>a</i> ,7,7 <i>a</i> ,13-hexahydro-1 <i>H</i> -4,12-methanobenzofuro[3,2- <i>e</i>]isoquinolin-7-ol
CAS #	76-57-3
Source	Reference Standard

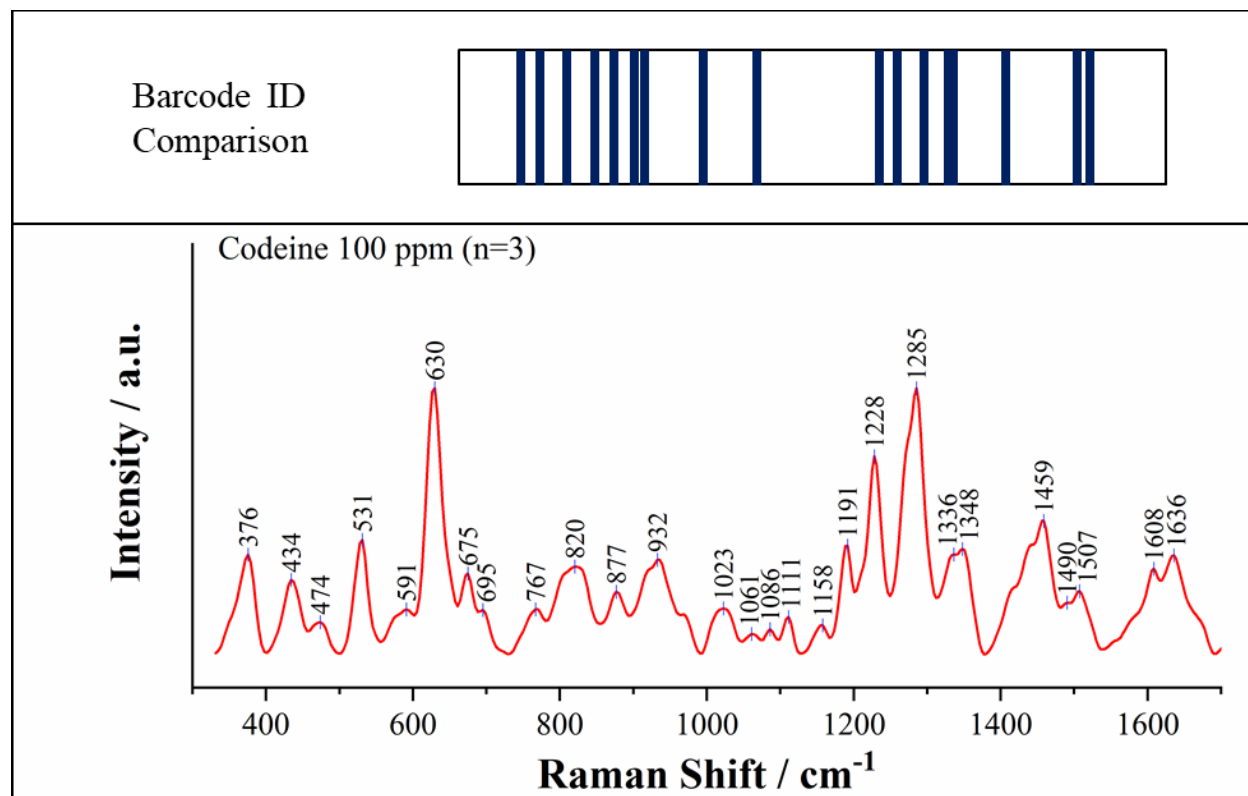
2. Chemical Data

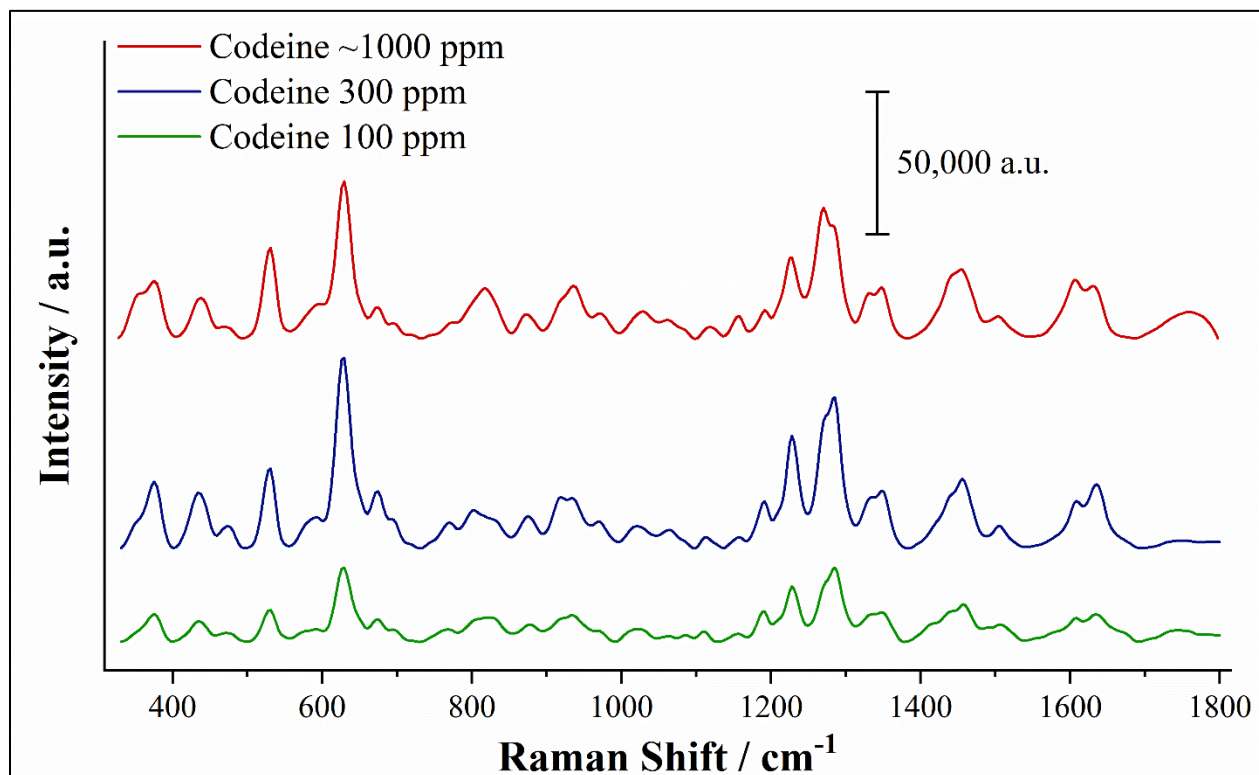
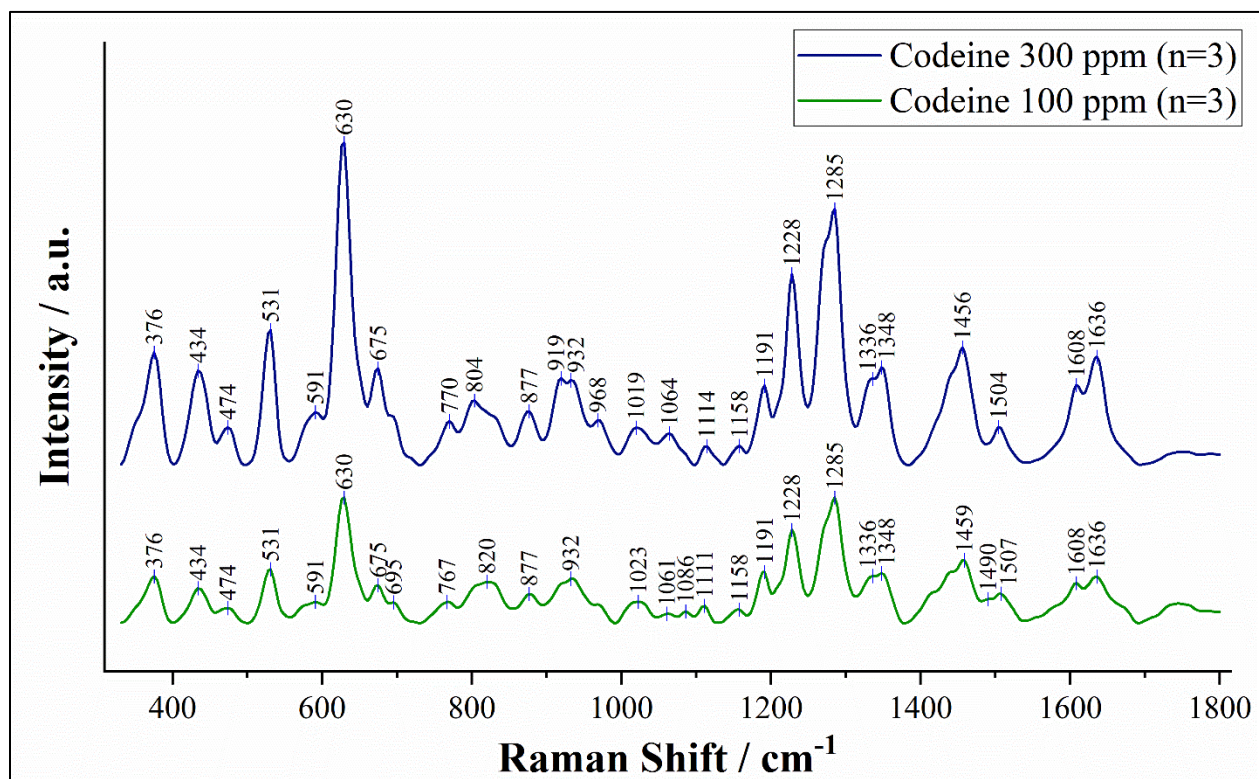
Chemical Formula	C ₁₈ H ₂₁ NO ₃
Molecular Weight	299.4 g/mol
pK _a	8.2



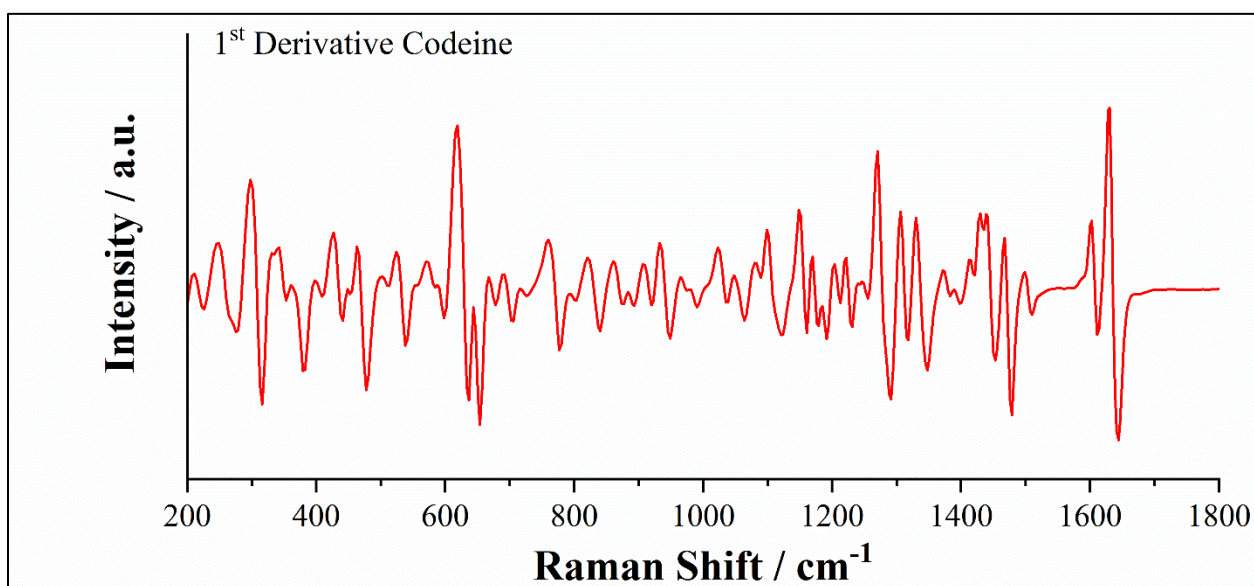
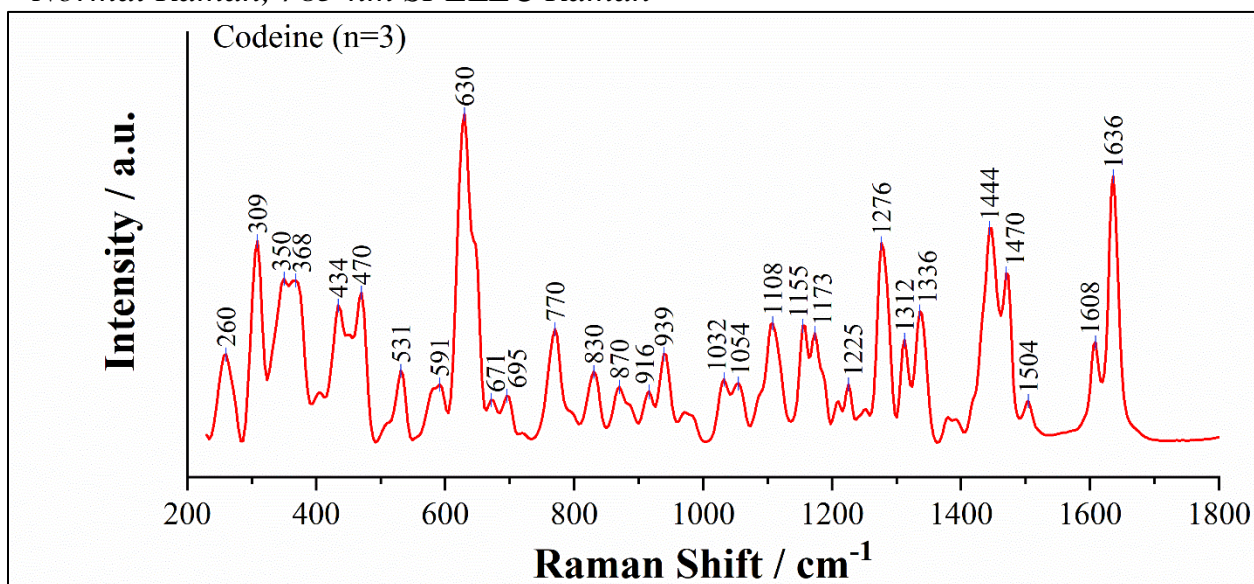
3. Qualitative Data

3.1. Nontargeted EC-SERS, 785-nm SPELEC Raman, Silver SPE

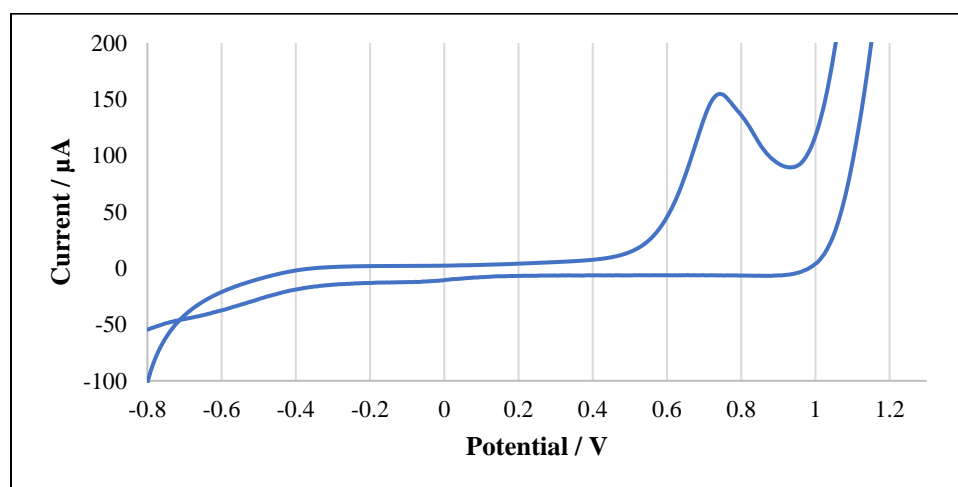




3.2. Normal Raman, 785-nm SPELEC Raman



3.3. Electrochemistry, SPCE, 0.1 M KCl



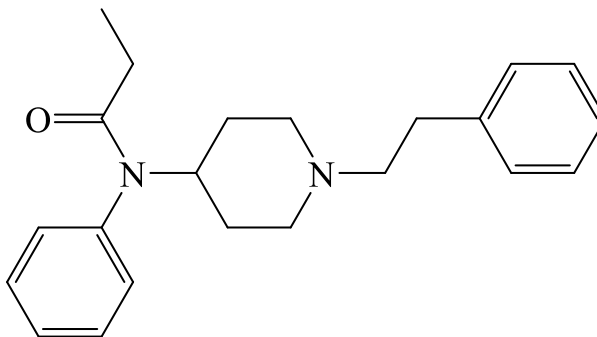
Fentanyl

1. General Information

IUPAC Name *N*-phenyl-*N*-[1-(2-phenylethyl)piperidin-4-yl]16ropenamide
CAS # 437-38-7
Source Reference Standard

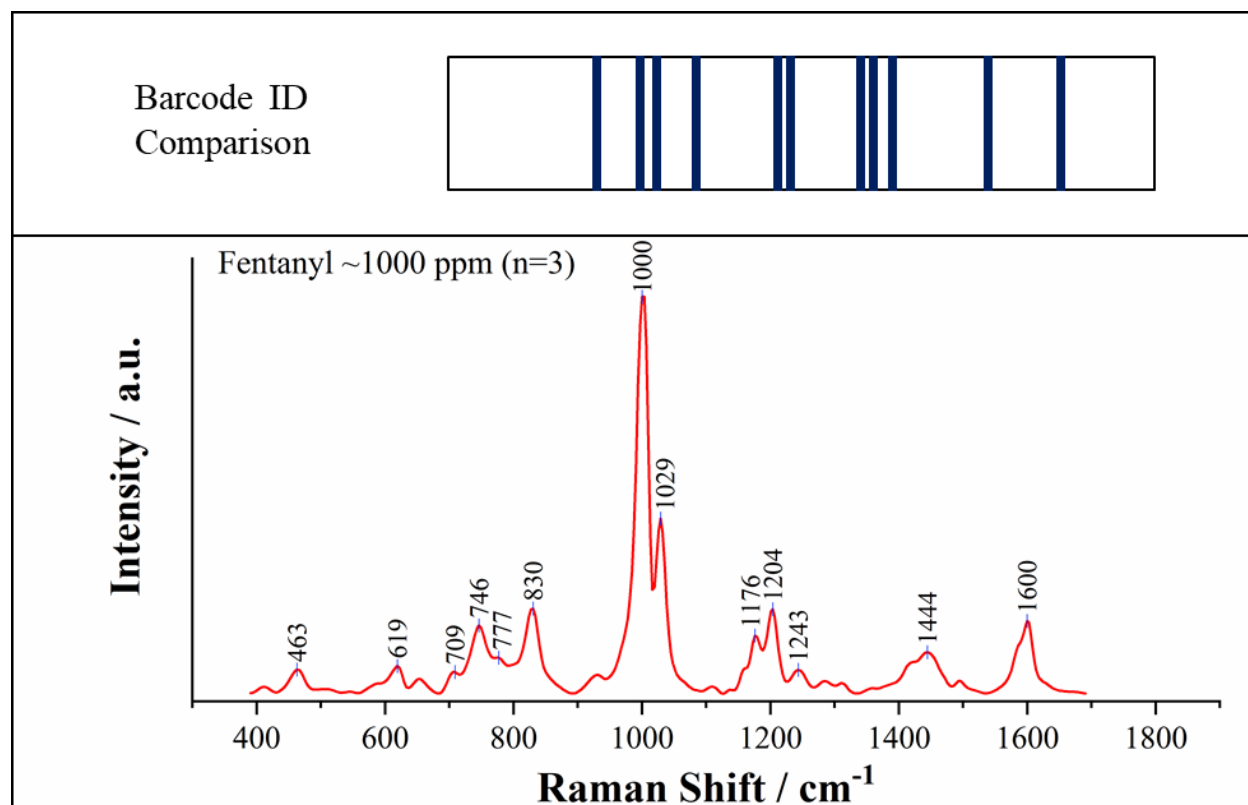
2. Chemical Data

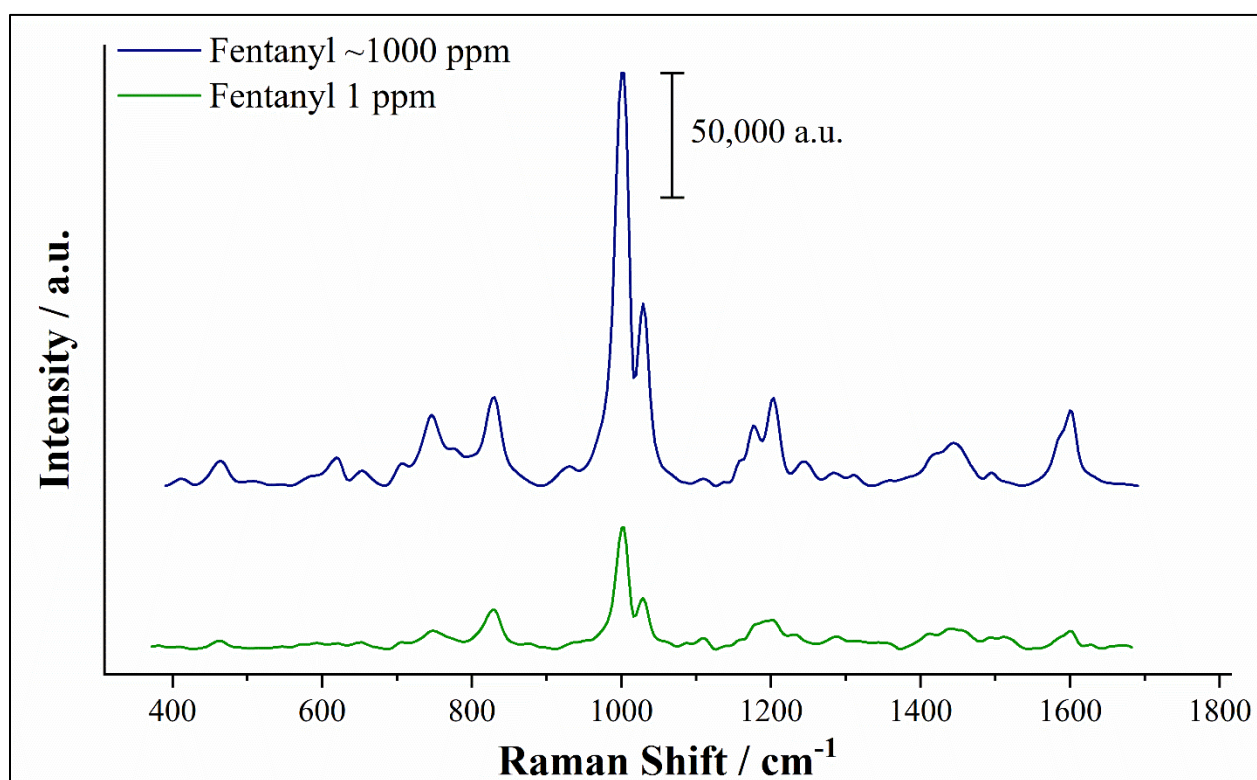
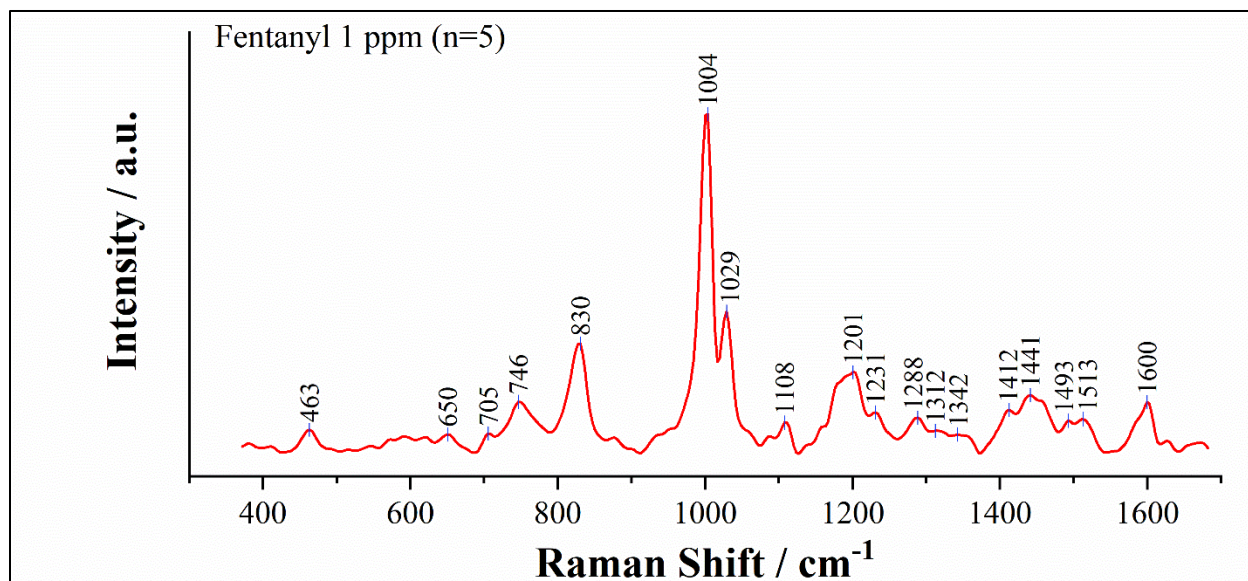
Chemical Formula $C_{22}H_{28}N_2O$
Molecular Weight 336.5 g/mol
pK_a 8.43



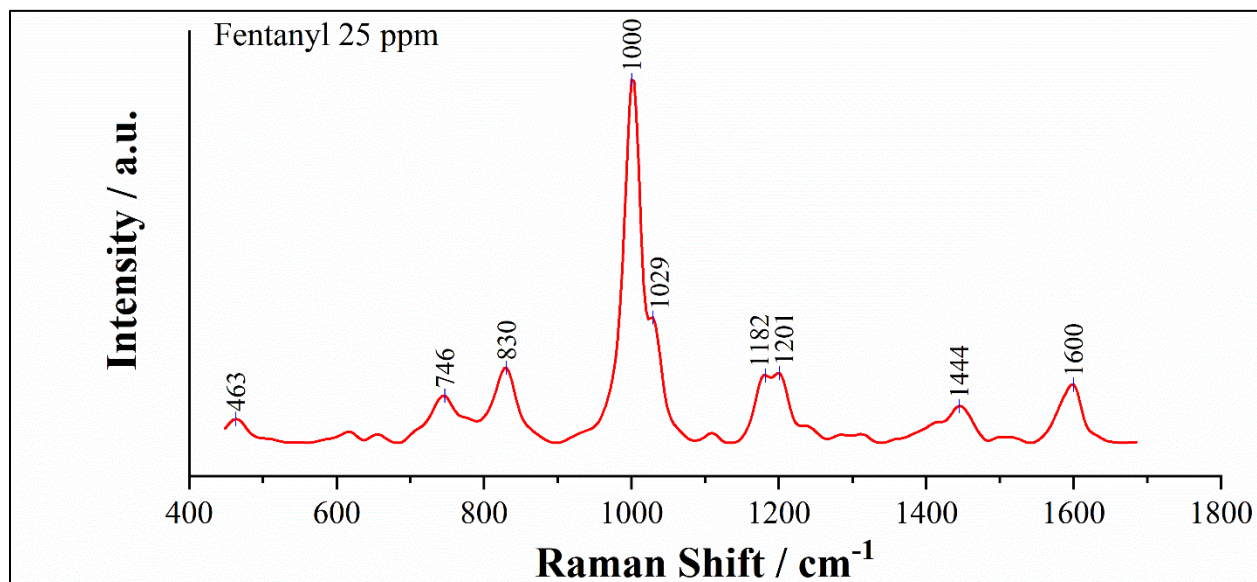
3. Qualitative Data

3.1. Nontargeted EC-SERS, 785-nm SPELEC Raman, Silver SPE

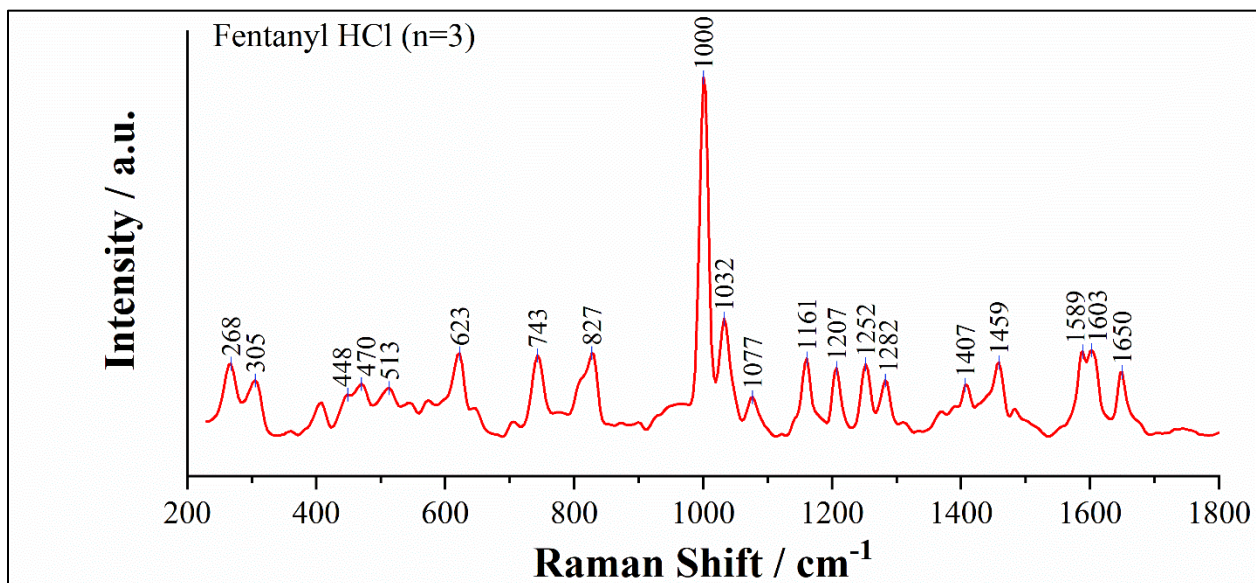


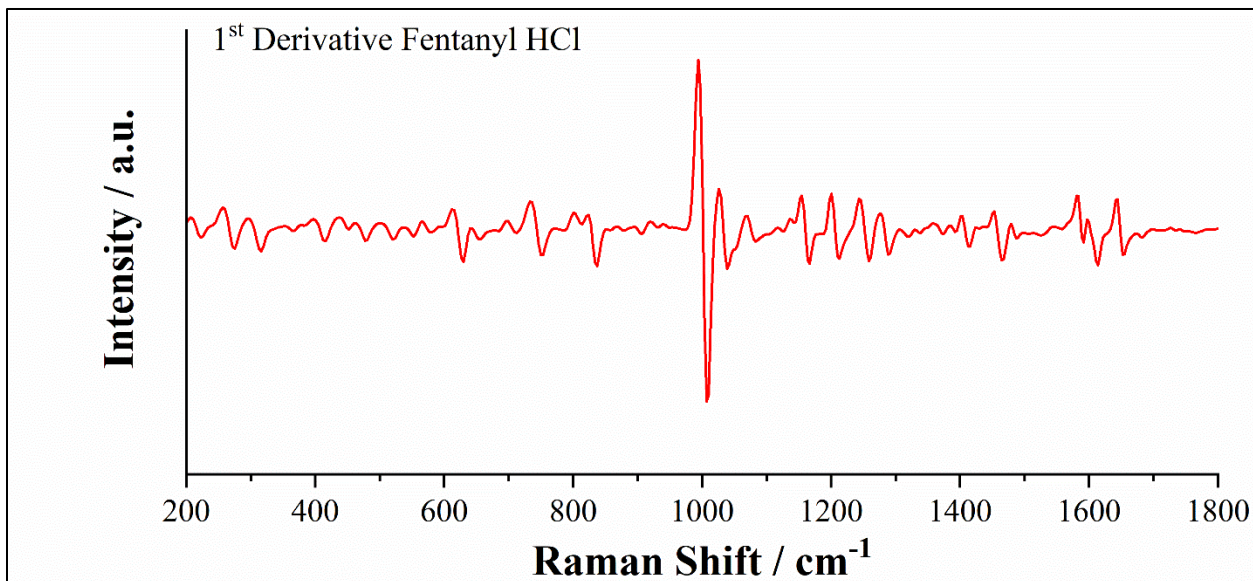


3.2. Targeted Fentanyl EC-SERS, 785-nm SPELEC Raman, Silver SPE

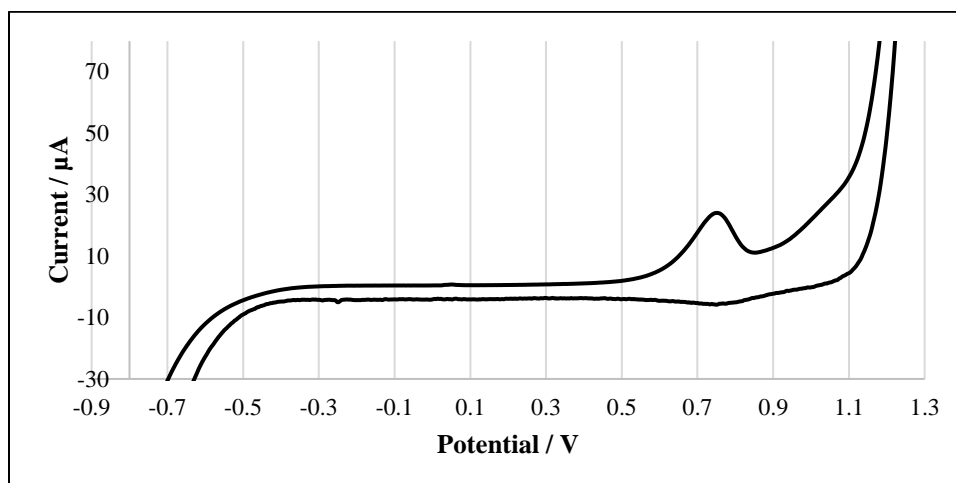


3.3. Normal Raman, 785-nm SPELEC Raman





3.4. Electrochemistry, SPCE, 0.1 M KCl



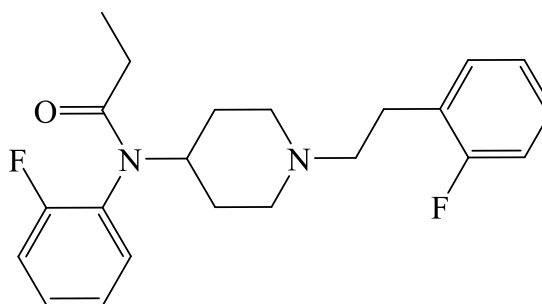
2'-fluoro *ortho*-Fluorofentanyl

1. General Information

IUPAC Name N-(2-fluorophenyl)-N-[1-[2-(2-fluorophenyl)ethyl]piperidin-4-yl]propanamide
CAS # NA
Source Reference Standard

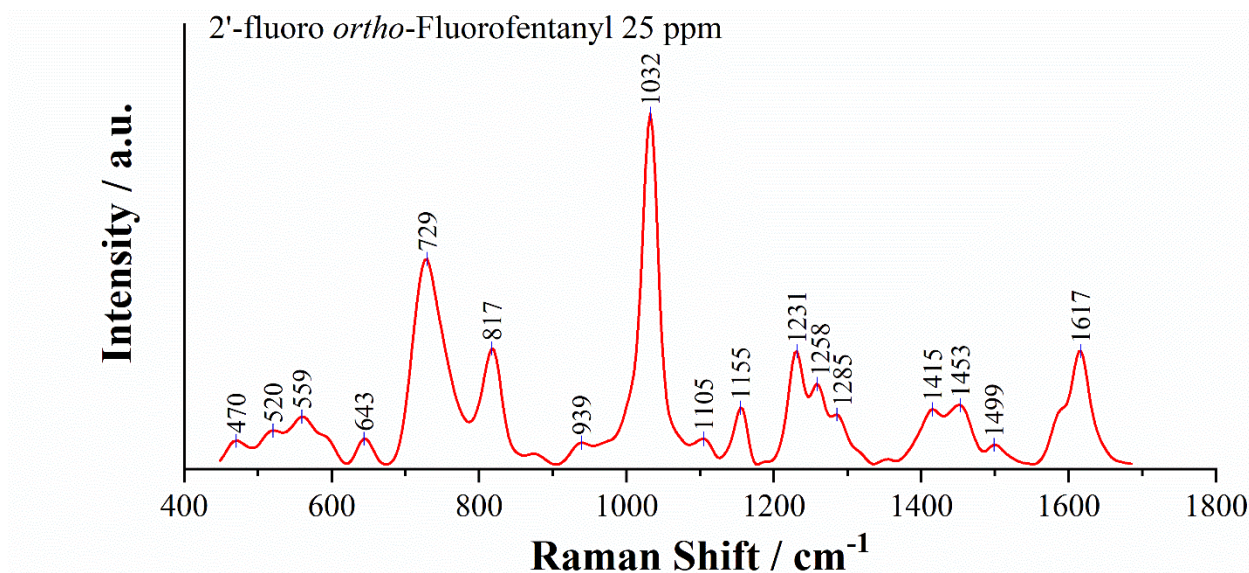
2. Chemical Data

Chemical Formula $C_{22}H_{26}F_2N_2O$
Molecular Weight 372.5 g/mol
pK_a NA



3. Qualitative Data

3.1. Fentanyl targeted EC-SERS, 785-nm SPELEC Raman, Silver SPE



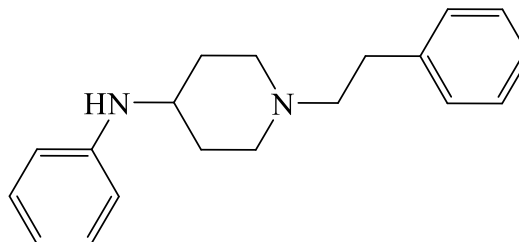
4-ANPP

1. General Information

IUPAC Name N-phenyl-1-(2-phenylethyl)piperidin-4-amine
CAS # 21409-26-7
Source Reference Standard

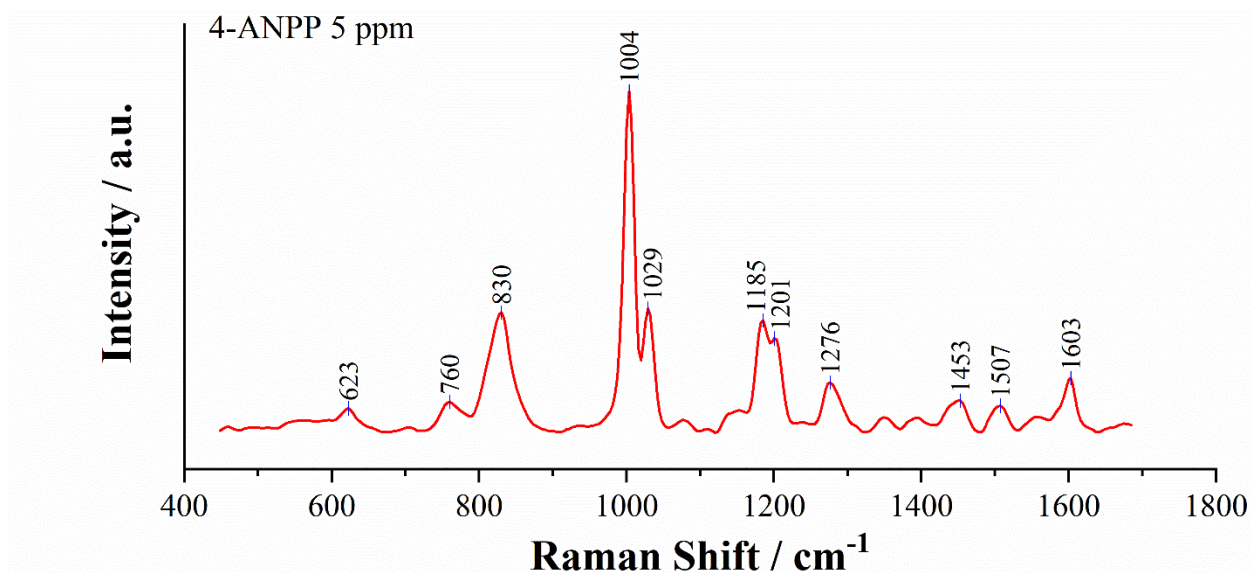
2. Chemical Data

Chemical Formula $C_{19}H_{24}N_2$
Molecular Weight 280.4 g/mol
pK_a NA



3. Qualitative Data

3.1. Fentanyl targeted EC-SERS, 785-nm SPELEC Raman, Silver SPE



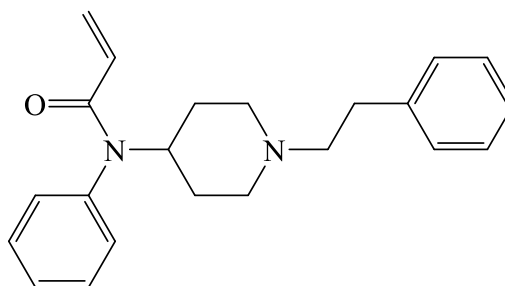
Acryl fentanyl

1. General Information

IUPAC Name	N-phenyl-N-[1-(2-phenylethyl)piperidin-4-yl]prop-2-enamide
CAS #	82003-75-6
Source	Reference Standard

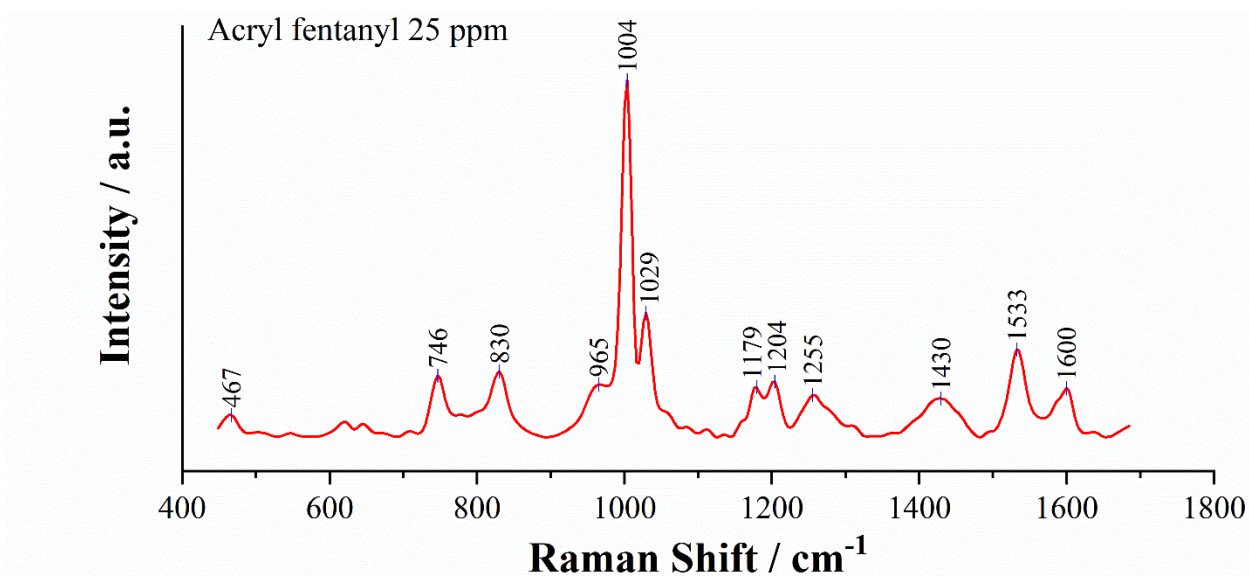
2. Chemical Data

Chemical Formula	C ₂₂ H ₂₆ N ₂ O
Molecular Weight	334.5 g/mol
pK _a	NA



3. Qualitative Data

3.1. Fentanyl targeted EC-SERS, 785-nm SPELEC Raman, Silver SPE



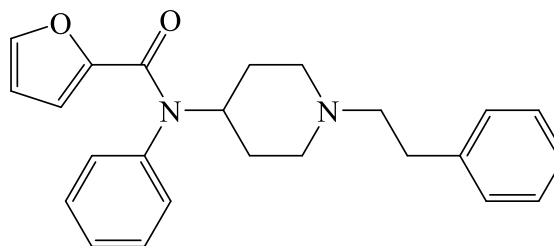
Furanyl fentanyl

1. General Information

IUPAC Name N-phenyl-N-[1-(2-phenylethyl)piperidin-4-yl]furan-2-carboxamide
CAS # 101345-66-8
Source Reference Standard

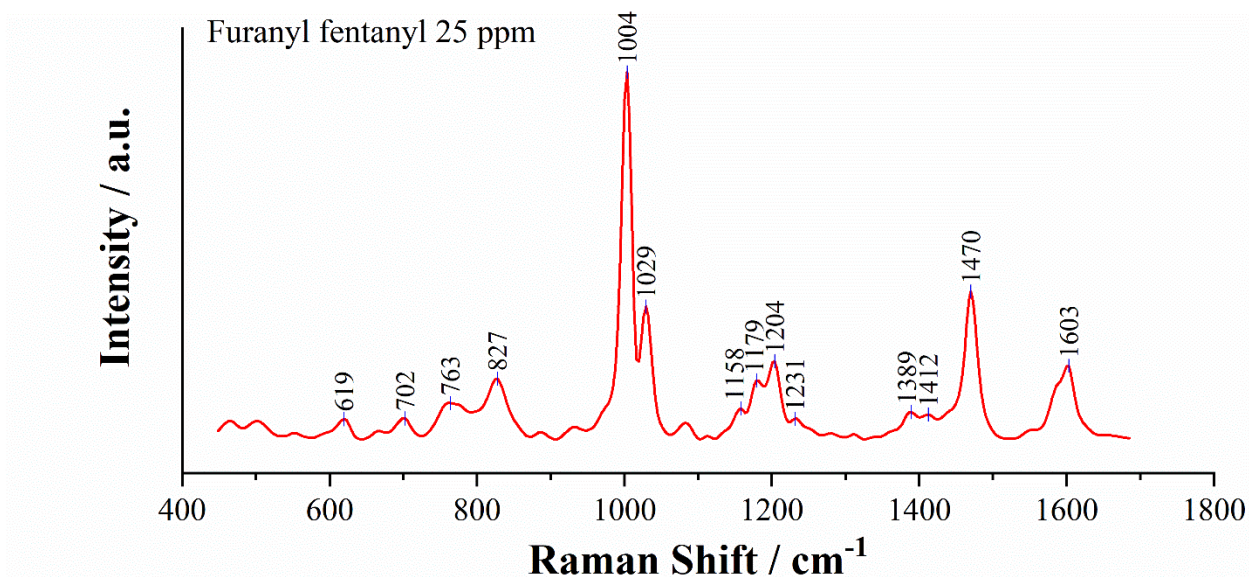
2. Chemical Data

Chemical Formula $C_{24}H_{26}N_2O_2$
Molecular Weight 374.5 g/mol
pK_a NA



3. Qualitative Data

3.1. Fentanyl targeted EC-SERS, 785-nm SPELEC Raman, Silver SPE



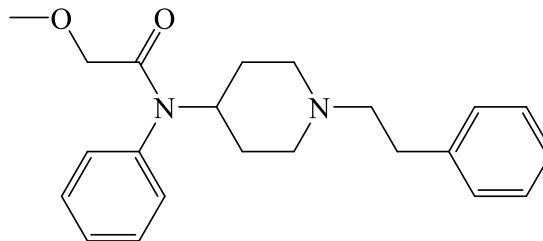
Methoxyacetyl fentanyl

1. General Information

IUPAC Name	2-methoxy-N-phenyl-N-[1-(2-phenylethyl)piperidin-4-yl]acetamide
CAS #	101345-67-9
Source	Reference Standard

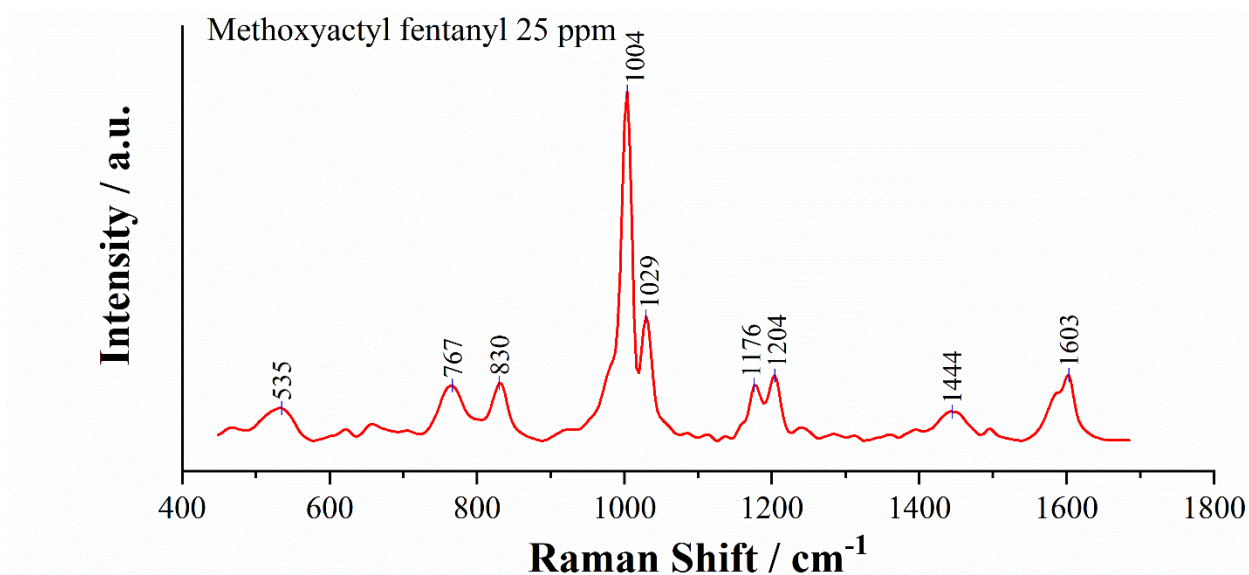
2. Chemical Data

Chemical Formula	C ₂₂ H ₂₈ N ₂ O ₂
Molecular Weight	352.5 g/mol
pK _a	NA



3. Qualitative Data

3.1. Fentanyl targeted EC-SERS, 785-nm SPELEC Raman, Silver SPE



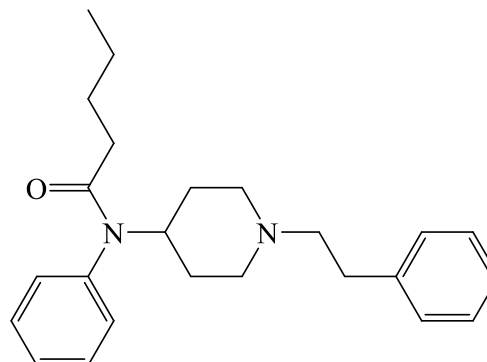
Valeryl fentanyl

1. General Information

IUPAC Name N-phenyl-N-[1-(2-phenylethyl)piperidin-4-yl]pentanamide
CAS # 122882-90-0
Source Reference Standard

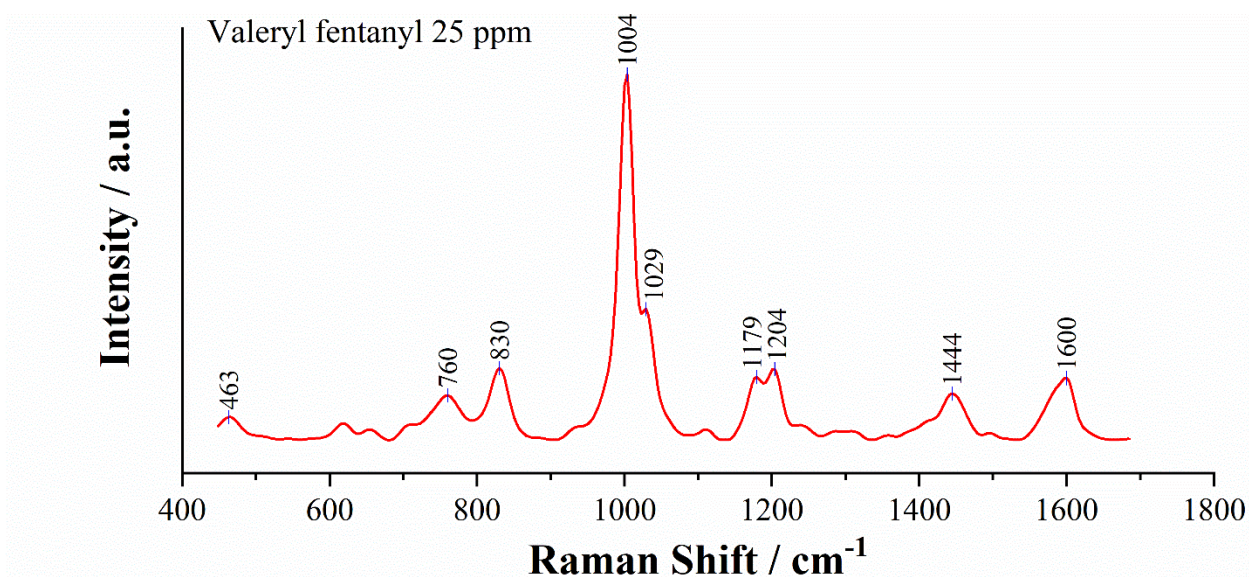
2 Chemical Data

Chemical Formula $C_{24}H_{32}N_2O$
Molecular Weight 364.5 g/mol
pK_a NA



3 Qualitative Data

3.2. Fentanyl targeted EC-SERS, 785-nm SPELEC Raman, Silver SPE



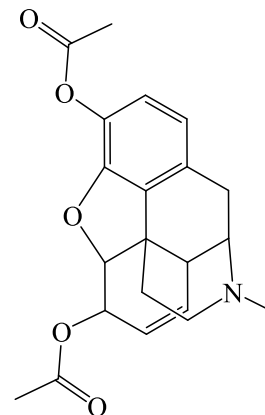
Heroin

1. General Information

IUPAC Name	[(4 <i>R</i> ,4 <i>aR</i> ,7 <i>S</i> ,7 <i>aR</i> ,12 <i>bS</i>)-9-acetyloxy-3-methyl-2,4,4 <i>a</i> ,7,7 <i>a</i> ,13-hexahydro-1 <i>H</i> -4,12-methanobenzofuro[3,2- <i>e</i>]isoquinolin-7-yl] acetate
CAS #	561-27-3
Source	Reference Standard

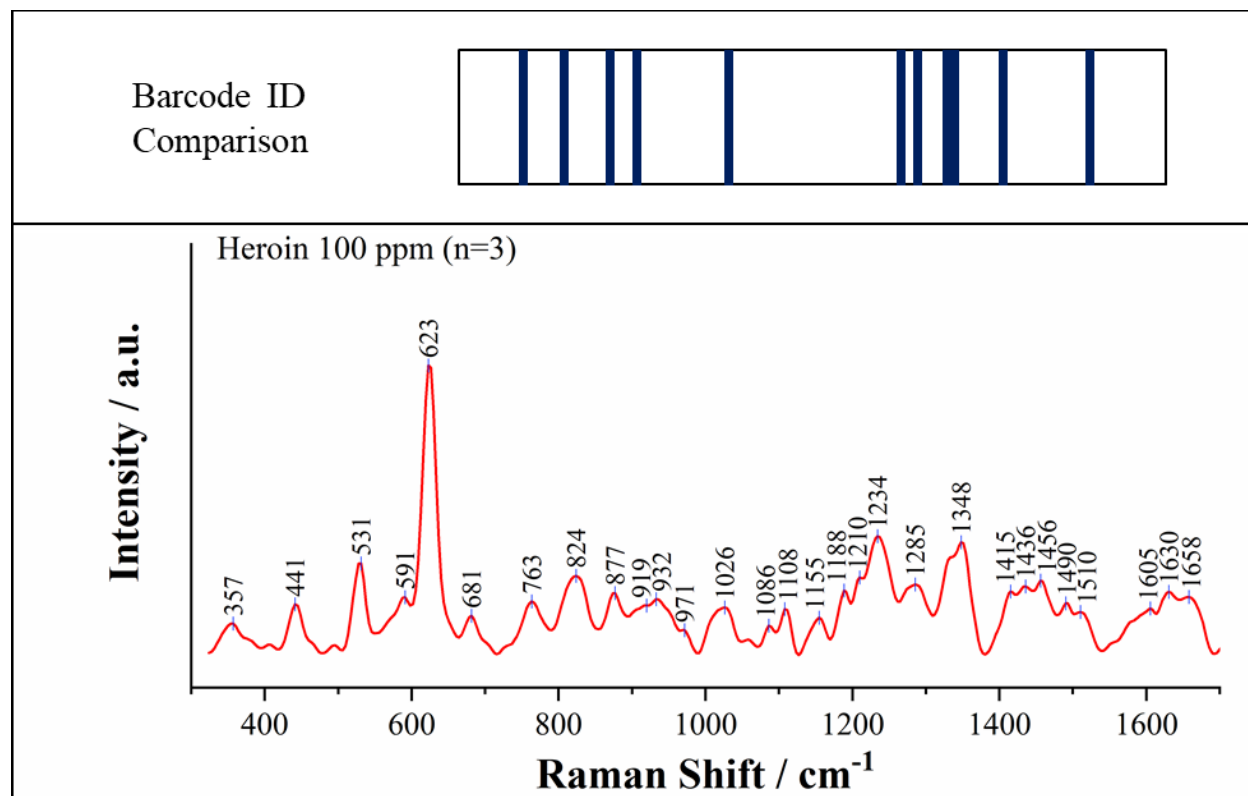
2. Chemical Data

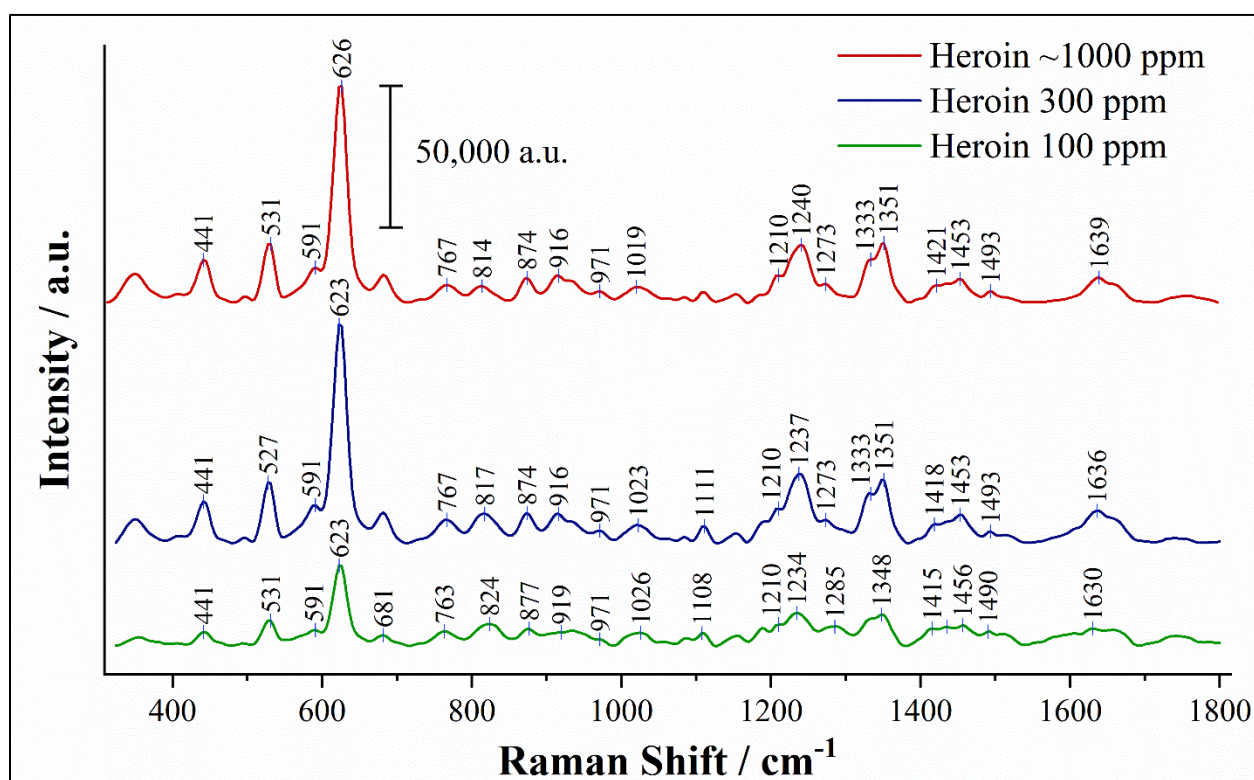
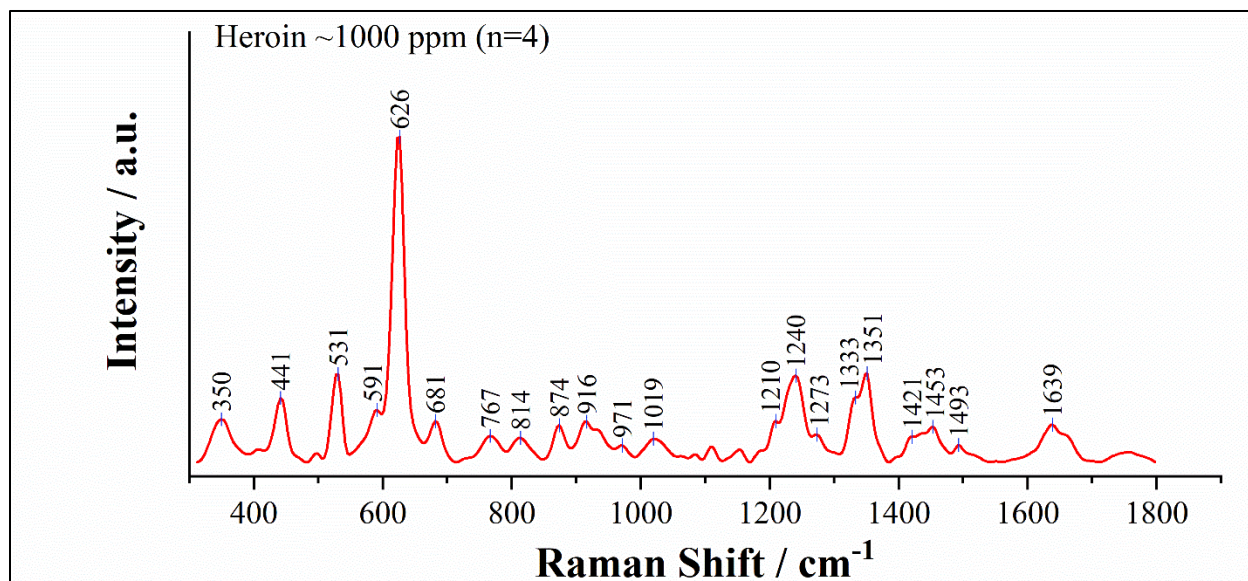
Chemical Formula	C ₂₁ H ₂₃ NO ₅
Molecular Weight	369.4 g/mol
pK _a	7.96



3. Qualitative Data

3.1. Nontargeted EC-SERS, 785-nm SPELEC Raman, Silver SPE

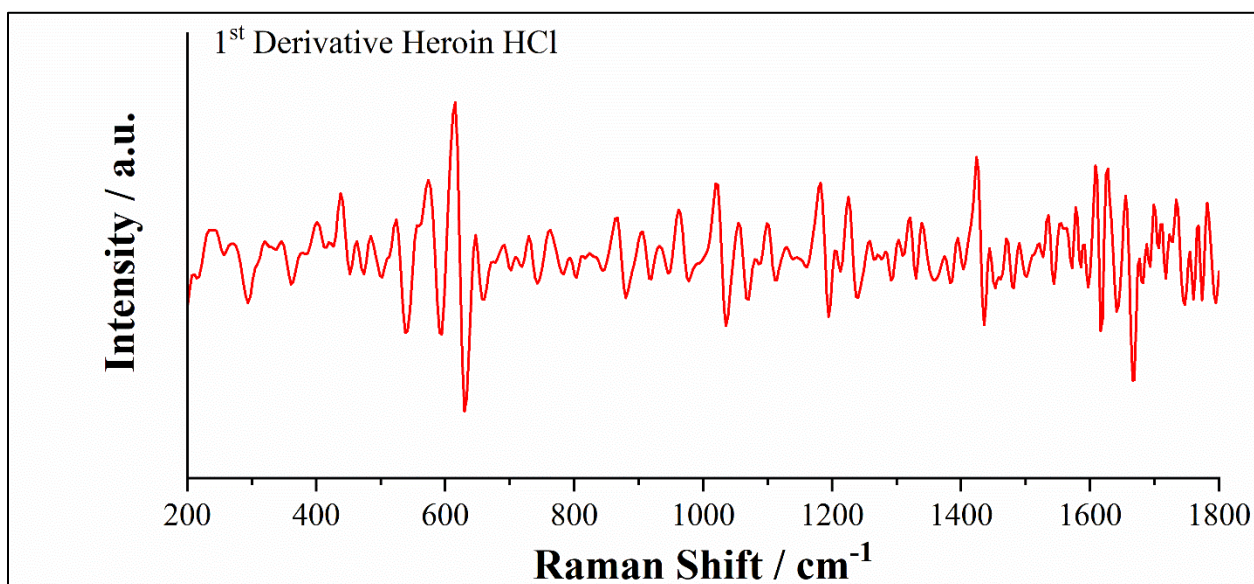
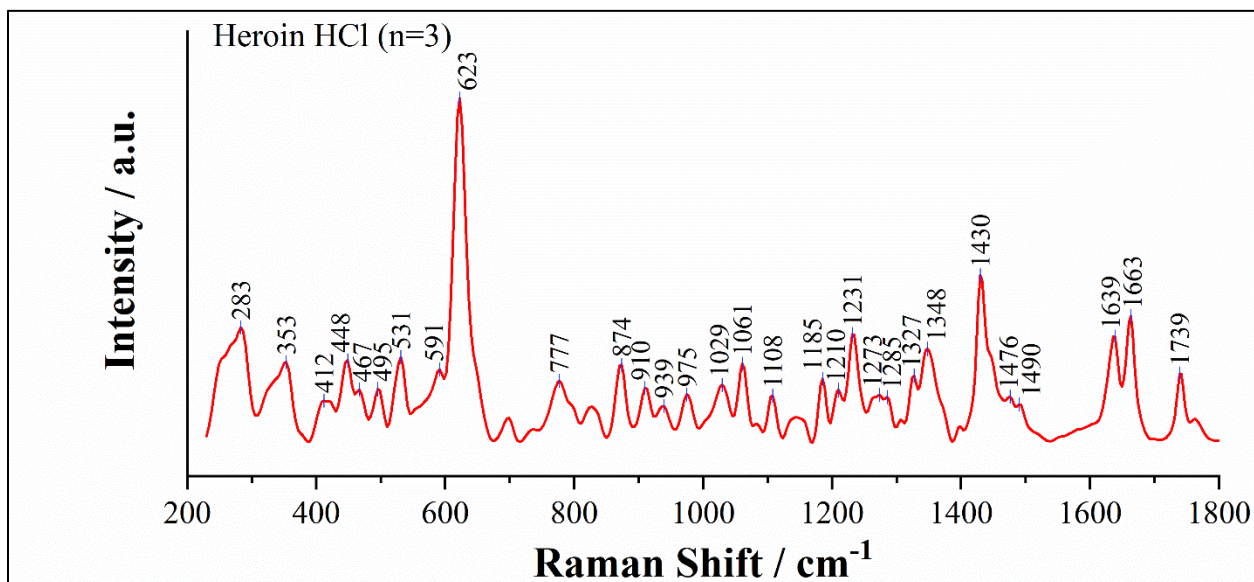




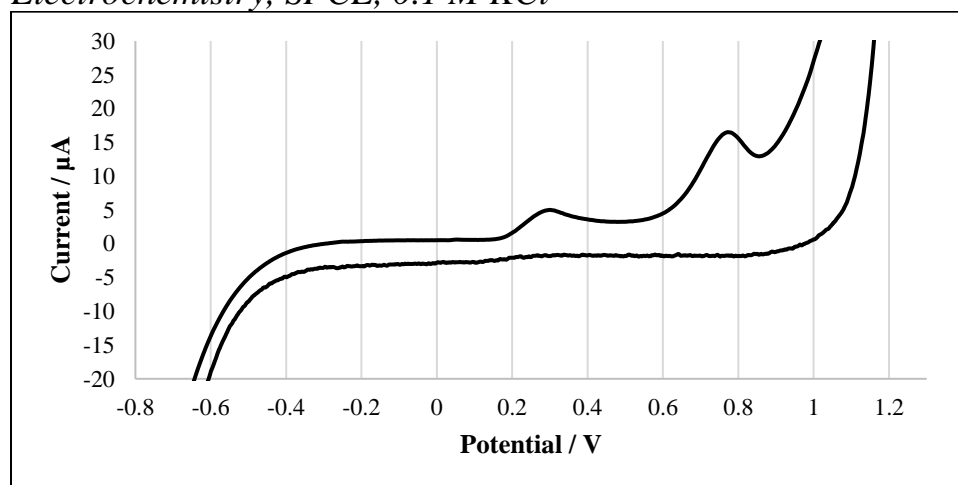
3.2. Fentanyl Targeted EC-SERS, 785-nm SPELEC Raman, Silver SPE

NO SIGNAL UNDER TESTED CONDITIONS

3.3. Normal Raman, 785-nm SPELEC Raman



3.4. Electrochemistry, SPCE, 0.1 M KCl



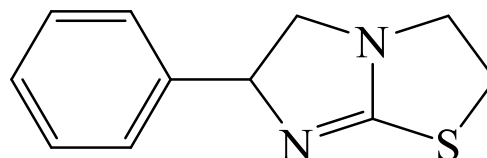
Levamisole

1. General Information

IUPAC Name (6*S*)-6-phenyl-2,3,5,6-tetrahydroimidazo[2,1-*b*][1,3]thiazole
CAS # 14769-73-4
Source Reference Standard

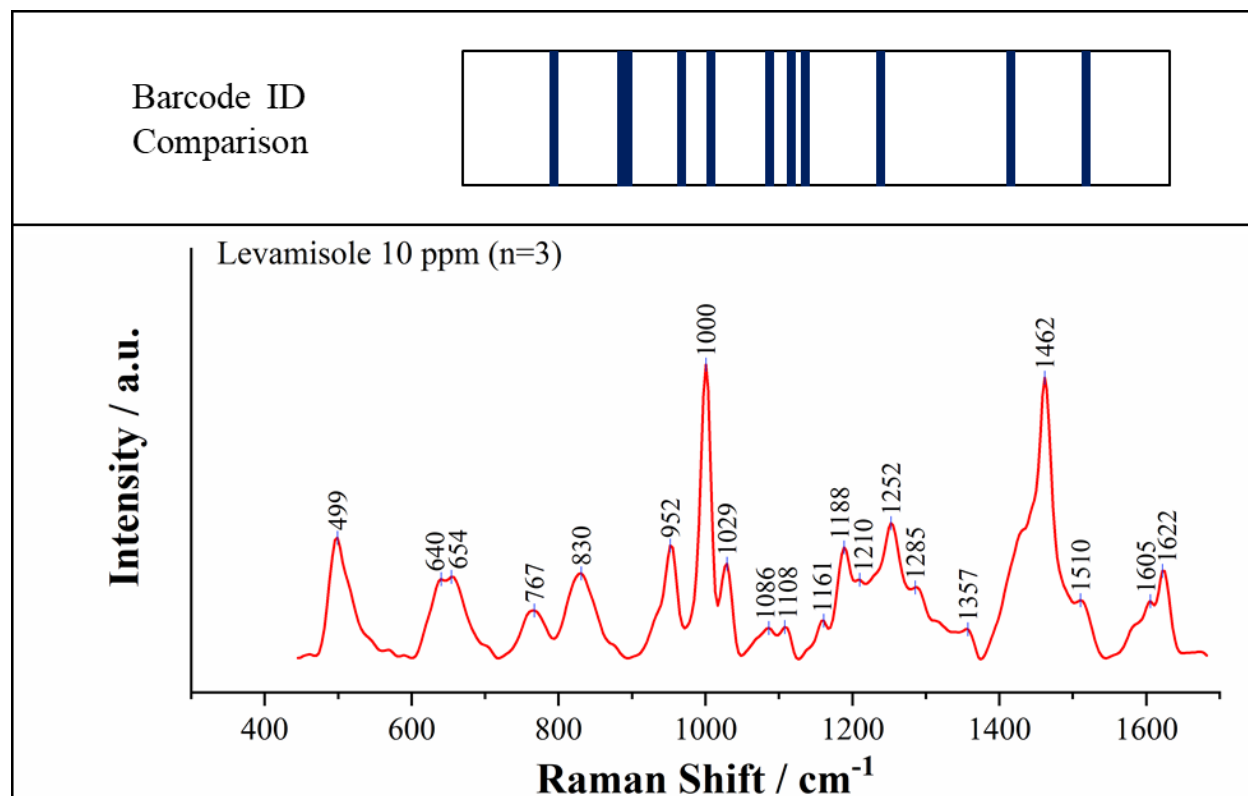
2. Chemical Data

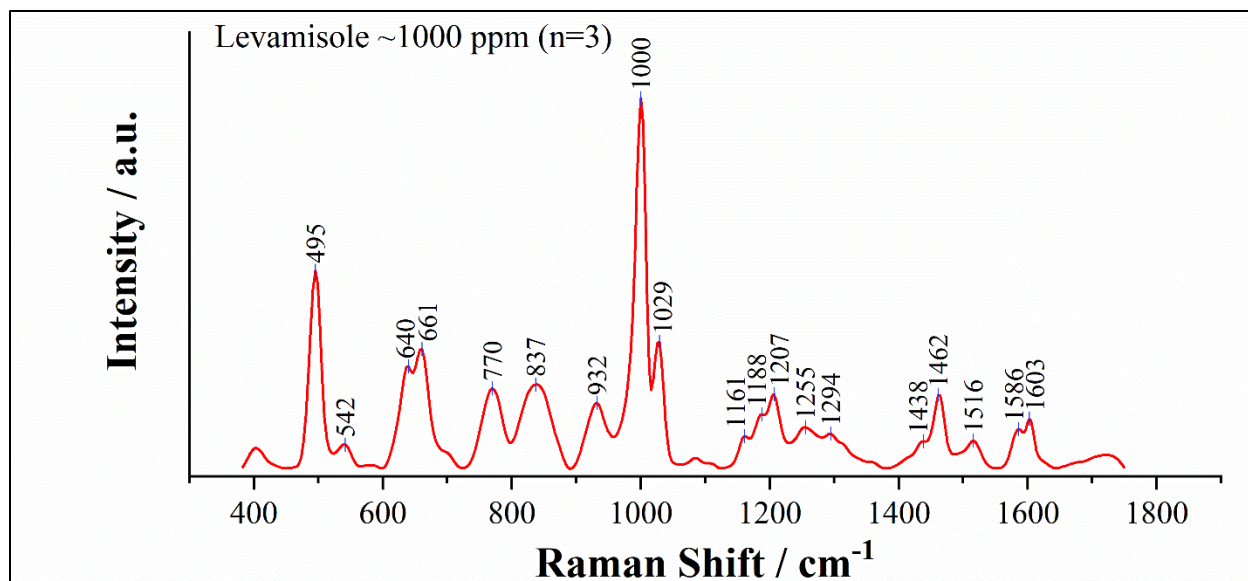
Chemical Formula $C_{11}H_{12}N_2S$
Molecular Weight 204.29 g/mol
pK_a Not Available



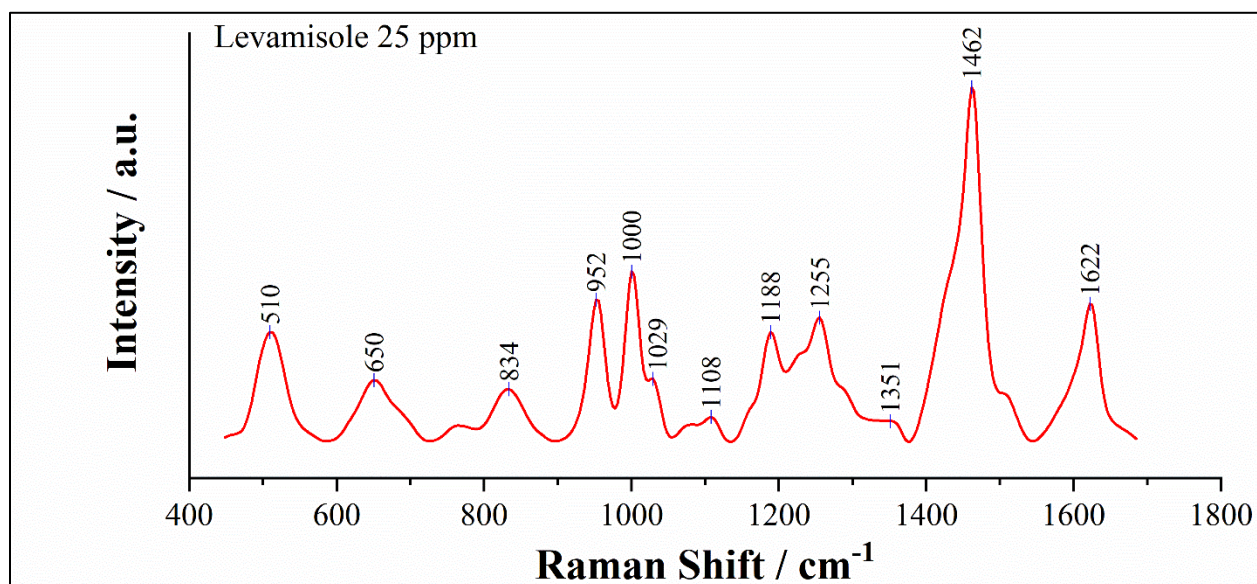
3. Qualitative Data

3.1. Nontargeted EC-SERS, 785-nm SPELEC Raman, Silver SPE

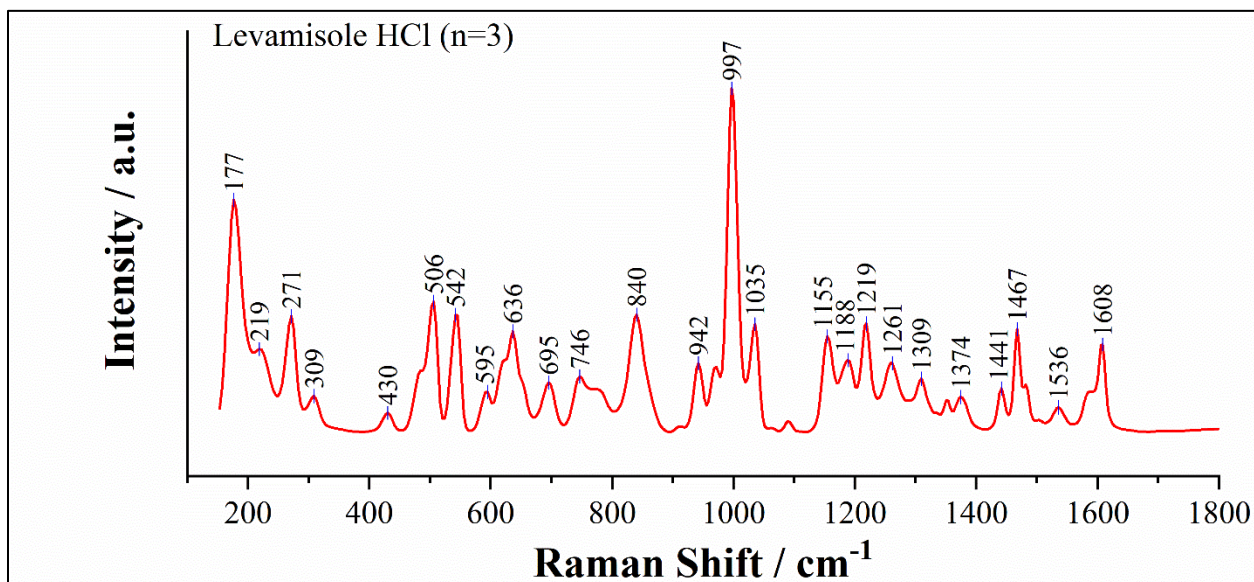




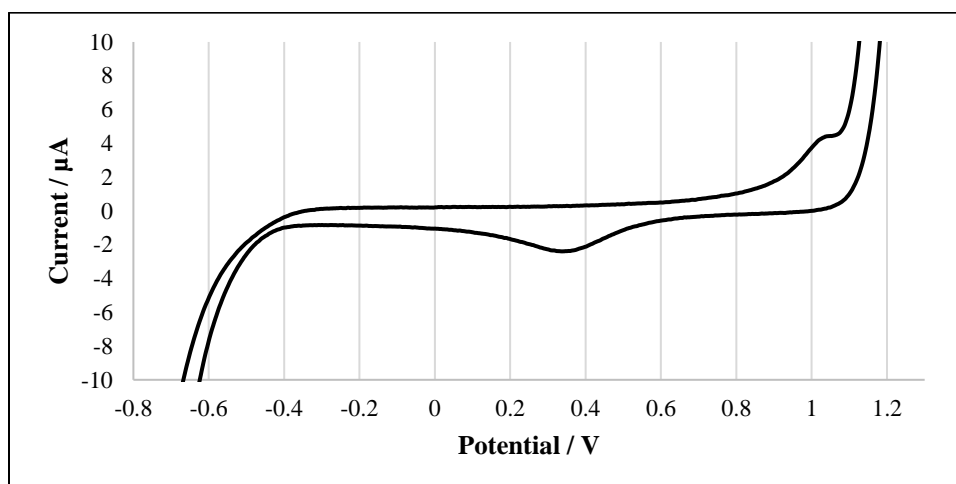
3.2. *Fentanyl Targeted EC-SERS, 785-nm SPELEC Raman, Silver SPE*



3.3. Normal Raman, 785-nm SPELEC Raman



3.4. Electrochemistry, SPCE, 0.1 M KCl



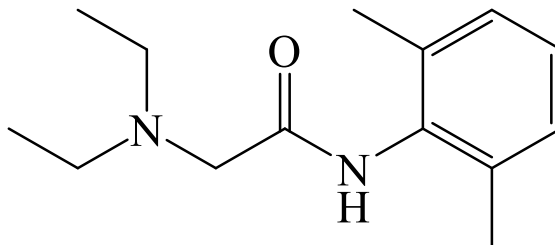
Lidocaine

1. General Information

IUPAC Name 2-(diethylamino)-*N*-(2,6-dimethylphenyl)acetamide
CAS # 137-58-6
Source Reference Standard

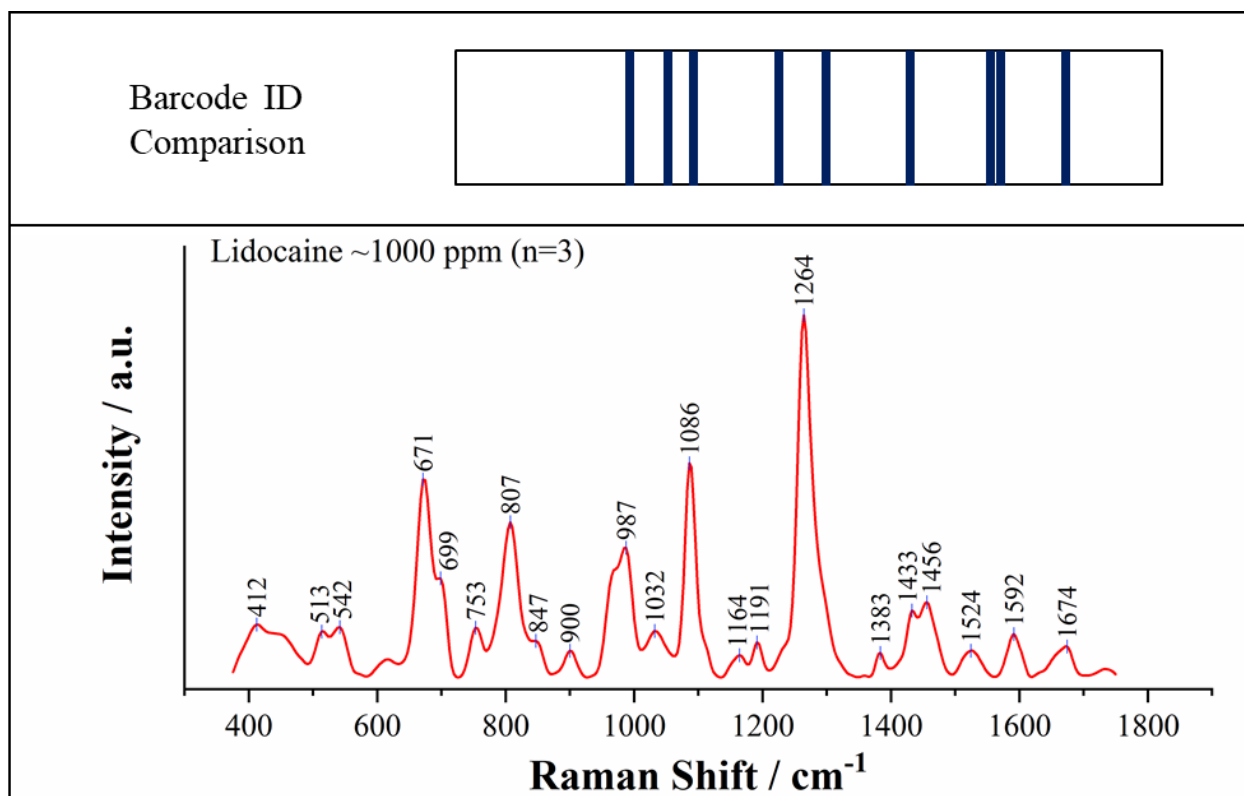
2. Chemical Data

Chemical Formula $C_{14}H_{22}N_2O$
Molecular Weight 234.34 g/mol
 pK_a 7.93

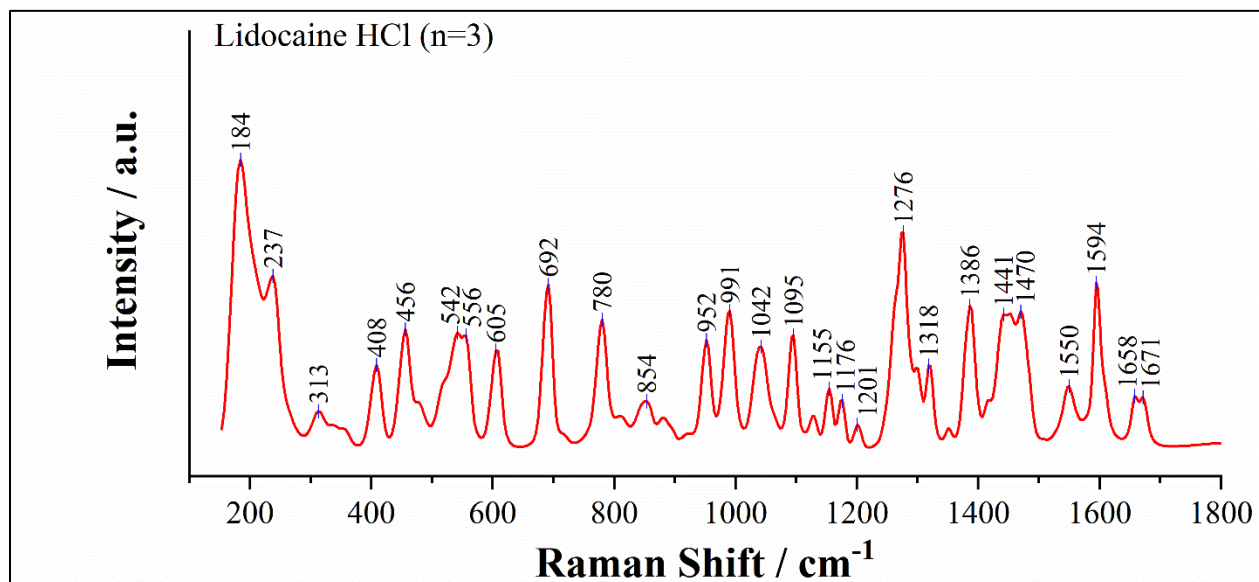


3. Qualitative Data

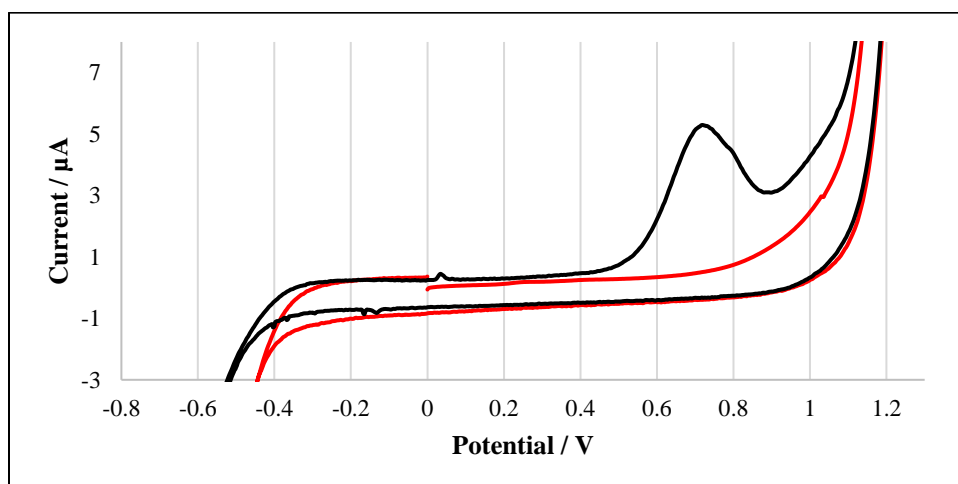
3.1. Nontargeted EC-SERS, 785-nm SPELEC Raman, Silver SPE



3.2. Normal Raman, 785-nm SPELEC Raman



3.3. Electrochemistry, SPCE, 0.1 M KCl



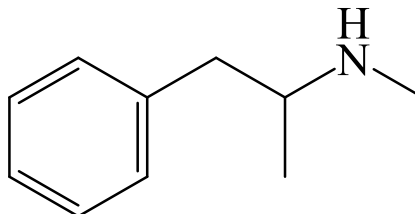
Methamphetamine

1. General Information

IUPAC Name (2*S*)-*N*-methyl-1-phenylpropan-2-amine
CAS # 537-46-2
Source Reference Standard

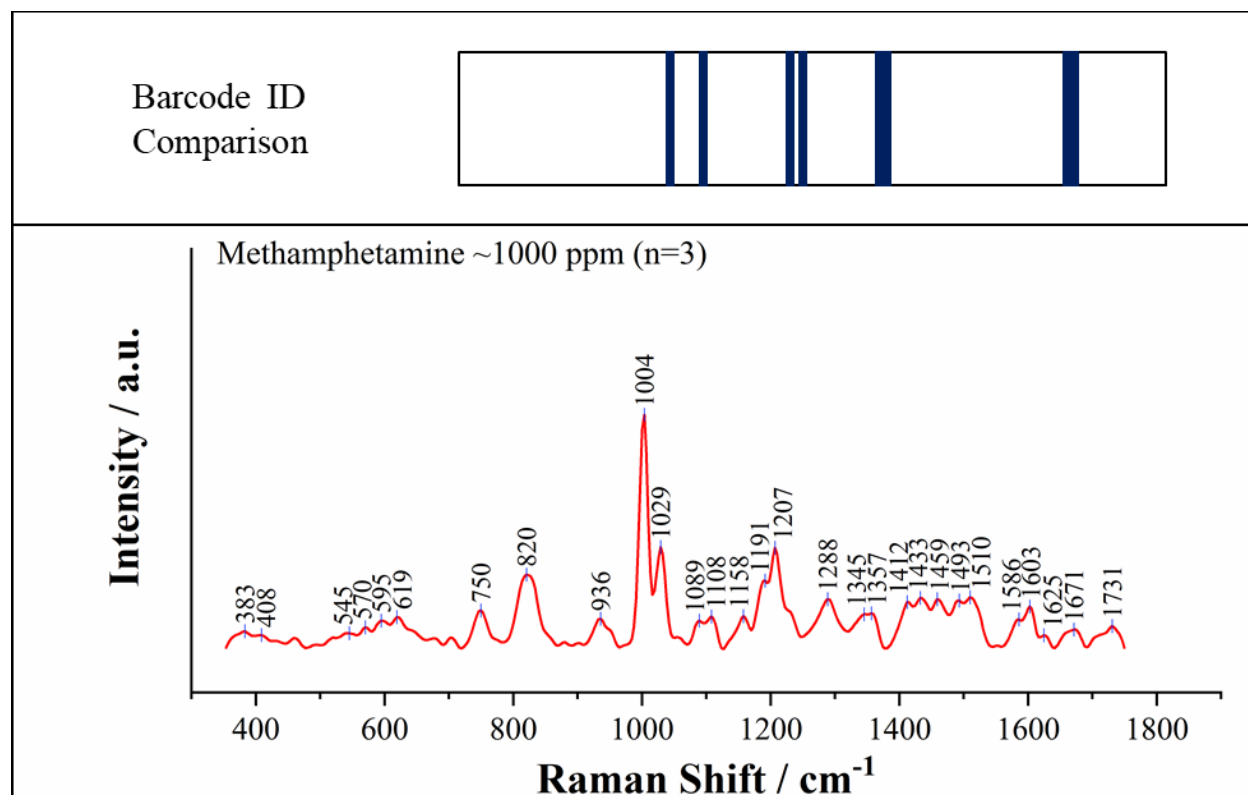
2. Chemical Data

Chemical Formula $C_{10}H_{15}N$
Molecular Weight 149.23 g/mol
 pK_a 9.99

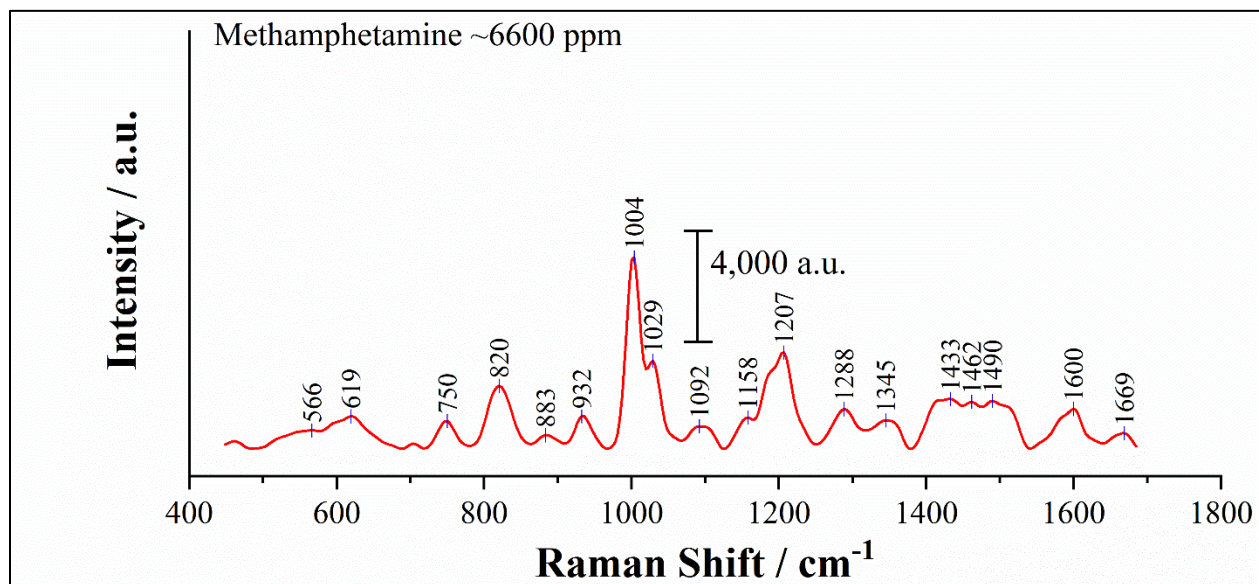


3. Qualitative Data

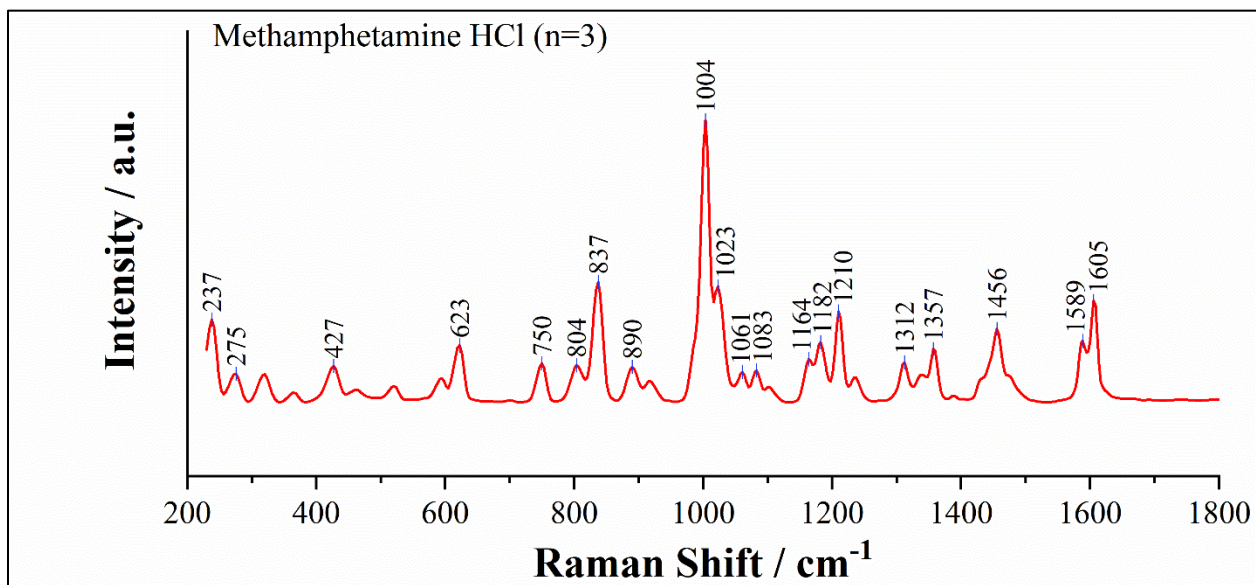
3.1. Nontargeted EC-SERS, 785-nm SPELEC Raman, Silver SPE

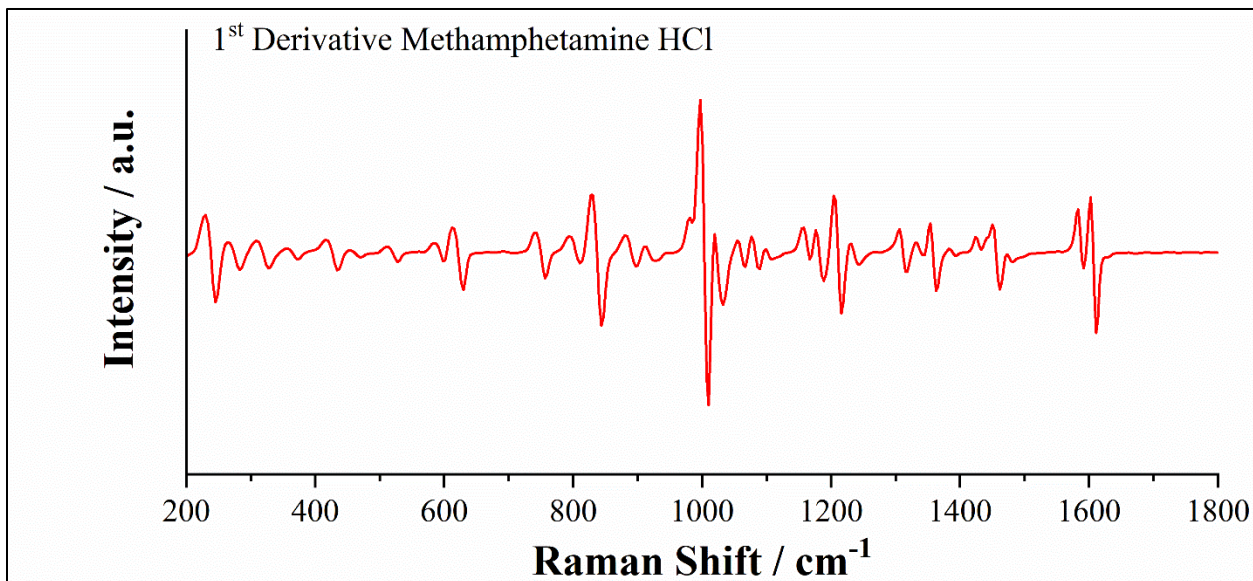


3.2. *Fentanyl Targeted EC-SERS, 785-nm SPELEC Raman, Silver SPE*

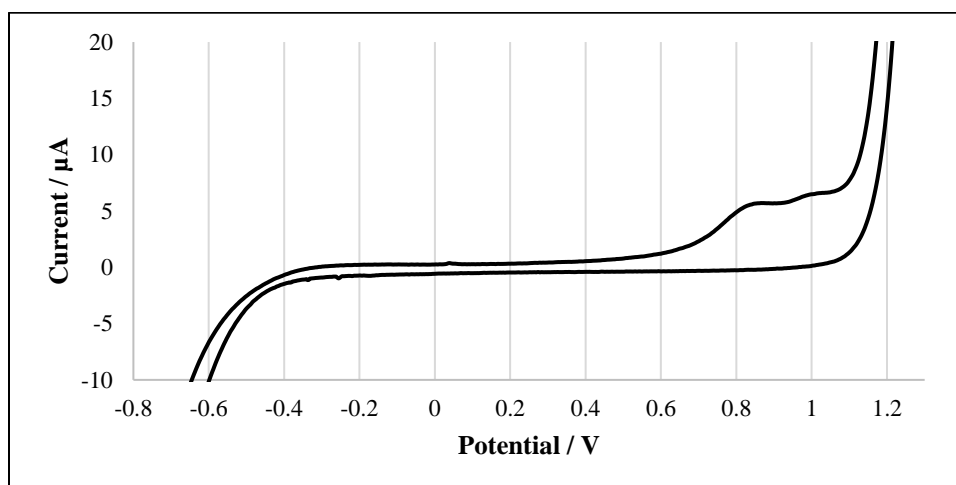


3.3. *Normal Raman, 785-nm SPELEC Raman*





3.4. Electrochemistry



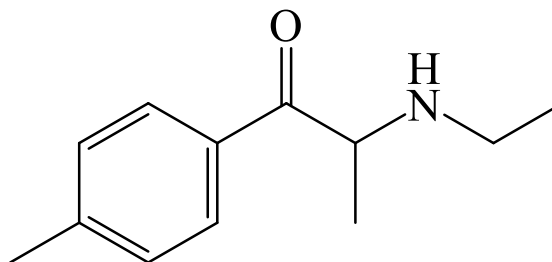
4-methylethcathinone

1. General Information

IUPAC Name 2-(ethylamino)-1-(4-methylphenyl)propan-1-one
CAS # 1225617-18-4
Source Reference Standard

2. Chemical Data

Chemical Formula $C_{12}H_{17}NO$
Molecular Weight 191.27 g/mol
 pK_a Not Available

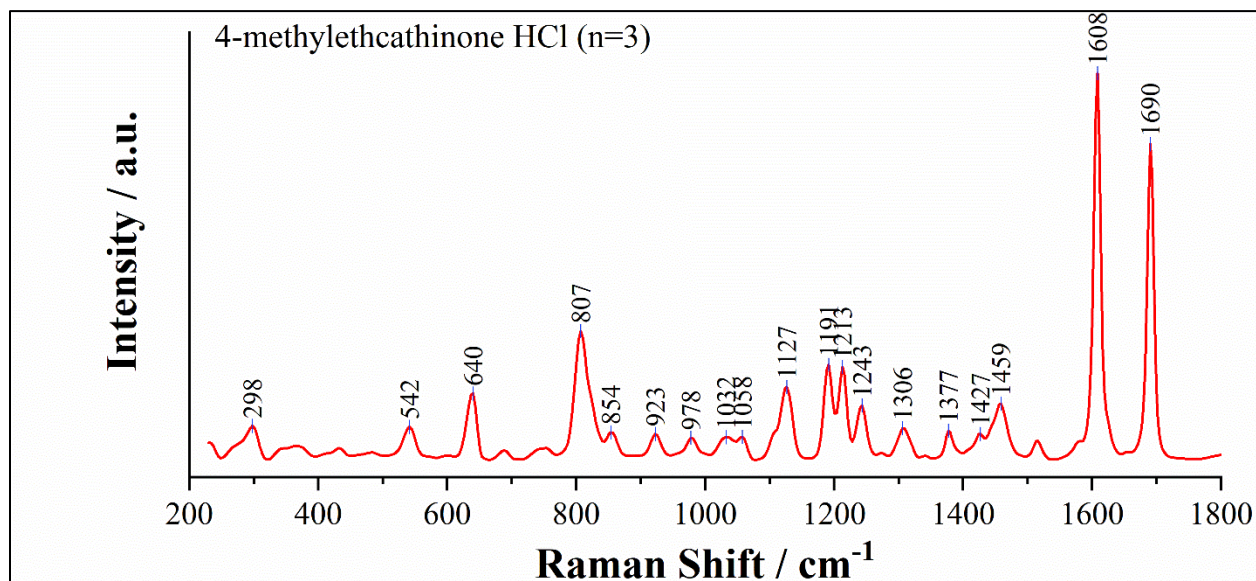


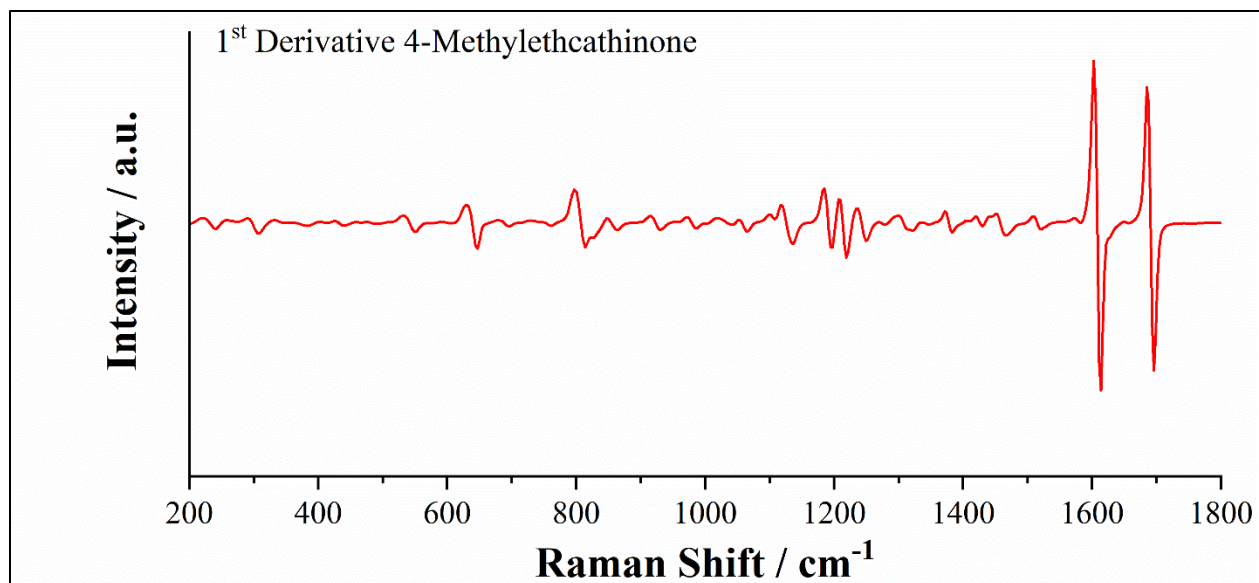
3. Qualitative Data

3.1. Nontargeted EC-SERS, 785-nm SPELEC Raman, Silver SPE

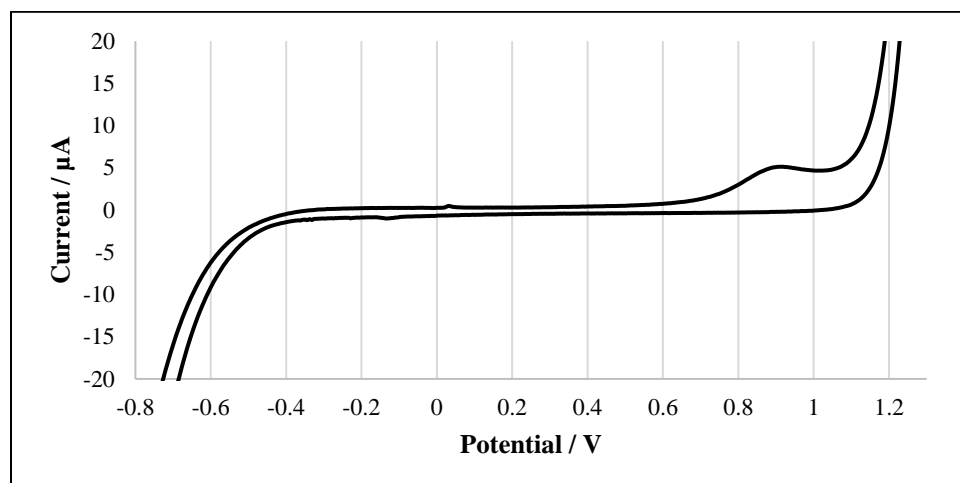
NO SIGNAL UNDER TESTED CONDITIONS

3.2. Normal Raman, 785-nm SPELEC Raman





3.3. Electrochemistry, SPCE, 0.1 M KCl



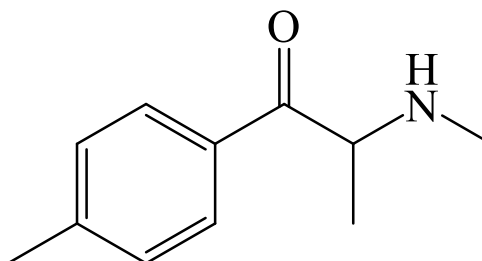
Mephedrone

1. General Information

IUPAC Name	2-(methylamino)-1-(4-methylphenyl)propan-1-one
CAS #	1189805-46-6
Source	Reference Standard

2. Chemical Data

Chemical Formula	C ₁₁ H ₁₅ NO
Molecular Weight	177.24 g/mol
pK _a	Not Available



3. Qualitative Data

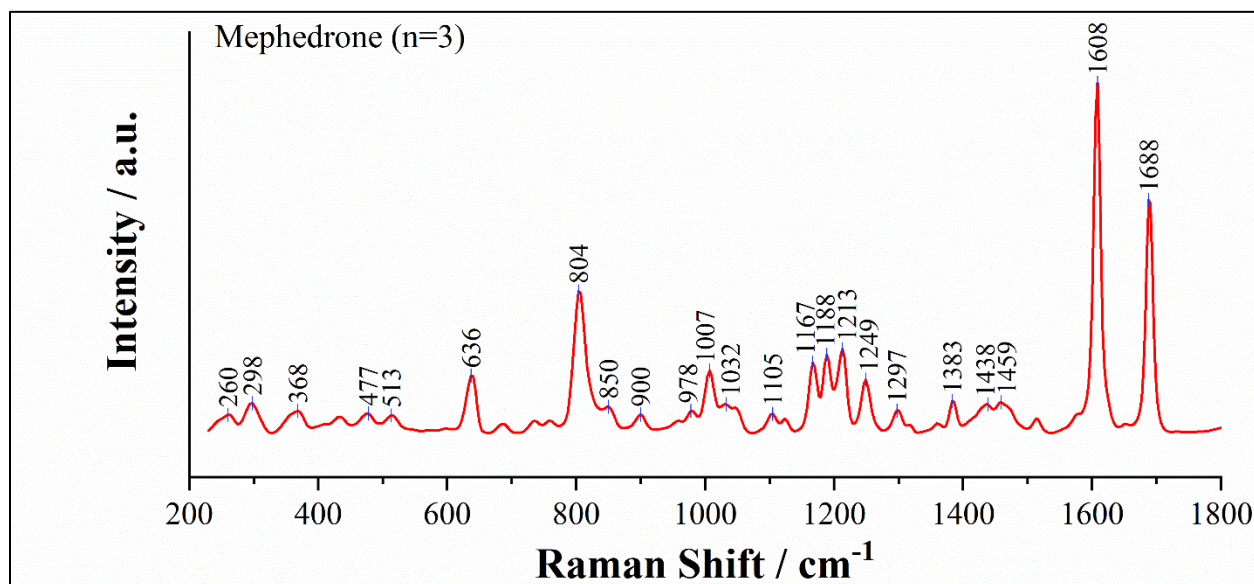
3.1. Nontargeted EC-SERS, 785-nm SPELEC Raman, Silver SPE

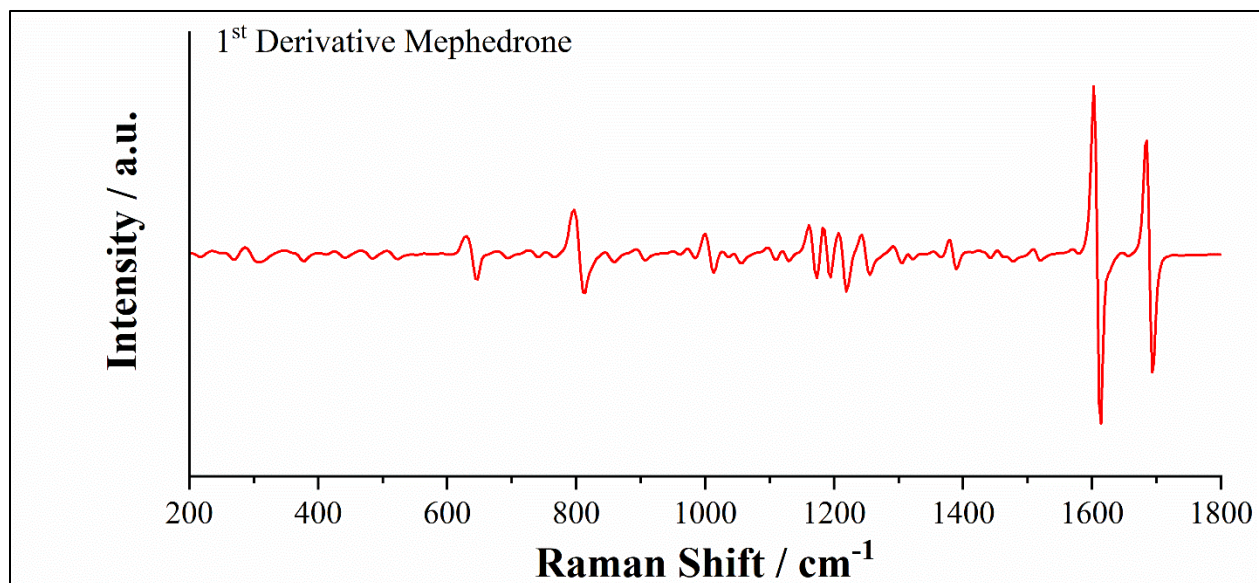
NO SIGNAL UNDER TESTED CONDITIONS

3.2. Fentanyl Targeted EC-SERS, 785-nm SPELEC Raman, Silver SPE

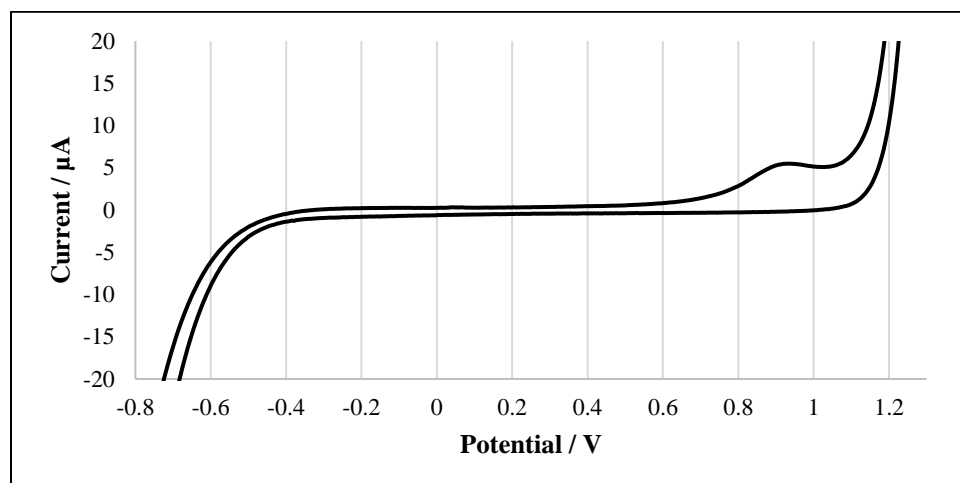
NO SIGNAL UNDER TESTED CONDITIONS

3.3. Normal Raman, 785-nm SPELEC Raman





3.4. Electrochemistry, SPCE. 0.1 M KCl



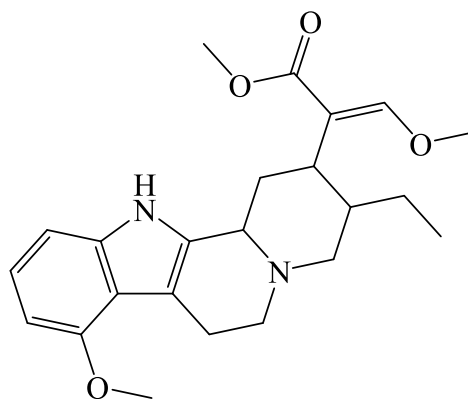
Mitragynine

1. General Information

IUPAC Name	methyl (<i>E</i>)-2-[(2 <i>S</i> ,3 <i>S</i> ,12 <i>bS</i>)-3-ethyl-8-methoxy-1,2,3,4,6,7,12,12 <i>b</i> -octahydroindolo[2,3- <i>a</i>]quinolizin-2-yl]-3-methoxyprop-2-enoate
CAS #	4098-40-2
Source	Reference Standard

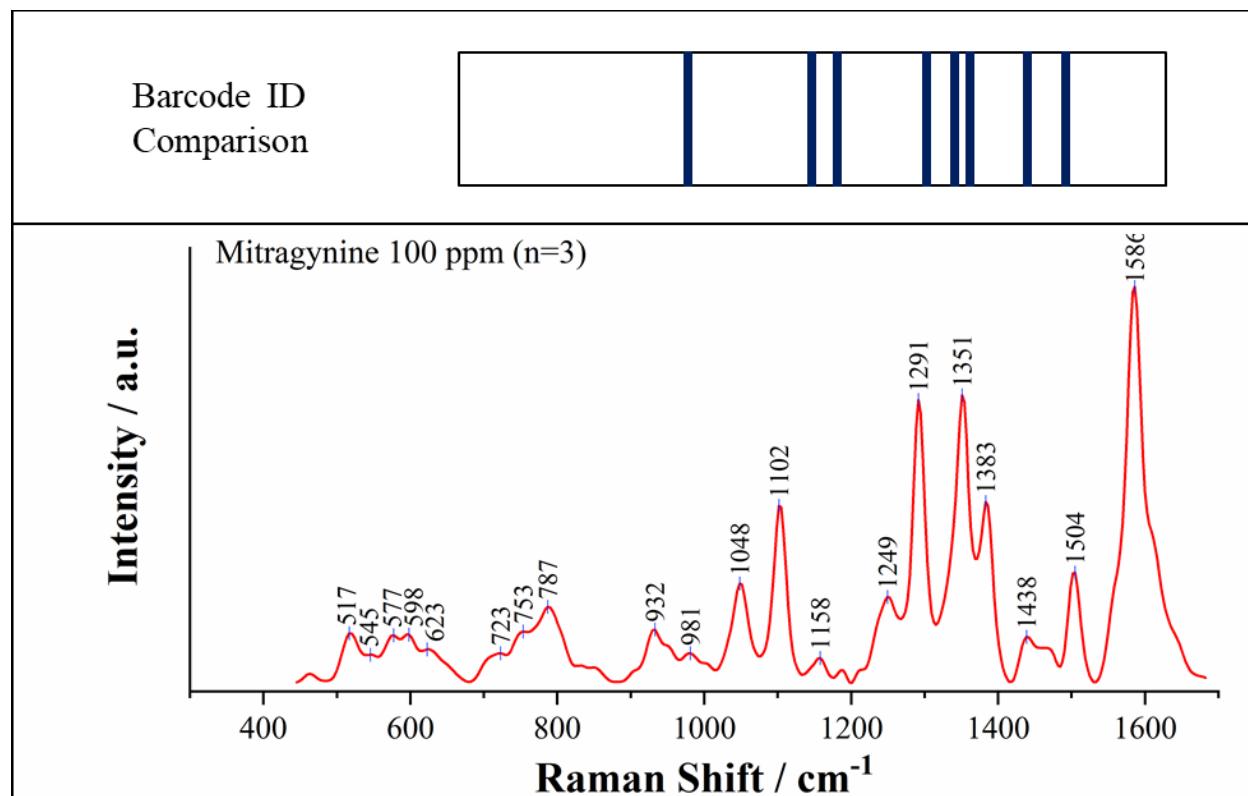
2. Chemical Data

Chemical Formula	C ₂₃ H ₃₀ N ₂ O ₄
Molecular Weight	398.5 g/mol
pK _a	Not Available

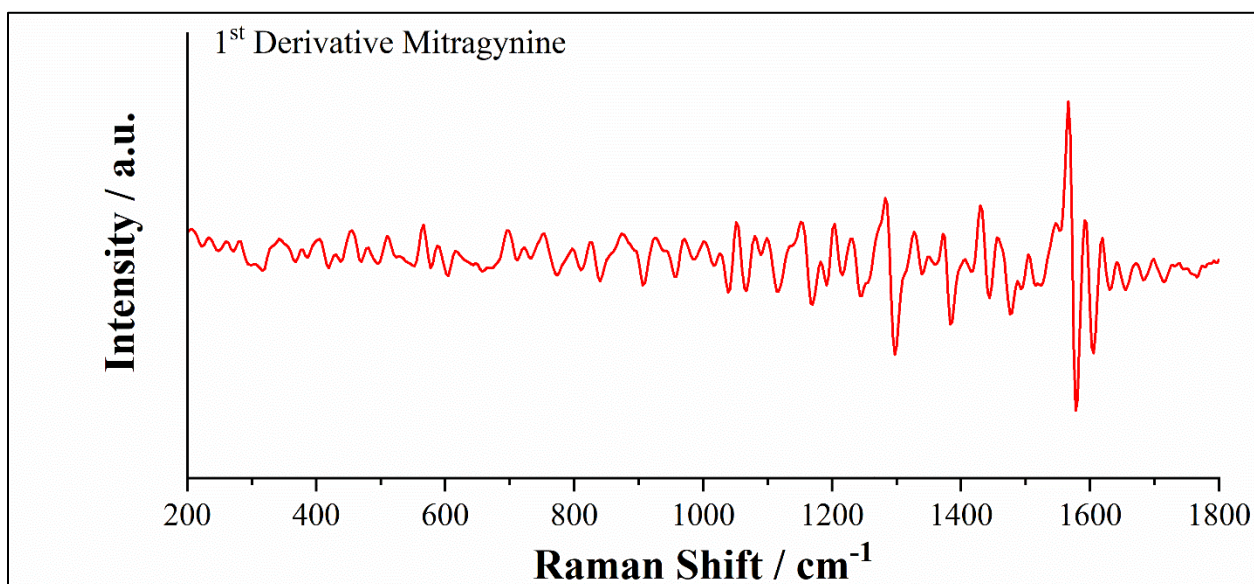
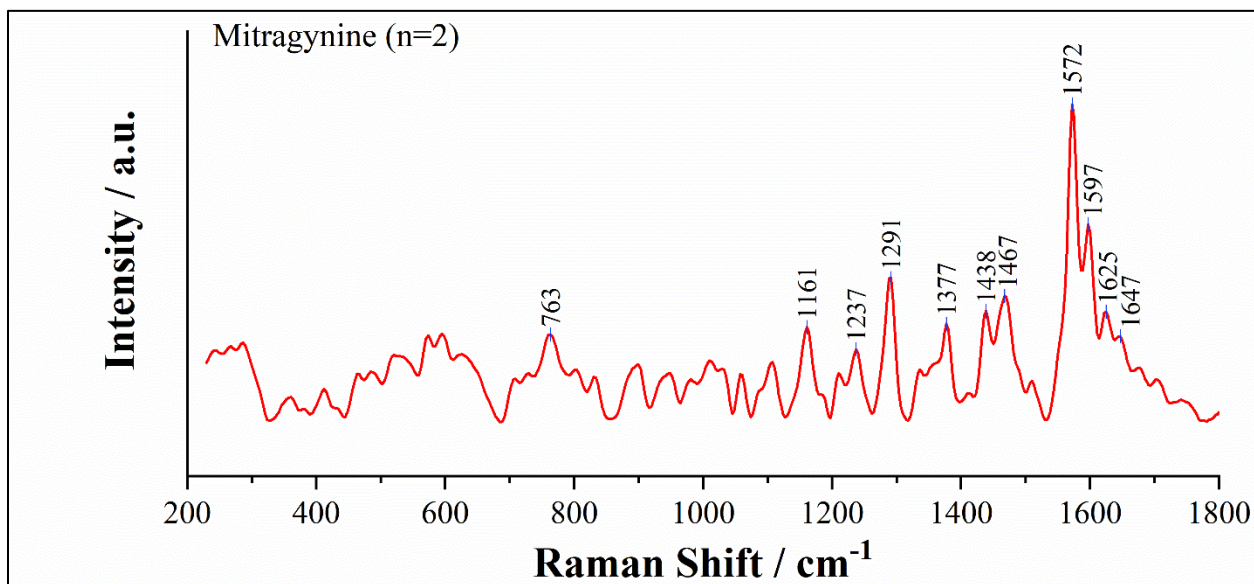


3. Qualitative Data

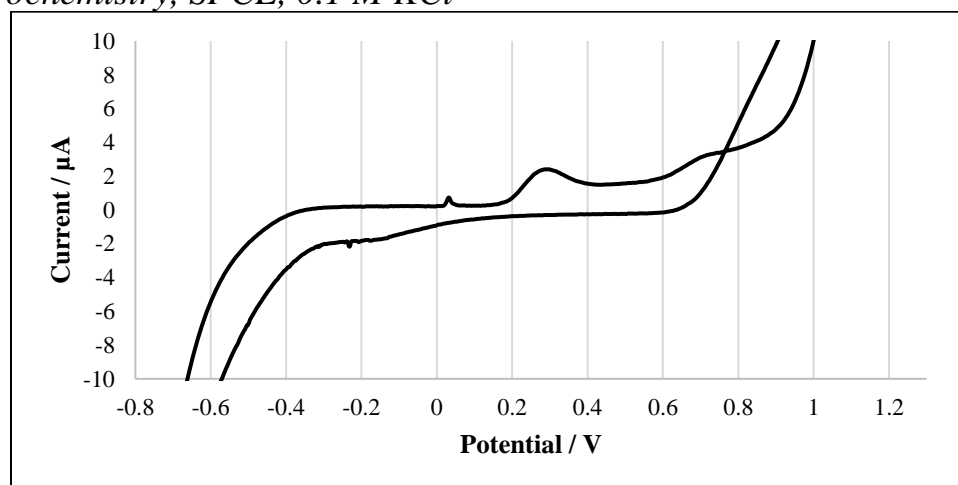
3.1. Nontargeted EC-SERS, 785-nm SPELEC Raman, Silver SPE



3.2. Normal Raman, 785-nm SPELEC Raman



3.3. Electrochemistry, SPCE, 0.1 M KCl



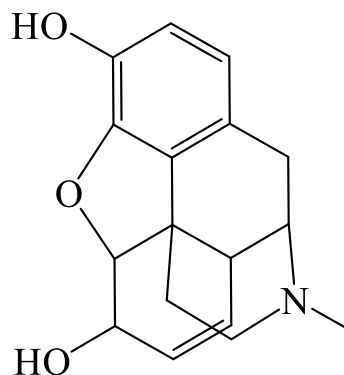
Morphine

1. General Information

IUPAC Name (4*R*,4*aR*,7*S*,7*aR*,12*bS*)-3-methyl-2,4,4*a*,7,7*a*,13-hexahydro-1*H*-4,12-methanobenzofuro[3,2-*e*]isoquinoline-7,9-diol
CAS # 57-27-2
Source Reference Standard

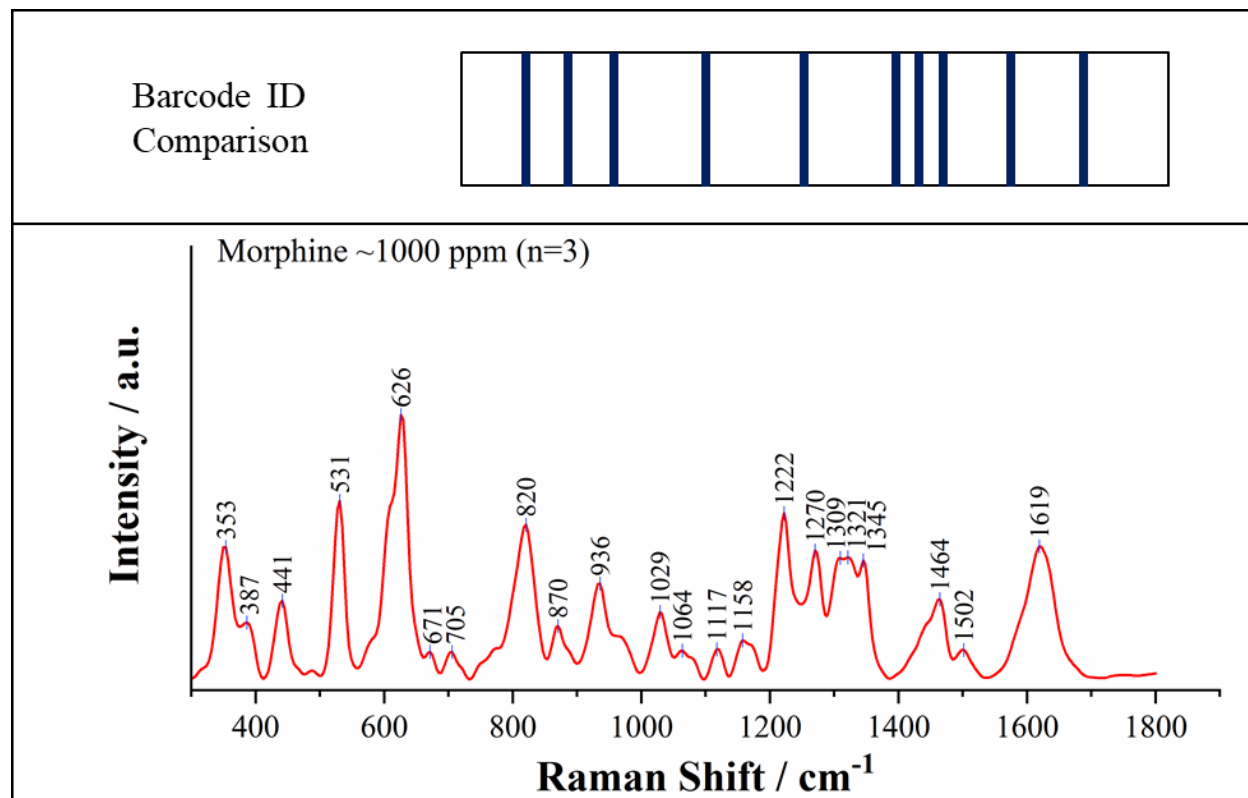
2. Chemical Data

Chemical Formula $C_{17}H_{19}NO_3$
Molecular Weight 285.34 g/mol
pK_a 8.18

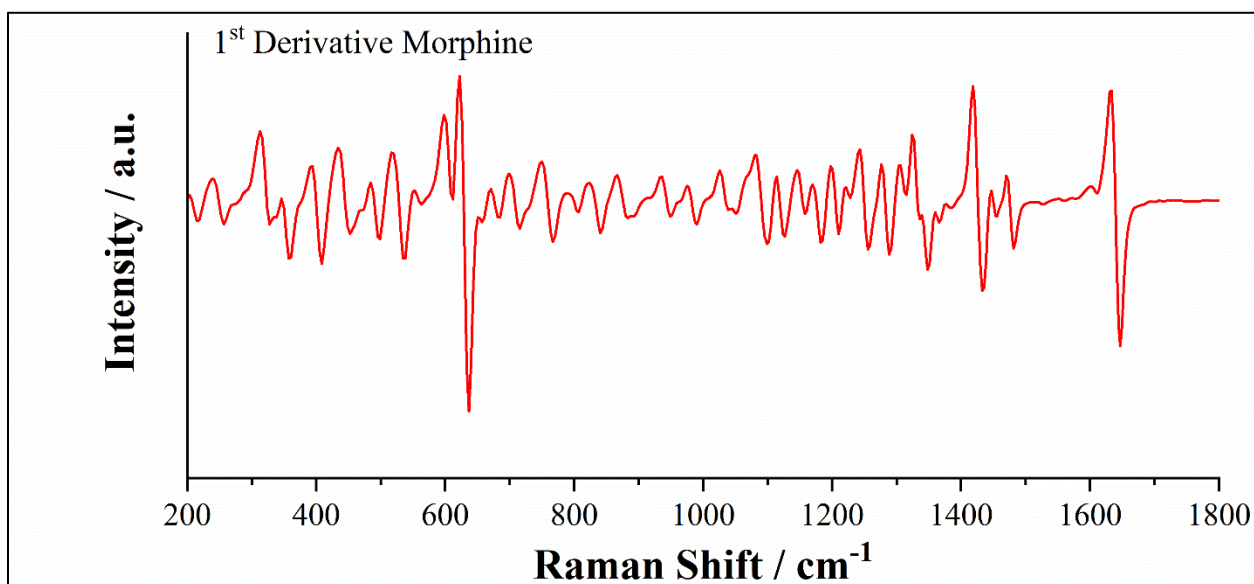
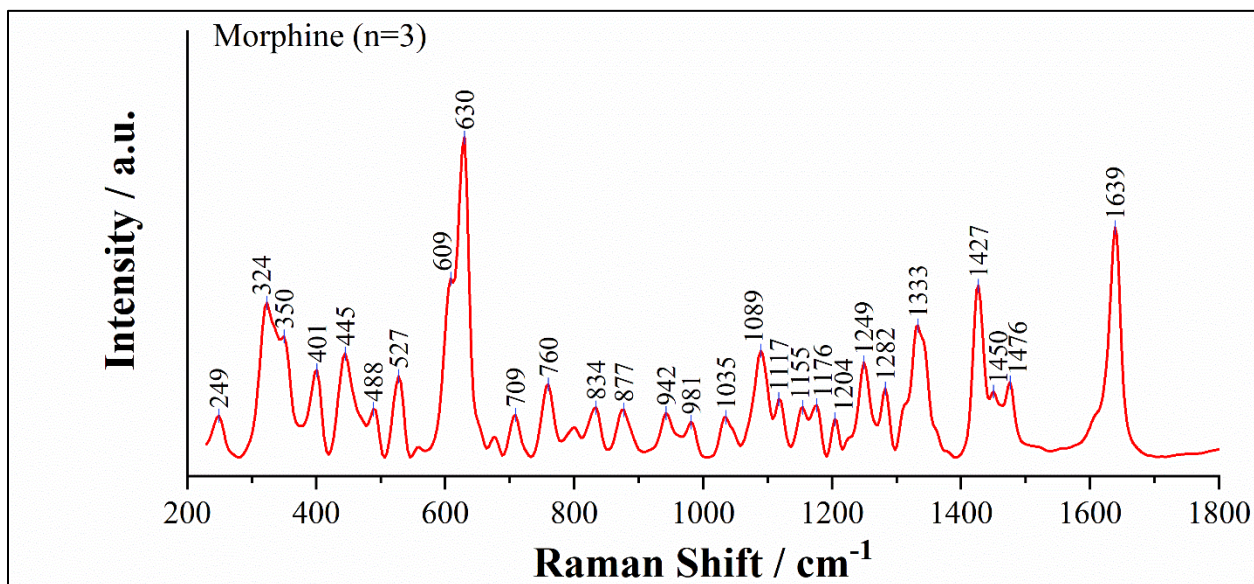


3. Qualitative Data

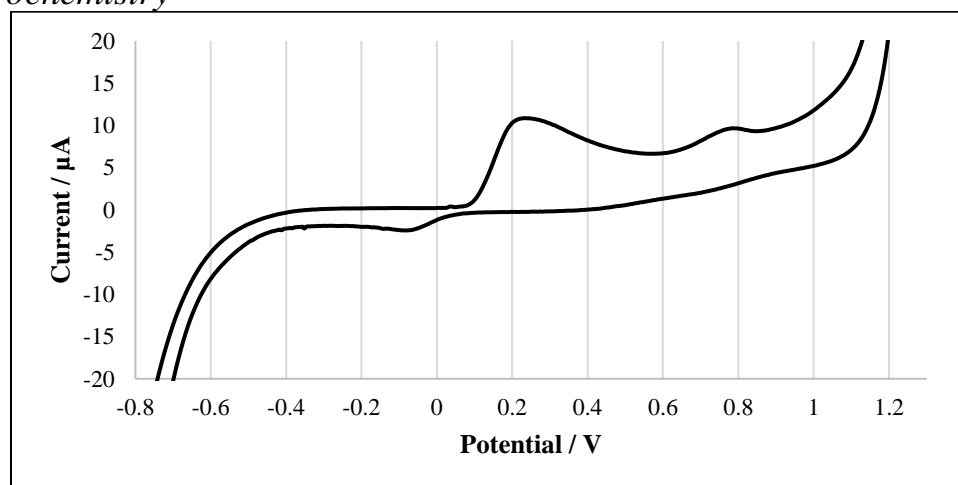
3.1. Nontargeted EC-SERS, 785-nm SPELEC Raman, Silver SPE



3.2. Normal Raman, 785-nm SPELEC Raman



3.3. Electrochemistry



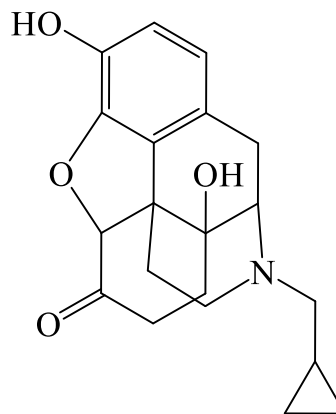
Naltrexone

1. General Information

IUPAC Name	(4 <i>R</i> ,4 <i>aS</i> ,7 <i>aR</i> ,12 <i>bS</i>)-3-(cyclopropylmethyl)-4 <i>a</i> ,9-dihydroxy-2,4,5,6,7 <i>a</i> ,13-hexahydro-1 <i>H</i> -4,12-methanobenzofuro[3,2- <i>e</i>]isoquinolin-7-one
CAS #	16590-41-3
Source	Reference Standard

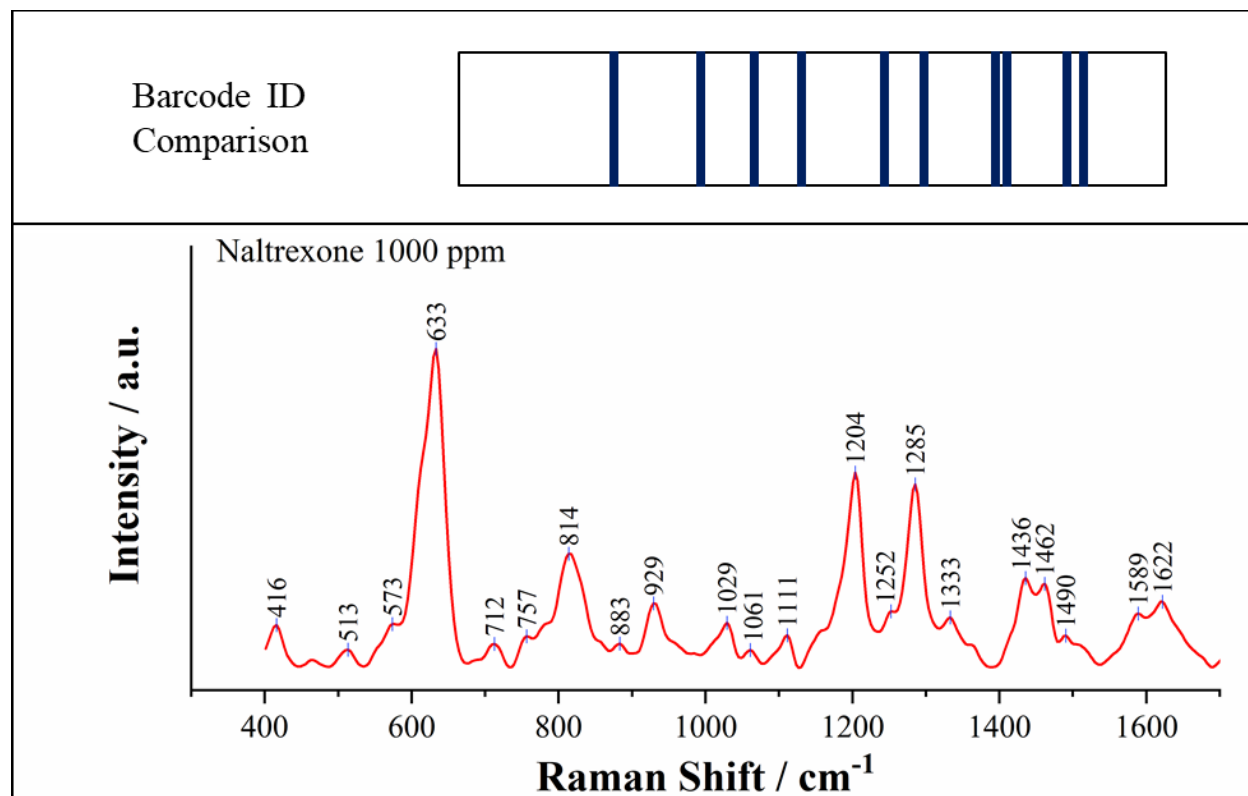
2. Chemical Data

Chemical Formula	C ₂₀ H ₂₃ NO ₄
Molecular Weight	341.4 g/mol
pK _a	8.38

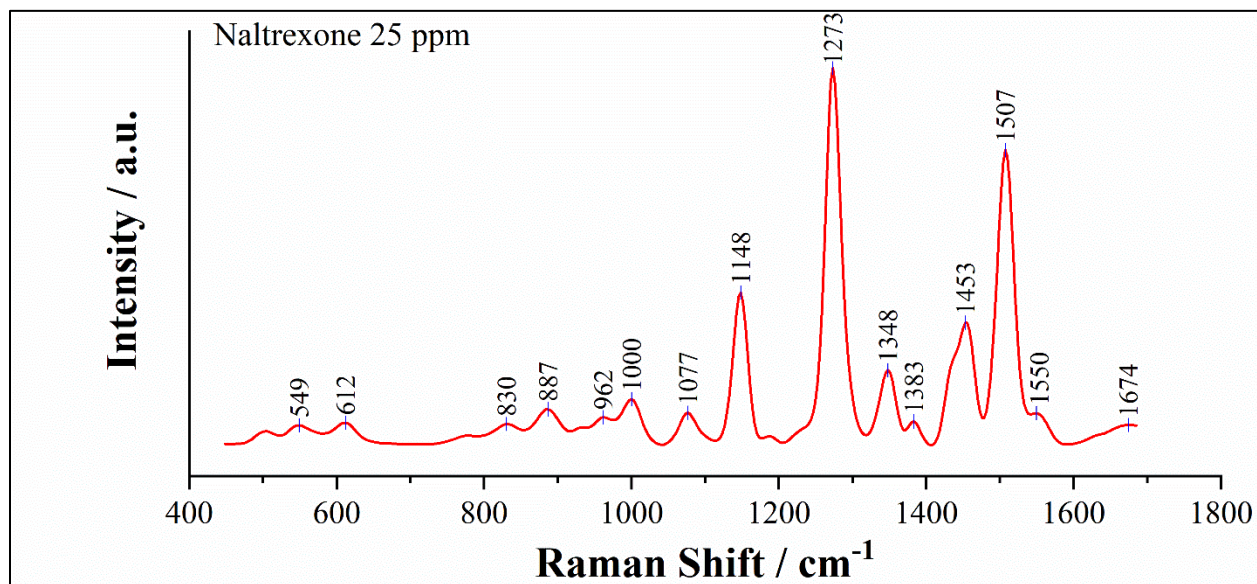


3. Qualitative Data

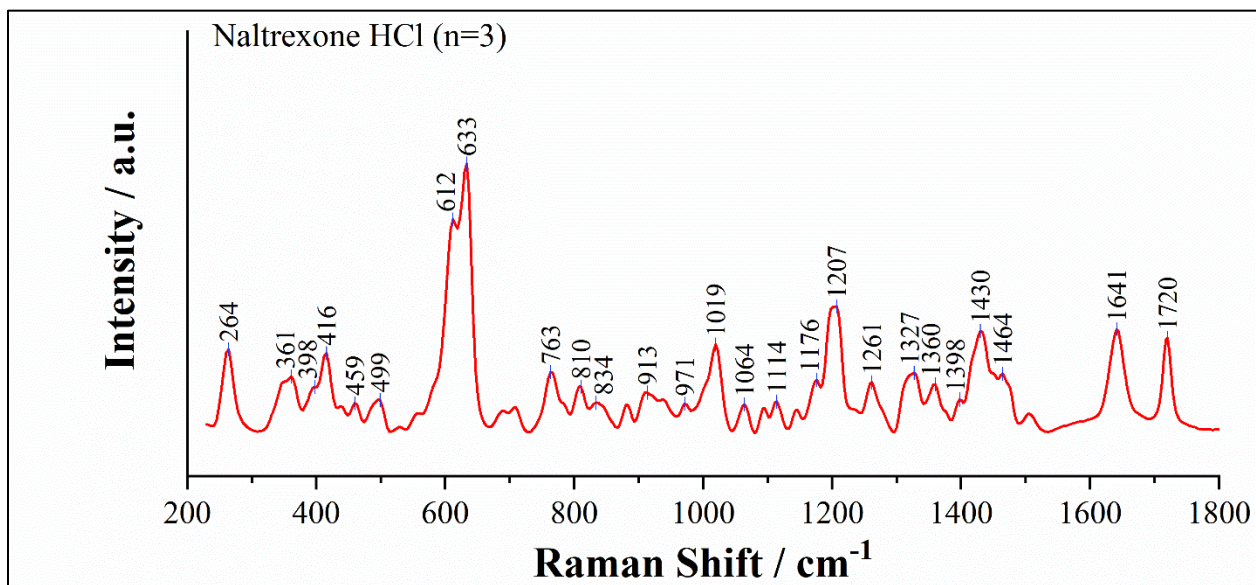
3.1. Nontargeted EC-SERS, 785-nm SPELEC Raman, Silver SPE

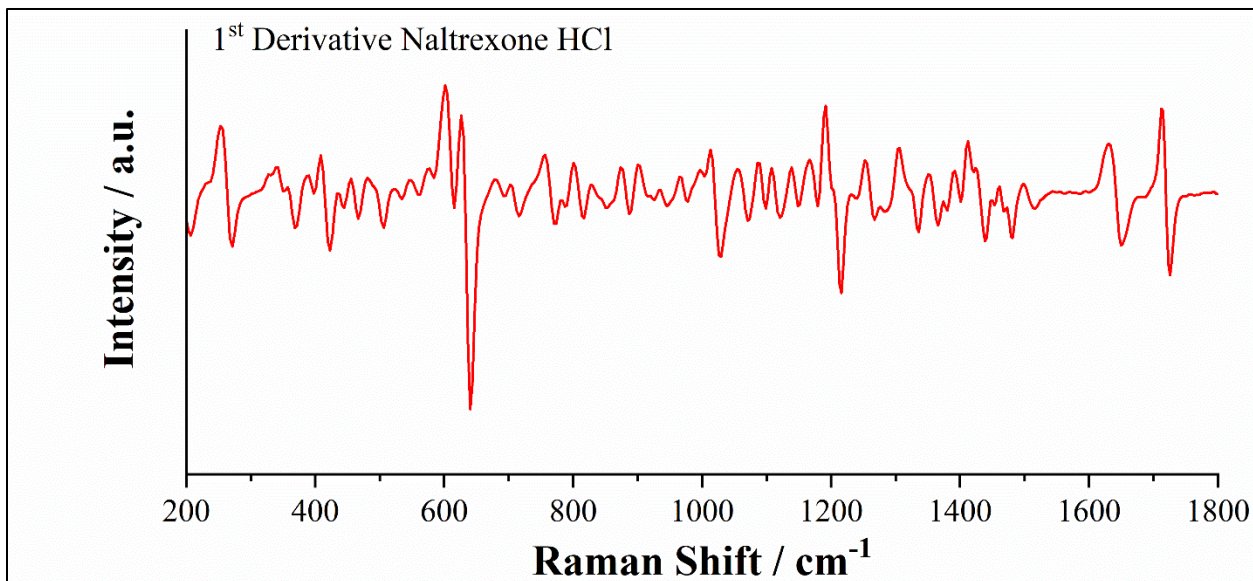


3.2. Fentanyl Targeted EC-SERS, 785-nm SPELEC Raman, Silver SPE

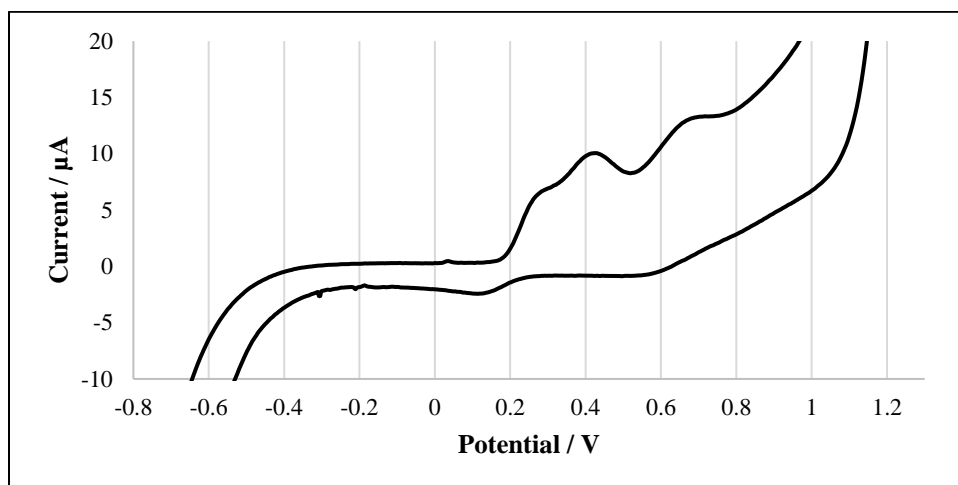


3.3. Normal Raman, 785-nm SPELEC Raman





3.4. Electrochemistry, SPCE, 0.1 M KCl



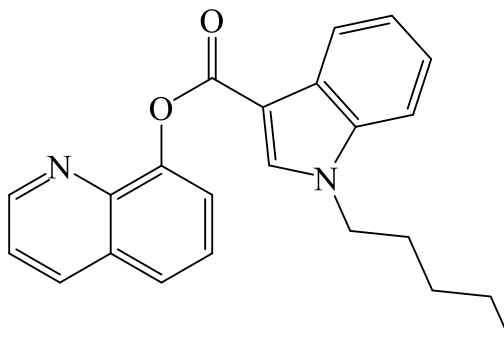
PB-22

1. General Information

IUPAC Name	1-pentyl-1 <i>H</i> -indole-3-carboxylic acid, 8-quinolinyl ester
CAS #	1400742-17-7
Source	Reference Standard

2. Chemical Data

Chemical Formula	C ₂₃ H ₂₂ N ₂ O ₂
Molecular Weight	358.4 g/mol
pK _a	Not Available

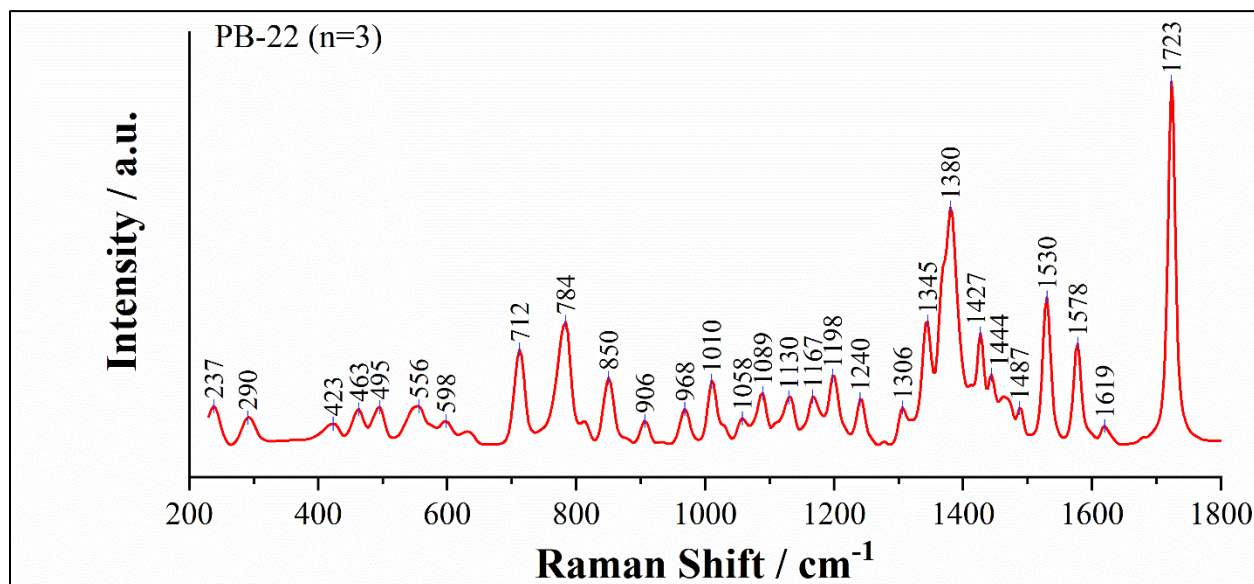


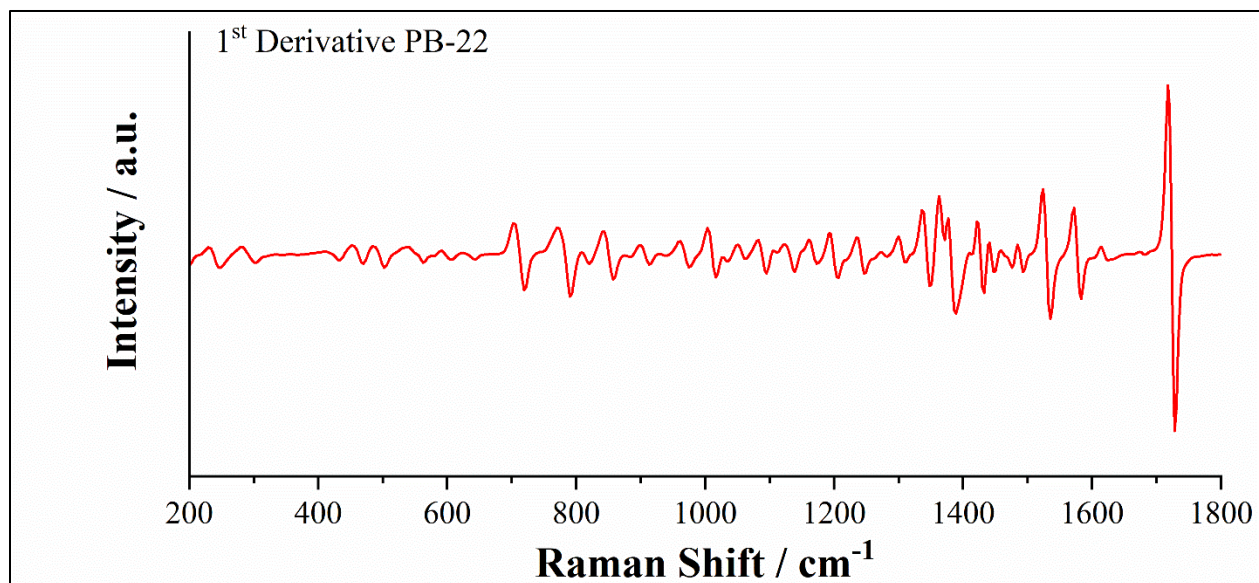
3. Qualitative Data

3.1. Nontargeted EC-SERS, 785-nm SPELEC Raman, Silver SPE

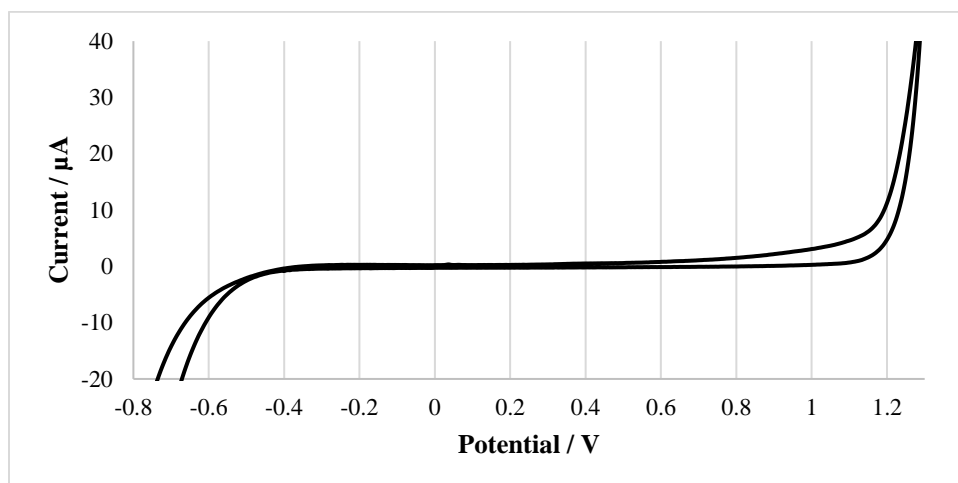
NO SIGNAL UNDER TESTED CONDITIONS

3.2. Normal Raman, 785-nm SPELEC Raman





3.3. Electrochemistry, SPCE, 0.1 M KCl



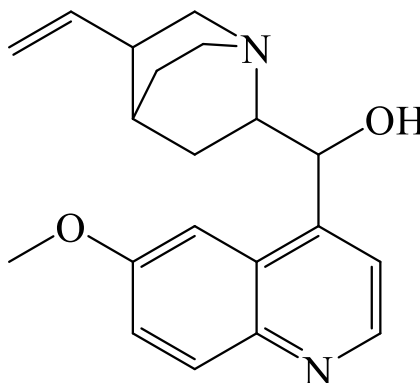
Quinine

1. General Information

IUPAC Name	(R)-[(2S,4S,5R)-5-ethenyl-1-azabicyclo[2.2.2]octan-2-yl]-(6-methoxyquinolin-4-yl)methanol
CAS #	72402-53-0
Source	Reference Standard

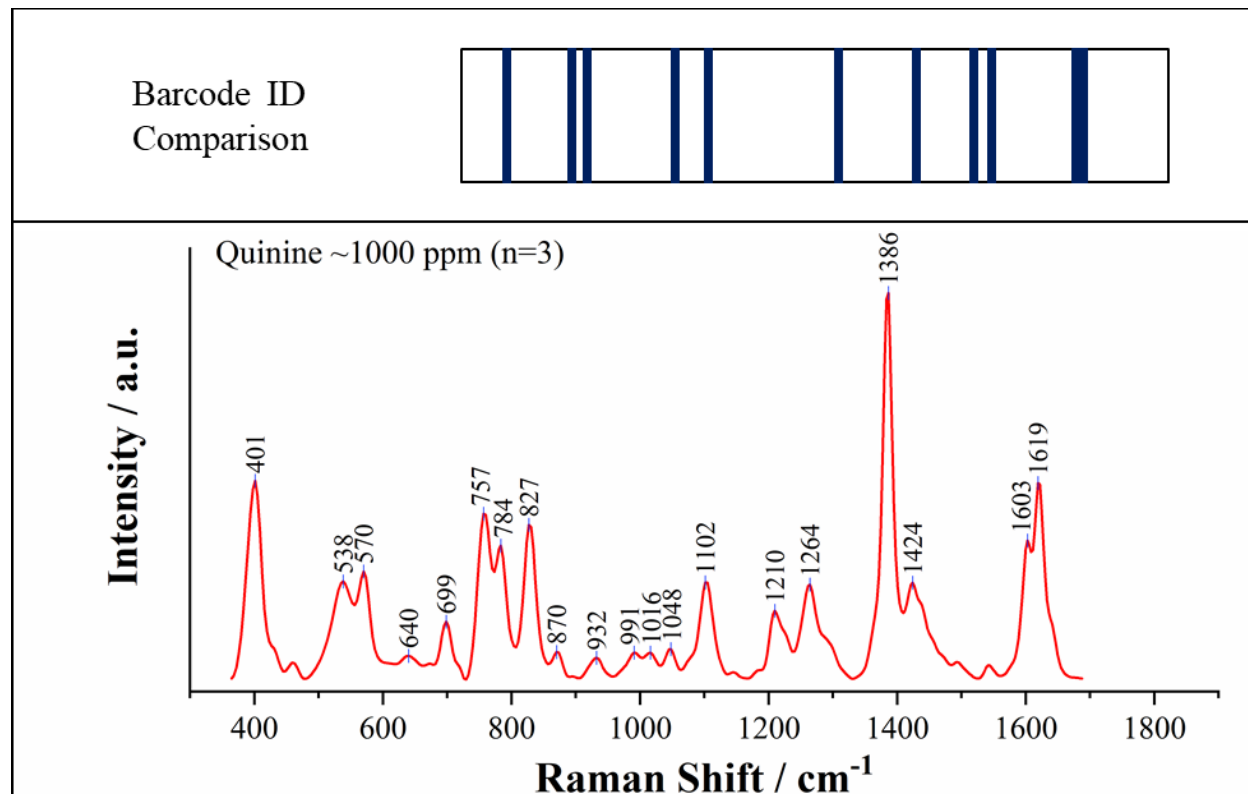
2. Chemical Data

Chemical Formula	C ₂₀ H ₂₄ N ₂ O ₂
Molecular Weight	324.4 g/mol
pK _a	8.56

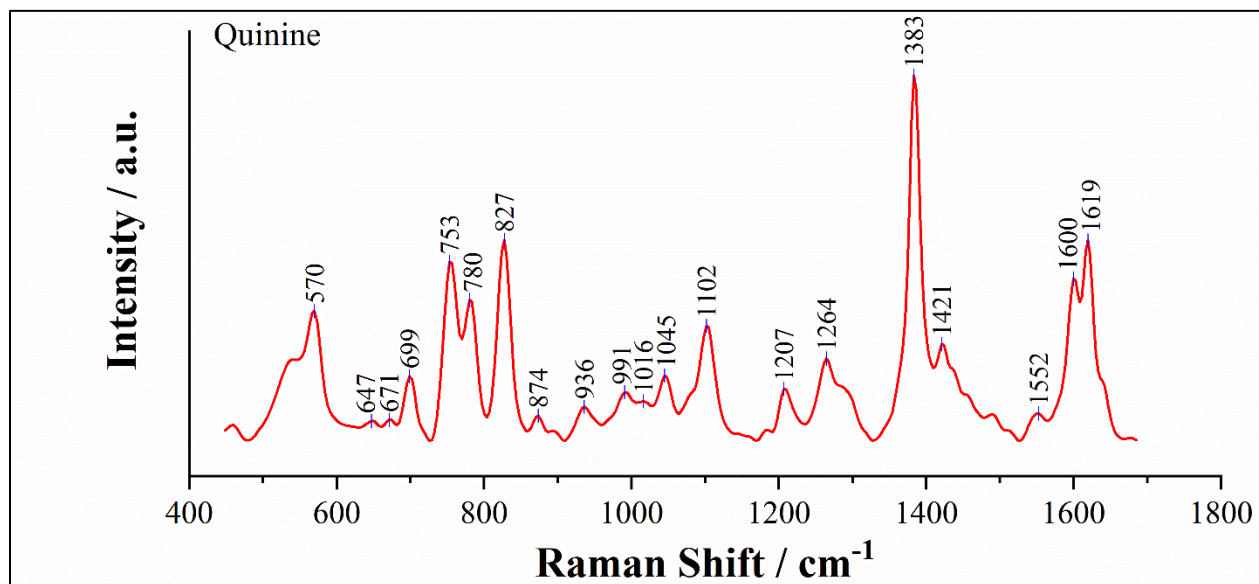


3. Qualitative Data

3.1. Nontargeted EC-SERS, 785-nm SPELEC Raman, Silver SPE



3.2. *Fentanyl Targeted EC-SERS, 785-nm SPELEC Raman, Silver SPE*



3.3. *Normal Raman, 785-nm SPELEC Raman*

DATA NOT COLLECTED

3.4. *Electrochemistry*

DATA NOT COLLECTED

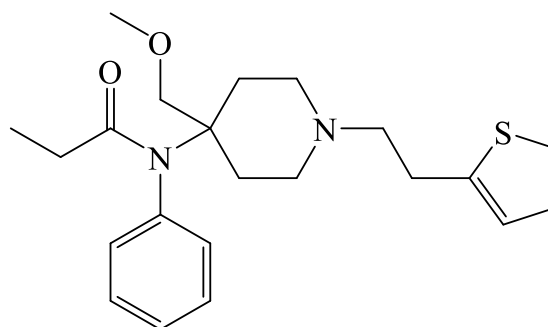
Sufentanil

1. General Information

IUPAC Name	<i>N</i> -[4-(methoxymethyl)-1-(2-thiophen-2-ylethyl)piperidin-4-yl]- <i>N</i> -phenylpropanamide
CAS #	56030-54-7
Source	Reference Standard

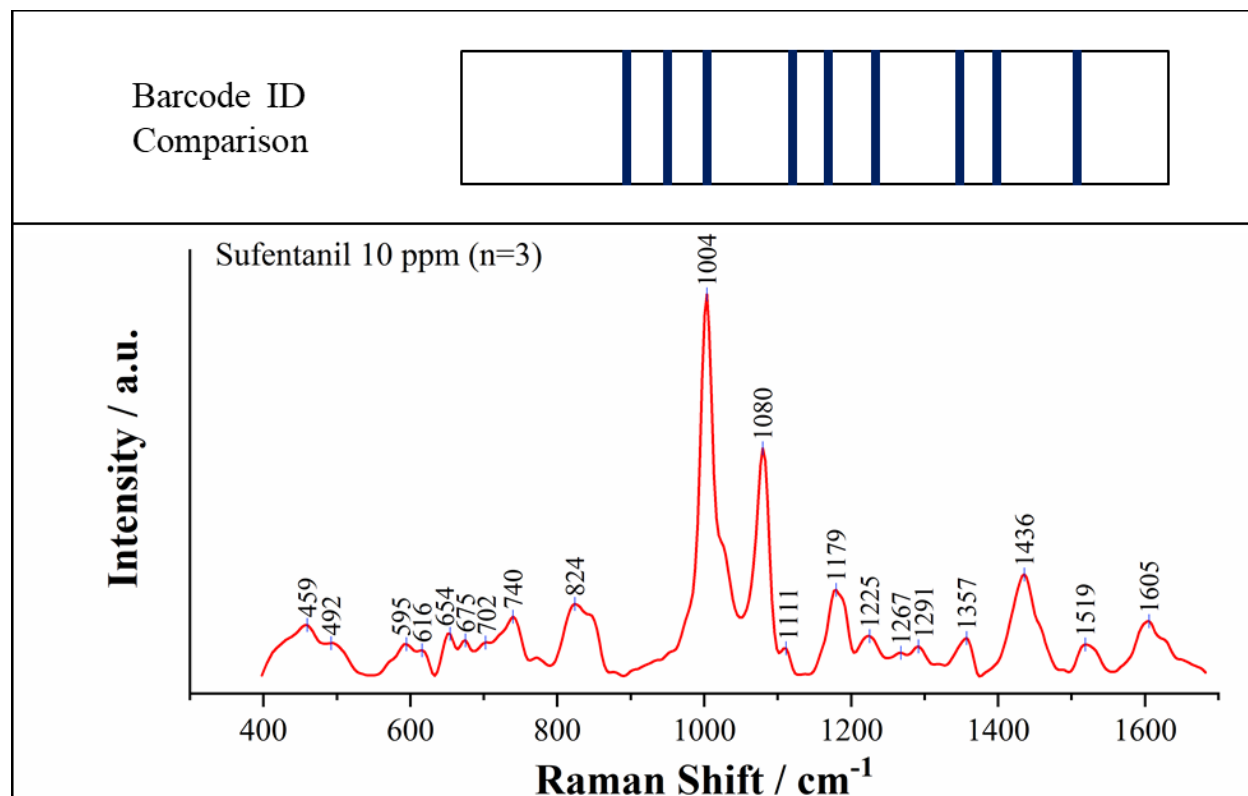
2. Chemical Data

Chemical Formula	C ₂₂ H ₃₀ N ₂ O ₂ S
Molecular Weight	386.6 g/mol
pK _a	7.85

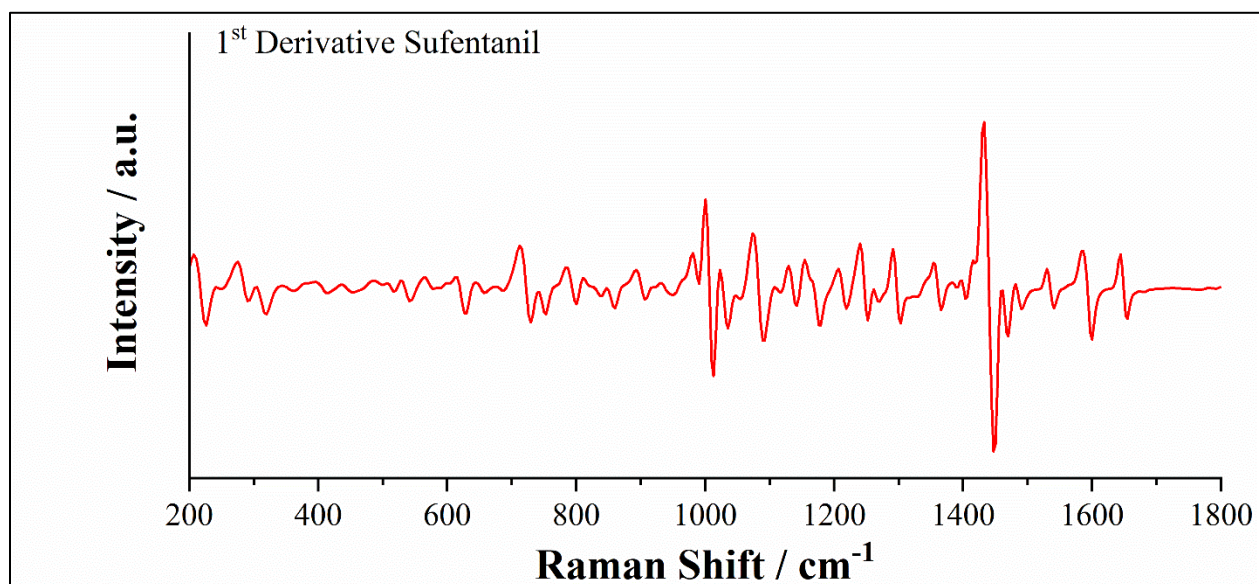
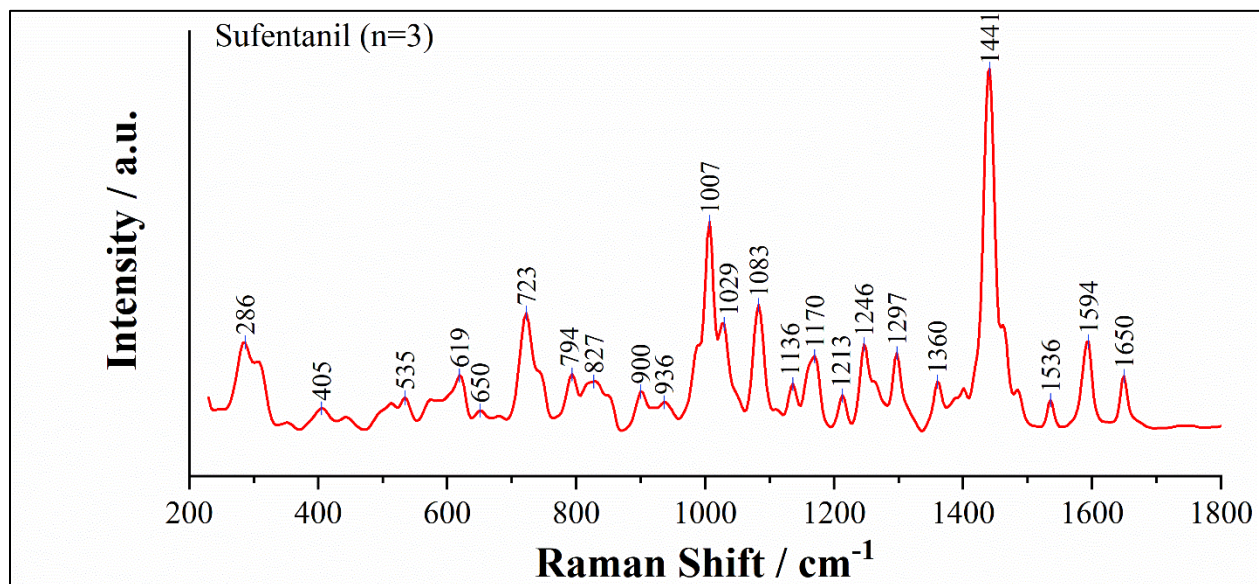


3. Qualitative Data

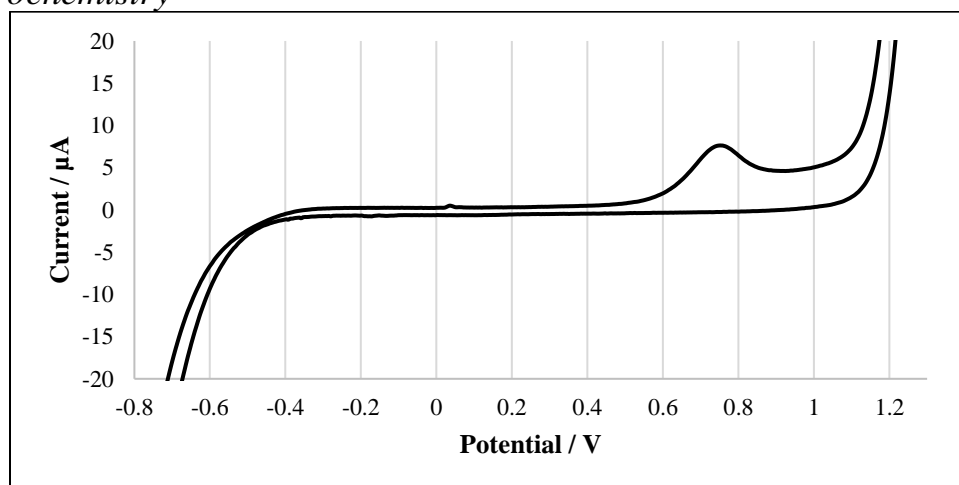
3.1. Nontargeted EC-SERS, 785-nm SPELEC Raman, Silver SPE



3.2. Normal Raman, 785-nm SPELEC Raman



3.3. Electrochemistry



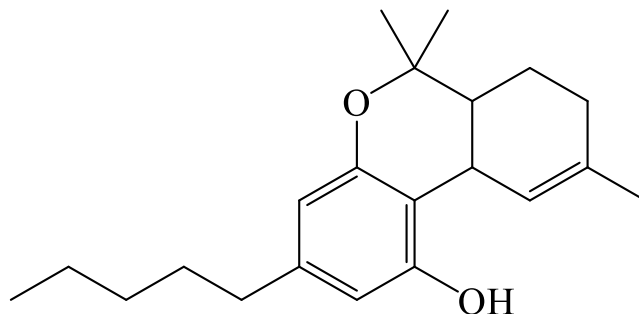
Delta-9-THC

1. General Information

IUPAC Name	(6 <i>aR</i> ,10 <i>aR</i>)-6,6,9-trimethyl-3-pentyl-6 <i>a</i> ,7,8,10 <i>a</i> -tetrahydrobenzo[<i>c</i>]chromen-1-ol
CAS #	1972-08-3
Source	Reference Standard

2. Chemical Data

Chemical Formula	C ₂₁ H ₃₀ O ₂
Molecular Weight	314.5 g/mol
pK _a	10.6

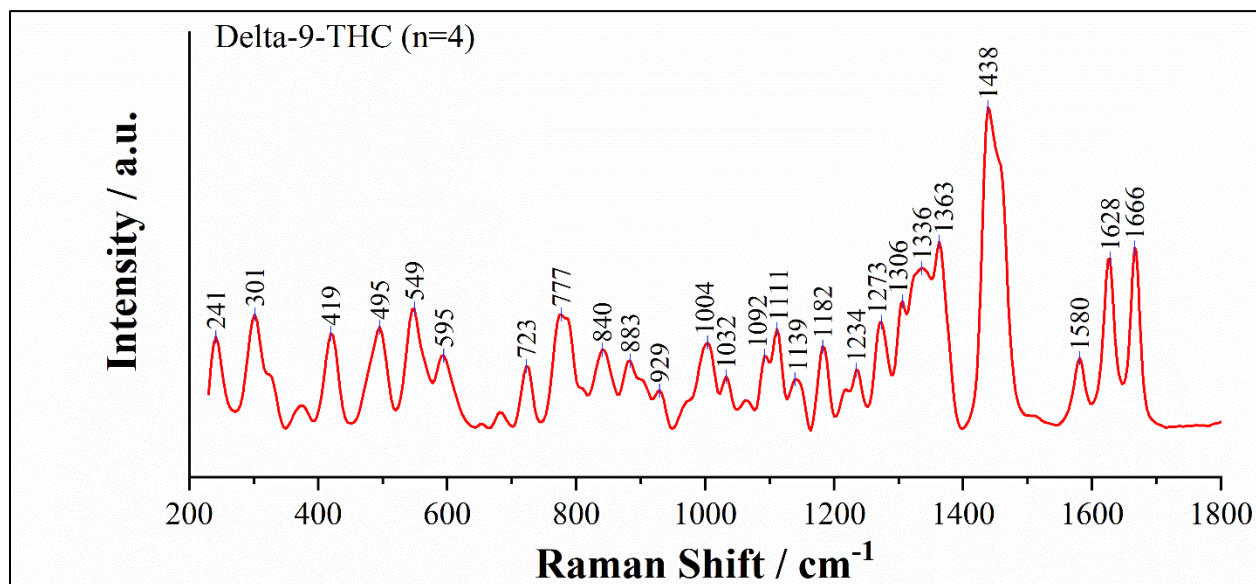


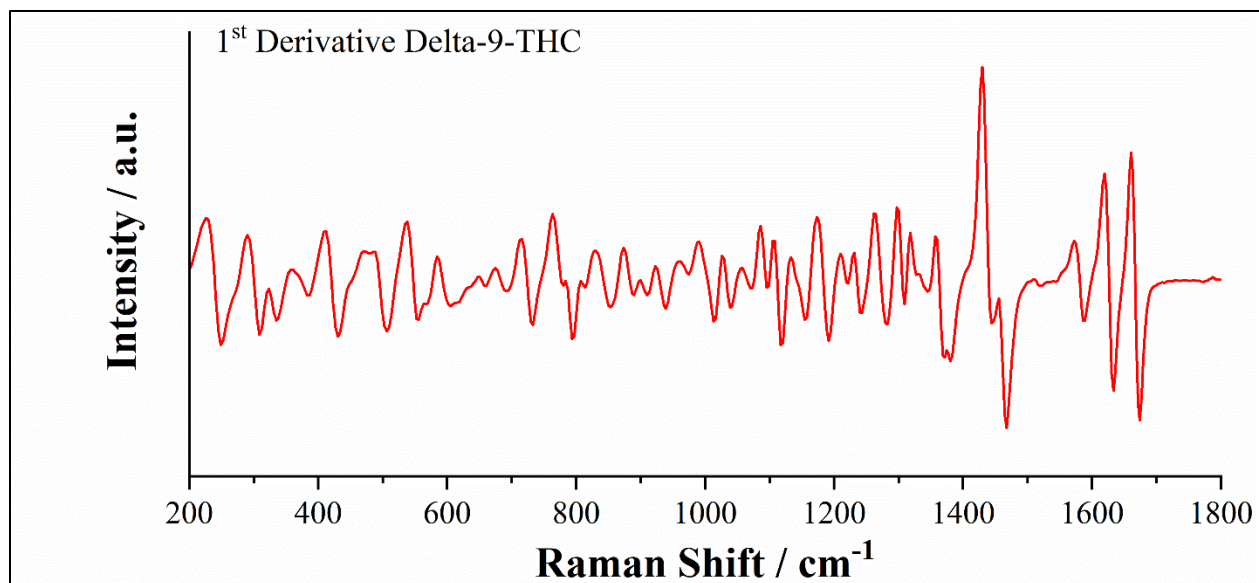
3. Qualitative Data

3.1. Nontargeted EC-SERS, 785-nm SPELEC Raman, Silver SPE

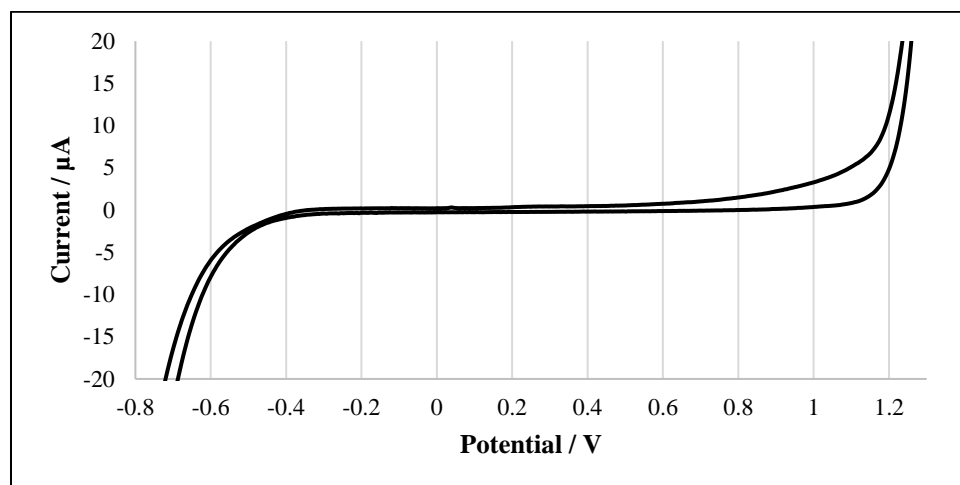
NO SIGNAL UNDER TESTED CONDITIONS

3.2. Normal Raman, 785-nm SPELEC Raman





3.3. Electrochemistry, SPCE, 0.1 M KCl



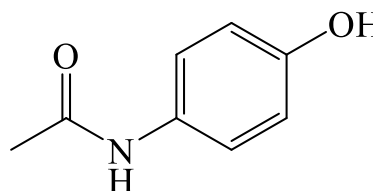
Acetaminophen

1. General Information

IUPAC Name	N-(4-hydroxyphenyl)acetamide
CAS #	103-90-2
Source	Reference Standard

2. Chemical Data

Chemical Formula	C ₈ H ₉ NO ₂
Molecular Weight	151.16 g/mol
pK _a	9.38



3. Qualitative Data

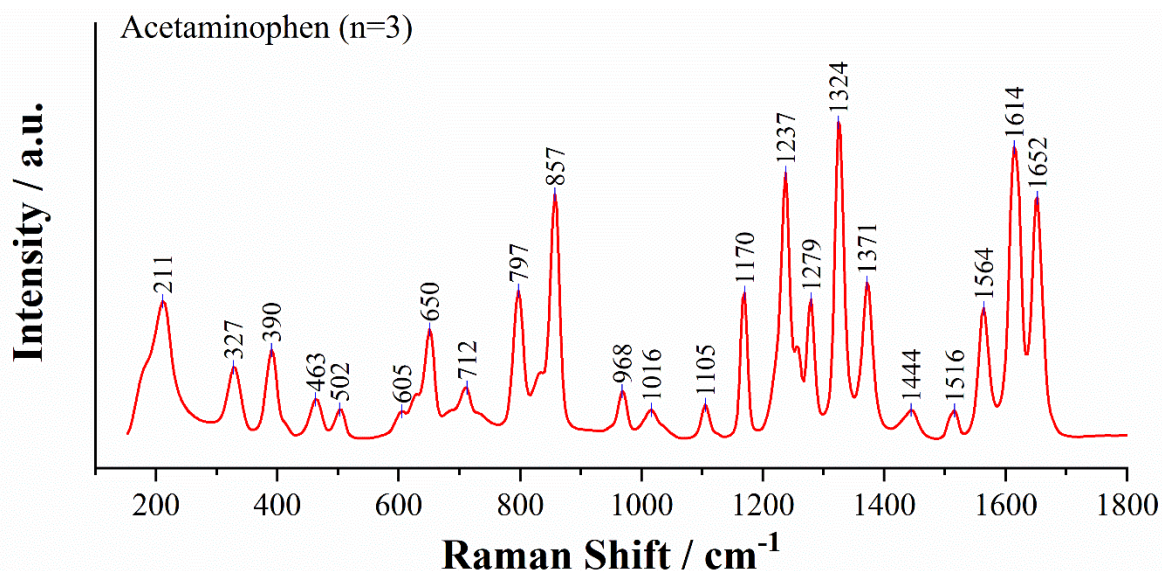
3.1. Nontargeted EC-SERS, 785-nm SPELEC Raman, Silver SPE

NO SIGNAL UNDER TESTED CONDITIONS

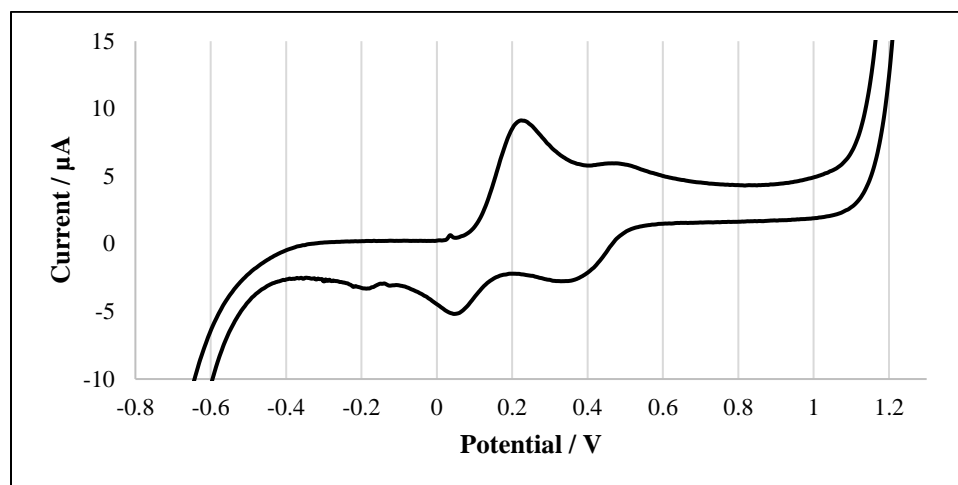
3.2. Fentanyl Targeted EC-SERS, 785-nm SPELEC Raman, Silver SPE

NO SIGNAL UNDER TESTED CONDITIONS

3.3. Normal Raman, 785-nm SPELEC Raman



3.4. Electrochemistry, SPCE, 0.1 M KCl



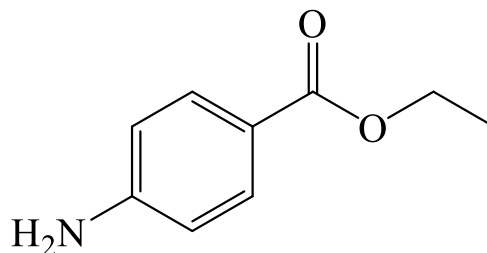
Benzocaine

1. General Information

IUPAC Name	ethyl 4-aminobenzoate
CAS #	94-09-7
Source	Reference Standard

2. Chemical Data

Chemical Formula	C ₉ H ₁₁ NO ₂
Molecular Weight	165.19 g/mol
pK _a	2.51

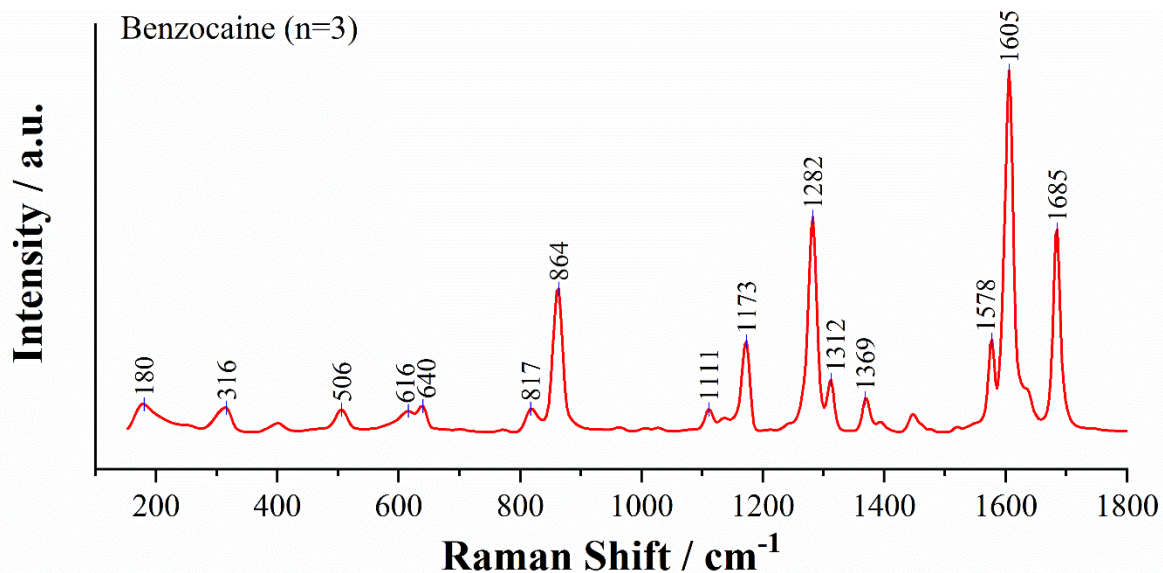


3. Qualitative Data

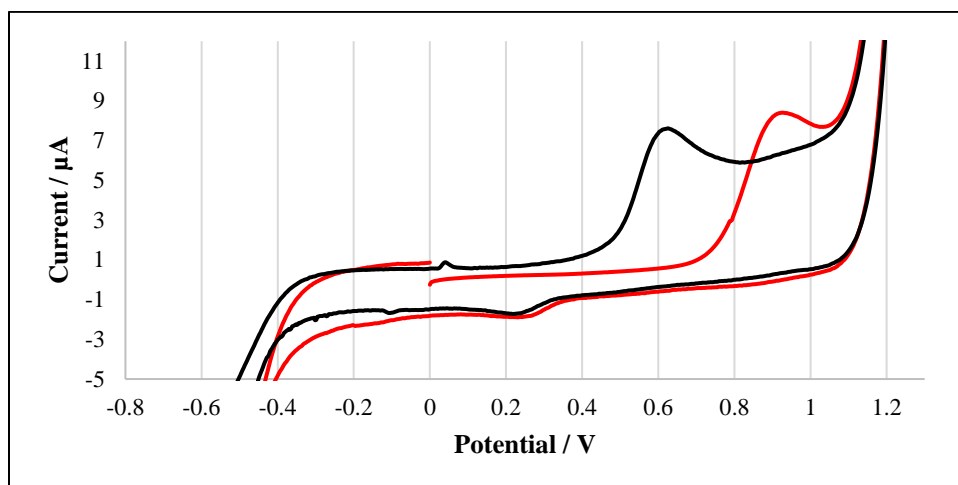
3.1. Nontargeted EC-SERS, 785-nm SPELEC Raman, Silver SPE

NO SIGNAL UNDER TESTED CONDITIONS

3.2. Normal Raman, 785-nm SPELEC Raman



3.3. Electrochemistry, SPCE, 0.1 M KCl



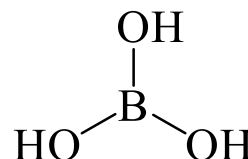
Boric acid

1. General Information

IUPAC Name	boric acid
CAS #	10043-35-3
Source	Reference Standard

2. Chemical Data

Chemical Formula	H ₃ BO ₃
Molecular Weight	61.84 g/mol
pK _a	9.24

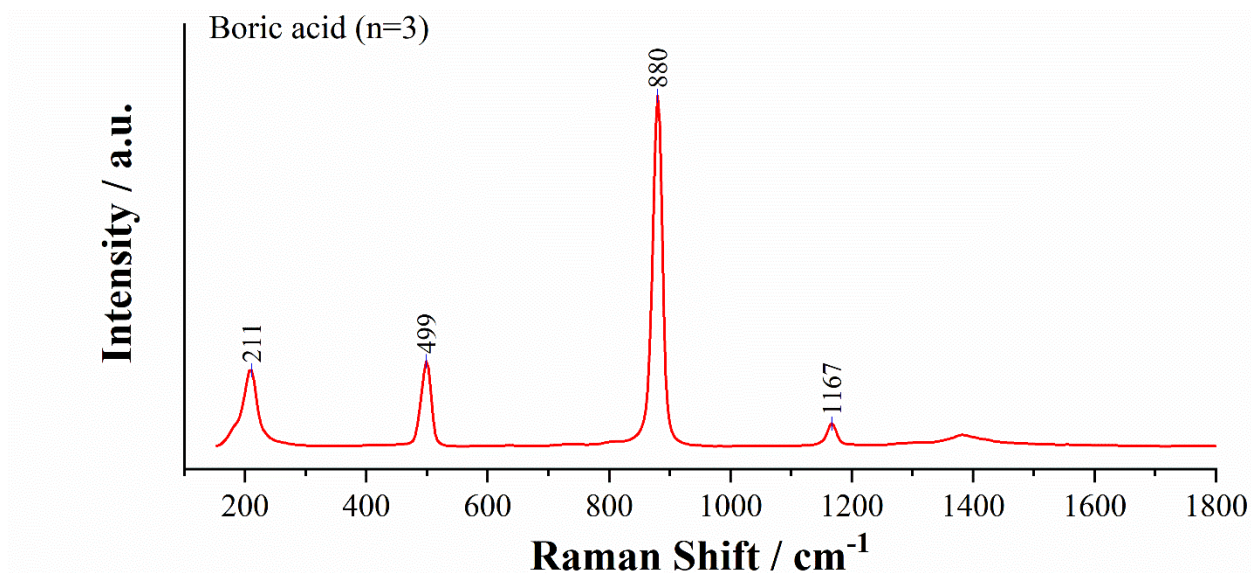


3. Qualitative Data

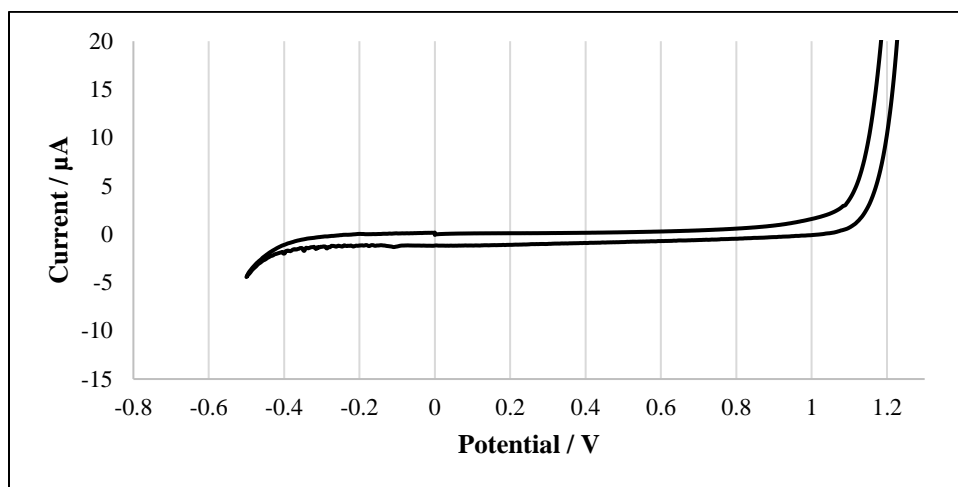
3.1. Nontargeted EC-SERS, 785-nm SPELEC Raman, Silver SPE

NO SIGNAL UNDER TESTED CONDITIONS

3.2. Normal Raman, 785-nm SPELEC Raman



3.3. Electrochemistry, SPCE, 0.1 M KCl



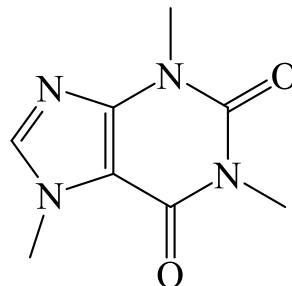
Caffeine

1. General Information

IUPAC Name	1,3,7-trimethylpurine-2,6-dione
CAS #	58-08-2
Source	Reference Standard

2. Chemical Data

Chemical Formula	C ₈ H ₁₀ N ₄ O ₂
Molecular Weight	194.19 g/mol
pK _a	14.0



3. Qualitative Data

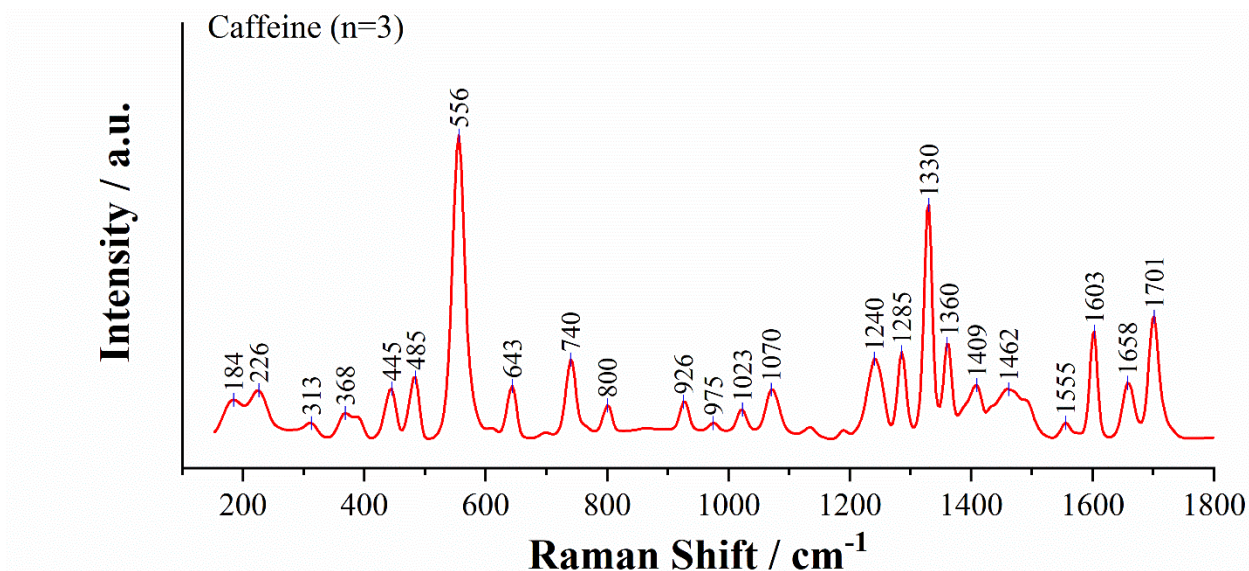
3.1. Nontargeted EC-SERS, 785-nm SPELEC Raman, Silver SPE

NO SIGNAL UNDER TESTED CONDITIONS

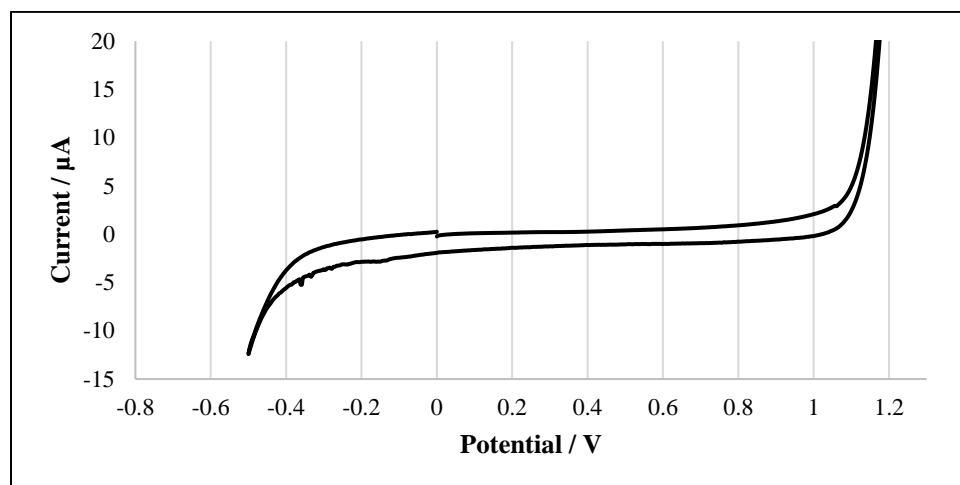
3.2. Fentanyl Targeted EC-SERS, 785-nm SPELEC Raman, Silver SPE

NO SIGNAL UNDER TESTED CONDITIONS

3.3. Normal Raman, 785-nm SPELEC Raman



3.4. Electrochemistry, SPCE, 0.1 M KCl



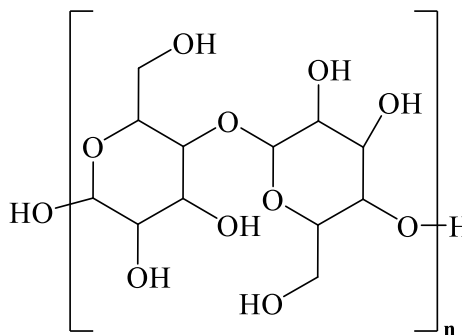
Corn Starch

1. General Information

IUPAC Name	2-(hydroxymethyl)-6-[[4,5,6-trihydroxy-2-(hydroxymethyl)oxan-3-yl]oxy]oxane-3,4,5-triol
CAS #	9005-25-8
Source	Reference Standard

2. Chemical Data

Chemical Formula	$(C_6H_{10}O_5)_n$
Molecular Weight	NA
pK _a	NA

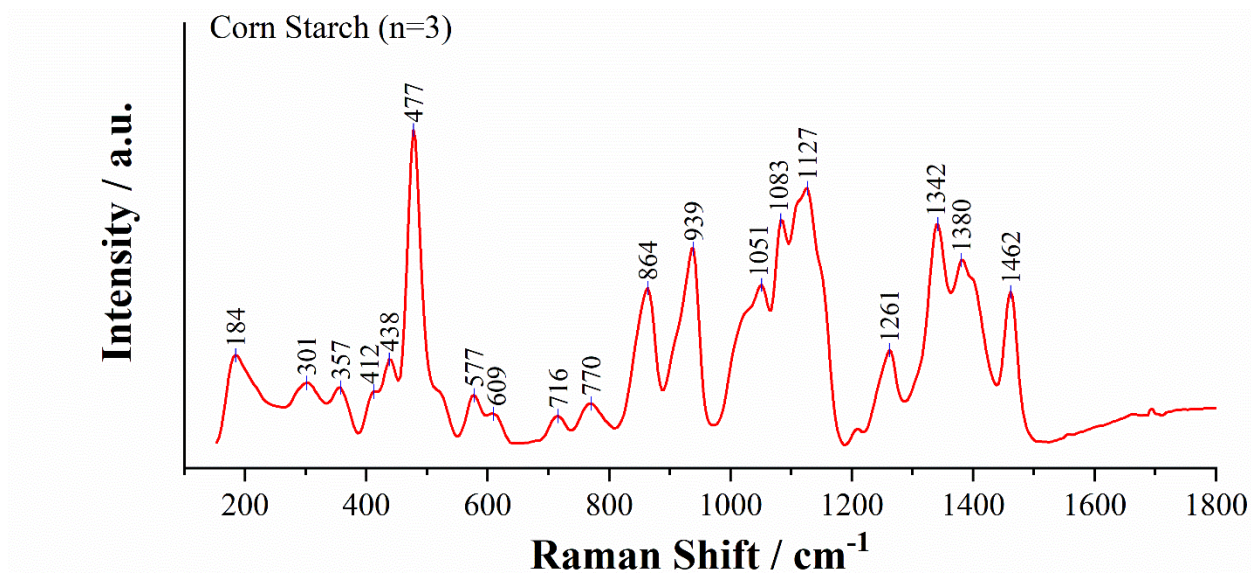


3. Qualitative Data

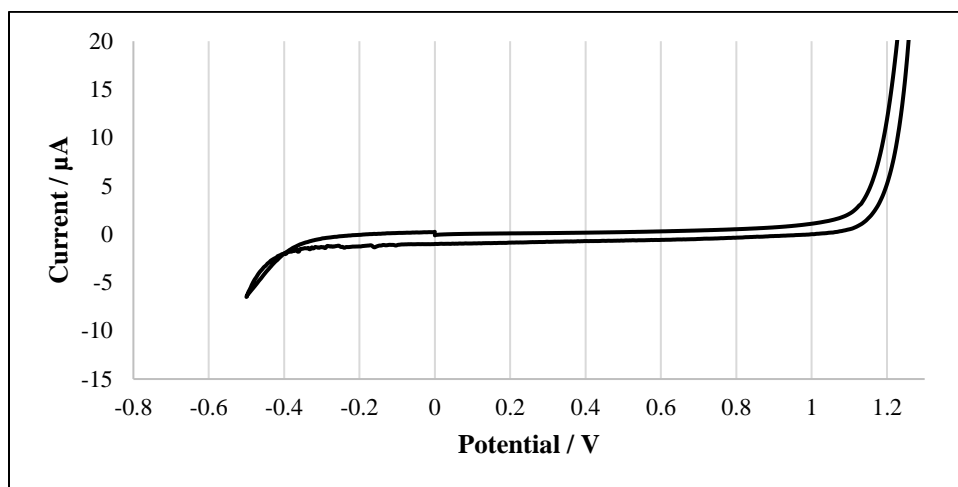
3.1. Nontargeted EC-SERS, 785-nm SPELEC Raman, Silver SPE

NO SIGNAL UNDER TESTED CONDITIONS

3.2. Normal Raman, 785-nm SPELEC Raman



3.3. Electrochemistry, SPCE, 0.1 M KCl



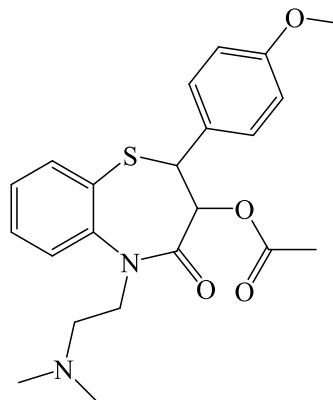
Diltiazem

1. General Information

IUPAC Name	[(2S,3S)-5-[2-(dimethylamino)ethyl]-2-(4-methoxyphenyl)-4-oxo-2,3-dihydro-1,5-benzothiazepin-3-yl] acetate
CAS #	56209-45-1
Source	Reference Standard

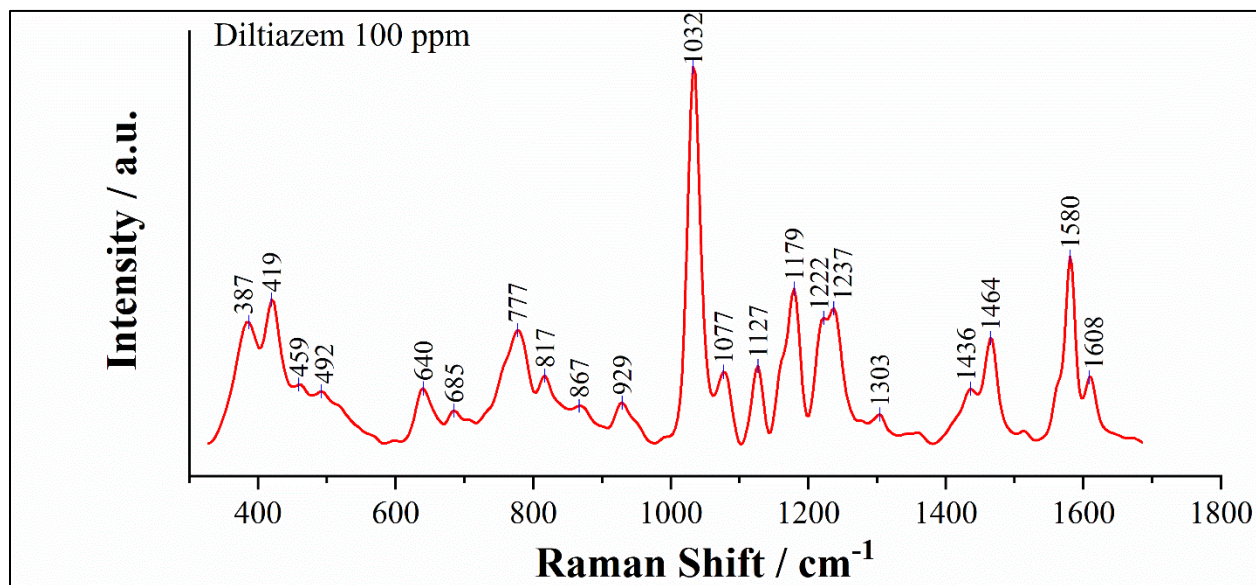
2. Chemical Data

Chemical Formula	C ₂₂ H ₂₆ N ₂ O ₄ S
Molecular Weight	414.5 g/mol
pK _a	8.06

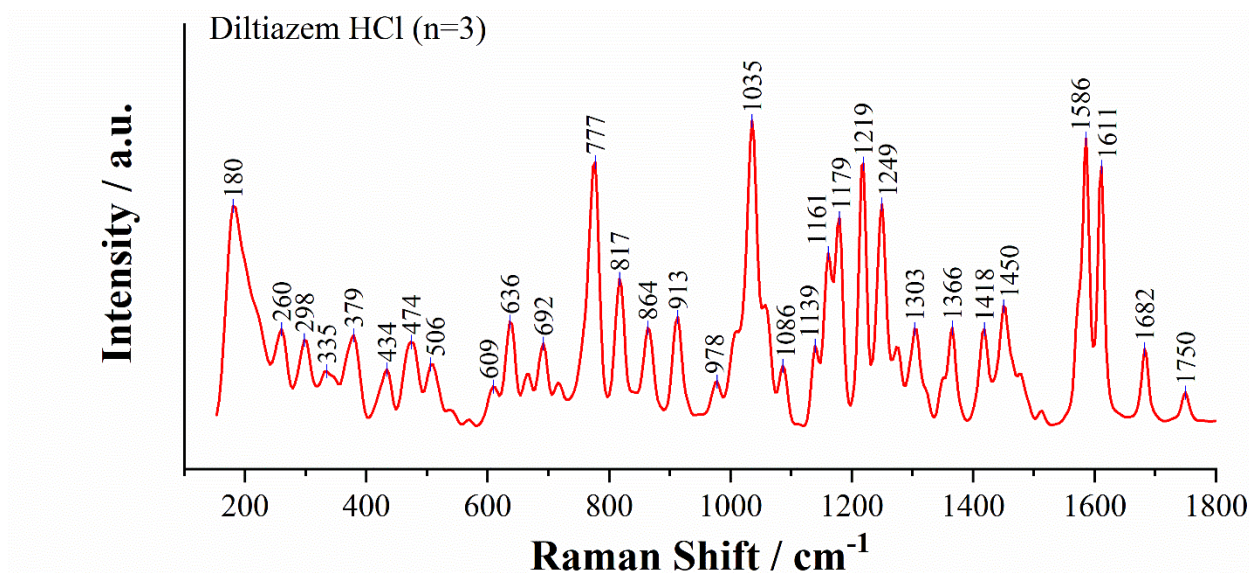


3. Qualitative Data

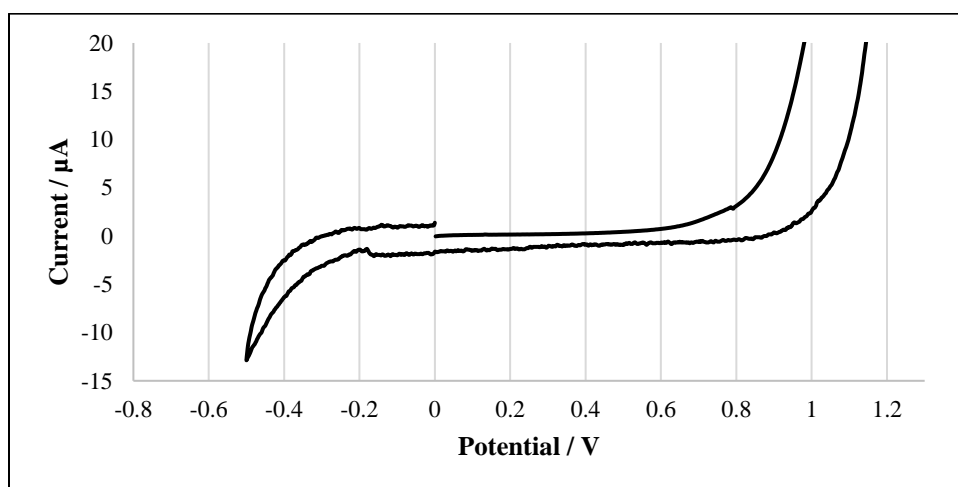
3.1. Nontargeted EC-SERS, 785-nm SPELEC Raman, Silver SPE



3.2. Normal Raman, 785-nm SPELEC Raman



3.3. Electrochemistry, SPCE, 0.1 M KCl



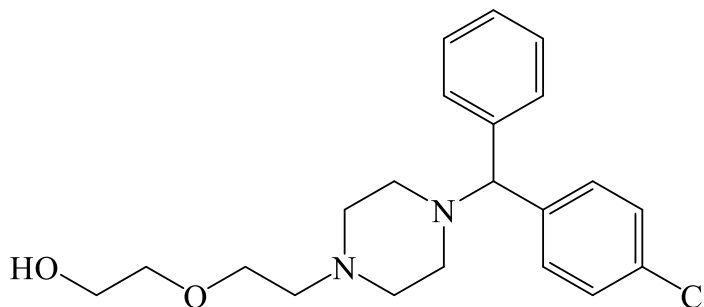
Hydroxyzine

1. General Information

IUPAC Name 2-[2-[4-[(4-chlorophenyl)-phenylmethyl]piperazin-1-yl]ethoxy]ethanol
CAS # 68-88-2
Source Reference Standard

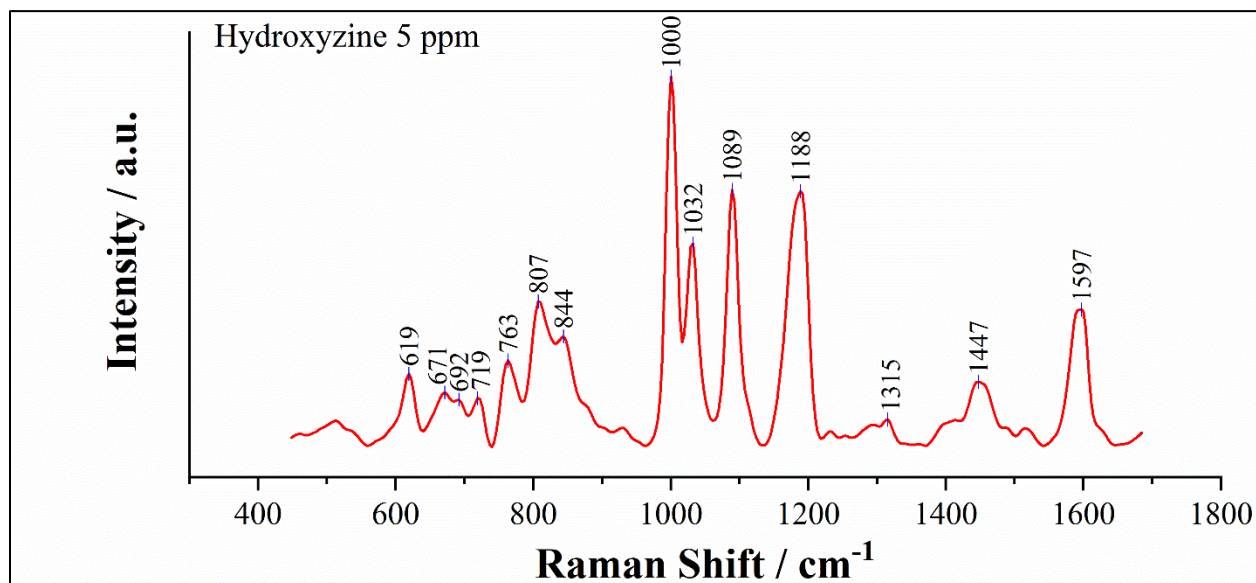
2. Chemical Data

Chemical Formula $C_{21}H_{27}ClN_2O_2$
Molecular Weight 374.9 g/mol
pK_a 2.47

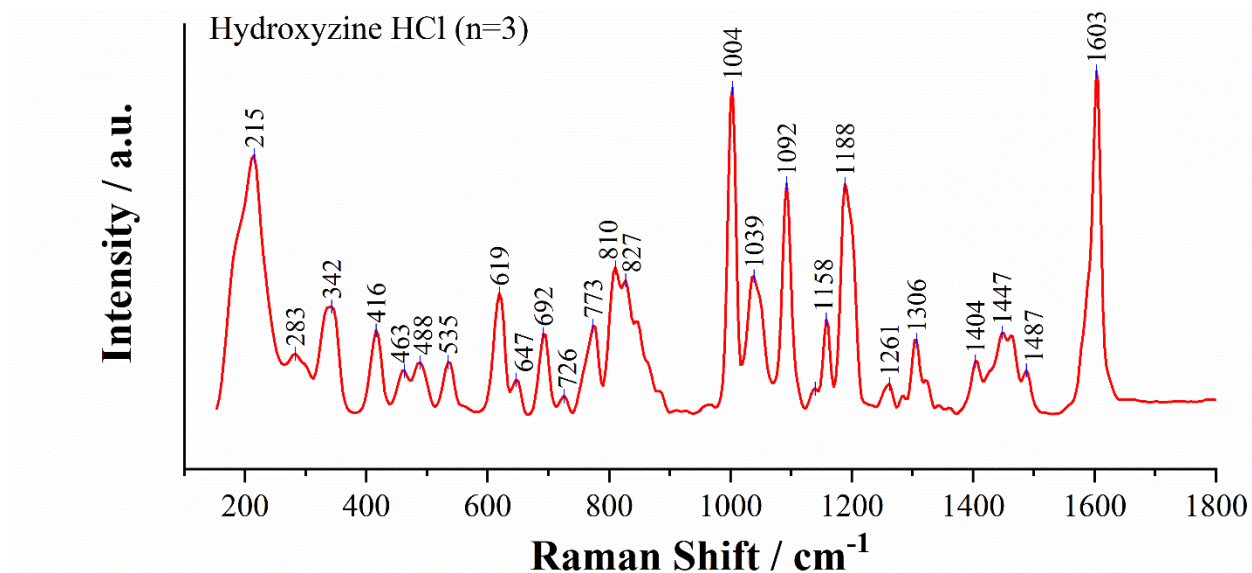


3. Qualitative Data

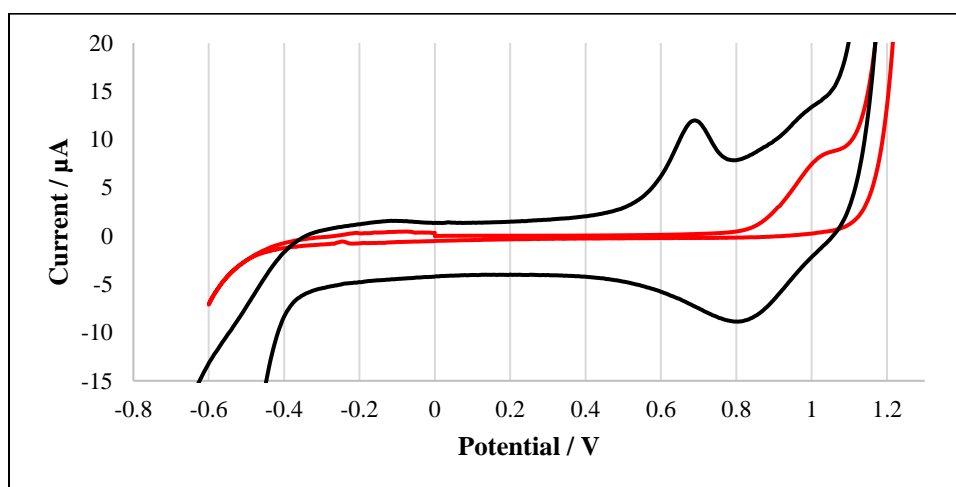
3.1. Nontargeted EC-SERS, 785-nm SPELEC Raman, Silver SPE



3.2. Normal Raman, 785-nm SPELEC Raman



3.3. Electrochemistry, SPCE, 0.1 M KCl



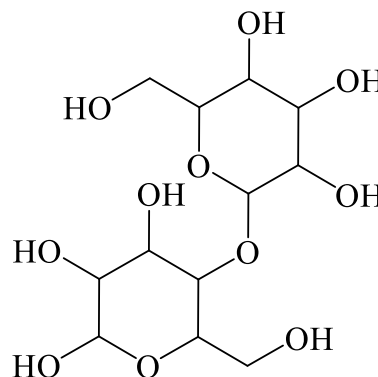
Maltose

1. General Information

IUPAC Name	(2R,3S,4S,5R,6R)-2-(hydroxymethyl)-6-[(2R,3S,4R,5R,6R)-4,5,6-trihydroxy-2-(hydroxymethyl)oxan-3-yl]oxyoxane-3,4,5-triol
CAS #	133-99-3
Source	Reference Standard

2. Chemical Data

Chemical Formula	C ₁₂ H ₂₂ O ₁₁
Molecular Weight	342.30 g/mol
pK _a	NA

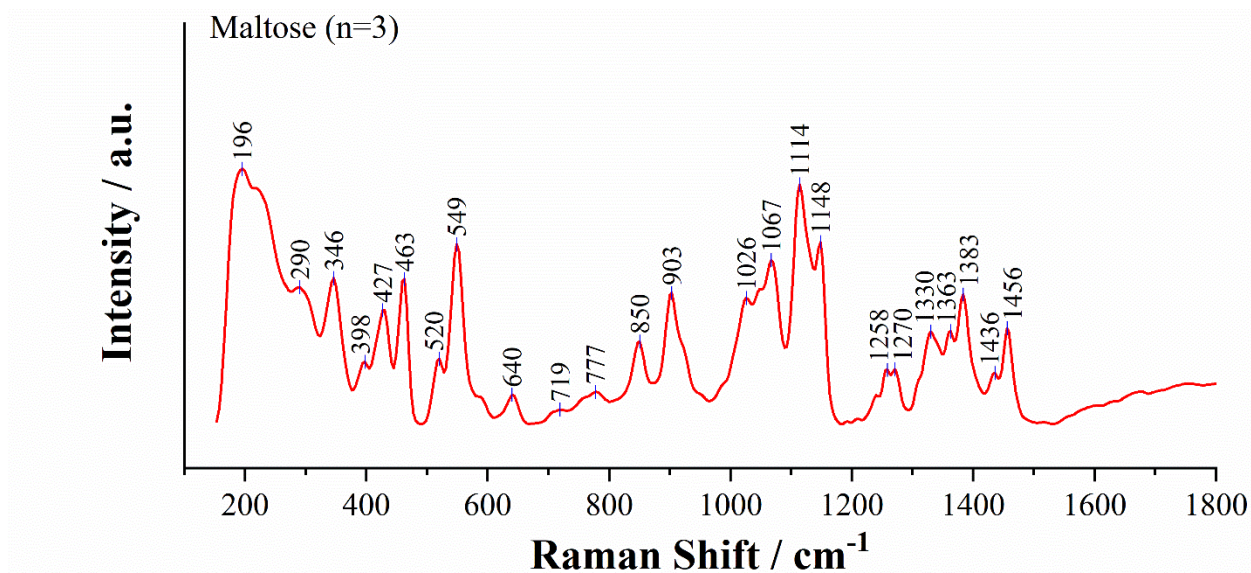


3. Qualitative Data

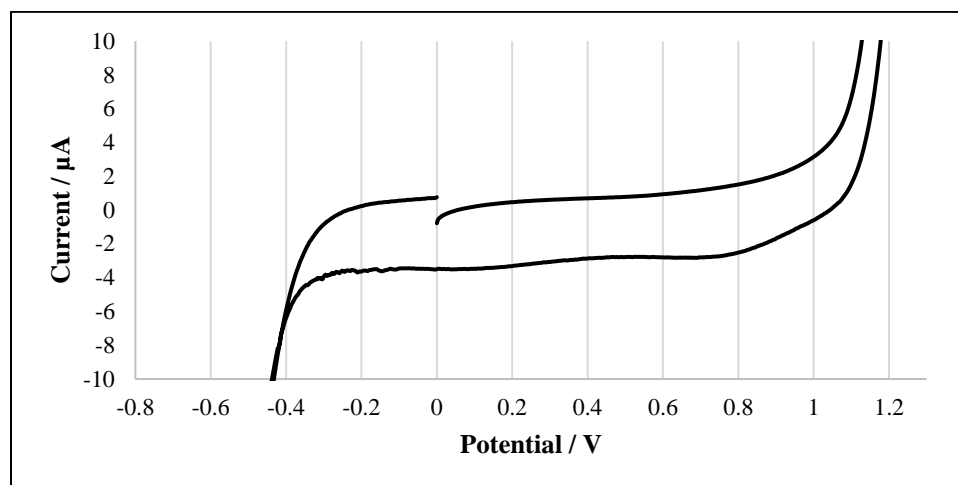
3.1. Nontargeted EC-SERS, 785-nm SPELEC Raman, Silver SPE

NO SIGNAL UNDER TESTED CONDITIONS

3.2. Normal Raman, 785-nm SPELEC Raman



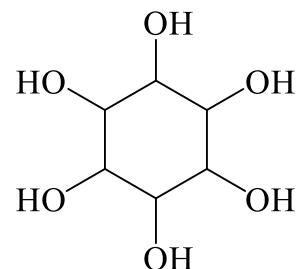
3.3. Electrochemistry, SPCE, 0.1 M KCl



Myo-Inositol

1. General Information

IUPAC Name	cyclohexane-1,2,3,4,5,6-hexol
CAS #	551-72-4
Source	Reference Standard



2. Chemical Data

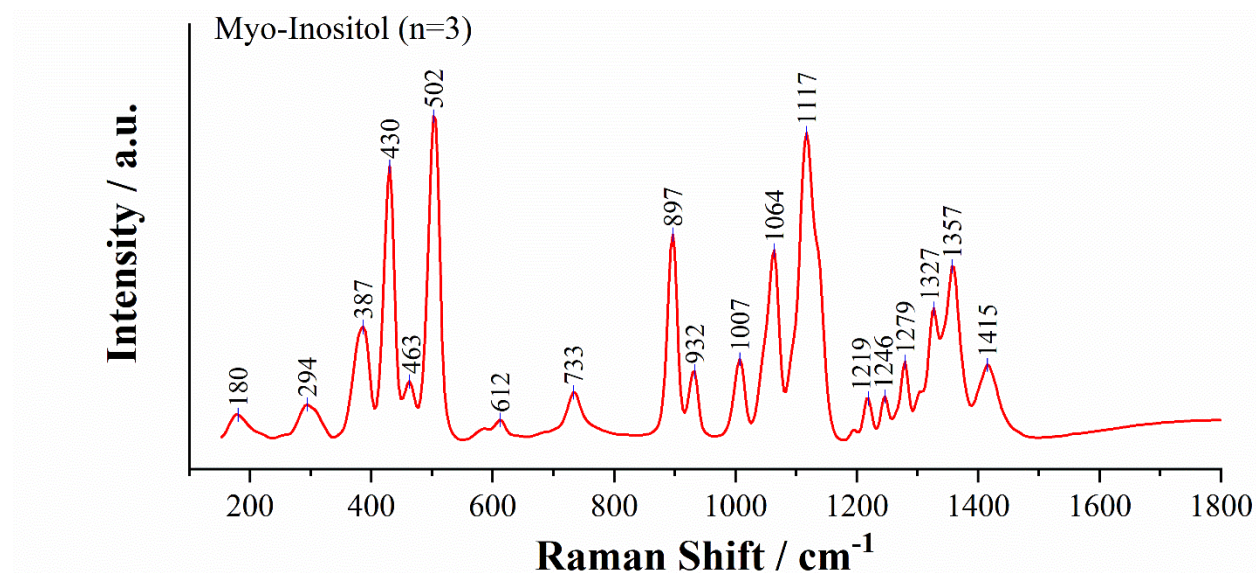
Chemical Formula	C ₆ H ₁₂ O ₆
Molecular Weight	180.16 g/mol
pK _a	NA

3. Qualitative Data

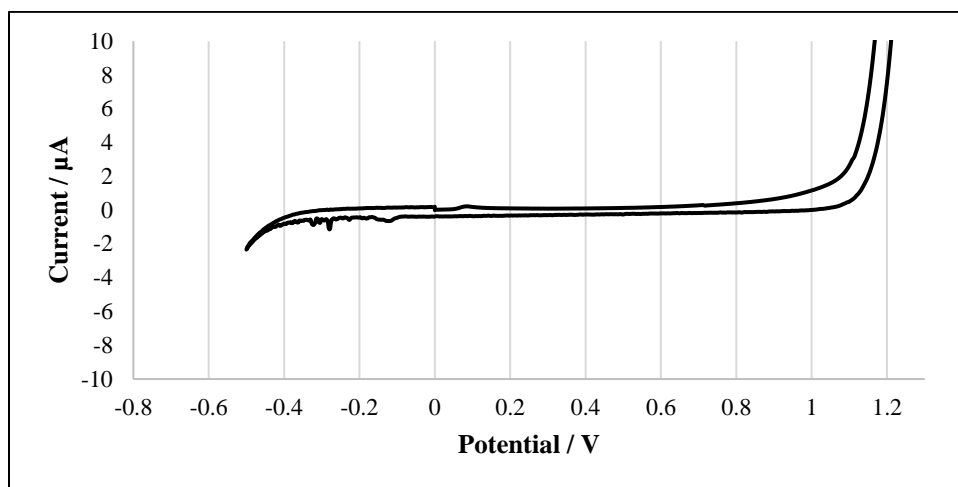
3.1. Nontargeted EC-SERS, 785-nm SPELEC Raman, Silver SPE

NO SIGNAL UNDER TESTED CONDITIONS

3.2. Normal Raman, 785-nm SPELEC Raman



3.3. Electrochemistry, SPCE, 0.1 M KCl



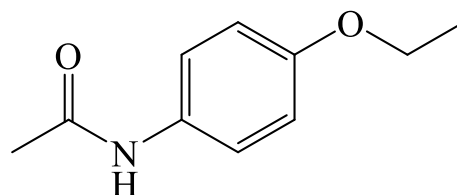
Phenacetin

1. General Information

IUPAC Name	N-(4-ethoxyphenyl)acetamide
CAS #	62-44-2
Source	Reference Standard

2. Chemical Data

Chemical Formula	C ₁₀ H ₁₃ NO ₂
Molecular Weight	179.22 g/mol
pK _a	NA

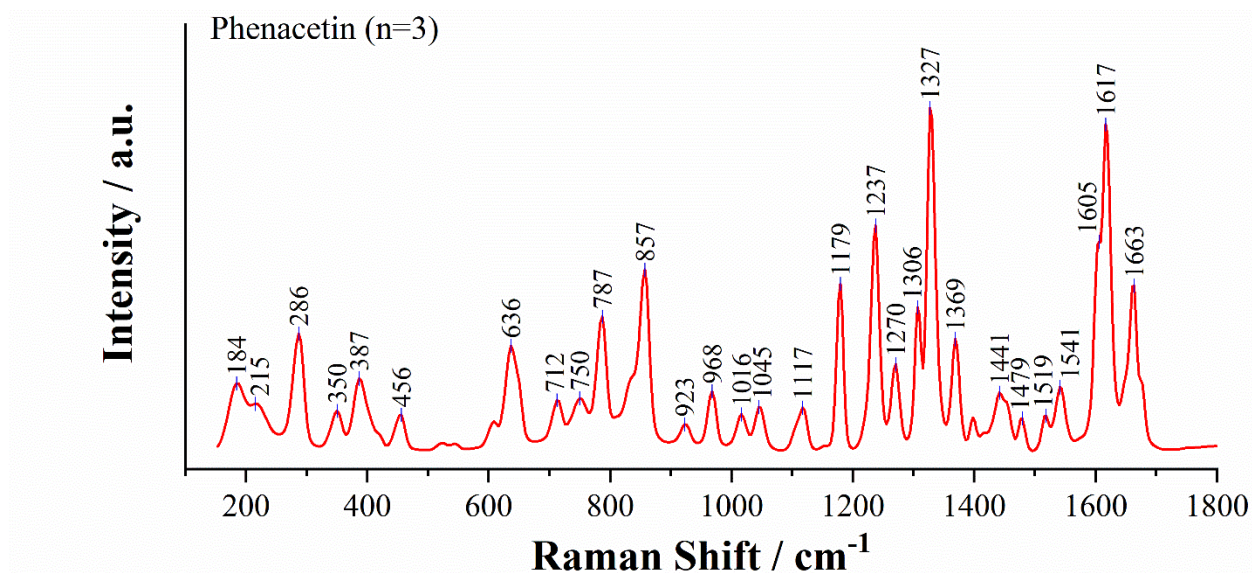


3. Qualitative Data

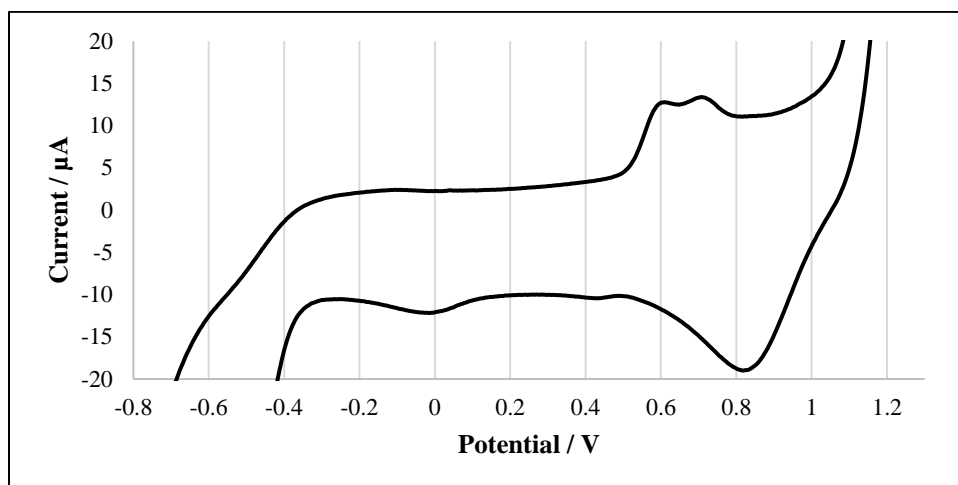
3.1. Nontargeted EC-SERS, 785-nm SPELEC Raman, Silver SPE

NO SIGNAL UNDER TESTED CONDITIONS

3.2. Normal Raman, 785-nm SPELEC Raman



3.3. Electrochemistry, SPCE, 0.1 M KCl



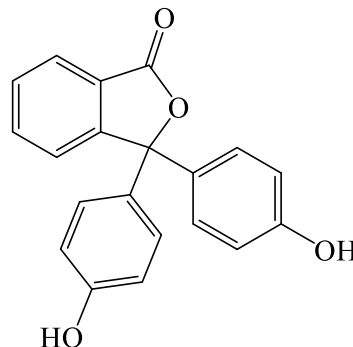
Phenolphthalein

1. General Information

IUPAC Name 3,3-bis(4-hydroxyphenyl)-2-benzofuran-1-one
CAS # 77-09-8
Source Reference Standard

2. Chemical Data

Chemical Formula $C_{20}H_{14}O_4$
Molecular Weight 318.3 g/mol
pK_a 9.7

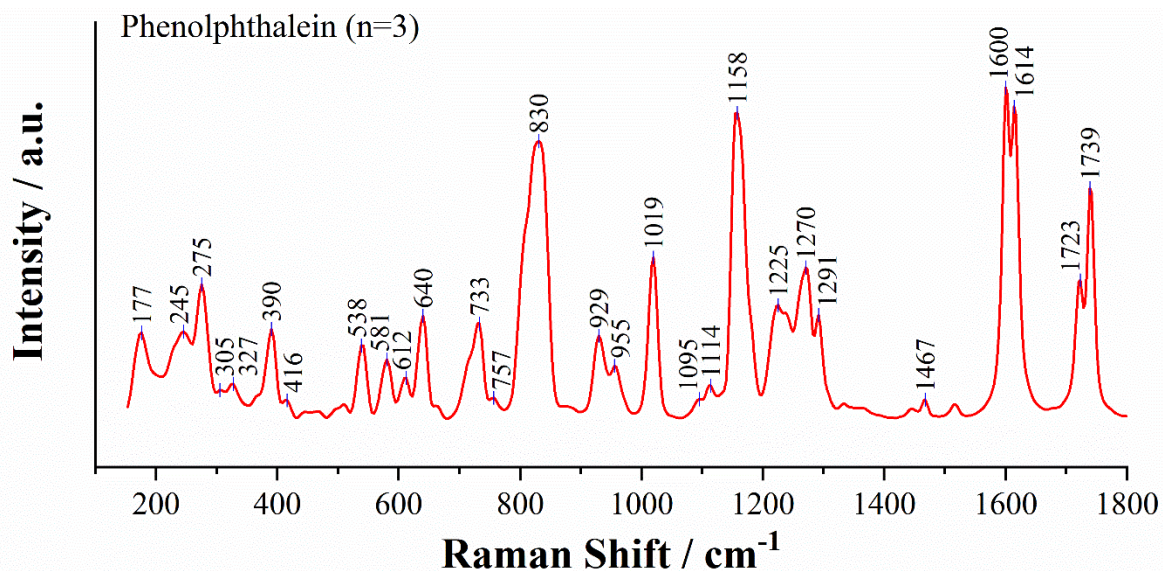


3. Qualitative Data

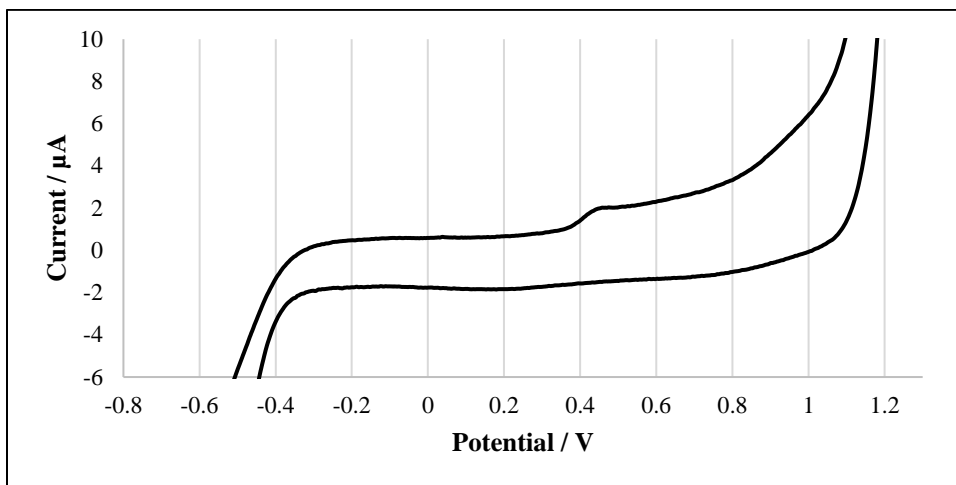
3.1. Nontargeted EC-SERS, 785-nm SPELEC Raman, Silver SPE

NO SIGNAL UNDER TESTED CONDITIONS

3.2. Normal Raman, 785-nm SPELEC Raman



3.3. Electrochemistry, SPCE, 0.1 M KCl



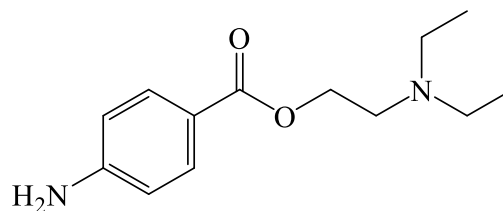
Procaine

1. General Information

IUPAC Name 2-(diethylamino)ethyl 4-aminobenzoate
CAS # 59-46-1
Source Reference Standard

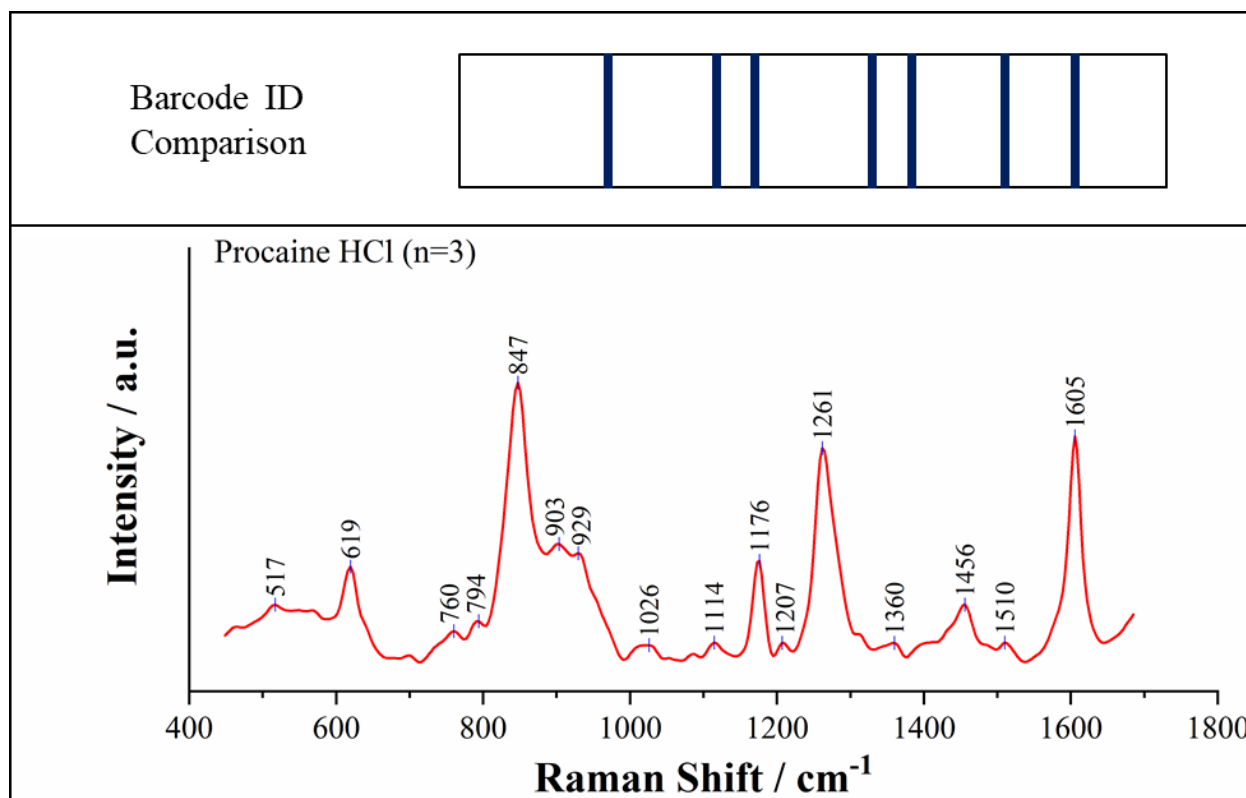
2. Chemical Data

Chemical Formula $C_{13}H_{20}N_2O_2$
Molecular Weight 236.31 g/mol
pK_a 9.04

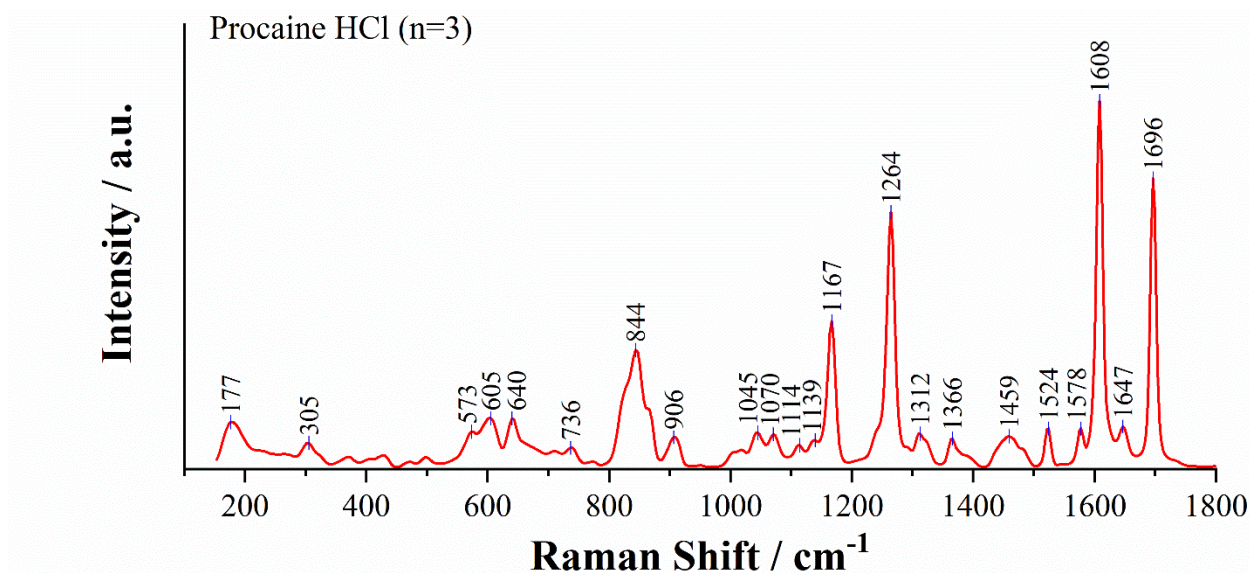


3. Qualitative Data

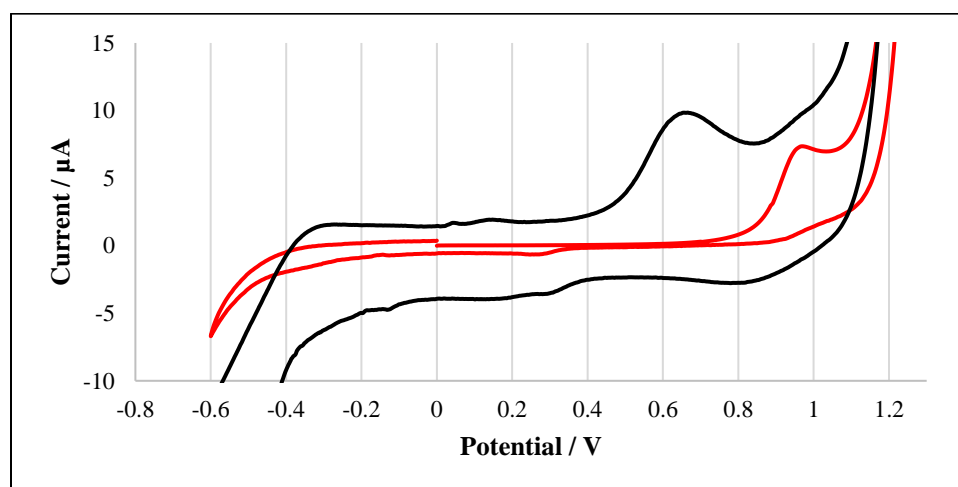
3.1. Nontargeted EC-SERS, 785-nm SPELEC Raman, Silver SPE



3.2. Normal Raman, 785-nm SPELEC Raman



3.3. Electrochemistry, SPCE, 0.1 M KCl



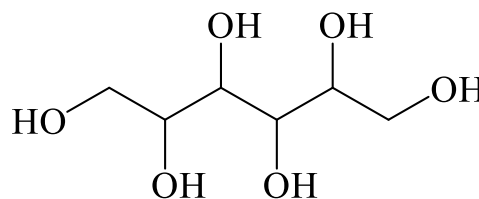
Sorbitol

1. General Information

IUPAC Name	(2R,3R,4R,5S)-hexane-1,2,3,4,5,6-hexol
CAS #	50-70-4
Source	Reference Standard

2. Chemical Data

Chemical Formula	C ₆ H ₁₄ O ₆
Molecular Weight	182.17 g/mol
pK _a	13.6

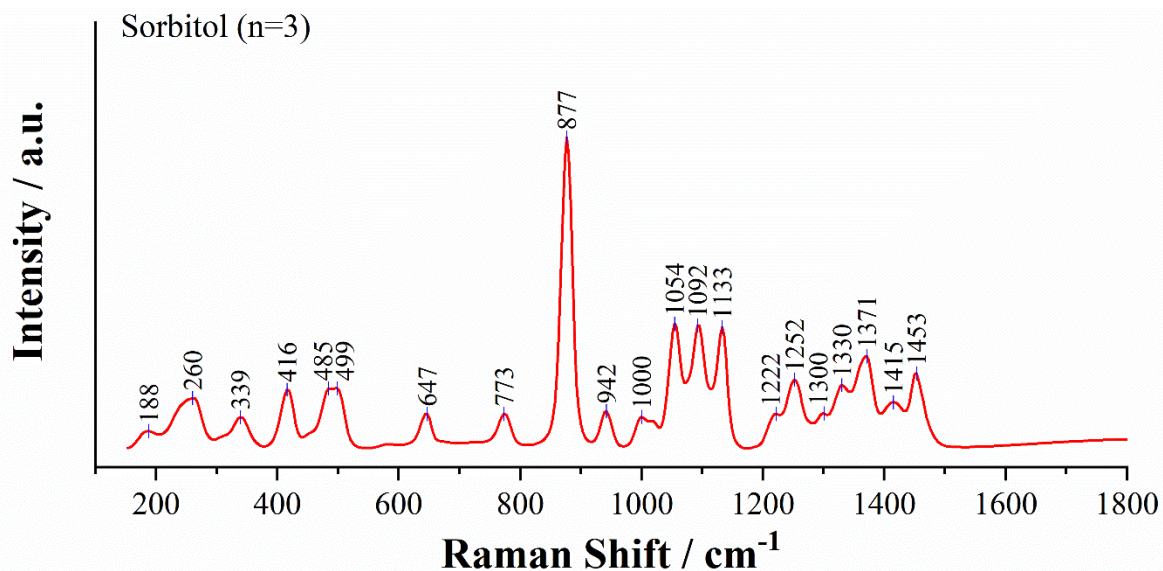


3. Qualitative Data

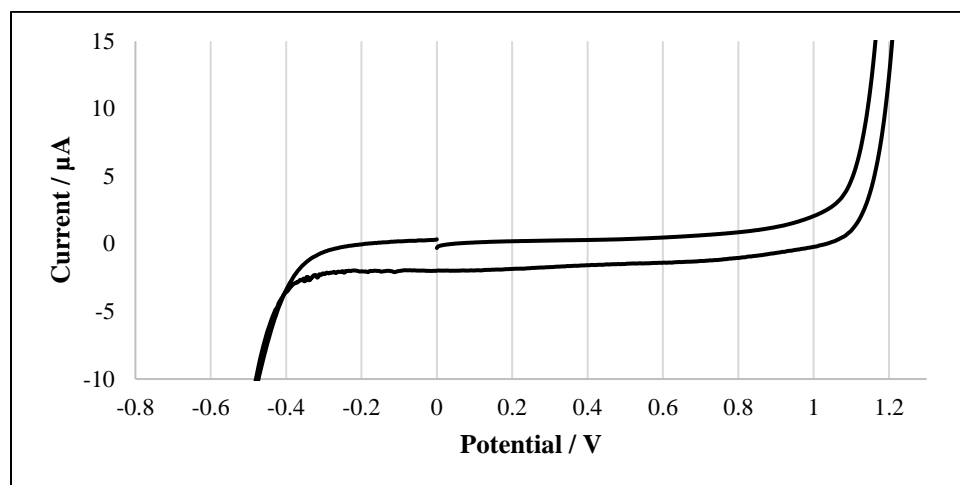
3.1. Nontargeted EC-SERS, 785-nm SPELEC Raman, Silver SPE

NO SIGNAL UNDER TESTED CONDITIONS

3.2. Normal Raman, 785-nm SPELEC Raman



3.3. Electrochemistry, SPCE, 0.1 M KCl



NOTES

The SPELEC Raman 785-nm combination potentiostat-Raman spectrometer was used for all measurements. Both targeted (multi-pulse amperometric detection + Raman) and untargeted (cyclic voltammetry + Raman) were used as EC-SERS methods. EC-SERS methods used 0.1 M perchloric acid supplemented with 0.01 M potassium chloride as the supporting electrolyte and silver SPEs (C013) from Metrohm DropSens USA, Inc. as the SERS substrate.

Baseline correction was performed for all spectra using DropView SPELEC software version 3.2.2 18LZ04.

Spectral band labels were generated using OriginPro 2023 software version 10.0.0.154 employing quick peaks using the 1st derivative method with no smoothing and a threshold of 5 %.

Electrochemistry was employed for the compounds using 0.1 M KCl as the supporting electrolyte and cyclic voltammetry between -0.8 V and +1.3 V or in some cases also included 0 V to +1.3 V to -0.5 V.

PubChem and/or Cayman Chemical was used as the reference for relevant compound information.

ChemDraw Professional software version 21.0.0.28 was used for the generation of the chemical structures.

This data was collected in relation to National Institute of Justice Award # 2019-DU-BX-0030 to West Virginia University. The opinions, findings, and conclusions are those of the authors and do not necessarily reflect those of the department of justice.